Synthesis by supercritical fluids methods of advanced additions for cementitious materials

PhD Thesis by

Marta Díez García

2017

Directed by:

Dr. Juan José Gaitero

Dr. Cyril Aymonier

"Le imprese più ardite vanno vissute con l'animo più semplice."

Italo Calvino. Il barone rampante.

ACKNOLEDGMENTS

This thesis is not an individual work, is the result of the hard work and support of many people to whom I'd like to thanks.

First of all to my directors Jontxu and Cyril who have given me the possibility to make this possible, sharing with me their knowledge and for helping me to develop my career as scientist. I'd like to thank Jontxu for the long conversations about the thesis and many other general aspects where you tried to put me the feet in the floor when I pretended to fight against the system. I know I'm more hardheaded than cement and I'm not easy to convince or to correct but we have finally arrived to a "methastable equilibria" in many "supercritical" situations and nevertheless, this thesis has come to fruition.

My thanks to Basque Government Research Group (IT781-13) directed by Dr. José T. San-José for their support on cement related experimental activities. I'd like to thank Tomás for helping me with the most ungrateful work, the administrative processes. I'd also like to thank the members of the tribunal who have valued my work and attend to my defense. Also to everyone who have given me scientific advice during these years: Jorge, Edurne, Sam, Silvina, Guido, Andrés, Hegoi, Marta, Alex, Josean…

En segundo lugar querría agradecer a mi familia, especialmente mis padres, mi hermana y Jaime, por apoyarme en todo momento. Habéis sido mi sustento emocional y económico durante muchos años, eso sí que es una beca. Gracias y siento haber pagado muchas veces con vosotros mis frustraciones por la tesis. A mis abuelas, tíos y primos por su apoyo cuando en navidad y verano estaba enfrascada con la tesis y no poder pasar todo el tiempo que hubiese querido con ellos. Quiero agradecer especialmente a Bruno, quien ha sido mi mayor apoyo y quien me ha hecho seguir adelante siempre. Creo que has sido más de ayuda tú para mi tesis de lo que yo lo fui para la tuya, pero lo importante es que los dos hemos llegado al final. Las tres semanas que pasé contigo en Nueva York fue el aporte de energía que necesité para escribir la parte más ardua, la introducción. Tu experiencia reciente con la tesis y tú visión más ingenieril me ha ayudado mucho a enfocar ciertos aspectos que no tenía claros. Muito obrigada.

Querría reservar un agradecimiento muy especial a todos mis compañeros de Tecnalia con quienes me he sentido muy a gusto para trabajar y de quien he aprendido

muchas cosas. Se trabaja muy bien con vosotros, y me habéis ayudado mucho en todo tipo de situaciones. Sólo he pasado con vosotros la mitad del tiempo de la tésis pero os habéis convertido en mi familia laboral. Gracias especialmente a mis compañeros de oficina y laboratorio Marta, Jone, Alex, Ana y Tamara, ha sido un placer compartir con vosotros todo tipo de situaciones desde risas hasta lagrimas, habéis sido un gran apoyo. También querría agradecer especialmente a Edurne con quién compartí mis primeros pasos en Burdeos y juntas nos peleamos con todos los reactores y las bombas hasta poder sacar algo en claro.

Esta cotutela no ha sido para nada fácil por temas administrativos y desacuerdos varios entre las dos universidades pero para ello estaban los "confusers" para ayudarme cuando necesitaba saber cómo resolver algunos papeles o con quien contactar para esto otro. Los problemas administrativos han sido desmoralizantes y nos han llevado muchos disgustos y quebraderos de cabeza, pero a pesar de todo es posible y poco a poco vamos saliendo hornadas (más o menos chamuscadas) de cotutelados UPV-UBX. Muchas gracias Aitor, Ainara, Ane, Ana y Olaia, creo que ya estamos capacitados para escribir la guía "cómo hacer una cotutela y no morir en el intento" para ayudar a los nuevos pupilos en este mar de burocracia.

El periplo en Burdeos tuvo muchos altibajos pero allí conocí gente maravillosa que me ayudó mucho a acentuar los altos y olvidar los bajos. Querría agradecer especialmente a Ester, Agustín, Ana, Aitor y Alicia porque esos pic-nic junto a la Garonne fueron lo mejor de ese año. También destacar divertidísimas clases de francés con Agustín y Ester. Querría agradecer a Blanca, Alicia y Suchittra que fueron mi gran apoyo en el ICMCB. También al resto de compañeros del ICMCB por ayudarme cuando lo necesité. Quisiera dar las gracias a Marie y a Charles (y mimi) porque fueron unos compañeros de piso maravillosos. Son de lo mejor que me llevo de mi estancia en Burdeos, ese piso en Sainte-Marie era mi refugio. Merci pour votre patience avec mon français et pour être mes maîtres, désolé pour n'être pas une bonne élève (au moins mimi m'entendait).

Por último agradecer a mis amigos por su constante apoyo y su paciencia conmigo cuando les posponía quedar una y otra vez por estar ocupada con la tesis: Naiara, Damián, Ortzi, Javi, Iciar, Ane, Amara, Izaskun, Olivia, Sandra…. Querría agradecer especialmente a Naiara por su ayuda con el diseño de la portada, ¡tienes mucho talento! Quiero agradecer a Tatiana y Raúl porque ellos son el motivo por el que

estoy haciendo la tésis ; aquella tarde en Etxebarri sí que fue un " yo solo iba a tomar un café y me lié".

GRACIAS A TODOS POR HABERME ACOMPAÑADO EN ESTA ETAPA

INDEX

GLOSSARY

CEMENT NOTATION

In cement chemistry there is a notation which is based on the following principles:

C= CaO

H=H_2O

S=SiO_2

A= Al_2O_3

Ŝ= SO_3

F=Fe_2O_3
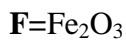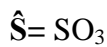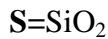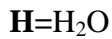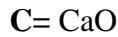
Based on this notation, several compounds are formulated as follows during this thesis:

C-S-H= Calcium silicate hydrate

C₂S= Ca_2SiO_4 ➔ Belite

C₃S= Ca_3SiO_5 ➔ Alite

C₃A= $Ca_3Al_2O_6$

C₆ASH₃₂= $(CaO)_6(Al_2O_3)(SO_3)_3 \cdot 32H_2O$ ➔ Ettringite

AFt= $Ca_3(Al,Fe)(OH)_6 \cdot 12\ H_2O]_2 \cdot X_3 \cdot nH_2O$ (where X represents a doubly charged anion or, sometimes, two singly charged anions.)

AFm= $[Ca_2(Al,Fe)(OH)_6)] \cdot X \cdot nH_2O$ (where X represents a singly charged anion or 'half' a doubly charged anion.)

ANALYSIS TECHNIQUES

XRD: X-Ray diffraction

NMR: Nuclear magnetic resonance

SEM: Scanning electron microscopy

TEM: Transmission electron microscopy

FTIR: Fourier-transformed infra red

XRF: X-Ray fluorescence

RESUMEN

El cemento es el material más utilizado en el mundo actualmente. Éste, fue utilizado por primera vez en tiempos de los romanos para argamasar las piedras en sus construcciones. Esta nueva técnica proporcionaba más durabilidad a las edificaciones y, en parte, gracias a ello aun podemos disfrutar de numerosos edificios construidos en aquella época. Tras un periodo oscuro durante la edad media, el conocimiento se perdió y hasta bien entrado el siglo XVIII no volvió a usarse algo similar al cemento romano. Entonces, se desarrolló lo que hoy en día conocemos como cemento Portland. Este nuevo material pronto se convirtió en un material imprescindible en la construcción por diversos motivos: su bajo coste, su fluidez y fácil trabajabilidad durante los primeros minutos de fraguado y su fácil uso. Sin embargo el cemento es frágil cuando es sometido a altas cargas de compresión, y también es susceptible a la degradación por agentes externos. Por este motivo se emplean diferentes adiciones en el cemento que modifican algunas propiedades finales o durante el proceso de fraguado. Entre ellas se encuentran los aceleradores del fraguado los cuales consiguen que la estructura de la matriz cementicia se desarrolle antes, consiguiendo una estructura más densa y resistente en menos tiempo. Entre los acelerantes existe un tipo de adiciones que actúan de semilla, que son puntos de nucleación para la formación de gel C-S-H en torno a ellos. La última generación de adiciones desarrolladas se basa en nanopartículas de silicato cálcico hidratado.

En este trabajo se estudiará la síntesis y el uso de dos nuevos tipos de nano-adiciones, la tobermorita y la xonotlita. La tobermorita es un silicato cálcico hidratado con Ca/Si=0,83. La elección de este compuesto de este compuesto se basa en las teorías que explican que el gel C-S-H, a pesar de su estructura amorfa, contiene algunos pequeños dominios cristalinos que presentan una estructura semejante al de la tobermorita. Así mismo, el descubrimiento de tobermorita cristalina en estructuras de cemento romanas sostienen la elección realizada. Ignoramos si esta tobermorita se introdujo junto con las pozzolanas o si fue un producto de hidratación posterior. En este último caso se desconoce en qué momento de los ~2000 años que tienen las estructuras llegó a cristalizarse la tobermorita. Existe la posibilidad de que la durabilidad del cemento romano venga proporcionado por este compuesto singular. La xonotlita es

también una silicato cálcico hidratado con una relación Ca/Si=1, su utilización como nano-adición también ha sido propuesta.

Tanto la tobermorita como la xonotlita son minerales poco comunes por lo que para su empleo industrial es necesario diseñar una ruta de síntesis efectiva. Hasta el momento la síntesis más común ha sido la hidrotermal a temperaturas en torno a los 130ºC para la tobermorita y 220ºC para la xonotlita. Sin embargo existe una gran controversia en torno a las condiciones de reacción de la tobermorita, ya que ésta es metaestable a altas temperaturas y puede transformarse en xonotlita. A pesar de ello aun no se conocen del todo las condiciones de equilibrio de estas dos fases.

En este trabajo presentamos un nuevo método de síntesis hidrotermal bajo condiciones supercríticas, es decir, por encima de 374ºC y 22,1MPa. El motivo de sintetizar xonotlita y tobermorita bajo estas condiciones es que el agua supercrítica tiene unas propiedades específicas que puede acelerar la cinética de la reacción. El estado supercrítico tiene propiedades de los líquidos y de los gases. La difusividad en este estado es muy alta y la viscosidad muy baja, por lo que favorece las reacciones. Este método de síntesis está empezando a despuntar debido a su versatilidad y se usa para la síntesis de multitud de materiales inorgánicos de tamaño nanométrico.

En primer lugar, tras una exhaustiva búsqueda bibliográfica, se realizó la síntesis de ambos productos en condiciones hidrotermales subcríticas. Esto nos sirvió para poder familiarizarnos con los compuestos y conocer cuáles son las condiciones más optimas de trabajo para llevar a cabo las síntesis y de este modo enfrentarnos a la síntesis en estado supercrítico de mejor manera.

Para la síntesis de xonotlita se estudiaron varios reactivos para conocer cuáles son mejores para producir xonotlita cristalina. Las condiciones de reacción empleadas fueron 225ºC y presión autógena durante 4 horas. Se pudo obtener xonotlita cristalina en todos los casos, obteniendo calcita ($CaCO_3$) o nitratina ($NaNO_3$) como producto secundario. En un segundo paso, una vez decididos los reactivos más adecuados, se llevó a cabo un estudio sobre el efecto de la temperatura y del tiempo de reacción sobre la síntesis. Se concluyó que el incremento de la temperatura de reacción de 215ºC a 250ºC favorecía la cristlización de la xonotlita y que el uso de tiempos de reacción más largos también favorecía la formación de xonotlita.

En el caso de la tobermorita, según la bibliografía, la introducción de una proporción pequeña de Al sustituyendo al Si en las cadenas de la estructura, proporciona estabilidad al compuesto. En este trabajo quisimos estudiar más a fondo este caso y conocer más en profundidad el efecto del Aluminio en la formación de la tobermorita. Por ese motivo se estudiaron cinco dosificaciones de Al: 0%, 6%, 10%, 15% y 20% respecto al silicio substituido. Se usaron como reactivos CaO, nano-SiO_2 (amorfo) y nano-Al_2O_3 en relación Ca/(Si+Al)=0,83. Todas las síntesis se realizaron a 215ºC durante 4 horas. Los análisis efectuados mediante difracción de rayos X destacaron el efecto del aluminio en la cristalización de la tobermorita. Se observó que cuanto mayor es la concentración de aluminio introducida, mayor es la cristalinidad del producto. La tobermorita cristaliza con dos morfologías diferentes, planar y fibrilar. Según lo descrito en la literatura, en las síntesis hidrotermales generalmente se obtienen partículas planas y aglomeradas a no ser que se empleen modificadores orgánicos que actúen de plantilla favoreciendo la formación de fibras. Así mismo la tobermorita tiene tres estructuras diferentes en función del grado de hidratación. Estas tres se diferencian por la distancia entre los planos de CaO siendo 14Å en la fase más hidratada, 11Å en la intermedia y 9Å en la menos hidratada. Mediante la síntesis hidrotermal obtuvimos en todos los casos 11Å tobermorita. Es posible deshidratar esta tobermorita sometiéndola durante al menos 24h a 300ºC. Existen dos tipos de 11Å tobermorita, la que se transforma en la de 9Å tras el tratamiento térmico, la cual recibe el nombre de normal y a la que no se transforma se le llama anómala. Efectuamos este proceso para diversas síntesis con diferentes %Al. Tras el tratamiento se encontró que en muestras con el mismo contenido de Al algunas presentaban un comportamiento anómalo mientras que en otras muestras era normal sin llevar un patrón definido y bajo las mismas condiciones de reacción. Se observó que, generalmente, las muestras con mayor cristalinidad eran las que se deshidrataban hasta 9Å. Sin embargo sería necesario hacer un estudio estructural más en profundidad para poder distinguir el comportamiento anómalo y normal.

Tras la síntesis hidrotermal se desarrollaron las síntesis en estado supercrítico con dos reactores diferentes, en continuo y en discontinuo. Para el caso del reactor en continuo fue necesario diseñar y realizar nuestro propio sistema, adaptándolo a la naturaleza de nuestro producto y modificándolo según se iban presentando problemas. Un sistema de reacción en continuo para agua supercrítica se compone principalmente de las bombas que controlan el flujo de entrada de los reactivos, un reactor (que consiste

en un tubo de inconel de longitud y tamaño variable), un controlador de la temperatura y un sistema de calentamiento para el reactor, un filtro, un sistema de enfriado (para parar la reacción) y una válvula que nos permita regular la presión del sistema. Para la síntesis en este sistema es necesario emplear productos que sean solubles para no bloquear las bombas, por ese motivo se empleó nitrato de calcio, metasilicato sódico y nitrato de aluminio (para la tobermorita). Tras varias pruebas y modificaciones fue posible conseguir xonotlita pura a 400ºC y 23,5 MPa y un tiempo de reacción apenas 20 segundos. El producto obtenido es muy cristalino y tiene morfología fibrilar.

Para la síntesis de tobermorita se añadió un porcentaje de 15% Al sustituyendo el Si. La reacción se llevo a cabo a 400ºC y 23,5 MPa durante 7 segundos obteniendo tobermorita pura. Si se aumenta el tiempo de reacción se obtiene xonotlita como producto secundario. Este reactor en continuo nos permite controlar la cinética de la reacción con alta precisión para poder parar la reacción antes de que se forme xonotlita. La tobermorita que se obtiene es muy cristalina y tiene una dirección preferente de crecimiento hacia la dirección (0,0,l). Tiene morfología fibrilar, al contrario de la obtenida con métodos subcríticos, por lo que se parecería más a la tobermorita mineral que es fibrilar. El agua supercrítica al ser altamente energética permitiría la formación de la morfología más estable; pero, para ratificar esto, sería necesario hacer estudios de modelización. En último lugar se estudió el tipo de 11Å tobermorita obtenida sometiéndolo a un tratamiento térmico a 300ºC durante 24 horas. En este caso el producto obtenido es anómalo. Con el objetivo de saber si la morfología en forma de fibras obtenida estaba relacionada con el hecho de realizarse la reacción en estado supercrítico, o si era debido a que se trataba de un reactor en continuo, se llevó a cabo la reacción supecrítica en un reactor discontinuo bajo condiciones supercríticas. Mediante este nueva vía de síntesis también se pudo obtener tobermorita cristalina. Sin embargo, dado que la reacción no ha sido optimizada y la dificultad en controlar la cinética mediante este modo, el producto no es puro. El análisis de microscopía electrónica demostró que el producto también era fibrilar por lo que se comprobó que la morfología viene dada por las condiciones supercrítica y no por el modelo de reactor.

De este modo queda demostrado que, a paesar de lo descrito en la literatura, es posible sintetizar tobermorita a altas temperaturas en condiciones metaestables si se controla la cinética de la reacción. Por otra parte se ha conseguido obtener dos nuevas

rutas sintéticas para tobermorita y xonotlita mediante las cuales se obtiene el producto final en cuestión de segundos en vez de horas como figura en la literatura.

El objetivo de sintetizar este tipo de partículas era emplearlas como semilla en pasta de cemento para comprobar si tienen un efecto acelerante en el fraguado. Para comprobarlo se hicieron medidas calorimétricas y test de resistencia. Para la xonotlita se comprobó su efecto acelarante en las primeras horas de fraguado, llegando a obtener resultados de resistencia a la compresión dos veces más alto que la referencia a las seis horas de fraguado. Para la tobermorita se midieron más parámetros, como la influencia del Al en la estructura, el modo de incorporación de las semillas en la pasta y por último la dosificación. Se comprobó que en todos los casos la tobermorita tiene un efecto acelerante con respecto a la referencia durante las primeras 24 horas de fraguado. Se vio que el % de Al en la muestra (y consecuentemente la cristalinidad de la muestra) no afecta al efecto semilla. En segundo lugar se comprobó que se obtenían mejores resultados añadiendo una dosis de 5% de tobermorita que cualquier otra dosis más bajas, obteniendo en este caso datos de resistencia a compresión hasta tres veces más que la referencia tras tan solo 6 horas de fraguado. En último lugar se comprobó que el modo de adicionar las semillas en la pasta de cemento. Dado que el producto hidrotermal es secado tras la síntesis, las partículas tienden a agregarse de manera que, cuando se adicionan a la pasta de cemento, los puntos de nucleación son más grandes y menos numerosos, y por lo tanto menor efecto semilla. Sin embargo si las semillas están dispersas en el agua de la síntesis (sin secar), están más dispersas y el efecto semilla es más acentuado debido al mayor número de puntos de nucleación. La resistencia mecánica a la compresión tras seis horas de fraguado para muestras usando semillas dispersas en una dosis del 2%, es seis veces mayor que la referencia y dos veces mayor respecto a la muestra con semillas secas. En este caso el agua está tan embebida en las partículas que resulta imposible añadir una dosificación de semillas mayor al 2% porque la trabajabilidad de la pasta de cemento.

Con todo esto podemos concluir que en esta tesis se ha estudiado el efecto del Al en la estructura de la tobermorita. También se ha desarrollado un nuevo método para la síntesis de xonotlita y tobermorita basado en la técnica de los fluidos supercríticos pudiendo reducir los tiempos de reacción descritos en la literatura de varias horas hasta apenas unos pocos segundos. También se ha comprobado la eficacia de estos dos compuestos como semilla en pastas de cemento y acelerar el proceso de fraguado.

RÉSUMÉ

Le ciment est le matériau le plus utilisé dans le monde de nos jours. Il fut d'abord utilisé à l'époque romaine comme mortier dans les constructions. Cette nouvelle technique donna plus de durabilité aux bâtiments et c'est en partie grâce à cela que nous pouvons encore profiter des nombreux bâtiments construits à cette époque. Après une période sombre au Moyen Âge, la maîtrise de cette technique fut perdue et il a fallu attendre le XVIII ème siècle pour redécouvrir un ciment semblable au romain. Ensuite, le matériau connu actuellement comme ciment Portland fut développé. Ce nouveau matériau est vite devenu indispensable dans la construction pour plusieurs raisons: son faible coût, sa fluidité et sa bonne maniabilité pendant les premières minutes du montage et son utilisation facile. Cependant, le ciment est fragile lorsqu'il est soumis à des charges élevées et il est susceptible d'être dégradé par des agents externes. Pour cette raison, différentes additions sont utilisées pour modifier le processus de prise ou les propriétés finales de la pâte de ciment. Parmi ces additions on y trouve les «accélérateurs de mise en place» qui développent la matrice de ciment plus rapidement. Il existe un type d'additions accélératrices qui agissent comme des graines; ce sont des points de nucléation pour la formation de gel C-S-H autour d'eux. La dernière génération d'additions accélératrices développées repose sur des nanoparticules de silicate de calcium hydraté.

Dans ce travail, on étudiera la synthèse et l'utilisation de deux nouveaux types de nano-additions, la tobermorite et la xonotlite. La tobermorite est un silicate de calcium hydraté avec un rapport Ca / Si de 0,83. Nous avons choisi ce composé car certaines théories soutiennent que le gel C-S-H, malgré sa structure amorphe, contient quelques petits domaines cristallins qui ont une structure semblable à la tobermorite. Aussi, la découverte de tobermorite cristalline dans les structures cimentaires de l'époque romaine soutient notre choix d'étudier ce composé. On ignore encore l'origine de cette tobermorite et si elle fut introduite avec les roches pouzzolanes employées dans la fabrication du béton ou si elle fut le résultat d'un produit d'hydratation postérieur. Dans ce dernier cas, on ne sait pas à quel moment, au cours des ~ 2000 ans de ces structures, la tobermorite s'est-elle cristallisée. On pense que la longue durée de vie des structures en ciment romaines pourrait s'expliquer par ce composé. La xonotlite est également un

hydrate de silicate de calcium avec un rapport Ca / Si de 1, et son utilisation comme nano-addition a également été proposée.

Aussi bien la tobermorite comme la xonotlite sont des minéraux rares. Il est donc obligatoire de concevoir une voie de synthèse efficace et rentable pour leur utilisation industrielle. Jusqu'à présent, la méthode de synthèse la plus courante a été la méthode hydrothermale, avec des températures atteignant 130 °C pour la tobermorite et 220 °C pour la xonotlite. Cependant, il existe une grande controverse concernant les conditions de réaction de la tobermorite, car ce composé est métastable à haute température et peut se transformer en xonotlite. Néanmoins, on ignore encore les conditions d'équilibre entre ces deux phases.

Dans ce travail nous introduisons une nouvelle méthode de synthèse qui repose sur la technologie de l'eau supercritique, c'est-à-dire au-delà de 374°C et 22,1MPa. La raison pour synthétiser la xonotlite et la tobermorite dans ces conditions est que l'eau supercritique a certaines propriétés spécifiques qui peuvent accélérer la cinétique de la réaction. L'état supercritique a des propriétés similaires aux liquides et aux gaz. La diffusivité est très élevée alors que la viscosité est très faible, ce qui favorise les réactions. Cette méthode de synthèse est de nos jours de plus en plus utilisée en raison de sa polyvalence et elle est utilisée pour la synthèse de multiples types de matériaux à l'échelle nanométrique.

D'abord, après une recherche bibliographique exhaustive, nous avons réalisé la synthèse des deux produits dans des conditions hydrothermales sous-critiques. Cette première étape nous a permis de nous familiariser avec les produits et de connaître les conditions de travail optimales pour la synthèse. De cette façon, il serait plus facile de faire face à la synthèse supercritique.

Pour la synthèse de la xonotlite, plusieurs précurseurs ont été étudiés afin de savoir lesquels étaient les plus convenables pour produire la xonotlite cristalline. Les conditions de synthèse utilisées étaient: 225°C et la pression autogène pendant 4 heures. Il a été possible d'obtenir la xonotlite cristalline dans chaque cas, obtenant aussi calcite ($CaCO_3$) ou nitritine ($NaNO_3$) comme sous-produits (selon les précurseurs utilisés dans chaque cas). Deuxièmement, une fois qu'il a été décidé quel précurseur était le plus convenable, nous avons réalisé une étude sur l'effet de la température et du temps de réaction dans la synthèse. Il a été conclu qu'augmenter la température de 215ºC à 250ºC favorise la cristallisation de la xonotlite. Nous avons aussi remarqué qu'à basses

températures, des temps de réaction plus longs favorisent également la cristallisation de la xonotlite.

Dans le cas de la tobermorite, selon la bibliographie, le remplacement d'une petite portion de Si par Al dans les chaînes donne une certaine stabilité au composé. Dans ce travail nous avons voulu approfondir l'étude de ce cas ainsi que le rôle de l'aluminium dans la cristallisation de la tobermorite. Pour cette raison, cinq doses d'Al ont été étudiées: 0%, 6%, 10%, 15% et 20% par rapport au Si atomique substitué. Comme précurseurs nous avons utilisé: CaO, nano-SiO_2 (amorphe) et nano-Al_2O_3 avec un rapport Ca/(Si + Al) = 0,83. Toutes les synthèses ont été effectuées à 215 ° C pendant quatre heures. Les analyses aux rayons X mettent en évidence l'effet de l'aluminium dans la cristallisation de la tobermorite. Ainsi, nous avons observé que la cristallinité du produit augmentait avec la teneur en aluminium. La tobermorite cristalline a deux morphologies, plaquettes et fibres. Il est décrit dans la littérature que, dans des procédés hydrothermiques sous-critiques, on obtient généralement des morphologies de plaquettes agrégées, à moins qu'un modificateur organique qui agisse comme patron ne soit utilisé pour favoriser la forme fibreuse. Aussi, la tobermorite a trois polytypes différents en fonction de son degré d'hydratation. Ce qui différencie ces trois polytypes est la distance entre les plans CaO: 14Å pour la phase la plus hydratée, 11Å pour l'intermédiaire et 9Å pour la moins hydratée. Grâce à la méthode hydrothermique sous-critique, nous avons obtenu dans tous les cas tobermorite 11Å. Il est possible de déshydrater cette tobermorite en la soumettant à 300ºC pendant au moins 24 heures. Il y a deux types de tobermorite 11Å: celle qui se transforme en tobermorite 9Å après le traitement thermique, qui est appelé normale, et celle qui ne se transforme pas, qui reçoit le nom de anormale. Ce traitement thermique a été appliqué pour plusieurs synthèses avec différents % d'Al. Après le traitement nous avons remarqué que, pour la même teneur en Al, certains échantillons présentaient un comportement anormal tandis que d'autres avaient un comportement normal sans motif apparent étant donné qu'ils étaient tous synthétisés dans les mêmes conditions. Nous avons observé que, généralement, les échantillons ayant une plus grande cristallinité étaient ceux qui se déshydratent à 9 Å. Cependant, il faudrait faire une étude plus approfondie afin de pouvoir distinguer entre le comportement anormal et le comportement normal.

Après la synthèse hydrothermale sous-critique, nous avons développé une nouvelle voie synthétique dans des conditions supercritiques avec deux réacteurs

différents, continu et batch. Dans le cas du réacteur continu, il a fallu concevoir et fabriquer notre propre réacteur, en l'adaptant à la nature de notre produit. Une synthèse supercritique continue pour l'eau se compose de pompes qui contrôlent le flux de revenu des précurseurs, le réacteur (un tube inconel de taille et longueur variables), un régulateur de température et un système de chauffage, un filtre, un système de trempage et une valve pour contrôler la pression. Pour la synthèse dans ce réacteur, il est nécessaire d'utiliser des précurseurs solubles afin de ne pas boucher les pompes, c'est pour cela que nous avons utilisé du nitrate de calcium, du métasilicate de sodium et du nitrate d'aluminium (dans le cas de la tobermorite). Après plusieurs essais et modifications, il a été possible d'obtenir de la xonotlite pure à 400ºC et 23,5 MPa en seulement 20 secondes. Le produit obtenu est très cristallin et d'une morphologie fibreuse.

Pour la synthèse de la tobermorite, nous avons ajouté une dose atomique de 15% d'Al substituant le Si. La réaction a été effectuée à 400 ° C et à 23,5 MPa pendant 7 secondes pour obtenir de la tobermorite pure. Lorsqu'on augmente le temps de réaction, la xonotlite se forme comme produit secondaire. Ce réacteur continu permet de contrôler la cinétique de la réaction avec une grande précision afin d'arrêter la réaction avant la formation de la xonotlite. La tobermorite obtenue est très cristalline et elle a une croissance préférentielle dans la direction (0,0,1). Elle a une morphologie fibreuse, contrairement à la plaquette obtenue avec des méthodes sous-critiques; ainsi elle est plus semblable à la morphologie fibreuse de la tobermorite minérale. L'eau supercritique est très énergique et cela permettrait la formation de la phase la plus stable; Cependant, pour prouver cela, il faudrait faire quelques études de modélisation. Pour compléter l'étude, la tobermorite 11Å obtenue a subie un traitement thermique sur l'échantillon à 300°C pendant 24 heures. Le produit est anormal. Afin de prouver si la morphologie obtenue était liée à l'état supercritique ou due au système d'écoulement continu, nous avons réalisé la réaction également dans un réacteur discontinu dans des conditions supercritiques. Nous avons pu obtenir de la tobermorite; Cependant, la synthèse n'est pas optimisée et le produit n'est pas pur. L'analyse d'image a montré que le produit est fibreux. Il a donc été prouvé que cette morphologie est liée à l'état supercritique et non au système continu.

Avec ces synthèses il a été démontré que, malgré ce qu'y est décrit dans la littérature, il est possible de synthétiser la tobermorite à des températures élevées dans

des conditions métastables si la cinétique est contrôlée. De plus, il a été possible de trouver deux nouvelles voies de synthèse pour la xonotlite et la tobermorite, obtenant le produit final en quelques secondes au lieu d'heures ou de semaines comme il est décrit dans la littérature.

L'objectif de synthèse de ce type de particules était de les utiliser comme germes de cristallisation dans des pâtes de ciment afin de vérifier si elles ont un effet accélérant pendant le processus de mise en place. Pour cela des mesures calorimétriques et des essais de résistance ont été effectués. Pour la xonotlite, son effet accélérant a été prouvé pendant les premières heures du réglage, obtenant des forces de compression deux fois supérieures à la référence après six heures de réglage. Pour la tobermorite nous avons mesuré plus de paramètres, tels que l'influence de la dose d'Al du produit, la façon dont les graines ont été introduites dans la pâte de ciment et le dosage. Il a été prouvé que dans tous les cas la tobermorite a un effet accélérant pendant les premières 24 heures de prise prenant comme référence une pâte de ciment sans additions. Nous avons observé que les différents % d'Al dans la tobermorite (et par conséquent la cristallinité de l'échantillon) n'ont aucune influence sur l'effet de semis. Deuxièmement, il a été prouvé que pour des dosages plus élevés (5%) on obtient de meilleurs résultats que pour des dosages plus faibles, ce qui donne des valeurs de résistance à la compression jusqu'à trois fois supérieures à la référence. Enfin, nous avons testé la méthode d'ajout des graines dans la pâte de ciment. Lorsque le produit hydrothermique suit un processus de séchage, les particules ont tendance à s'agréger de sorte que lorsqu'elles sont ajoutées à la pâte de ciment, les points de nucléation sont grands et moins nombreux, et l'effet d'accélération est plus faible. Cependant, lorsque les graines sont dispersées dans l'eau de synthèse, elles ne sont pas très agglomérées et l'effet d'ensemencement est plus élevé en raison de l'augmentation des points de nucléation. La force mécanique de compression après six heures de prise, lors de l'utilisation de graines non séchées, est six fois supérieure à celle de la référence, tandis que pour les graines séchées elle est deux fois plus élevée. Malheureusement, cette méthode ne peut être utilisée que pour des doses faibles (inférieures à 2%), car la pâte à ciment est très peu usinable.

Tenant compte de tout cela on peut conclure que dans cette thèse l'effet de l'Al dans la structure de la tobermorite a été étudié. Nous avons également développé une nouvelle méthode de synthèse pour la xonotlite et la tobermorite qui repose sur la technologie de l'eau supercritique et il a été possible de réduire les temps de réaction des

synthèses décrites dans la littérature de quelques heures à quelques secondes seulement. L'efficacité des deux composés comme graines dans les pâtes de ciment et leur effet accélérant pendant la prise ont été également démontrés.

ABSTRACT

Cement is the most widely used material in the world today. It was used for the first time by the Romans to mortar the stones in their constructions. This new technique provided more durability to the buildings and, partly, thanks to it we can still enjoy many buildings built at that time. After a dark period during the Middle Ages, the knowledge was lost and only in the eighteenth century it was used again something similar to Roman cement. Then it was developed what we know as Portland cement. This new material soon became an essential material in the construction for diverse reasons: its low cost, its fluidity and easy workability during the first minutes of setting and its easy use. However, the cement is brittle when subjected to high compression loads, and is also susceptible to degradation by external agents. For this reason different additions are used in the cement to modify some final properties or the setting process. One type of these additions are the accelerators of the setting which develop the structure of the cementitious matrix earlier, achieving a structure more dense and resistant in less time. Among the accelerants there is a type of seed-acting additions, which are nucleation points for the formation of C-S-H gel around them. The latest generation of additions developed is based on hydrated calcium silicate nanoparticles.

In this work we will study the synthesis and the use of two new types of nano-additions, tobermorite and xonotlite. The tobermorite is a calcium silicate hydrated with Ca/Si=0.83. The first reason for the use of this compound is based on theories that explain that the C-S-H gel, despite its amorphous structure, contains some small crystalline domains that have a structure similar to that of tobermorite The second reason is given by the discovery of crystalline tobermorite in Roman cement structures. The origin of this one is not known nor if it was introduced together with the pozzolanes or if it was a product of hydration later; And, if so, it is unknown at what point in the 2000 years that the structures have, did it crystallize the tobermorite. There is a possibility that the durability of the Roman cement is provided by this unique compound. Secondly it was also studied the possibility of using xonotlite, another type of hydrated calcium silicate with Ca / Si = 1, as nano-addition.

Both tobermorite and xonotlite are rare minerals so, for industrial use, it is necessary to design an effective synthetic route. So far the most common synthesis has been the hydrothermal at temperatures around 130ºC for the tobermorite and 220ºC for

the xonotlite. However, there is great controversy about the reaction conditions of the tobermorite, since it is metastable at high temperatures and can be transformed into xonotlite. However, the equilibrium conditions of these two phases are not yet fully known.

In this work we present a new method of hydrothermal synthesis under supercritical conditions, that is, above 374ºC and 22.1MPa. The reason for synthesizing xonotlite and tobermorite under these conditions is that supercritical water has specific properties that can accelerate the kinetics of the reaction. The supercritical state has properties of liquids and gases. The diffusivity in this state is very high and the viscosity very low, so it favors the reactions. This method of synthesis is beginning to emerge due to its versatility and is used for the synthesis of multitude of inorganic materials of nanometric size.

First, after an exhaustive bibliographical search, the synthesis of both products was carried out under subcritical hydrothermal conditions. This helped us to become familiar with the compounds and to know the optimal conditions of work to carry out the synthesis and thus to face the synthesis in a supercritical state in a better way. For the synthesis of xonotlite several reagents were studied to know which precursors are better to obtain crystalline xonotlite. The reaction conditions employed were 225 °C and autogenous pressure for 4 hours. It was possible to obtain crystalline xonotlite in all cases, obtaining calcite (CaCO3) or nitratine (NaNO3) as secondary product. In a second step, once the most suitable reagents were decided, a study was carried out on the effect of temperature and reaction time on the synthesis. It was concluded that increasing the reaction temperature from 215 °C to 250 °C favored the crystallization of xonotlite and that the use of longer reaction times also favored the formation of xonotlite.

In the case of tobermorite, according to the literature, the introduction of a small proportion of Al replacing the Si in the chains of the structure provides stability to the compound. In this work we wanted to study this case more thoroughly and to know more in depth the effect of the aluminum in the formation of the tobermorite. For this reason 5 dosages of Al: 0%, 6%, 10%, 15% and 20% with respect to the substituted silicon were studied. CaO, nano-SiO_2 (amorphous) and nano-Al_2O_3 were used as Ca/(Si+Al) reactants=0.83. All syntheses were run at 215°C for 4 hours. The X-ray diffraction analysis highlighted the effect of aluminum on the crystallization of the

tobermorite. It was observed that the higher the concentration of aluminum introduced, the greater the crystallinity of the product. The tobermorite crystallizes with two different morphologies, planar and fibrillar. In hydrothermal syntheses, generally, flat and agglomerated particles are obtained unless organic modifiers are used which act as a template favoring the formation of fibers. Also the tobermorite has three different structures depending on the degree of hydration. These three are differentiated by the distance between the planes of CaO being 14Å in the most hydrated phase, 11Å in the intermediate and 9Å in the least hydrated. By hydrothermal synthesis we obtained in all cases 11 tobermorite. It is possible to dehydrate this tobermorite by subjecting it for at least 24 hours at 300 ° C. There are two types of 11Å tobermorite, the one which is transformed into 9Å after the heat treatment is called normal, and the one which is not transformed is called anomalous. We performed this process for various syntheses with different %Al. After the treatment it was found that in samples with the same Al content some showed an anomalous behavior while for others was normal without a defined pattern and under the same reaction conditions. It was observed that, generally, the samples with greater crystallinity were those that were dehydrated up to 9Å. However, a more in-depth structural study would be necessary to distinguish anomalous and normal behavior.

After the hydrothermal synthesis, the syntheses were developed in supercritical state with two different reactors, continuous and in discontinuous. For the case of the continuous reactor it was necessary to design and realize our own system, adapting it to the nature of our product and modifying it as problems were presented. A continuous reaction system for supercritical water consists mainly of the pumps that control the inlet flow of the reactants, a reactor consisting of a tube of inconel (being possible to vary the volume as a funciton of the tube used and the length), a temperature controller, a heating system for the reactor, a filter, a cooling system (to quench de reaction) and finally a valve that allows us to regulate the pressure of the system. For the synthesis in this system it is necessary to use products that are soluble so as not to clog the pumps, for that reason calcium nitrate, sodium metasilicate and aluminum nitrate (for the tobermorita) were used. After several tests and modifications it was possible to obtain pure xonotlite at 400 ° C and 23.5 MPa and a reaction time of only 20 seconds. The obtained product is very crystalline and has fibrillar morphology.

For the synthesis of tobermorite was added a percentage of 15% Al substituting Si. The reaction was carried out at 400 ° C and 23.5 MPa for 7 seconds to obtain pure tobermorite. If the reaction time is increased xonotlite is obtained as by-product. This continuous reactor allows us to control the kinetics of the reaction with high precision in order to stop the reaction before xonotlite is formed. The tobermorite obtained is very crystalline and has a preferential direction of growth towards the direction (0,0,1). It has fibrous morphology, unlike that obtained with subcritical methods, so it would look more like mineral tobermorite which is composed of fibers. The supercritical water, being highly energetic, would allow the formation of the more stable morphology, but to ratify this would be necessary to do modeling studies. Finally the type of 11Å tobermorite obtained was subjected to a heat treatment at 300 ° C for 24 hours. In this case the obtained product is anomalous. In order to know whether the fiber-like morphology obtained was related to the fact that the reaction was carried out in the supercritical state, or if it was due to a continuous reactor, the supecritical reaction was carried out in a batch reactor under supercritical conditions. By means of this new route of synthesis also it was possible to obtain crystalline tobermorite. However, since the reaction was not optimized and due to the difficulty to control the kinetics, the product obtained was not pure. Among other things, xonotlite was obtained as a by-product. The electron microscopy analysis showed that the product was also fibrillar, so it was found that the morphology is given by the supercritical conditions and not by the reactor model.

Thus, the possibility of synthesizing tobermorite at high temperatures under metastable conditions is demonstrated if the kinetics of the reaction is controlled, although the literature up to now said that it was not possible due to its metastability. On the other hand, it has been possible to obtain two new synthetic routes for tobermorite and xonotlite by means of which the final product is obtained in a matter of seconds instead of hours as it appears in the literature.

The objective of synthesizing this type of particles was to use them as seed in cement paste to check if they have an accelerating effect on the setting. Calorimetric measurements and strenght tests were performed to verify this. For the xonotlite, it was verified its accelerating effect in the first hours of setting, obtaining results of compression strength two times higher than the reference to the 6 hours of setting. For tobermorite, more parameters were measured, such as the influence of Al in the

structure, the mode of incorporation of the seeds in the paste and finally the dosage. It was verified that in all cases the tobermorite has an accelerating effect with respect to the reference during the first 24 hours of setting. It was found that the% Al in the sample (and consequently the crystallinity of the sample) does not affect the seed effect. Secondly, it was found that better results were obtained by adding a dose of 5% tobermorite than any other lower dose; obtaining in this case compression strengths up to three times more than the reference after only six hours of setting. Finally, it was verified that the way of adding the seeds in the cement paste affects considerably the mechanical resistance to compression. When the seeds are dried and added to the paste in this way, there are fewer and bigger nucleation points, and therefore less seed effect. However if the seeds are included without having previously dried them, they are more dispersed and the seeding effect is more pronounced. The mechanical strength at compression after six hours of setting for samples with a dose of 2% of the seeds without drying, is six times higher than the reference and two times higher than the sample with dry seeds. In this case the water is so embedded in the particles that it is impossible to add a higher seed dose than 2% because the workability of the cement paste.

With all this, we can conclude that in this thesis the effect of Al in the structure of the tobermorite has been studied. Also, a new method has been developed for the synthesis of xonotlite and tobermorite based on the technique of supercritical fluids which can reduce the reaction times described in the literature from several hours to only a few seconds. The accelerating effectiveness of these two compounds as seed in cement pastes has also been proved.

GENERAL INTRODUCTION

Cement is the most used material in the world just after water. The society nowadays demands more and more fast and cheap civil structures and houses and cement is a very versatile material and can satisfy this demand. The advances in this technology have optimized the building industry, improving the mechanical resistances, the durability, the construction times… Nowadays many houses and constructions are built from precast pieces made of concrete that considerably reduce the time required to rise a building, or to do a civil structure and therefore, the cost is also reduced. However, the cement industry is also one of the most pollutant ones in the world due to the high production volumes annually. In spite of the construction crisis in Europe, the global production and consumption of cement has been increased during the last year and it is estimated to keep on growing during the following years.

Given the importance of this industry, it is very important to propose innovative solutions in order to fulfill the necessities of the society and remediate the weak points of this material. Some are made to change esthetic character such as the texture or the color, others search to improve the durability of the cement, others try to assess the workability of the cement paste and others regulate the setting times of the concrete. This work is framed in this last case as the objective of this work is to synthesize and test the performance of new accelerating additives in cement pastes. The objective is to shorten the setting process; this is required for cold climates where the hydration water can freeze, in the precast concrete industry to produce faster and also, in the civil structures or in the classic house building industry to gain strength at short times. The last generation of accelerating additives are based on nanometric calcium silicate hydrates. This trend is based on the good compatibility of these materials with the cement paste. In this PhD we have mainly worked on two calcium silicate hydrates: xonotlite and tobermorite and proposed a new synthesis method using supercritical water. The aim is to find a new synthesis route that can optimize and make more profitable the hydrothermal routes that exist nowadays which generally are very long. The synthesis in supercritical conditions can reduce drastically the reaction times and the continuous technology that will be developed also makes the reaction more sustainable.

In the first chapter of the thesis we introduce the main concepts that are going to be developed during the whole work. First, it is introduced the cement material explaining the history and evolution of this compound up to nowadays and the properties that make it so special and demanded. It will be explained the chemistry that involves the hydration process of the cement and it will be explained the function of the accelerating additives and which are the most used nowadays. In the second part of this chapter it will be done an extensive structural description of xonotlite and tobermorite and their politypes. In the last part of the chapter it will be introduced the hydrothermal synthesis, the history of this kind of process and the advantages derived from it in comparison with other methods. Then, it will be described what the literature tells about the hydrothermal synthesis of xonotlite and tobermorite. This information is completed with an extended summary of the syntheses in Annexes 1 and 2.To conclude it will be introduced the supercritical water system, the special properties in this domain of the phase diagram and the advantages of using it for hydrothermal syntheses.

In the second chapter is described all the equipments and materials used for the synthesis of the material under sub and supercritical hydrothermal methods and the characterization techniques for the product. It is also described the equipment employed to prepare the cement paste and the machines used in the mechanical tests.

In the third chapter is described the experimental work done related to the synthesis of xonotlite and tobermorite. The first part explains the subcritical hydrothermal syntheses carried out, the reaction conditions and the variables studied for both xonotlite and tobermorite. Then there is a long characterization of the phases produced in order to throw some light about some aspects that were still not clear about these two phases. In the second part it is described the supercritical hydrothermal synthesis. As it is carried out in a home-made continuous system, the first step was to adapt a generic continuous set-up to our necessities, as function of the problems found during the optimization process. Once the optimal rector was obtained, both the synthesis of xonotlite and tobermorite were carried out and their product was carefully characterized as it had never been synthesized before under these conditions.

In the last chapter it is described the accelerating effect of the xonotlite and the tobermorite synthesized under subcritical hydrothermal methods. This seeding effect was studied both with calorimetric measurements and with mechanical test.

To summarize, this thesis follows the complete path from the hypothesis that xonotlite and tobermorite could work as acceleration additions in cement paste, up to the test of their effect in cement paste, passing through the development of a new synthesis route to produce them.

CHAPTER I: INTRODUCTION

I.1   **INTRODUCTION TO CEMENTITIOUS MATERIALS**

I.2   **C-S-H PHASE SYSTEM**

I.3   **HYDROTHERMAL SYNTHESIS**

I.4   **CONCLUSIONS**

I.1   *Introduction to cementitious materials*

I.1.1   History of cementitious materials

The first civilization to use cement, as we know it nowadays, was the Roman [1]. Previously other cementing materials had been used; for example, the Mesopotamian civilization used a mixture of lime, sand, and gravel [2]. However, the Romans were the first ones using hydraulic cement, which means that it reacts with water (like the one we use nowadays). The quality of this cement they invented is unquestionable as we can still visit hundreds of ancient Roman buildings that have resisted over time in good conditions. Vitruvius in his writings "ten books on architecture," around the year 25 BC, described the recipes to be followed to achieve different types of lime mortars. The Romans used for the first time pozzolanic sediments as silicious source original from volcanic eruptions, to make the cement paste more resistant to aqueous atmospheres[3]. Vitruvius described the seawater concrete that they prepared as "it can neither be dissolved in the waves, nor by the power of water." [4]

Afterward, during the dark middle ages, all the knowledge acquired during the Roman period was lost, and they kept on using poor mortars for their construction.

The year 1756 meant an inflection point in cement's history. In that year the British constructor John Smeaton was asked to repair Eddystone's lighthouse. Due to the difficulties found to build a building so exposed to sea tides and severe weather, he decided to investigate how to create a mortar that could set and develop some strength in twelve hours, the time available to build between one high tide and the following one.

If when the tide rises again, the mortar is not hardened enough, it would be damaged, and the building would not last that long. So he made some research on the lime production in the country. He found out a direct relation between the quality of the lime (the hydraulicity) and the clay content of the limestone which served as raw material for the lime: the higher content of clay, the better was the hydraulicity [5][6]. From the results of the research, he obtained the suitable cement to be employed in a lighthouse.

In 1818 L.J.Vicat did a deep research on hydraulic lime, and he arrived at the conclusion that a hydraulic lime should contain both silica and alumina in its composition. As a result of this study, it was possible to synthesize a synthetic hydraulic lime calcining a ground mixture of calcareous stone and lime.[6]

As a result of this research in 1824, Mr. Joseph Apsdin made the first step for the production of Portland cement using clay and lime as raw materials and patented it. It was finally Isaac Charles Johnson the one who developed Apsdin's idea and made what is nowadays know as Portland cement. The innovation that he introduced was related to the production's temperature, increasing the process temperature up to the vitrification point of the products and this way he obtained the clinker used nowadays.[6]

Since then, Portland cement production has been changing and improving its properties. These attributes have enabled it to become the leader in the construction materials production during the last decades (Figure I.1-1).
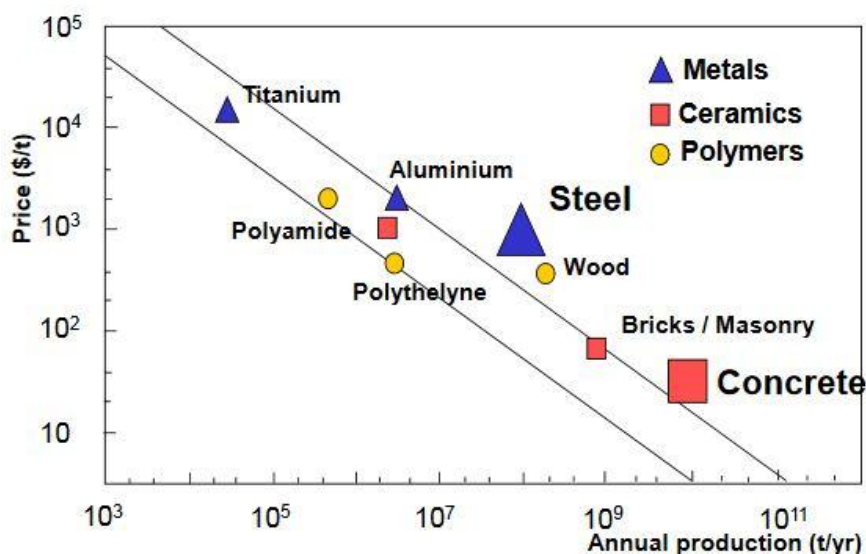
Figure I.1-1: Diagram of the annual production of different construction materials in tons per year related to its prize per ton.[7]

Nowadays cement is the most consumed material (after water) in the world due to several reasons:

- It is very cheap (around 60-70€/ton)[8],
- The fresh cement paste can flow into the prefabricated formwork,
- It has good mechanical properties in compression,
- It is easy to use,
- It is resistant to fire.

Despite the construction crisis in Europe (which has caused a decrease in cement production to levels lower than those of 2001), the world cement production (Figure I.1-2), and consumption (Figure I.1-3) continue increasing each year. This effect is especially accentuated in developing countries such as China and India, and it will continue increasing in the future (Figure I.1-4).
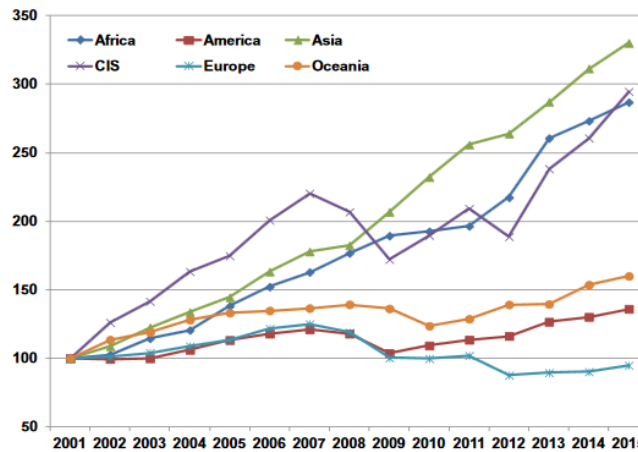
Figure I.1-2: Total cement production (in ton millions) per region from 2001 to 2015. CIS: commonwealth of independent states [9]

Figure I.1-3: Geographical comparison of cement consumption in 2010 and 2015 [10]
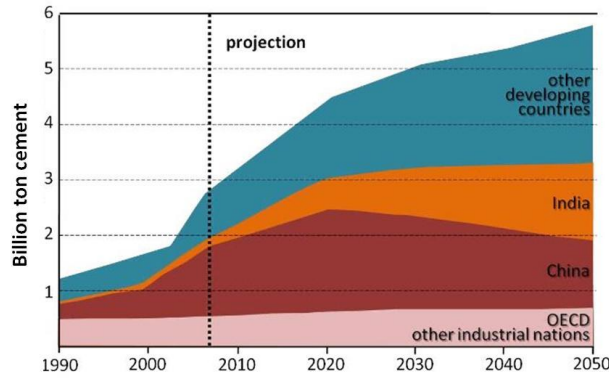
Figure I.1-4: Graphic of the prediction of cement demand in the next years[11]

Each person consumes around three tons of cement per year, as a consequence, cement industry generates around 5% of the total CO_2 anthropogenic emissions to the atmosphere. Half of the emissions comes from the clinker manufacturing process, 40% from burning fuel and 10% from electricity use and transportation, while the other half of the emissions is originated during the calcination process of limestone to obtain CaO[12]. Each ton of ordinary Portland cement (OPC) produced requires 60-130 kg of fuel oil (depending on the kind of cement) and 110 KWh of electricity. In total the estimation of the CO_2 emissions is about 0.9 ton per ton of clinker produced [13]. On the following table, there is a resume of the worldwide environmental footprint of the cement industry.

Table I.1-1: Environmental footprint of cement industry [14]

	1990	2010	2011
Clinker production (in tons)	421	634	665
Cement production (in tons)	511	840	888
Gross specific CO_2 emissions (kg CO_2/ton cement)	761	654	646
Net specific CO_2 emissions (kg CO_2/ton cement)	756	638	629
Thermal energy consumption in clinker fabrication (MJ/ton)	4259	3584	3561
Electric energy consumption in cement fabrication (MJ/ton)	116	110	107
Volume of alternative fossil fuel used (millions of tons)	2.4	13.4	12.8
Volume of biomass fuel used (millions of tons)	0.3	5.0	5.3

It can be observed that despite the fact that the cement production has been increased gradually in last decades, the CO_2 emissions have decreased due to more restrictive environmental legislation, the improved efficiency of the production processes and the incorporation of energetic alternative sources in the production. Because of the importance of cement, and its ecological footprint, it is very important to continue investigating in this field to produce more ecological cement (through energetically optimized manufacturing or improving the performance of the concrete).

Some solutions are being used to improve this environmental footprint [13]. For example:

- Using clean energies for the manufacturing process,
- Placing the production plants close to quarries and the clients to avoid transportation of raw materials and final product,
- Employing waste materials as raw materials or addition for the production of cement.

This necessity to optimize cement production has also an economic reason because as the fuel reservoirs are depleting, the energy cost is increasing and it is estimated that, by 2030, the prize will be doubled [15].

I.1.2 Manufacturing

(a) Industrial process

For the Portland cement production are needed two main components: calcium oxide and silica. The most abundant in the mixture is the calcium which is extracted from several sources such as limestone, chalk, marl, sea shells and aragonite. The composition and the impurities of the raw materials vary from one quarry to another. Some limestone sources are quite pure in calcium carbonate, while others contain some impurities of silica which are more favorable to the production of cement (as it reduces the silica source income needed), or pyrite (FeS_2) which is undesirable because it increases the SO_2 emissions during the manufacturing process. The silicon sources are mainly pit-sand or clay. Also, aluminum and iron oxides are added in lower amounts to the mixture. [16]

In the first step of the manufacturing process, the raw materials are dried to a humidity level under 1%. The proper proportion of both raw materials is ground to obtain a thin homogeneous powder. This mixture is then introduced into a rotary cylindrical furnace called "cement kiln" (Figure I.1-5) where the mixture is heated to temperatures up to 1500ºC. At that temperature, the material is melted, and several chemical reactions happen which will be explained in the next section. The obtained product is called clinker. Afterward, this clinker is ground, and mixed with some additions to improve some specific characteristics of cement. Gypsum is the most common additive in Portland cement. It is used to prevent the "flash setting" effect (rapid development of rigidity in freshly mixed portland cement paste) on the cement paste. It is also used to facilitate the clinker's grinding step, avoiding the agglomeration and coating the mill wall's surface. Organic compounds such as glycols, alkanolamines, and phenol-type are also often added as grinding aids to avoid powder agglomeration and low the energy employed in the process[17]. At this point is obtained what we know as cement.
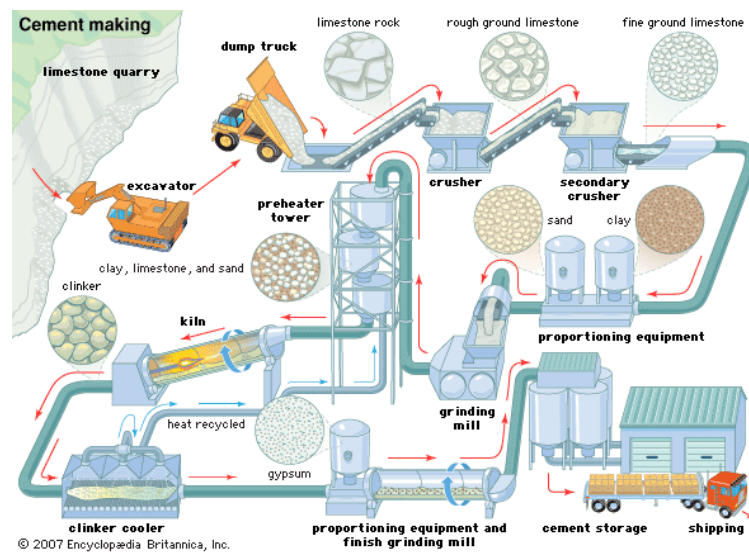
Figure I.1-5: Cement manufacturing plant [18]

(b) Chemical synthesis

In this section, it will be addressed the cement from a structural point of view, starting with the chemical processes that transform raw materials in cement, analyzing the different processes traversed. From this point, we will refer to Portland cement (OPC) every time that we talk about cement.

When the raw materials (calcareous and siliceous) are heated, depending on the temperature, different transformations occur[19]:

- 70-100 ºC: Raw materials are dried under a 1% of moisture.
- 400-600 ºC: Clay is discomposed in its principal oxides; mainly SiO_2 and Al_2O_3.
- 600-1100 ºC: Belite is formed:

$$2CaCO_3 + SiO_2 \rightarrow Ca_2SiO_4 + 2CO_2 \qquad \text{(Equation 1)}$$

The calcite excess is discomposed:

$$CaCO_3 \rightarrow CaO + CO_2 \qquad \text{(Equation 2)}$$

- 1100-1450 ºC: Alite is formed:

$$Ca_2SiO_4 + CaO \rightarrow Ca_3SiO_5 \qquad \text{(Equation 3)}$$

Apart from alite and belite, it is also composed of other minority compounds such as $Ca_3Al_2O_6$ and $Ca_2Al_2Fe_2O_{10}$ which come from the aluminum and iron oxides present in the raw materials[20].

I.1.3   Hydration Process

The hydration process involves many physical changes and chemical reactions. However, because the clinker has lots of impurities, there are too many variables to control, and for this reason, this process is still not completely understood.

All hydration stages involve lots of reactions. Alite is the principal component of the clinker and main responsible of cement hardening. The hydration process takes more than 28 days, and after those days, only 70% of the clinker alite has reacted. After a year, it could be considered that the reaction is finished.[21] The hydration process in alite is the following one:

$$2Ca_3SiO_5 + 6H_2O \rightarrow Ca_3Si_2O_7 \cdot 3H_2O + 3Ca(OH) \qquad \text{(Equation 4)}$$

| C-S-H gel | Portlandite |
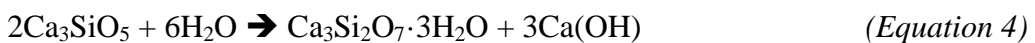
Belite is the second predominant compound in the clinker; its hydration kinetic is even slower than the one of alite. So after 28 days, only 30% of belite has reacted and 90% in one year[21]. The hydration reaction of belite is the following one:

$$2Ca_2SiO_4 + 4H_2O \rightarrow Ca_3Si_2O_7{\cdot}3H_2O + Ca(OH)_2 \qquad \textit{(Equation 5)}$$

C-S-H gel	Portlandite
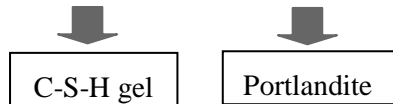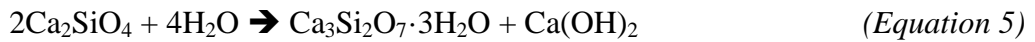
Another component of the clinker is the tricalcium aluminate (C_3A). This compound is very reactive with water, and this affects the cement paste rheology. For this reason, gypsum is added to the mixture; this compound reacts with tricalcium aluminate to avoid the "flash setting." During that process, ettringite is formed[22]. The ettringite is the main compound of the AFt phase which is also composed of different calcium sulfoaluminate hydrates.

$$Ca_3Al_2O_6 + 3CaSO_4{\cdot}2H_2O + 30H_2O \rightarrow Ca_6Al_2(SO_4)_3(OH)_{12}{\cdot}26H_2O \quad \textit{(Equation 6)}$$

Ettringite

If the gypsum added to the clinker is not enough, calcium aluminate phases are formed (known as Afm phases).

The hydration process is commonly divided into five stages [23][19][24][21]. Figure I.1-6 shows the calorimetric curve of the reaction and each of the steps described in this section. Figure I.1-7 shows the morphological changes in the reaction which will also be described in the following lines.
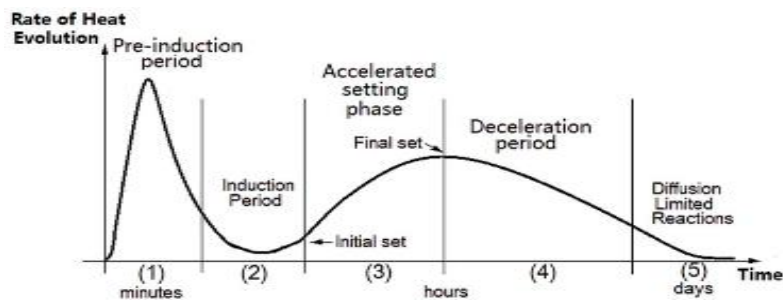
Figure I.1-6: Heat evolution during Portland cement hydration process [25]**.**
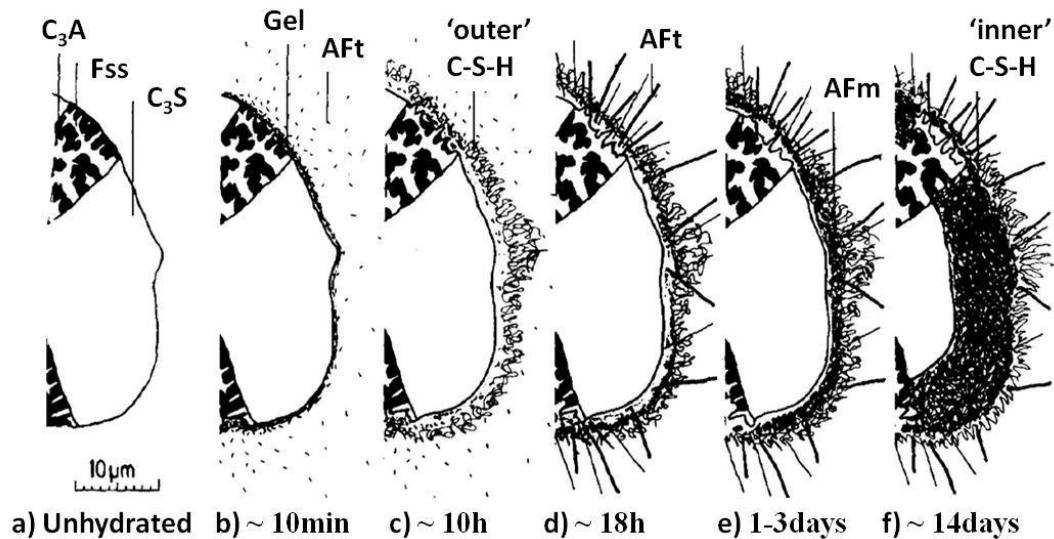
Figure I.1-7: Microstructure evolution of the Portland cement paste during hydration process[21]

- *Stage 1: Pre-induction*

    In the first step, the clinker grains (Figure I.1-7a). are fast dissolved, liberating some Si^{4+}, Ca^{2+}, and OH^- ions to the solution.

    The Si^{4+} ions are dissolved up to a limit where the calcium silicate hydrate gel (C-S-H gel) starts to form, from that moment the Si^{4+} free ions diminish. Due to the different Ca/Si ratio between the clinker composition and the C-S-H gel, when all the Si^{4+} are consumed, there are still Ca^{2+} and OH^- ions in the medium.[26] During this stage, stubby rods of AFt phase, composed mainly of ettringite (C_6ASH_{32}), are formed on the outer face of the gel layer. The ettringite crystals start to appear due to C_3A dissolution, and, if gypsum is not added as an admixture to the clinker, flash setting occurs. At this point, the particles measure up to 250 nm long [27][28]. This stage is represented in Figure I.1-7b.

- *Stage 2: Induction*

    In this step, the hydration slows down, and the cement paste is still fluid. Some authors claim that during stage 2 a continued thin layer is formed over the C_3S grains avoiding their dissolution and therefore their reaction[29][30]. The composition of that protective layer is still unknown, but it is thought to be a metastable calcium silicate hydrate. It can also vary depending on the composition of each clinker. At the end of this step, some pores are formed over the surface of the protective layer allowing the dissolution of the C_3S grains.

- *Stage 3: Acceleration*

    As a consequence of the pore formation in the previous step, the reaction re-starts and C-S-H gel precipitates on the surface of the layer. As the gel is thermodynamically stable, it forms all around the grain. The more C-S-H nuclei form and grow the faster is the hydration process.

    As second reaction product, the portlandite precipitates in the medium. As a consequence, the amount of dissolved Ca^{2+} and OH^- ions diminishes, and the dissolution of calcium silicates and aluminates is accelerated again. In this stage happens a strong heat evolution characterized by the fast formation of C-S-H and portlandite. They grow in the space previously occupied by water, their bigger size and high amount may engulf some small cement grains. The C-S-H at the same time continues growing and involving the AFt rods [31][27]. A second stage C-S-H gel is formed, while portlandite and ettringite continue growing. The end of this stage corresponds to the end of the setting period and the maximum of heat release.

    The growing is shell-shaped, after 12h the C-S-H layer is 0.5-1 μm thick and some close grains start coalescing each other; this point coincides with the end of the setting. At this moment, there is some space (up to 0.5 μm wide) between the C-S-H shell that has been formed and the anhydrous cement that remains unreacted. This space is thought to be filled with a colloidal dispersion. This stage is represented in Figure I.1-7c.

- *Stage 4: Deceleration*

    After some hours reacting, the cement grain's surfaces are coated by the hydration products. In this stage, the kinetics is not anymore controlled by the solution index or the crystal nucleation, but by the diffusion of Ca^{2+} and Si^{4+} ions in the product which are capable of breaking through the porous structure of the C-S-H shell [32]. The reaction slows down as the hydration product is formed. Due to SO_4^{2-} consumption, the ettringite is transformed into monosulfoaluminate (if there is not enough gypsum in the medium), producing a shoulder in the reaction heat diagram (Figure I.1-6). At the end of this period the AFt crystals start growing again with acicular shape; they reach a measure of 2-10 μm long [33][31][28]. This stage is represented in Figure I.1-7d.

- *Stage 5: Diffusion*

In this stage, the C-S-H gel microstructure becomes denser. The rest of species (specially portlandite and monosulfoaluminate) keeps on growing. Consequently, the diffusivity in the reaction medium decreases and the reactions are slowed as the cement matrix gains strength. In the late period, the C-S-H shell becomes less permeable, and the new gel starts to be formed mainly inside the shell. The smaller particles ($<5\mu m$) have completely reacted at the beginning of this period, and the bigger ones are considerate that the core-shell space has been filled after seven days [32]. In this period the SO_4^{2-} concentration drops down inside the shell, and the AFt begins to transform into AFm as a result of the aluminate reaction[32][33]. After the core-shell interspace has been filled, the reaction is much slower, and the mechanism is topochemical. This stage is represented in Figure I.1-7e. The final product is the cement matrix (Figure I.1-7f), and it will be explained more in detail in the following section.

I.1.4 Cement matrix

As it has been mentioned before, the C-S-H gel is the principal hydration product of the cement; it constitutes up to a 70% of the total volume of the set cement. Although the cement is a widely employed material around the world, its real structure is still unknown.

Apart from the C-S-H gel, other crystalline phases that we can find are portlandite and ettringite. The portlandite, forming big hexagonal crystals, and also ettringite which is found forming tiny crystals over the C-S-H amorphous structure (Figure I.1-8).

From the macroscale point of view, cement paste can be considered as a homogeneous material with some macropores ($>5~\mu m$). The observation of the cement at microscale shows a different structure. The C-S-H gel is an amorphous phase that surrounds all the crystalline aggregate. At this scale, there are capillary pores of a size ranging from 10 nm to 5 μm.

Figure I.1-8: SEM image of hydrated cement paste. [34]

At this scale, the pores are associated to the vacancies left when the hydration products replace the spaces initially occupied by water and cement. The pores abundance depends on the water/cement ratio used in the mixture; the higher is the ratio, the more porous is the paste.

At nanoscale it is more difficult to explain the cement structure; the C-S-H structure has not been yet 100% elucidated. There are also pores at this scale that corresponds to the intrinsic C-S-H structure. So, as the exact structure has not been experimentally demonstrated, some theories have been presented to explain the C-S-H gel's structure. It could be defined as some silicate chains linked by CaO layers, forming a stratified structure with variable stoichiometry. The space between layers is occupied by water and Ca^{2+} or Na^+ ions dissolved in it (Figure I.1-9). The chains are ordered following a "drierketter" structure; this means that the structure is repeated each three silicon tetrahedras. The chains can have different lengths, following this rule: 2,5,8,….,3n-1 silicon tetrahedra (n=integer)[35][36][37][38].
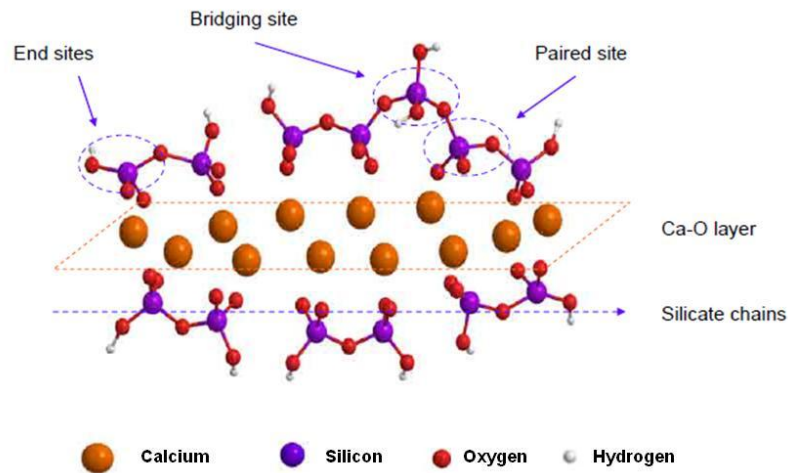
Figure I.1-9: Proposed C-S-H structure[39]

The structure and composition of the C-S-H gel have been widely discussed for years. Le Chatelier et al. (1905) [40] first described it as a $CaO·SiO_2·2.5H_2O$ phase, but he specifies that the ratio between the components was assigned because it was the only calcium silicate that he had been able to synthesize. Newberry and smith[41] agreed that it was a calcium silicate hydrate but with a Ca/Si ratio of 1.5-2. A few years later Bogue in his book "The Chemistry of Portland Cement"[42] concluded that the probable composition was close to $1.5CaO·SiO_2·(aq)$. Recent studies point out a variable Ca/Si ratio ranging from 0.7 to 2.3[43].

Many experimental techniques have been employed to try to elucidate the nanostructure of the C-S-H gel (NMR, FT-IR spectroscopy, TEM, X-ray, nanoindentation, and gas absorption [44][45]) but due to its variable and amorphous nature, it has been impossible to clarify it yet. Bernal[46] and Taylor[47][48] did some XRD analysis on hydrated C_3S paste that allowed him to classify the C-S-H gel into two types, the C-S-H (I) and the C-S-H (II). Calcium silicate hydrate (I) had a layer structure, with the layers elongated in one direction that resulted in a fibrous structure, and showed similarities to tobermorite [49][50][51], and the second is similarly related to jennite[52]. Both are considerably more crystalline than the material formed in cement pastes under normal conditions. From this model, it can be explained a general structure of the C-S-H gel which is a layered structure where calcium silicate oxides flank on both sides the silicate chains while in the interlayer space there are free calcium ions and water molecules.

However, the real C-S-H gel is not completely composed of ordered crystalline tobermorite and jennite phases (only some short-range order). It is a disordered structure full of defects and imperfections which can look similar to the mentioned minerals, but the entire structure is more variable than the ideal one. Tobermorite has a Ca/Si ratio of around 0.8 and the jennite of 1.5 while the C-S-H gels in average have a ratio of 1.7 [36]. The main difference between natural tobermorite and the phase found in C-S-H gel (type I) can be explained by the lack of some bridging tetrahedra, by the omission of entire segments of silicate chains and the inclusion of Ca^{2+} ions in the gap[53][54]. This theory is sustained by ^{17}O-NMR[55] and FT-IR analysis[56]. However, there are other models that differ from this where they highlight the importance of a combination of tobermorite-like + jennite-like structure[35][57][58]. More recently this has also been studied by computational simulation using different models arriving at the conclusion that, in the C-S-H formation, there are two different growth mechanisms that depend on the amount of Ca and Si ions giving place to the two known structures[59]. Dolado et al.[43] in their study propose a solution to the structure of C-S-H gels: at low Ca/Si the systems formed are composed of long polymerized chains (pentamers and more) with 11Å tobermorite, 14Å tobermorite, and Jennite structures. At high Ca/Si the polymeric chains are short (dimmers), and they are basically formed by 14Å tobermorite and jennite.

Tobermorite is thought to be a key point for the durability of Roman structures[60].This phase has been found in some Roman cementitious binders, so some authors claim that the durability of this cement is related to the tobermorite. Marie Jackson et al. [61] published a paper where they describe the discovery of Al-tobermorite in the analysis of Roman archeological submarine cementitious structures. The origin of the Al-tobermorite is related with the pyroclastic puzzolans (Al-rich and Si-poor) employed in the concrete mixture.

I.1.5   Mechanical Properties of Cement Matrix

The mechanical strength of cement is one of the main characteristics that defines it. The hydration process is the one that procures to the cement its mechanical properties. During this period, it is created a structure that held together the cement's particles, as it has been explained previously.

The mechanical properties commonly measured in the cement/concrete are the flexural (Figure I.1-10a) and the compression strength (Figure I.1-10b). The one that characterizes cement for its high performance is the compressive one. There are several factors that control this type of strength of the cement paste[21]:

- The clinker composition and microstructure,
- The water/clinker ratio and the air content in the admixture,
- The mixing conditions,
- Temperature and relative humidity during the curing process,
- The age.
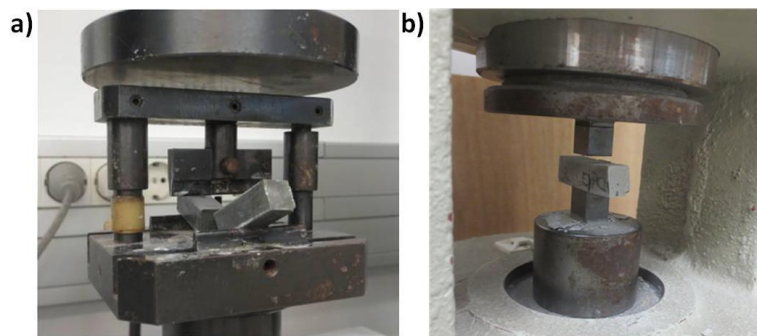
Figure I.1-10: a) flexural test b) compression test

I.1.6 Concrete Admixtures/Additions

Admixtures are those ingredients in concrete other than Portland cement, water, and aggregates that are added to the mixture immediately before or during mixing. Their purpose is to improve some lacks of OPC under specific circumstances (such as climatic).

Already the Romans used some admixtures such as urea or egg white. After the Portland cement invention, the first admixture introduced was the $CaCl_2$ to control the setting process. Some admixtures have been developed to modify the concrete according to its final use to modify and improve some of the problems that the plain cement paste can have. In the following section, most representative admixtures will be introduced in relation with their utility. All the different admixtures types are described in the report ACI 212.3R-16 [62] and the normative the ASTM-C494 [63].

Water-reducing: The amount of water is a determining factor to obtain the adequate workability in the cement paste. Depending on the mixture composition, the

workability of the concrete can worse, and it might need some more water; however, the increase in the water/cement ratio can affect the durability of the concrete. For this reason, water-reducing products were developed. The addition of them to the mixture improves the workability of the cement paste without adding more water; they are commonly called superplasticizers. They are based on polymeric structures, the first ones appeared in the 1930s, and they were based on lignosulfonates, nowadays they are based on polycarboxylate ether, these being polycarbonate chains with an ionic extreme. The aim of this product is to work as dispersant avoiding segregation and improving the flow. The dosage needed is very low between 0.1 and 0.3% by weight of cement. The ASTM C494/C494M regulation names them as Type A.

Setting time-modifier: These compounds affect the setting time for different uses; they can be accelerators or retardants.

The retarding ones are used in very hot climate places where the cement starts the hydration very fast and loses its workability in a short time. For some applications, such as concrete roads, it is necessary to have longer times to apply the mixture properly. The compounds used as retardants are, generally, lignosulfonic acids and their salts, hydroxylated carboxylic acids and their salts, carbohydrate-based compounds such as sugars and inorganic salts[62].

The accelerating ones speed up the setting process and improve the resistance at shorter times. They are used for specific purposes, especially in cold places to reduce the risk of frost damage. It is also applied in precast structures to accelerate the setting process and remove the mold as soon as possible to produce a structure in shorter times. Precast structures are now very used in construction, and the optimization of the process can minimize the cost of construction. Traditionally calcium chloride is used . However, the chloride affects the steel structure and causes corrosion, so other compounds replaced it such as calcium nitrate, sodium nitrate, triethanol-amine, calcium formate, and thiocyanate[62]. Nowadays new compounds are being studied based on silicates such as finely divided silica gels, soluble quaternary ammonium silicates, and silica fume. They have an accelerating effect due to the decrease in the concentration of calcium and hydroxyl ions during the first minutes of the hydration process, and the promotion of the formation of the hydrated layer on the surface of the clinker [64][65][66][67][68]. During the last years, other accelerating compounds based on nano-calcium silicate hydrates[69][70][71] have been proposed; they act as seeds accelerating the hydration

process. This seeding effect means that some calcium silicate hydrate nuclei are introduced into the mix and promote the formation of the C-S-H gel[72][73][74]. The difference between these compounds and the previously mentioned (not nanometric ones) is that the hydration products are formed both on the surface of the clinker and also at the particles surface in the pore space of the cement paste. The small size of nanoparticles provides very large surface areas which improve the seeding effect. Also, they occupy the spaces that bigger particles cannot occupy, and the hydration products grown from those nuclei induce the early higher compression strength[74]. According to the ASTM C494/C494M Standard, these admixtures are classified as Type C. In this work the aim is to synthesize some new additions based on the nano-calcium silicate hydrates type to act as accelerator in the cement composites.

As it was mentioned in the previous section, the C-S-H gel has some structural similarities with tobermorite. Also, tobermorite is thought to be the cause of the durability of Roman cementitious structures. So, it was thought to employ nanoparticles of this compound as a seed in the hydration process to accelerate the setting during the first hours and obtain higher resistances during the beginning of the setting. Toguether with the tobermorite, a second calcium silicate hydrated seeding agent was proposed, the xonotlite. The main advantage of these two phases in comparison to other classical additions is its nature very similar to the C-S-H gel that would induce an autocatalytic effect in the hydration process.

G.Land et al.[74] in 2015 published an article introducing these accelerating agent in cementitious materials. However, they use natural products, and the particle size is not nanometric, so the effect was not very clear. They start from the hypothesis that low C/S ratio calcium silicate hydrate seeds have a stronger impact in the accelerating process [71] and for that reason, they center their study on tobermorite and xonotlite. The seeding effect of mineral tobermorite was studied following a calorimetric analysis to see the heat exchange difference. The result of the study is shown in Figure I.1-11a, the seeds added at 10% by weight acts as an accelerator in the system.

In Figure I.1-11b it is possible to observe the effect of mineral xonotlite when it is added as a seed to the cement paste. At high dosages (4 wt% and 10 wt%) the accelerating effect is clear.
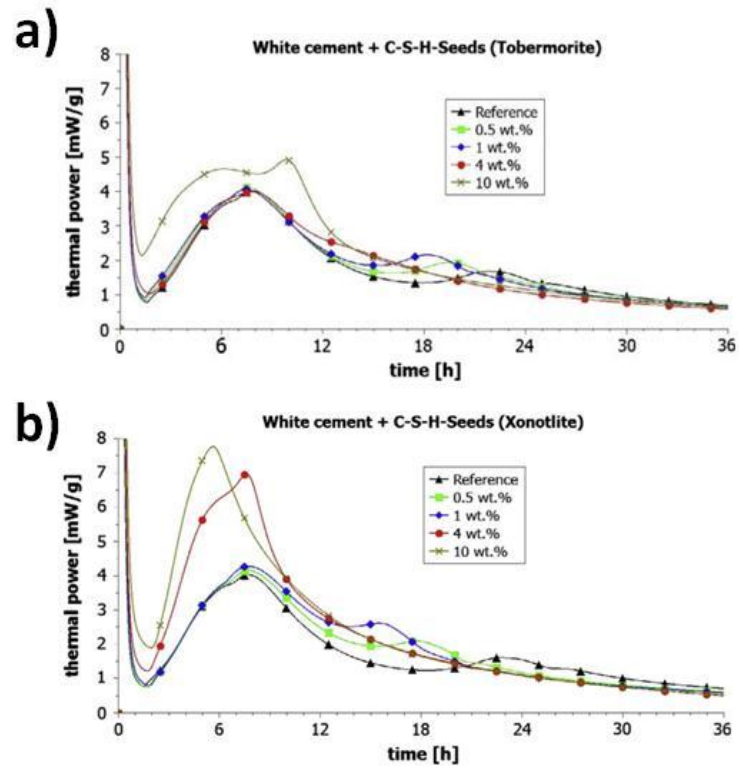
Figure I.1-11: Calorimetric analysis of the a) tobermorite and b) xonotlite as addition into cement paste [74]

In this work, we will synthetise both xonotlite and tobermorite, study carefully the physicochemical properties, and we will use them as a seed. The synthetic products are thought to have nanometric size and, therefore, better performance as a seed in cement paste in comparison with the mineral products used by G.Land et al.

I.2 Tobermorite and xonotlite

I.2.1 Tobermorite

Tobermorite receives its name from the location where it was first found in 1880, Tobermory (Scottland). The interest for this mineral emerged from the publication of the theory that said that the structure of the C-S-H gel could be related to the one of tobermorite[49][50]. From that point, the number of publications and the research around tobermorite increased (Figure I.2-1) as the interest from then was not only geological but also industrial because knowing that the structure of the C-S-H gel could be helpful to improve the mechanical properties of the cement matrix. Some studies have also explored the possibility of using natural ground tobermorite as seeding addition for cement composites [74] or as a stabilization agent for the capture of contaminants [75][76]. In this work, it will be studied a new point of view that is the use of synthetic tobermorite and xonotlite as seeding agents in cement pastes.
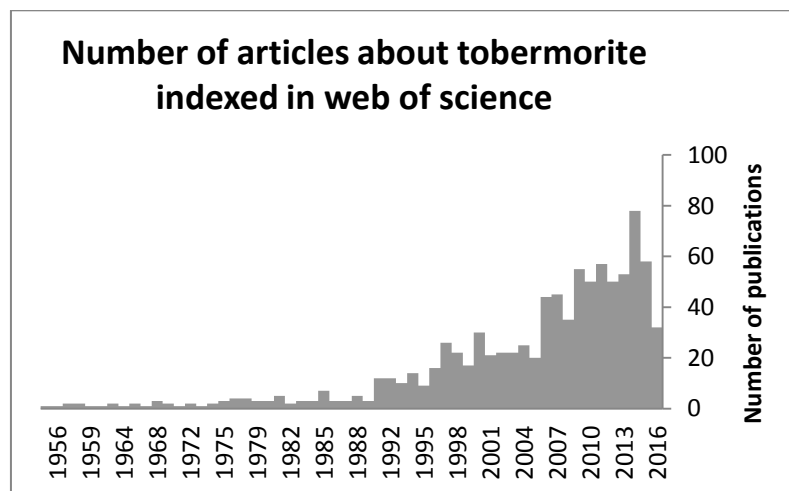
Figure I.2-1: *Illustration of the number of publications indexed in "web of science" related to tobermorite*

Tobermorite is considered as a rare mineral that in nature only crystallizes under hyper-alkaline hydrothermal conditions[77], normally in cavities at the contact of limestone and dolerite (one type of basaltic rock) or granodiorites (similar to granite) [78]. In fact, the difficulty of obtaining large and pure crystals is one of the main reasons why its structure has been a matter of debate for many years. Nevertheless, it is

generally accepted that calcium oxide forms layers perpendicular to the c-axis and flanked on both sides by chains of silicate tetrahedra [77][79]. Natural tobermorite crystallizes in the form of fibers or plates [80][81][82] with three different degrees of hydration. Depending on the amount of water, the basal distance between two consecutive layers of calcium oxide changes from 14Å to 11Å or 9Å giving place to the so-called 14Å tobermorite, 11Å tobermorite or 9Å tobermorite. The most common structure under ambient conditions is tobermorite 11Å, but the variety with more resemblances to the cementitious C-S-H gel is 14Å tobermorite [49][51]. Among the three polymorphs, there are also some differences in the structure, and they will be explained in the following paragraphs.

(a) Structure of tobermorite polymorphs

(1) *14Å tobermorite*

14Å tobermorite, commonly known as plombierite, is the most hydrated polymorph formulated as $Ca_5Si_6O_{16}(OH)_2 \cdot 7H_2O$. The structure of tobermorite is composed of complex layers, formed by sheets of sevenfold coordinated calcium cations, flanked on both sides by silicate chains with dreierketten distribution (Figure I.2-2). The space between two complex layers contains calcium cations and H_2O molecules. It has a monoclinic unit cell with space group B11b. In this polymorph the silicate chains belonging to adjacent layers are not condensed to form double chains (as we will see later that it happens in 11Å tobermorite), the layers are moved apart and locate in between some H_2O molecules. The single chains are shifted b/2 with respect to each other (b is the lattice parameter of the unit cell) [83]. 14Å tobermorite dehydrates and transforms into 11Å tobermorite after a heat treatment at 80-100 ºC.
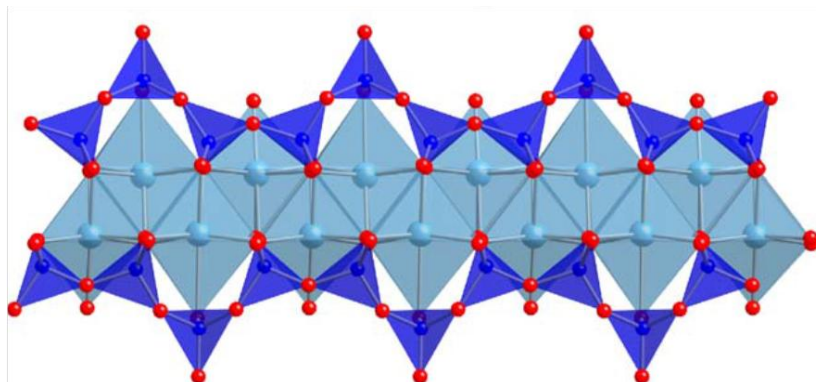
Figure I.2-2: Crystal structure of 14Å Tobermorite. Si atoms in dark blue, Ca atoms in light blue and O in red.

(2) *11Å tobermorite*

The structure of 11Å tobermorite is slightly more complex than the one of the 9Å tobermorite because there are two classes of this specy and the exact formulation is still not clear. Many authors describe the structure of this compound with different compositions. The two different polymorphs are normal and anomalous. The main difference between them is that while the normal form transforms into 9Å tobermorite upon heating at 300ºC, the anomalous one remains stable (in spite of the loss of water molecules) [80,84,85].

As aforementioned it is especially hard to elucidate the structure of this mineral as most specimens are poorly crystalline or microcrystalline with high structural disorder. The first group who studied the crystallography of this compound was McConnel (1954)[86] using a sample from Northern Ireland which they described as normal tobermorite. It was described as orthorhombic with a space group of C222. The preference growing direction is along the c axis which indicates that the mineral is built of perfect structural blocks perpendicular to c with structural defects in between them. This study attributed to the specimen two possible formulas: $Ca_5Si_6O_{17} \cdot 5H_2O$ or $Ca_5Si_6O_{16}(OH)_2 \cdot 4H_2O$.

Only two years later it was published a similar study by Megaw and Kelsey[87] using a specimen of the same origin. According to their description, the "pseudo-orthorhombic" structure is based on layers parallel to (001) built up by a central sheet of CaO. This sheet has in both sides' silicate chains with dreierketten arrangement. Those layers are stacked in a way that the ridges of each layer are precisely facing those of adjacent layers. The remaining Ca ion, and the water molecules are placed in the cavities between the ridges and some hydrogen atoms are attached to the silicate chains. The proposed formula for this model is $Ca_5Si_6O_{16}(OH)_2 \cdot 4H_2O$.

In 1981 Hamid[88] analyzed a sample from Germany (without specifying if it was normal or anomalous). He classified the structure in the Imm2 group. It was described as a continuous sheet of seven-coordinated calcium polyhedral with dreierketten silicon chains in both sides. These calcium sheets occupy two alternative positions displaced by b/2. In his work, he proposed two causes of the disorder in the structure; the bridging tetrahedral might take two different mirror orientations perpendicular to the a axis. Also, the calcium cations in the cavities between the layers present only half occupancy which

would be correlated with the orientation of the bridging tetrahedral. The proposed structure, in this case, was $Ca_{4.5}[Si_6O_{15}(OH)_3] \cdot 2H_2O$.

As there was not concordance with the structures previously proposed, Merlino et al.[89] did a deep study to elucidate the structure of 11Å tobermorite. They used a sample from Wessels (South Africa) which had extraordinary well-developed crystals and could make this work easier. The proposed structure did not differ that much with the previous ones, but the measure was more accurate and allowed to obtain what they call the "real" structure. They define the tobermorite as infinite layers of sevenfold-coordinated calcium polyhedra parallel to the direction (001). The characteristic that differs this conformation from the other tobermorite is at the apical sites of the pyramidal parts of the calcium polyhedral where OH⁻ anions and water molecules regularly alternate along the b axis (in the other ones they are oxygen atoms instead of hydroxyls). They agree with the basic structure of silicate chains in dreierketten conformation along the b direction link together to two successive calcium polyhedral layers. The symmetry of the structure could be classified as 2mm. Also, some wide channels were described along the b direction where three water molecules are hosted and sometimes also calcium ions. The proposed structure is the following one: $Ca_{4+x}Si_6O_{15+2x}(OH)_{2-2x} \cdot 5H_2O$ (x varies from 0 to 1).
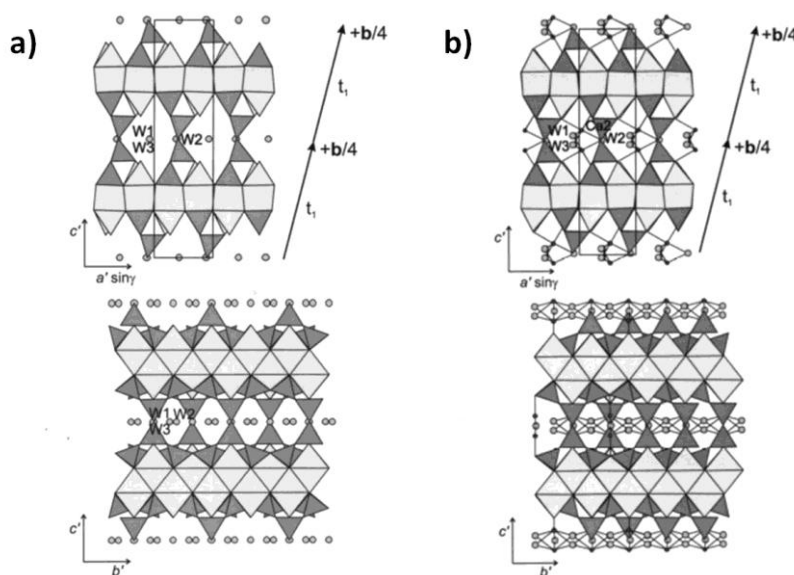
Figure I.2-3: *a) Crystal structure of the monoclinic polytype of the anomalous 11Å tobermorite and b) crystal structure of the monoclinic polytype of the normal 11Å tobermorite silicate chain in dark gray and CaO layers in light gray, dark dots are additional Ca cations, and the light gray dots represent the zeolitic water molecules*[78].

For the structural differences between the normal (Figure I.2-3b) and the anomalous tobermorite (Figure I.2-3a) some authors claim that: only in anomalous tobermorite silicon chains are attached to different calcium layers linked together by Si-O-Si bonds giving place to a rigid structure [85]. However, Merlino et al. [89][78] argue that such links exist in both cases, and the difference is solely due to the presence of zeolitic calcium ions tightly bonded to three water molecules in the normal variety which are lost in the dehydration process. During this step, there is a chain condensation that gives place to the 9Å tobermorite. The presence of such zeolitic calcium ions would also be bound to a small change in stoichiometry that, according to Merlino et al., varies from $Ca_{4.5}Si_6O_{16}OH \cdot 5H_2O$ in normal tobermorite to $Ca_4Si_6O_{15}(OH)_2 \cdot 5H_2O$ in the anomalous one [78]. Even though, the mechanism of the transformation during the dehydration is still not clear.
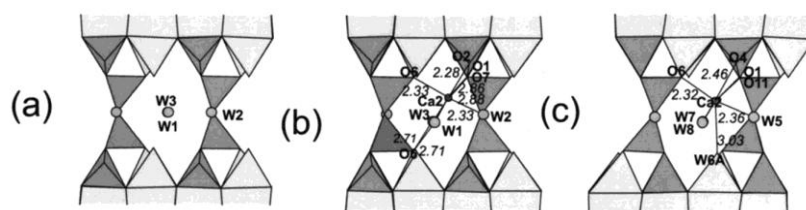
Figure I.2-4: Schematic drawing of the structural cavities, as seen along [010] in (a) anomalous tobermorite 11Å, (b) normal tobermorite 11Å and (c) clinotobermorite [78]

It has been proved the existence of a third polytype of 11Å Tobermorite which is called clinotobermorite[78,89] (Figure I.2-5). In this case, the structure and the zeolitic organization is very similar to the normal 11 Å tobermorite, with the difference that in normal 11Å tobermorite the zeolitic calcium occupation is just partial which is reflected in the different Ca/Si for each polytype (Figure I.2-4). Another difference is in the symmetry that in the clinotobermorite is C12/m1 with two possible unit cell configurations, monoclinic and triclinic, while the symmetry of the normal 11Å tobermorite is C2mm with a monoclinic unit cell. This phase also changes to 9Å tobermorite under dehydration conditions. The formula proposed for this type is $Ca_5Si_6O_{16}(OH)_2$.
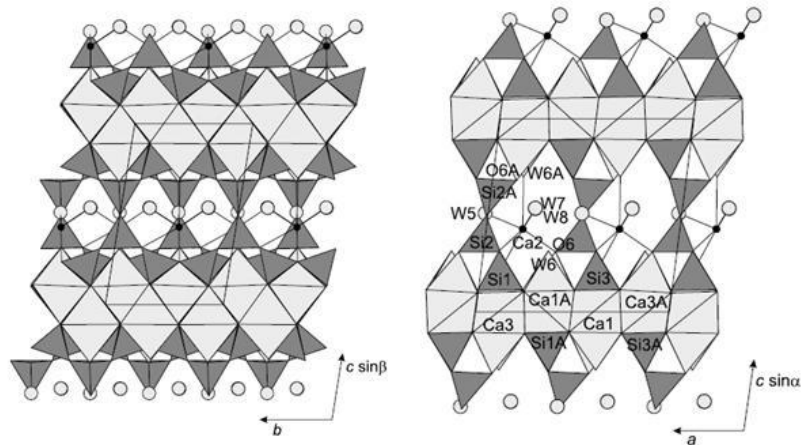
Figure I.2-5: Crystal structure of the triclinic polytype of clinotobermorite. Silicate chain in dark gray and CaO layers in light gray[89]

.

(3)   9 Å tobermorite

The 9Å tobermorite is obtained as a product of dehydration of clinotobermorite or normal 11Å tobermorite under a heating treatment at 300ºC obtaining 9Å clinotobermorite and riversideite, respectively. The typical structure[89,90] repeated in all the previously named conformations is also observed in this one (Figure I.2-6); the calcium layers parallel to (001) but in this case, they are closer to each other and connected through single chains of silicates with dreierketten conformation. Four of the five water molecules that are in the 11Å tobermorite disappear and the remaining one is in the form of hydroxyl (SiOH). The zeolitic channels are now narrower after the dehydration, and they only host Ca^{2+} in positions slightly displaced with occupancy 0.5. The structure is formulated as follows: $Ca_5Si_6O_{16}(OH)_2$.
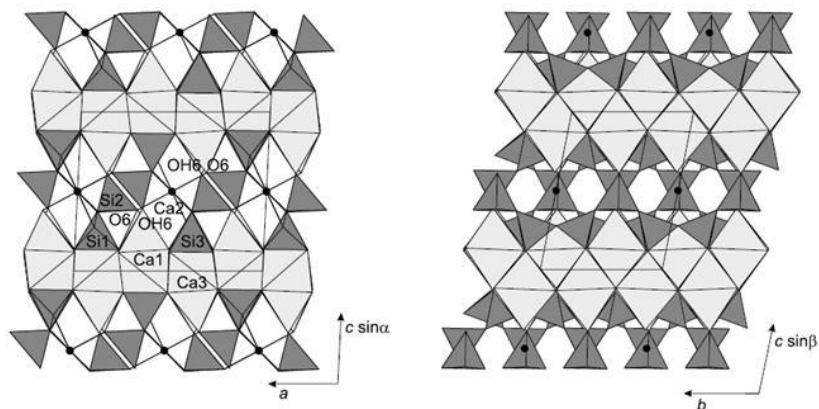
Figure I.2-6: Crystal structure of the triclinic polytype of 9Å tobermorite. Silicate chain in dark gray and CaO layers in light gray[89].

(4)   _X-substituted Tobermorite_

Tobermorite can present a partial substitution in its structure with aluminum and, on fewer occasions, with other elements like Fe, Mg, Na… It has been widely demonstrated the occurrence of this in natural formations where it is more common to find the Al-substituted one rather than the pure one[91]. However, it has also been produced in the laboratory. The degree of substitution and the structural changes when the Al is incorporated have also been very discussed in the literature, and it will be explained in the following paragraphs.

It is believed that aluminum provides tobermorite some stability versus the transformation into xonotlite under specific hydrothermal conditions[77,92–95].

Many authors have discussed the way that the Al enters into tobermorite's structure. In some silicate minerals with a layer structure, the Al^{3+} can assume tetrahedral coordination where it would enter as a substitution of the Si^{4+}, or assume a higher coordination and substitute the Ca^{2+} ions[96]. However in the case of tobermorite, it has been widely demonstrated that the aluminum occupies the position of the silicon. Diamond et al. [97] showed this with measurements by X-ray fluorescence spectroscopy. Kalousek[96] proposes the different possibilities of Al^{3+} entry into the crystal according to the principles of isomorphous substitution. The first one is the substitution of Al^{3+} + H^+ for one Si^{4+}, a second one is the substitution of $2Al^{3+}$ for Si^{4+} + Ca^{2+}, and the last one is the substitution of $4Al^{3+}$ for $3Si^{4+}$. This last one would imply special geometrical arrangements, and this is not the case. The first option is the most probable one but the second one can also happen punctually.

The position that the Al^{3+} cation takes in the chain has also been discussed by many authors. In general, most of them agree that the substitution of Al for Si does not occur in terminating positions of the chains; bridging and branching sites are the preferable ones[98]. In Figure I.2-7 are described all the possible positions for the Si and the Al according to the description of Wang et al.[99]
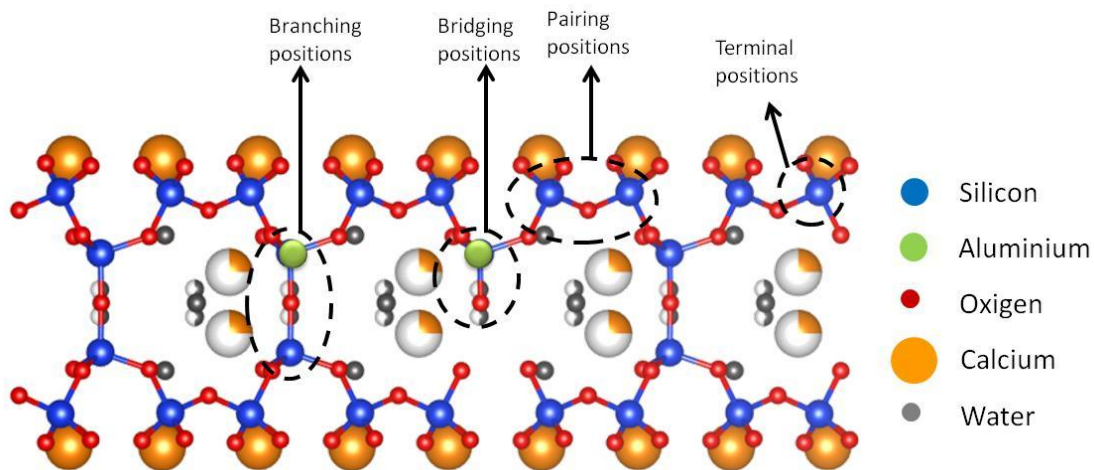
Figure I.2-7 Description of the Si and Al atoms in the tobermorite structure according to Wang et al [99] The spheres with one part in white represent the portion of the atom that belongs to another unit cell.

There are plenty of research works that have demonstrated, experimentally, the advantage of adding Al for the stabilization of tobermorite, and many of them highlight that the optimum Al/(Si+Al) molar ratio is 0.15 [77][93][95]. Above that ratio, some authors have demonstrated the formation of hydrogarnet as a secondary product[96][100].

Aluminum is not the only ion that can enter into the structure of tobermorite. Diamond et al.[101] also studied the effects of iron and magnesium, and Barnes et al. [100] the addition of sodium. The effect of sodium is relevant because it can give the tobermorite "ion-exchange" properties [102]. In the structure it would occupy the position of the H+ in the interlayer space and the Al-Na- tobermorite could have this formulation $Ca_5Na_{0.7\pm0.2}Al_{0.8\pm0.15}Si_{5.2\pm0.2}O_{16}(OH)_2\cdot4H_2O$ [100]. The calcium in the zeolitic spaces of Al-Na-tobermorite is very hydrated; this effect gives the tobermorite the exchanging properties, as the Cs^+ has more affinity for the Na^+ instead of Ca^{2+}[102]. Other alkalis can also be part of the structure such as K^+ and Rb^+ but the affinity is lower [104]. Selective Cs^+ exchange on such tobermorite may be useful in decontaminating circulation water in nuclear reactors and radioactive waste solutions [102]. The exchanged Cs^+ could be exchanged by Pb^{2+} and Cd^{2+} [103]. Al-Na-Tobermorite is known to have a partial or total exchange of structural Ca^{2+} for divalent ions such as Co^{2+}, Ni^{2+}[104], Cd^{2+} and Zn^{2+}[105]. Tobermorite could also be applied to clean waters which are polluted with heavy metals [106] and phosphates. In this case, the Ca^{2+} exchange promotes the formation of hydroxyapatite ($Ca_5(PO_4)_3(OH)$) coat over the tobermorite which would retain the phosphates and clean the water [75].

I.2.2   Xonotlite

Xonotlite is a monoclinic crystal which chemical formula is $Ca_6Si_6O_{17}(OH)_2$. The origin of the name is related to Xonotla (Mexico), the place where it was first discovered in 1866[107]. It is considered a rare mineral that only forms in nature under hyper-alkaline hydrothermal conditions [77]. Usually, it appears related to other minerals of the same family such as wollastonite, tobermorite and rosenhahnite. It is considered as a product of Ca-metasomatosis and it is found close to a contact of calcium bearing rocks with igneous rocks[108].

The basic structure of the xonotlite is described by Hejny et al. (2001)[108]. It is formed by dreierketten-like $[Si_3O_9]$ chains. As it has been previously explained, the dreierketten structure consists of repetitive structures of 2n-1 SiO_4 tetrahedral where two of them are paired together, and the third one is in bonding position with the consecutive chain through the apical oxygen of the tehtrahedra, forming what is known as "dreier-doppelkette" (Figure I.2-8a). The two chains are related to each other by a inversion center, a two-fold axis, and a mirror plane perpendicular to the two-fold axis. The symmetry is 2/m. There are two types of calciums as function of their coordination in the structure. One of them is sevenfold coordinated in a trigonal prism shape; six of the coordinated oxygens are in the apices of the prism and the seventh one in the middle of one of the faces (this is represented as B and B' in Figure I.2-8 b). The calcium with octahedral coordination is edge-sharing to form an infinite chain along the b-axis (represented as A in Figure I.2-8b). All the chains are joint together by the edge-sharing to form a layer (001) parallel to BAB' structure. The chains B and B' are related by a two-fold axis parallel to b and a mirror plane perpendicular to it. The OH group is located at the free apices of the calcium octahedral where no SiO_4 tetrahedra are bonded.
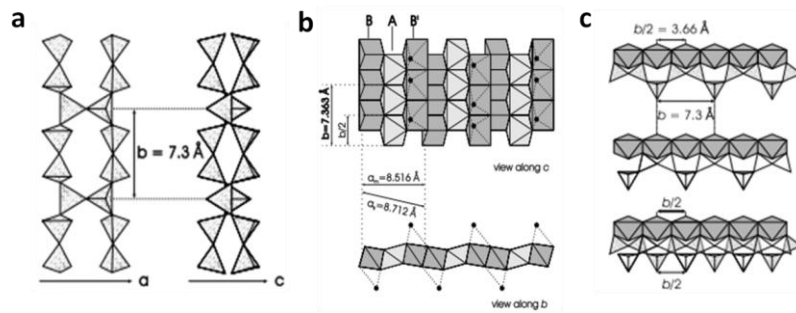
Figure I.2-8: a) Representation of the Silicon tetrahedral "dreier-doppelketten" structure in xonotlite, b) representation of the two coordination of the Calcium and their organization into the structure of xonotlite and c) representation of the two coordination possibilities for the dreier-doppelketten chains wich give place to the different xonotlite polytypes. [108]

The "dreier-doppelkette" has the same length as two calcium polyhedra; this gives place to two possibilities of attaching to the double chain of SiO_4 (Figure I.2-8c). This positional duality gives place to the various polytypes of xonotlite[108][109][110] with triclinic or monoclinic primary cell [109].

Xonotlite structure can suffer from some changes when some of the elements in the structure are changed for others with similar characteristics. The Si^{4+} can be substituted by Al^{3+} up to 5% [111][109]. The Ca^{2+} can be almost completely substituted by Co^{2+}, or Ni^{2+}[112] and partially by Mg^{2+}[113]. Natural xonotlite can also have some impurities from other elements such as Na^+, K^+, Mn^{2+} and Fe^{3+}[109].

It has been studied the use of xonotlite for several industrial applications, such as: friction extender in brake pads of automobiles[114], pigment in paper and dye industry, thixotropic agent in composites, flame retardant, drip suppressant in composites[108] and filler material to improve flexural strength of cement matrices[115][74]. It is also one of the compositions that are formed in well cement[116]. Also, some research works have explored the possibility of using xonotlite nanofibers as a precursor for the formation of wollastonite nanofibers for biological and orthopedic applications [117][118][119][120][121][122]. Nevertheless, a more recent work has proved the feasibility of using xonotlite nanofibers directly for those same orthopedic applications simplifying and reducing the cost of the synthesis process [123].

I.3   *Hydrothermal Synthesis*

I.3.1   Hydrothermal methods

The word hydrothermal makes reference to the reactions in aqueous media under high pressure and temperature conditions and closed systems [124]. This media is very suitable for the dissolution and recrystallization of insoluble materials under normal conditions.

Hydrothermal synthesis was born from the idea of mimicking natural geothermal reactions, which take place under extreme conditions of pressure and temperature in the sea volcanoes to form minerals. The first person who made reference to the term hydrothermal was the British geologist Roderick Murchison in the XIX century. With this idea, a large number of compounds have been synthesized under hydrothermal conditions.

To carry out the reactions in hydrothermal conditions two achievements were very important to develop the technology. The first one was the development of Morey's vessel; it consisted on an autoclave made of inert metal like silver, gold or platinum. It made possible to carry out the reactions under high pressures (up to 80 MPa)[125]. The second discovery was the Bridgeman seal for reactor vessels which allowed to increase the pressure up to 700 MPa [126].

This type of reactions were carried out for the first time by Schafhault in 1845 to produce quartz[127]. In the 19th century, it was developed the first industry based on the use of hydrothermal synthesis for the production of large single quartz crystals [128] and zeolites[129]. During world war II the hydrothermal method became very important for the production of extremely pure crystals with specific physical properties[130]. Also, the development of electronic industry demanded pure single crystal units which were only possible to obtain under hydrothermal conditions. After the discovery of this method, lots of rare minerals, which were expensive to buy due to their scarcity, have been able to be synthesized under hydrothermal condition. This technology has made possible the development of new applications of those compounds. Also, the possibility to obtain pure phases was very interesting for specific purposes. For instance, the sapphire is very expensive but the synthetic one is more affordable, and it is now commonly employed

in laboratories[131].

Traditionally the inorganic solids are prepared through a "solid-solid" reaction at high temperatures. At those high temperatures, one or more components are in the liquid state (melt), so it can be considered a solid-liquid reaction. Through this process, it is hard to identify the phases and the mechanism of the reaction. At room temperature solids do not react because they need high energy to reorganize their internal structures. At high temperatures, it is possible to break bonds, the atom migration and the restructuration of the structure[132]. This traditional synthesis method favors the formation of the most thermodynamically stable phases, for that reason, metastable new phases would be very difficult to obtain.

In the hydrothermal process, the reactions are carried out using water as a solvent at high temperatures and pressures (over 25ºC and 1atm), it is called solvothermal if the solvent is different from water, but we will only center on water as a solvent. The advantages of using water are several. The first one is that water is non-toxic, non-flammable, non-carcinogenic and non-mutagenic; so this is already a big advantage in comparison with most of the organic solvents employed for many syntheses.
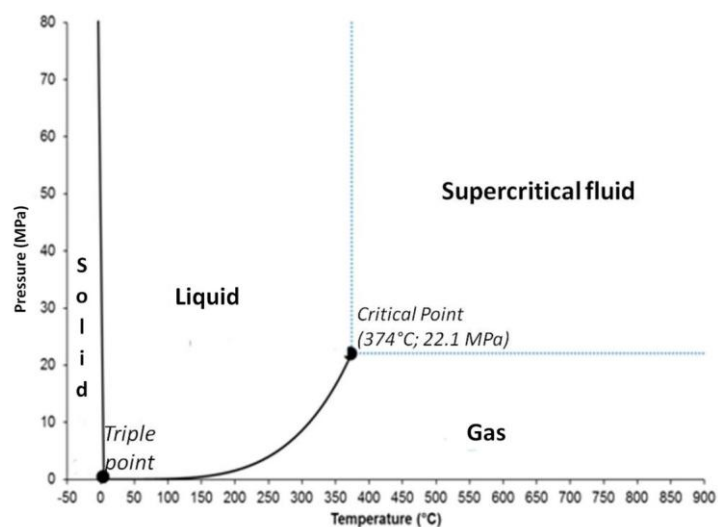
Figure I.3-1: Water phase diagram with the different states.

In these kind of reactions, the water is not only a solvent but also the medium that transfers the pressure so the physicochemical properties of water at high temperatures must be taken into account. These, for water, have been widely studied, and they are well known. Figure I.3-1 shows the water phase diagram. The hydrothermal reactions are carried out following the saturated steam curve. As it will be

explained in the next section, the reaction conditions change drastically in supercritical conditions (above 374ºC and 22.1 MPa). While heating the mixture in a closed vessel, the pressure reached is the autogenous one.

In subcritical conditions, some physicochemical changes are produced in the media. The ion product increases sharply with pressure and temperature; at very high PT conditions (15000-20000 MPa and 1000ºC) water is completely dissociated into H_3O^+ and OH- behaving like a molten salt and the density increases. Under these conditions, non-polar compounds are miscible[133]. The Figure I.3-2*a* shows the temperature-density diagram that allows calculating the density of each phase (liquid and gas) under each temperature and pressure conditions. It can be seen that as the temperature increases, more molecules are transferred from the liquid phase to the gaseous, so the density of the liquid phase decreases and the one of the gas phase increases up to the supercritical point where only one phase is present.

Under hydrothermal conditions the viscosity is lower; this fact facilitates the diffusivity in the media and therefore the reactivity [134][135]. One of the most important advantages of using hydrothermal methods is that the change in the density directly affects its solvation power and, therefore, its feasibility to react.

An important parameter to take into account during hydrothermal batch reactions is the initial vessel filling degree. Figure I.3-2b represents the effect of the vessel filling. When the vessel is initially filled less than 32%, at the critical temperature, the pressure is still not the critical one. Just a few degrees before arriving at the critical point, the saturation vapor line is passed, the superheated vapor is obtained, and the vessel is only filled with gas. At higher filling degrees, the water will expand to fill the autoclave at temperatures below the critical temperature. This process will result in a steep increase in the pressure inside the autoclave, due to differences in compressibility of gas and liquid. If the reactor is filled up to 80% or more, the critical pressure is reached before arriving at the supercritical temperature, but the only phase present is liquid. If the system keeps on heating, and the temperature is increased over the critical one, the system arrives at the supercritical state. So, if the objective of the synthesis is to achieve the supercritical state, the minimum volume of liquid in the reactor should be 32%.
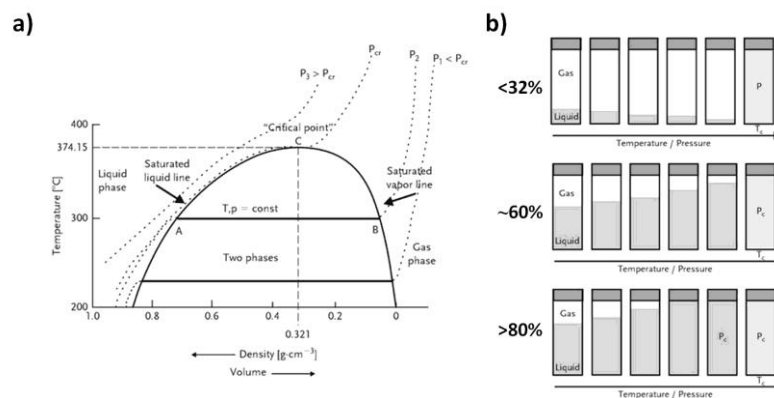
Figure I.3-2: a) Density change of the liquid and gas phase in a closed vessel as the temperature is increased. The dotted lines are lines of constant pressure. b) effect of the vessel filling over the pressure. [135]

I.3.2 Hydrothermal stability of the crystalline phases that compose the CaO-SiO$_2$-H$_2$O System

The CaO-SiO$_2$-H$_2$O system is very complex; it is composed of about thirty crystalline phases. The big ionic radius and the electropositive character of calcium allow many types of coordination with oxygen and therefore the formation of many different species[136]. Most of the phases can be formed in hydrothermal conditions. There are many parameters that control the formation of one species or another; some of the variables which control it are: the Ca/Si ratio, the temperature of the reaction and the time. The syntheses of the species that form this system are very complicated due to the high difficulty to obtain a pure single-phase compound with high crystallinity. Most of the studies are centered in the stability between the following species: tobermorite, xonotlite, Z-phase, gyrolite, and truscottite[137][138][77][139]. Figure I.3-3b represents how those phases are distributed in the phase diagram. However, this diagram is not very exact as it does not take in count other factors such as time and pressure. Another recent study made by S.Y. Hong et al.[140] (2004) proposed a phase diagram based on experimental results obtained from several hydrothermal reactions at different Ca/Si ratios (from 0.85 to 2.0) (Figure I.3-3b). In the third diagram (Figure I.3-3c) all the phases are represented, and under which temperature and pressure conditions they are stable[137].The stability curve that we are interested in for this work is the one that involves tobermorite and xonotlite (the V line in Figure I.3-3c). Many authors have discussed the conditions at which the tobermorite changes to xonotlite. However, so many parameters should be taken into account to identify this change properly, that no

information in literature arrives at a clear conclusion [141][142][92][77][138][137]. The lowest temperature at which the formation of xonotlite has been reported is 160ºC with a starting Ca/Si ratio of 1[143]. However, a well crystallized synthetic tobermorite showed signs of changing to xonotlite at 185ºC. So with this information, Harker et al.[137] considered that the xonotlite/tobermorite boundary region is at 170ºC ± 20ºC.
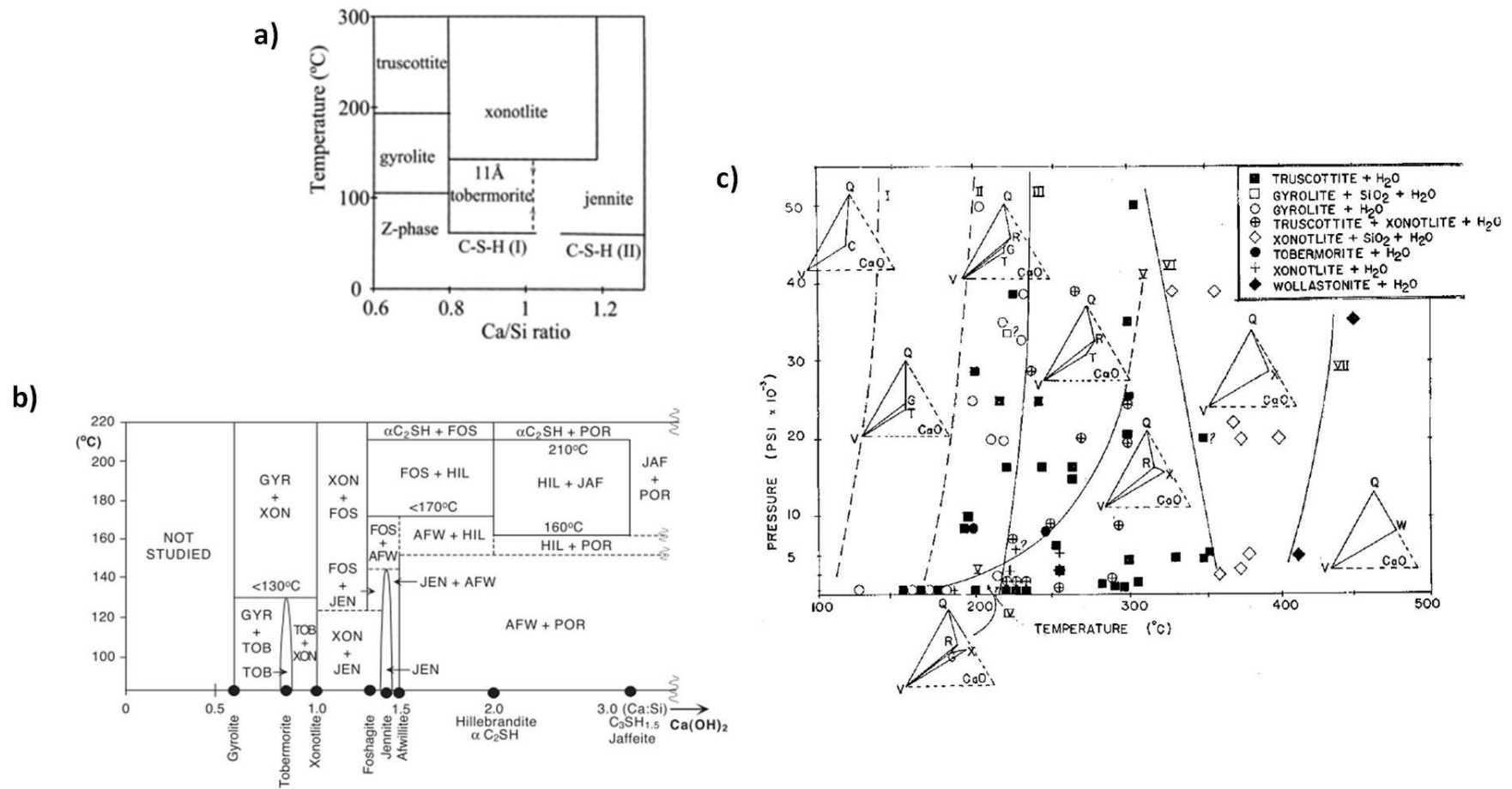
Figure I.3-3: *a) CaO-SiO₂–H₂O phase diagram from Ca/Si of 0.6 to 1.3 and range of temperatures from 0ºC to 300ºC*[77]*, b) phase diagram obtained from several hydrothermal experiments, the dashed lines indicate uncertainties* [140] *and c) Phase boundaries of the CaO-SiO₂–H₂O system components as function of temperature and pressure. Q=quartz, C = CSH(I), T = tobermorite, G = gyrolite, R =truscottite, X = xonotlite, W = wollastonite, and V = H₂O* [137]*.*

According to Buckner et al.[141] the thermal stability between tobermorite and xonotlite also depends on the Ca/Si; they claim that the tobermorite is more stable at ratio 0.8 rather than 1. In their work, they also describe the effect of high pressures in the tobermorite-xonotlite equilibria [141]. In Figure I.3-4*a* it can be observed that, at high pressures (up to 207 MPa), the phase change occurs at 280ºC. However, in these experiments, the kinetic factor time is not represented (not all the experiments lasted the same) and it is a key point to understand the equilibrium. This experiment would, nevertheless, demonstrate that, at higher pressures and temperatures, the tobermorite becomes more stable.
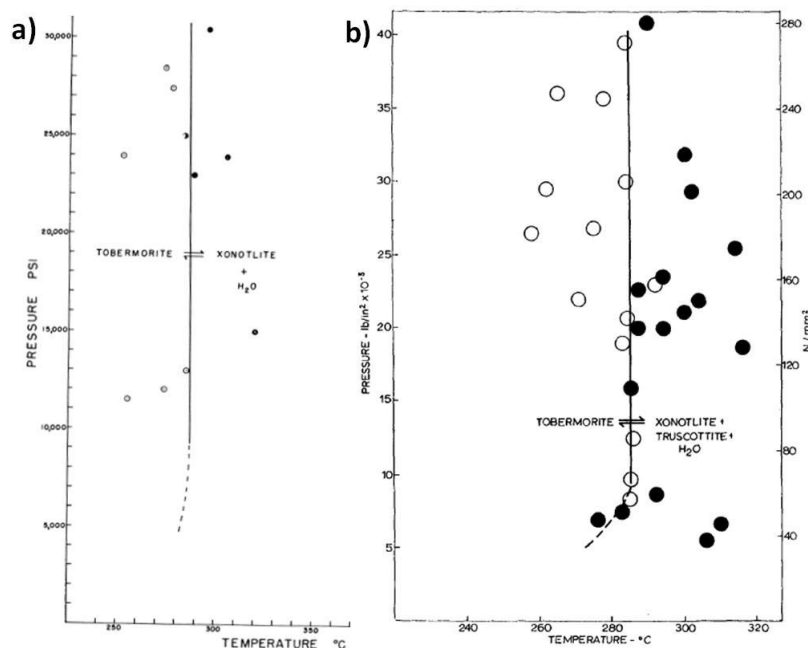
Figure I.3-4: Tobermorite - xonotlite phase boundary at high pressures[141] [144]

Speakman[144] carried out a very similar experiment. He concluded that tobermorite is formed in a very narrow temperature range; below 100°C only amorphous C-S-H is formed, and above 140°C xonotlite starts to form. So this author sets in this last temperature the equilibrium boundary between both phases. However in experiments carried out at high pressures (up to 275 MPa) he confirms that tobermorite becomes stable up to 285°C (Figure I.3-4*b*).

Shaw et al. [77] studied the effect of the atomic substitution of structural Si for Al in the mix to stabilize the tobermorite (Figure I.3-5). They proposed a mechanism for the formation of tobermorite as a result of a thorough kinetic study with *in-situ* synchrotron spectroscopy in the temperature range 235-310ºC. In a first step a disorder

C-S-H gel forms at room temperature, then CaO layers become ordered, and an increasing periodicity in the (0,0,l) direction is developed until tobermorite crystallizes. In this process, as mentioned above, temperature plays a very important role to avoid xonotlite formation. At high temperatures, the system is thermodynamically unstable.
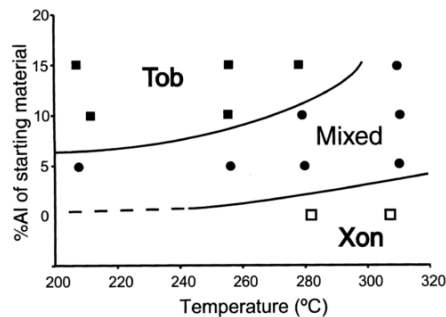
Figure I.3-5: *Phase diagram of tobermorite-xonotlite system, introducing %Al as a variable.*[77]

L.Black et al. [142] describe that the 11Å tobermorite has lower polymerization comparing with xonotlite because in the structure occurs a combination of single "dreienfachketten" silicate chains with the typical double chains. They propose that the stability of the double chains in tobermorite is not as high as in xonotlite and this leads to its instability at high temperatures.

As it has been shown, the C-S-H system is very complex, and also it is the tobermorite-xonotlite boundary. The high number of factors that can affect the system makes it very hard to study and to extract conclusions about which are the conditions where each species is stable.

(a)   Hydrothermal synthesis of xonotlite

The synthesis of xonotlite has also been widely reported in the literature. In the following paragraphs, it will be described the most important contributions while in the appendix I there is a list with a compilation of some xonotlite reactions reported in the literature.

E.P. Flint et al.[145] (1938) did a very wide study of the C-S-H system at different Ca/Si ratios, temperatures, pressures, and timings. They used silica gel and lime as precursors. For the case of xonotlite, it was produced from three different Ca/Si ratios: 0.8, 1 and 1.5. However, the one of 1.5 gives place to an unknown secondary phase. For the other two ratios, it was possible to obtain pure xonotlite within a range of

temperatures from 175°C to 390°C. The higher was the temperature, the shorter was the reaction time; the reaction took 79 days at 175°C while only four days at 390°C. This is the only work that reports the use of supercritical water to synthesize xonotlite. However, the process is not well described and the product is not properly characterized. After this experiment, there is no other publication which reports the formation of xonotlite in supercritical water.

K.Speakman [144] (1968) studied the stability of the tobermorite-xonotlite system; he did a broad number of syntheses at different Ca/Si ratios, temperatures and pressures. He demonstrated the stability of xonotlite at high pressures within a wide range of temperatures.

The most common precursors employed for the synthesis are SiO_2 (crystalline or amorphous) and CaO [145][144][139][115][146][142][147][140][148][82][149][150]. However, other authors studied the possibility to use other precursors such as $Na_2SiO_3 \cdot 9H_2O$ as silicon source[151][152] and $Ca(NO_3)_2 \cdot 4H_2O$[151] or carbide slag[153] as a calcium source. W. Tan et al.[152] added Na_3AlO_3 to the reaction, although it is not demonstrated the stabilizing effect of the Aluminum in xonotlite as it is in tobermorite. They claim that the addition of this compound can reduce the reaction time from eight hours to just one, having as a result, the same high crystalline product.

Although most of the reactions are carried out under classical hydrothermal conditions, some authors have studied other routes. X. Li et al.[123] employed a microemulsion (using TEOS, CTAB, $Ca(NO_3)_2 \cdot 4H_2O$ and NaOH as precursors) for the formation of xonotlite, and they obtained well-crystallized xonotlite after 30 hours of synthesis. L. Black et al. [142] introduced a milling step before the hydrothermal treatment, however, the effect of this step is not clear.

(b) Hydrothermal synthesis of tobermorite

In this section we will summarize the hydrothermal synthesis of 11Å tobermorite because in literature there is no information about the synthesis of 14Å tobermorite, which has only been found in nature, or about the synthesis of 9Å tobermorite wich is obtained through a dehydration thermal treatment to 11Å tobermorite but it is not produced hydrothermaly. In this case, the reaction conditions are more controverted than in the case of xonotlite. As mentioned before, xonotlite's stability is higher, and it

is easier to get xonotlite in a more or less wide range of temperatures than for tobermorite.

During the last decades, many research groups have focused their attention into 11Å tobermorite, and they have proposed a wide variety of routes to synthesize it. Most of them intend to obtain highly crystalline 11Å tobermorite, understand the xonotlite-tobermorite phase boundary and/or study the effect of the substitution of Si in the silicate chains for Al in the structure. As it can be observed in appendix II, the variability of the conditions to obtain 11Å tobermorite under hydrothermal conditions is very big, and there are not clear conclusions about the optimal conditions to synthesize 11Å tobermorite.

Many authors have studied how different parameters affect the kinetic of the reaction. These parameters are reaction time, Ca/Si ratio, temperature, pH, precursors and partial substitution of aluminum for silicon. Some research works have also investigated the effect of some different precursors on the synthesis of 11Å tobermorite such as EDTA [154], Borosilicate [155], sucrose [156] or Ca-formate [157]. Most of them used CaO and SiO_2 as precursors, but other products like calcsilicate alkoxide gel [77] or $Ca(NO_3)_2$ and Na_2SiO_3 [158] have also been used. It has also been studied the synthesis using as precursors, industry waste products such as oil shale ash[159], cement kiln dust[160], soda-lime-silica container glass[105] and paper recycling residues[161]. In some cases, a milling step of the precursors was included before the hydrothermal treatment [162][142]. Reaction times vary from some hours to months, with synthesis temperature rarely exceeding 200ºC. It has been found that some of the works are contradictory among them; for example, K. Speakman[144] employs 196 days to synthesize tobermorite from CaO and quartz (Ca/Si=0.8) at 140ºC without the addition of Al while S. Hamid et al.[139] need only 60 hours to obtain the 11Å tobermorite in the same reaction conditions and, apparently, same precursors. Some works from the literature will be explained in more detail in the next paragraphs.

E.P Flint et al. [145] in 1938 was the first one to report the synthesis of 11Å tobermorite. He did three syntheses using CaO and SiO_2 with a ratio of 0.8 at three temperatures 150°C, 225°C and 250°C obtaining 11Å tobermorite after 42, 14 and 7 days, respectively. He demonstrated that a higher temperature but shorter reaction times could give place to the same product.

G. Kalousek et al.[96] (1957) did a deep study about 11Å tobermorite formation with the aim of understanding the stable conditions for the formation of the pure product. As a first variable, he modified the Ca/(Si + Al) ratio. He did a first set of experiments of ratio 0.80 where he modified the Al content. For these syntheses, he kept a reaction time of 24h and a temperature of 175°C. They concluded that with low quantities of Al (0.4%), they could obtain 11Å tobermorite. With the addition of a higher amount of Al (12%) the major part of the product was 11Å tobermorite (95%), but it also formed a small quantity of katoite (C_3ASH_4). The more Al was added, the more C_3ASH_4 was produced. In the second set of experiments, he used a Ca/(Si + Al) ratio of 1 and variable quantities of Al. In this occasion, he sets a temperature of 170°C and a reaction time of 72h. The Al content varied from 0.45% to 50%, and in every case, he obtained 11Å tobermorite mixed with hydrogarnet ($Ca_3Al_2(SiO_4)_{3-x}(OH)_{4x}$). He did one last reaction in different conditions, Ca/Si + Al ratio of 1, 0.45% Al, 170°C and 15h, on this occasion he obtained pure tobermorite. With this experiment, he demonstrated that the Al stabilizes the formation of 11Å tobermorite, but with a limit, ~12%, above that limit secondary phases are formed.

A similar experiment was carried out by T. Mitsuda et al. (1975)[95]. In this occasion, he introduced a new variable, the silica source. He employed three different precursors: colloidal SiO_2, aluminosilicic gel and clinoptilolite ($Ca_3(Si_{30}Al_6)O_{72}·20H_2O$). For every compound, he tried two different Ca/(Si+Al) ratio: 0.8 and 1. For each ratio, the %Al was also studied carrying out the experiments at three composition ratios 0%, 5%, 10% and 15% at two different temperatures each, 90°C and 120°C. These experiments highlighted that the addition of aluminum in low quantities stabilizes the tobermorite formation. Also, the formation of the desired phase is more favorable when the Ca/(Si+Al) ratio is 0.8 rather than 1. The use of higher temperatures promotes a faster crystallization of tobermorite. Among the three siliceous sources, apparently, the use of aluminosilicic gel gives place to better results, but this fact is not completely clear. H. Sato et al. (1992) also studied the effect of the silica source in the reaction. He used as reaction conditions Ca/(Si+Al) ratio: 0.8, 120°C, water/solid=5 and variable times. He checked the efficiency of three precursors: quartz, silicic acid, and colloidal silica fume. For the quartz, he needed only 4 hours of reaction to get high crystalline tobermorite, for the other two precursors it was needed longer reaction times,

8 and 24 hours, respectively, and nonetheless, the crystallinity degree is not as high as the one obtained using quartz as a precursor.

El-Hemaly et al.[92] carried out a deep study on the formation of anomalous and normal tobermorite. Despite they did not arrive to clear conclusions about which are the conditions that determine the formation of one type or another they did an exhaustive work about the synthesis of tobermorite in general. They used a wide combination of precursors to study the system. As silicon precursors they employed: quartz (10-20 μm), colloidal silica, quartz (<10μm), silica by-product and cristobalite. They also tested the effect of the addition of alumina and alkali products. The temperatures range employed were 120-180°C and the reaction time ranged from 2 hours to 14 days. The synthesis conditions are very variable, and every case is described in appendix II.

As it was previously mentioned, tobermorite can be found in two different morphologies, as platelets, and as fibers. Most of the hydrothermal reactions in literature obtain as result platy tobermorite, but some modifications in the synthetic route can give fibers as well. X. Huang et al.[163][154] proposed the use of EDTA to obtain fibers at pH 13, at lower pH instead, they obtain platelets. K. Lin et al.[158] employed a microemulsion method to obtain fibers; the addition of CTAB to the mixture could work as a template to form the fibers.

Most of the reactions in literature have been carried out under hydrothermal conditions, but some other methods have also been studied. L. Black et al.[142] and D. Palubinskaite et al.[162] added a milling step to the synthesis previous to the hydrothermal process; they wanted to demonstrate that the decreasing of the particle size through this step could cause an increase in the process rate because of the improvement of the diffusion and the reactive surface. However, the effect of this process was not as big as expected. As a second method S. Tränke et al.[164] proposed the use of microwaves to assist the hydrothermal method. However, the results demonstrated that the obtained tobermorite had lower quality than the particles obtained through traditional hydrothermal method.

This summary highlights the current knowledge about the synthesis processes of tobermorite, the kinetics of the reaction and the stability of the product. In this work, we will study new reaction conditions that had never been studied before, the formation of tobermorite in supercritical water.

I.3.3   Synthesis in Supercritical Water

In this thesis will be intrudece a new synthesis route for xonotlite and tobermorite using supercritical water. A supercritical fluid is the domain of the matter over its critical point for pressure and temperature, and below the pressure required to condense into a liquid[165].

(a)   History of supercritical state

Supercritical phase was first discovered in 1822 by the French scientist Baron Cagniard de la Tour[166]. He was doing experiments about acoustics when he introduced a flint ball in a digester, half filled with a liquid. Upon rolling the device, a splashing sound appeared when the ball was placed in the liquid-gas interphase; while heating the closed system the sound continued up to a point where it disappeared, that point was the supercritical point, where the two phases disappeared, and the sound is not transmitted. After this first observation, he continued doing experiments with alcohol [167], observing that the liquid increased twice its volume upon heating up to a point where suddenly disappear the two phases and a kind of homogeneous vapor appeared. When decreasing the temperature, he observed that at the critical point was produced a kind of thick opaque cloud and then, again, the two phases appeared. In an ulterior article, he studied the critical point with water, alcohol, ether and carbon bisulphide[168]. He estimated the supercritical temperature for water at 362ºC which is not so different from the real one 374ºC.

At that time the rest of the scientists did not assume that point as the generic state of the matter but only a specific phenomenon for those compounds. Some known scientists made reference to this discovery, Faraday in 1844 [169] called it ”Cagniard de la Tour's state,” and Dimitri Mendeleev in 1861[170] referred to it as "absolute boiling point." Only in 1869 was coined the term that we know nowadays, the supercritical state; the one who did it was Thomas Andrew when he published a paper[171] related to the pressure-volume curve of the liquid-vapor coexistence line of carbonic acid.

Afterward, this new knowledge started to be applied for different uses[172]. The first researchers to describe the solvation power of the supercritical state were Hanay and Hogarth in 1879[173]. They did some experiments with metal chlorides in supercritical ethanol, and they discovered that the concentration of the metal chlorides

in the supercritical state was much higher than in the vapor phase and when they decreased the pressure they precipitated "like snowflakes." Although some works about extraction in supercritical fluids had been done during the first half of the XXth century, the highest impact discovered was made in 1970 by Zosel [174]. He patented the process to extract caffeine from coffee using supercritical CO_2. This process was very revolutionary, and still nowadays it is employed by coffee industry.

Supercritical hydrothermal synthesis is now developed from the beginning of the 90's [175][176]. Supercritical water exhibits specific properties favoring high kinetics and burst nucleation for inorganic material formation [177]. These unique properties have been used to produce many oxides, metals and sulfides with desired sizes [178] and morphologies (preferred growth in particular directions, particle size, etc.) and/or control the degree of crystallinity [176,178–184]. The success of the synthesis under supercritical conditions is based not only on the special properties of the compounds in supercritical conditions but also on the feasibility to adapt the technology to specific reaction conditions.

(b)   Physical and thermodynamic properties

The thermodynamic and transport properties of supercritical water are very different from those of water at room temperature[124] (*Table I*.3-1). It is usually described as a media which shares properties from both liquid and gas phases. As it was previously mentioned, once the saturated steam curve arrives at the critical point, the two phases transform into a unique one, the supercritical phase. The critical point of water is at 374ºC and 22.1 MPa. Under that point there are strong hydrogen bonds between water molecules. Under supercritical conditions, the order of hydrogen bond is reduced, and the physical properties change drastically.

The polarity of the water decreases, and also does the dielectric constant, due to the disruption of the hydrogen-bond network. This effect together with the density fluctuation can explain that at high pressure (and high density) substances with ionic bonds are dissolved while at low pressures (and low densities) non-polar organic compounds dissolve[185]. The viscosity also drops, related to the decrease of the polarity, and therefore the molecular mobility increases[124].

Table I.3-1 Physico-chemical properties of water as function of pressure and temperature [185]

	"normal" water	Subcritical water	Supercritical water		Superheated steam
T [ºC]	25	250	400	400	400
P[MPa]	0.1	5	25	50	0.1
ρ[gcm^{-1}]	0.997	0.80	0.17	0.58	0.0003
ε	78.5	27.1	5.9	10.5	1
pK$_W$	14.0	11.2	19.4	11.9	-
C$_P$[kJKg^{-1}K^{-1}]	4.22	4.26	13	6.8	2.1
η[mPas]	0.89	0.11	0.03	0.07	0.02
λ[mWm^{-1}K^{-1}]	608	620	160	438	55

The diffusivity in supercritical water is very high[186], this improves the transport properties because supercritical water behaves as dense as liquids and as fluid as gas. The surface tension is very low which facilitates the permeability into other materials. All these properties make the supercritical water very suitable for some applications such as the extraction processes.

Some other properties, like the heat capacity at constant pressure or the speed of sound, have opposite extreme behaviors, the first one approaches infinity under supercritical conditions while the second approaches to zero[187].

I.4   Conclusions

In this chapter, it has been done a wide introduction to the main topics concerning this thesis. First, it has been presented the importance of the cement through the history and in the present, and it was introduced some estimations about the evolution of the use of this material in the future. Also, it was introduced the concern about the CO_2 emissions derived from the production of cement and how is that problem being solved in the present and the proposals for the future. To know better about this material it has been introduced the production process of the cement and the reactions that occur when it is hydrated, and the cement paste is formed. It was also introduced the admixtures that exist nowadays to modify the hydration process.

In the second part of the chapter, it was highlighted the role of the tobermorite in the cementitious world. Many important authors described the similarities between the structure of the tobermorite and the C-S-H gel; despite not being the same thing because the C-S-H phase is an amorphous phase and the tobermorite a well crystalline one. Xonotlite was also selected for the synthesis due to its composition and for being in thermodynamic equilibria with tobermorite under some hydrothermal conditions. For these reasons, they were proposed as seeding agents in cement pastes. Previous to the synthesis of both materials it was done a deep bibliographic study to accurately describe the structures and polytypes of both tobermorite and xonotlite. They are complex structures, and in some aspects, they are still not completely known, and this work pretends to throw some light to this. For example in the case of tobermorite, the structural differences between the anomalous 11Å tobermorite and the normal one are still not clear. It is also unknown the reason why one or the other is formed.

In the third part of the chapter is summarized the knowledge about the hydrothermal synthesis of tobermorite and xonotlite up to the date. After a deep study and a thorough compilation of synthesis under a broad range of conditions, no clear synthesis route of tobermorite was found. The metastable behavior under certain conditions made it very hard to find the optimal synthesis route avoiding the production of xonotlite as a secondary product. As a consequence of the messy compilation of information in the literature, it was highlighted the necessity to find some key points to understand the tobermorite-xonotlite system. Therefore, it was proposed this new

synthetic route based on supercritical water. No calcium silicate had been synthesized up to now under supercritical conditions. As there is a high controversy about the formation of tobermorite and its equilibria with xonotlite, it was decided to study the synthesis under supercritical conditions. The peculiarities of this phase were described in the last part of this chapter. As it has been mentioned, the physicochemical properties of supercritical water are very interesting for the synthesis of materials as many parameters are controlled, and it is possible to make reactions in very short times.

CHAPTER II: EXPERIMENTAL TECHNIQUES

II.1   SYNTHESIS REACTORS

II.2   CEMENT PASTE PREPARATION INSTRUMENTAL

II.3   CHARACTERIZATION TECHNIQUES

II.1   Synthesis reactors

II.1.1   Subcritical hydrothermal batch reactor

A batch reactor is a hermetically closed vessel where reactions can be carried out at high temperatures and autogenous pressures. It is normally composed of a tank with an agitator and integral heating/cooling system. In this system, the product is only recovered when the reaction has finished, and the tank is open or discharged from the bottom. This reactor was used in Tecnalia

The batch reactions were carried out in a Büchi Glass Uster (Figure II.1-1) composed of:

- Two-liter stainless steel reaction vessel "limbo 350ls" with hermetic nut-closing. The temperature and pressure limits are 350ºC and 35 MPa. For an effective hermetic closing, there is a silver o-ring in the closing system. The vessel is thermostated externally by a coil jacket and controlled with the "tc450" system,

- Magnetic stirrer system "cyclone 075 magnetic drive" with an agitator blade up to 3000 rpm,

- Piezoresistive Transmitter Pressure sensor "Keller PA-21-400" connected to an electronic pressure display "bds.sc.",

- A jacket cooling system controlled by a refrigerating system "MTA, TAE-evo".

Figure II.1-1: Subcritical hydrothermal batch reactor.

II.1.2   Supercritical continuous reactor

The continuous supercritical units are, generally, home-made units ensemble together following a classic general scheme composed of one, two or more pumps, a mixing fitting tool, a reactor made of tubing, a heating system + temperature controller, a quenching bath, a filter and a back pressure regulator to control the pressure. This reactor was developed at the ICMCB.
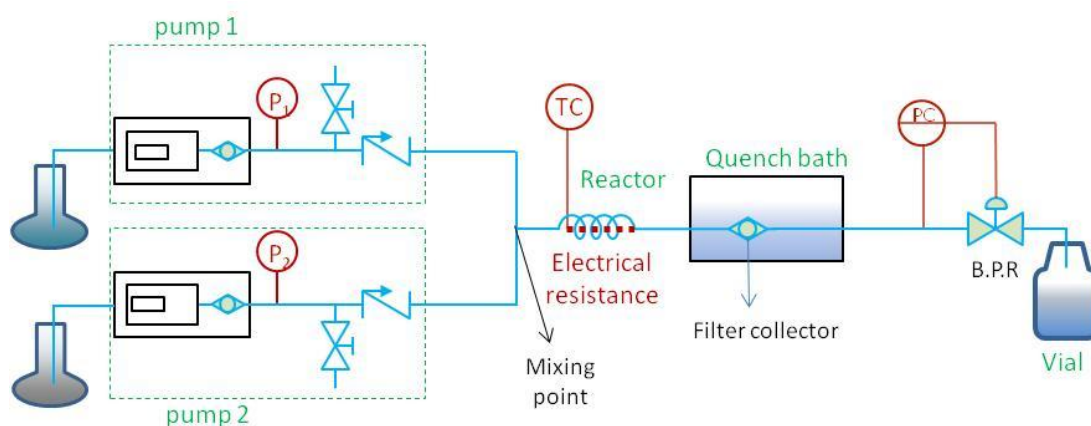
Figure II.1-2: General scheme of a supercritical continuous reactor. P: pressure transducer, TC: temperature controller, PC: pressure controller and B.P.R: back pressure regulator.

The supercritical continuous reactor is composed of:

- **Pump:** The model used for the experiments was a PU-2080 Isocratic HPLC Pump (Figure II.1-3a), it has a flow rate precision over the flow rate range of 1 μL to 10 mL per minute. The flow is pulse free, so it is constant during the reaction. In our system two pumps were used, one for each precursor. The pressure limit is 50 MPa for a flow less than 5ml/min and 35 MPa for a flow higher than 5 ml/min.

- **Tubing /reactor:** To process supercritical water all the tubing has to be made of Inconel 625 alloy. The sizes used at lab scale are usually 1/32", 1/16", 1/8" and 1/4" of diameter (Figure II.1-3b). The tube fittings have to be adapted to high pressures. The length of the reactor is chosen in accordance with the maximum and minimum flow of the pump and to reach a wide range of residence times just varying the flow.

- **Mixing point:**The precursors are introduced into the system through two different pumps, and the mixing should ideally take place close to the reactor entrance. The tools used for a coflow mixing (one flow from the outer tube and a second flow from the inner tube) are like the ones in Figure II.1-3c.

- **Heating system:** The reactor is thermostatted with a Eurotherm with a power of 1000W to control the temperature at every moment of the reaction. Depending on the set-up and the reactor the heating system can be different; in our experiments, it has been used three types (Figure II.1-3d). The cartridge is used with 1/16" reactors, the ceramic band heater is used with the 1/8" reactors and the wire with the 1/4" reactors. In the first case, the reactor is rolled around the cartridge and then protected with a metallic tube and glass wool to insulate. In the second case, the reactor is rolled around a metallic tube filled with glass wool and placed inside the ceramic band heater. In the last case, the wire is rolled around the reactor and protected with glass wool.

- **Filter collector:** A stainless steel fritted filter with 50μm porous size, is used to collect the particles as they were flowing out of the reactor; the fritter was inside a vessel with an input and output (Figure II.1-3e). The filter is kept inside a cold bath to cool down the outer flow of the reactor.

- **Back pressure regulator:** To control the pressure of the system is used a Tescom back pressure regulator. As it is explained in the diagram of Figure

II.1-3f, the valve is regulated by a needle adjusting with a polymeric piece. The closing of the valve compresses the two pieces and exerts a pressure in the system as the water is flowing. The pressure is measured by the pump that allows a pressure up to 50 MPa (depending on the flow).
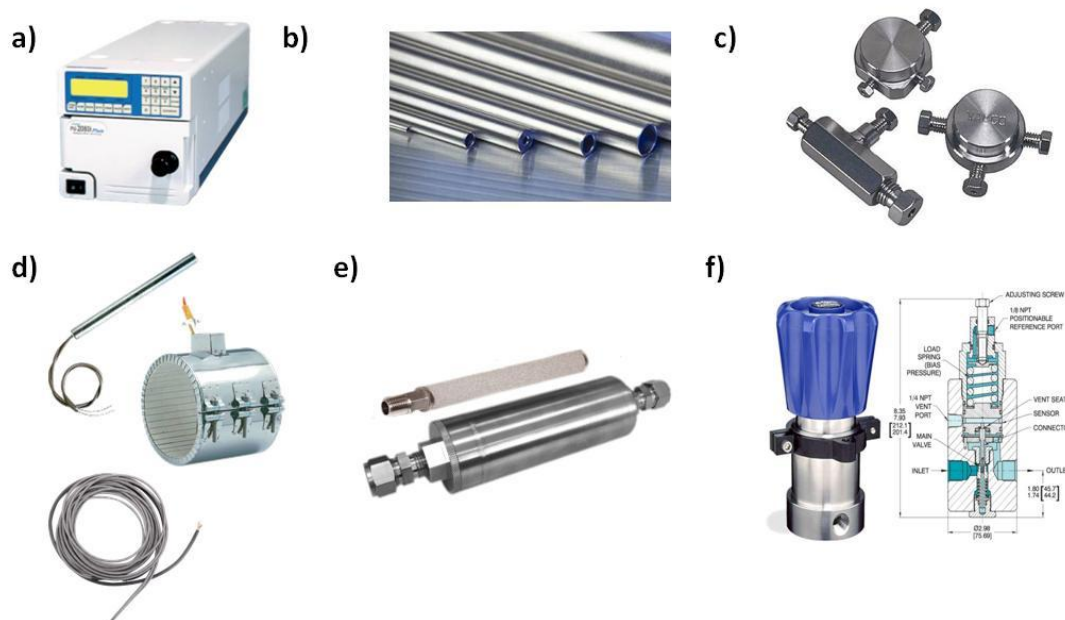
Figure II.1-3 Components of the supercritical hydrothermal continuous reactor. a) PU-2080 Isocratic HPLC Pump, b) different size Inconel tubes, c) co-flow tee fitting tools, d) heating systems: cartridge, ceramic band and wire, e) stainless steel fritted filter and its vessel and f) Tescom back pressure regulator.

II.1.3   Supercritical batch reactor

The supercritical batch reactor is a multifunctional Sparex design (Figure II.1-4). It has three configurations for different uses: continuous for CO_2, semi-batch oxidation reactions with supercritical water and batch for supercritical water reactions.   The experiments with this reactor were carried out in Tecnalia. The whole system configuration is composed by

- Two HPLC pumps. The first one is a Separex CO_2 piston pump with a flow rate range from 5 to 50 g/min and pressure limit of 1000 bar. The second one is a co-solvent pump "SSI, prep 36" with a flow rate range from 0 to 36 mL/min and pressure limit of 40 MPa,
- Two preheating units with heating range from 20 to 600ºC,
- One liter Inconel vessel with an electrically heated jacket. The vessel has a hermetic closing system composed of a hand tight screw type lid with

conical metallic sealing. The temperature and pressure limits are 600ºC and 35 MPa. It has an Inconel "basket" with a 2µm filter in the bottom,

- An Euroterm system for heating, controlling and also data logging. It memorizes all the data during the experiments (temperature, pressure and agitation speed) and it is possible to export those data in a USB key,

- Dynamic magnetic coupling mixer with a rotation speed range of 0-2000 rpm,

- Tescom back pressure regulator

Figure II.1-4: Supercritical batch reactor scheme.

For the batch configuration, only the vessel with the mixer and the heating system is employed. When the reaction is finished, it has to be cooled down before removing the pressure for security reasons. As the equipment doesn't have a quenching system, the reaction time is harder to control. The equipment is in high temperature for some hours until it is cooled down (as it doesn't have external help).

II.2 Cement paste preparation tools

- **Ultrasonic dispersion system:** The sonication system employed was a Bandelin HD 2070 with a Sonopuls MS73 microtip (Figure I.2-2a).

- **Cement paste mixer:** To mix the cement paste, it was used a Heidolph™ Electronic Electronic Overhead Stirrer - RZR 2102 Control Z with a stirring rod (Figure I.2-2b).

- **Moulds:** The cement samples were molded in a hexa-mold in stain steel. The dimension or each sample is 1x1x5 cm. These were tailor-made for this purpose (Figure I.2-2c).

- **Cement compacting machine:** To compact and remove the bubbles trapped in the cement paste samples, a compactor machine was used. This machine gives one bump per second (Figure I.2-2d).
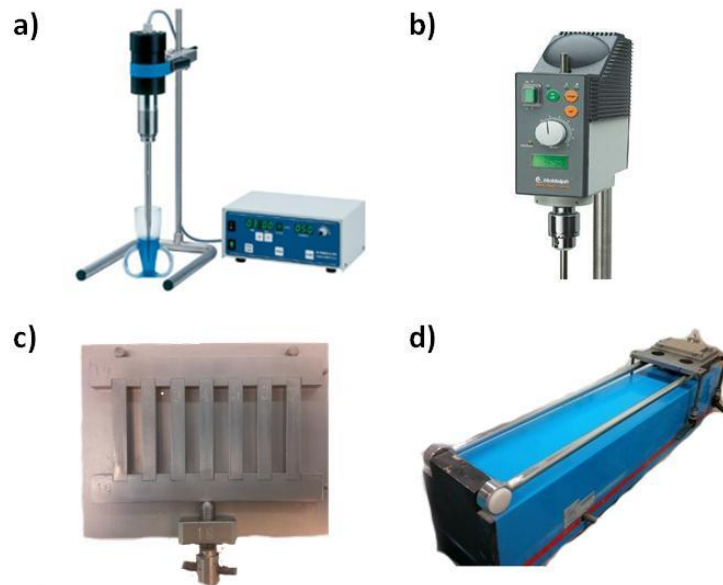
Figure II.2-1 Cement paste preparation tools a) ultrasonic dispersion system, b) stirrer, c) mold for the cement paste samples and d) compacting machine.

II.3   Characterization Techniques

II.3.1   X-Ray Diffraction:

Two X-ray diffractometers (XRD) were used for the analysis. They were both similar equipments, but the measuring conditions were different, so they will be detailed in Table II.3-1. The analyses were carried out for powder samples.

Both equipments at ICMCB and at Tecnalia were a Philips PANalytical X'Pert powder X-ray diffractometer model PW 1820 with an automatic sampler. The software employed to study the measurements is X'Pert Hight score plus which is provided with a specific library for cementitious compounds.

A quantitative XRD-Rietveld analysis was asked to the University of Málaga. The Rietveld method uses a least squares approach to refine a theoretical line which matches with the experimental one. The technicians first analyzed the powder samples in a Philips PANalytical X´Pert PRO MPD equipment and then identified the phases using the X'Pert Hight score plus software with a specific PDF database. The quantitative Rietveld analysis was carried out with the Bruker TOPAS software using Zincite (ZnO NIST SRM676- a) as an internal standard.

Table II.3-1: Measurement specifications of the X-Ray diffractometer.

	ICMCB	Tecnalia
Radiation source:	$CuK_{\alpha1}$ (1.5406 Å)	$CuK_{\alpha1}$ (1.5406 Å)
Starting position [º2 θ]:	5.01	2.01
Ending position [º2 θ]:	79.98	74.99
Step [º2 θ]:	0.017	0.020
Measuring time per step [s]:	149.86	2.00
Generator settings:	45 kV, 40 mA	40 kV, 40 mA
Divergence slit type:	Fixed	Fixed
Fixed divergence slit size [º]:	0.5	1.0

II.3.2 Nuclear Magnetic Resonance Spectroscopy

Two types of magic-angle NMR (54.7°) were carried out, one based on the ^{29}Si isotope and the other on the ^{27}Al isotope. The analyses were carried out in the solid state NMR department of the SGIKER-UPV/EHU general services.

The equipment used was a Bruker Ultrashield 9.4 T (400MHz) equipped with a MAS-DVT probe. The samples were turning at a speed of 10 kHz, the specifications for each measurement are summarized in Table II.3-2. The data were collected and processed by the technician of the service. The deconvolutions of the spectra were carried out with the software Omnic 7.2.

Table II.3-2 NMR measurements specifications

	^{29}Si MAS	^{27}Al MAS
Nucleus frecuency (MHZ)	79.49	104.79
Nucleus pulse	4.0	2.0
Delay between scans	10	1
Number of scans	4096	1024

II.3.3 Scanning Electron Microscopy

Three different scanning electron microscopes were employed during the research. At ICMCB it was employed a Jeol JSM 6360A, it has a beam voltage of 0.4 kV-40kV; a resolution of 10 nm and a magnification ×10 to ×300 000. The samples were supported on a carbon tape and coated with gold using a 108 manual sputter coater equipment.

In the general services SGIker-UPV/EHU a high-resolution field emission microscope Jeol JSM-7000F with Wolfram filament was used. It has a beam voltage of 300V-30kV and a resolution of 1.2 nm. The samples were supported on a carbon tape and coated with platinum.

At tecnalia the SEM images were acquired using a FEI Quanta 200 ESEM with a correlated EDAX company X-ray energy dispersive fluorescence spectrophotometer, Genesis 4000 system. The SEM images were acquired using uncoated samples at a sample chamber pressure of 60 Pa, accelerating voltage of 30 keV and a working distance of 10.7 mm.

In all the equipments, the imaging can be obtained with two detectors; the one that uses secondary electrons to obtain fine surface topographical features and the one with backscattered electrons which give contrast based on atomic number.

II.3.4   Transmission Electron Microscopy:

The transmission electron microscope used was a *JEM-2200FS/CR* in the BioGUNE research center. It is equipped with an UltraScan 4000 SP (4008×4008 pixels) cooled slow-scan CCD camera (GATAN, UK). The electron source is a ZrO/W (100) filament, and the maximum beam is 200 KeV, and the resolution is 0.14 nm. The sample was supported on a copper-carbon grid. The images were treated with the Digital Micrograph software.

II.3.5   Infra-Red Spectroscopy:

In this project, two infrared spectrometers were employed. At ICMCB it was a BRUKER Equinox FTIR equipped with an attenuated total reflection (ATR) unit. The sample was diluted in KBr which is transparent to infrared light, and the transmittance was measured. At Tecnalia, a Perkin-Elmer Spectrum 100 FTIR was employed, in this case, the samples were prepared in KBr pellets, and also the transmittance was measured.

II.3.6   X-Ray fluorescence:

A Bruker® M4 tornado μXRF scanner equipped with a Rh source (excitation of 30W) and a XFlash 430 Silicon Drift detector was used for obtaining the μXRF measurements. All line scan measurements were executed under vacuum conditions (20 mbar), with a 25 μm spot size and with a 3 second dwell time per point.

II.3.7   Calorimetry

The calorimetric equipment employed is a "TAM air isothermal calorimeter" with eight channels. The equipment is thermostatted at 25±0.02ºC. The sample is introduced into a 20mL hermetic glass bottle, and the measurement is done using water as reference. The experiments run independently in each of the eight channels and the final data obtained is the calorimetric curve.

II.3.8   Electromechanical Test Machine

This equipment is employed to carry out the three point bending test and compression tests. It is a "ibertest ELIB-10-W" machine with two modules for the different tests. The module for the three point bending test has two support points and one loading point in between to break the specimen in two (Figure II.3-1a). The compression module has two square 1cmx1cm surfaces (the same one as the section of the specimen), one of them is the support, and the other one is the loading point to apply the compression strength (Figure II.3-1b).

Two different sets of loads were employed depending on the nature of the specimens. Short-time cured samples (6 and 8 hours) loading rates of 1 and 10 [N/s] were set for bending and compression test, respectively, and for longer times (16, 24, 48 and 72 h) the loading rates were 5 and 100 N/s, respectively.
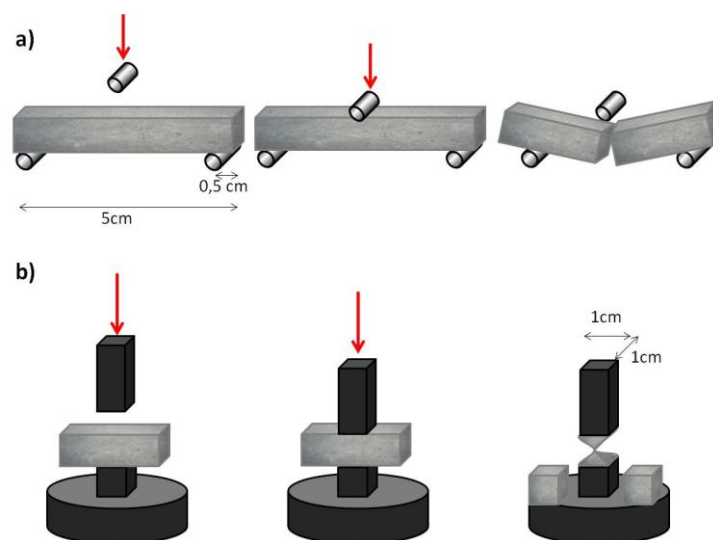
Figure II.3-1: a) three points bending test and b) compression test process with 1cmx1cm square support.

CHAPTER III: SYNTHESIS OF TOBERMORITE AND XONOTLITE

III.1   **SUBCRITICAL** HYDROTHERMAL SYNTHESIS

III.2   **SUPERCRITICAL HYDROTHERMAL SYNTHESIS**

III.3   **CONCLUSIONS**

III.1   *Subcritical hydrothermal synthesis*

The first approach of the synthesis was under subcritical conditions to follow the guidelines of the previous knowledge in the area. After the study of a huge number of reactions summarized in the appendix I and II, the most suitable conditions for each product (xonotlite and tobermorite, respectively) were selected. As it was mentioned before, the tobermorite is metastable at high temperatures. So as, apparently, the synthesis of xonotlite is easier, we decided to start with this one. The reactor employed in this synthesis is the one explained in section II.1.1.

III.1.1   Subcritical synthesis of xonotlite

In the literature it can be found many hydrothermal routes for the synthesis of xonotlite (appendix I). One of the variables studied in some cases are the precursosrs used for the synthesis. The most common precursors employed for the synthesis are SiO_2 (crystalline or amorphous) and CaO [145][144] but other authors studied the possibility to use other precursors such as $Na_2SiO_3 \cdot 9H_2O$ as silicon source[151][152] and $Ca(NO_3)_2 \cdot 4H_2O$[151] or carbide slag[153] as a calcium source.

For this reason the first step was to study the syntheses using different precursors with the objective of identifying the differences among the obtained products. The proposed precursors for this synthesis are summarized in

Table III.1-1.

Table III.1-1: Summary of the precursors used in the subcritical synthesis of xonotlite.

	Amorphous nano-SiO_2	$Na_2SiO_3 \cdot 9H_2O$	$Na_2SiO_3 \cdot 5H_2O$	Waterglass (Sodium silicate)	$Ca(NO_3)_2 \cdot 4H_2O$	CaO
Comercial distributor	Akzonobel levasil	Sigma-Aldrich	Sigma-Aldrich	Panreac	Sigma-Aldrich	Sigma Aldrich
Description	Colloidal dispersion in water (45%)	Transparent small crystals	Small white balls	Viscose liquid	Transparent small crystals	White powder
Purity	100%	98%	99%	Na_2O 8.9% SiO_2 29.2%	99%	96-100.5%
Pretreatment	//	//	//	//	//	Calcination 800ºC 4h

The syntheses were carried out at 225ºC for 4 hours. The Ca/Si ratio in every case was one, and the total volume of the synthesis 1.5L. The syntheses were prepared as indicated in Table III.1-2:

Table III.1-2: Formulation of each of the syntheses carried out under subcritical conditions.

		Reaction 1	Reaction 2	Reaction 3	Reaction 4	Reaction 5	Reaction 6
Si Source	**Na$_2$SiO$_3$·5H$_2$O (g)**	10.61	//	//	//	//	//
	Na$_2$SiO$_3$·9H$_2$O (g)	//	6.96	//	//	13.93	//
	Waterglass (g)	//	//	10.29	//	//	35.48
	Levasil 100 (g)	//	//	//	9.37		//
Ca Source	**Ca(NO$_3$)$_2$·4H$_2$O (g)**	11.81	5.90	11.81	//	//	//
	CaO (g)	//	//	//	4.15	2.80	8.4

XRD analyses of the products obtained from the syntheses are summarized in Figure III.1-1.
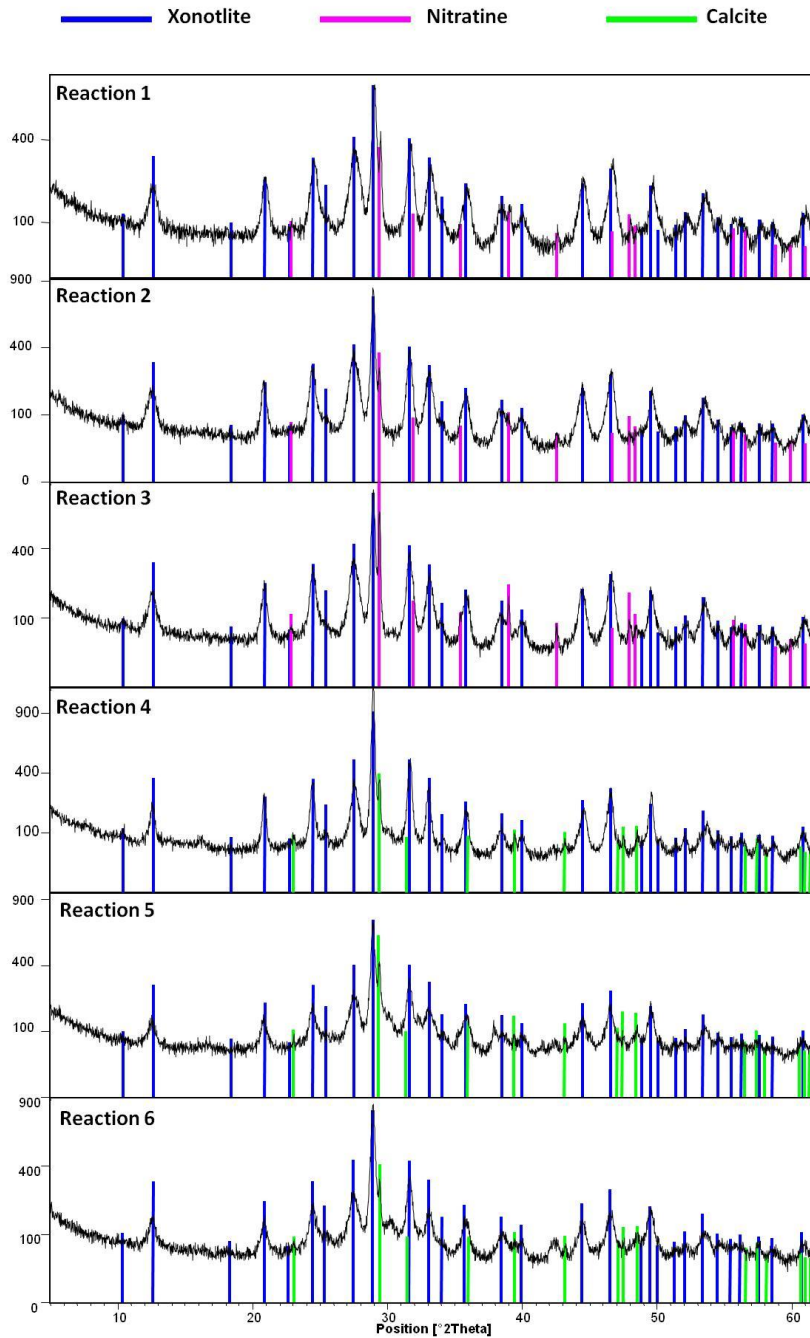
Figure III.1-1: XRD patterns of the products obtained under subcritical conditions with the different precursors summarized in Table III.1-2.

For every reaction, it was possible to obtain crystalline xonotlite. However, it was not pure. Depending on the precursors used, different byproducts were formed. For those syntheses employing calcium nitrate as precursor (reactions 1, 2 and 3), nitratine (sodium nitrate) was obtained as a by-product. For those using CaO as a precursors (reaction 4 and 5), calcite (calcium carbonate) was obtained as by-product due to the

presence of atmospheric CO_2 or disolved in the water. The synthesis that has fewer impurities (in comparison of the intensity of the secondary product with the intensity of the xonotlite signal) are the number 4 and 6, the ones that use CaO as Ca source and Levasil 100 and waterglass as source of Si.

A deeper study about the effect of the temperature and reaction time in the syntheses was carried out. For this study it was selected as reference the reaction 6.
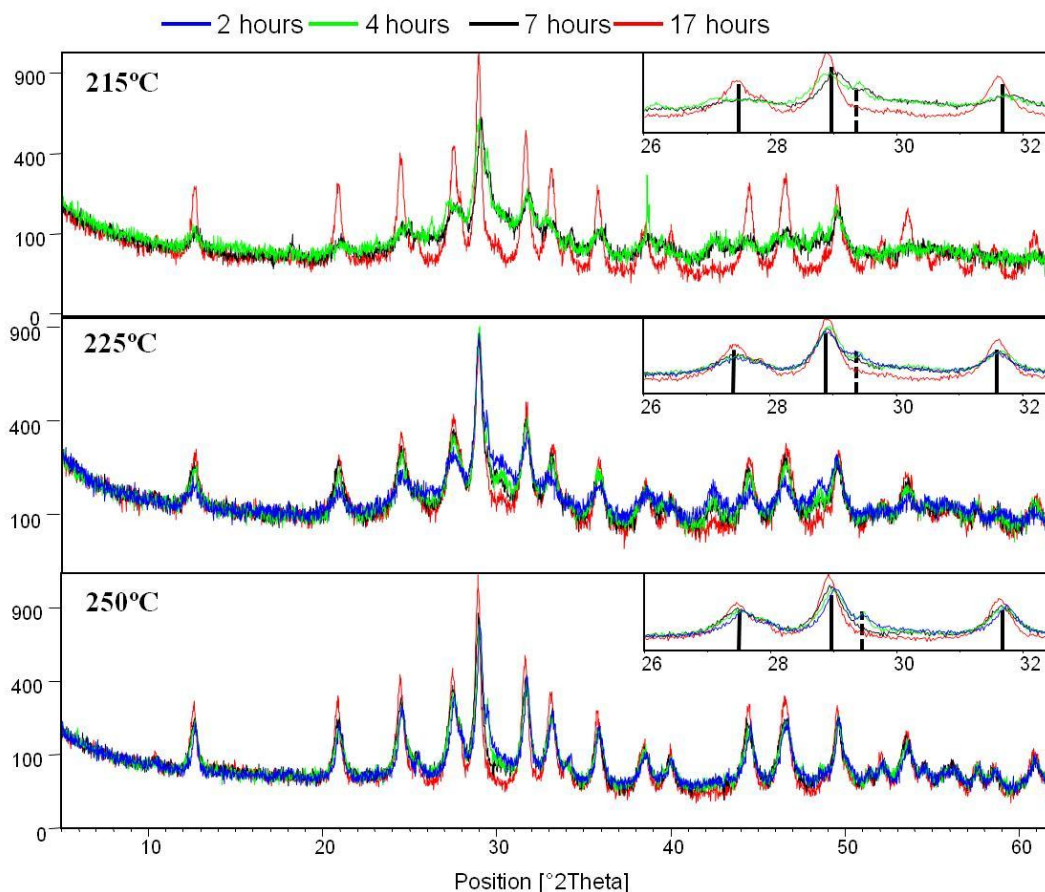
Figure III.1-2 Subcritical hydrothermal synthesis of xonotlite using waterglass and CaO as precursors at 215ºC, 225ºC and 250ºC, varying the residence time (2,4,7 and 17 hours). In the zoom image are highlighted the XRD signals of tobermorite with continuous line and the signal of calcite with dashed line.

As it can be observed in Figure III.1-2, the two variables studied affect to the crystallinity of the xonotlite and also to the formation of calcite as a secondary product. It can be observed that as the temperature is increased, no matter the time, the crystallinity of the xonotlite is increased. At 215ºC there is a big difference between the samples that reactioned during 4 hours and the ones that did it during 17 hours. However at 250ºC there is no difference observed between the temperatures. This proves that at low temperatures (215ºC) longer reaction times are required to obtain a

crystalline phase. However, at higher temperatures (250ºC) already at short reaction times, it can be obtained the crystalline phase and longer times do not change it. One of the differences observed among the products obtained at different reaction times is the presence of calcite as secondary product. As it can be observed in the zoom images of the Figure III.1-2, at longer reaction times for every reaction temperature, the calcite amount is lower.

In order to know the morphology of the xonotlite phase, a SEM analysis was carried out. In Figure III.1-3 are represented the images obtained of the samples synthesized at 215ºC and 250ºC for 17 hours. Both have fibrous morphology, the characteristic one of xonotlite. The fibers are nanometric and no significative difference is observed among the ones produced at 215ºC and at 250ºC.

215ºC **250ºC**
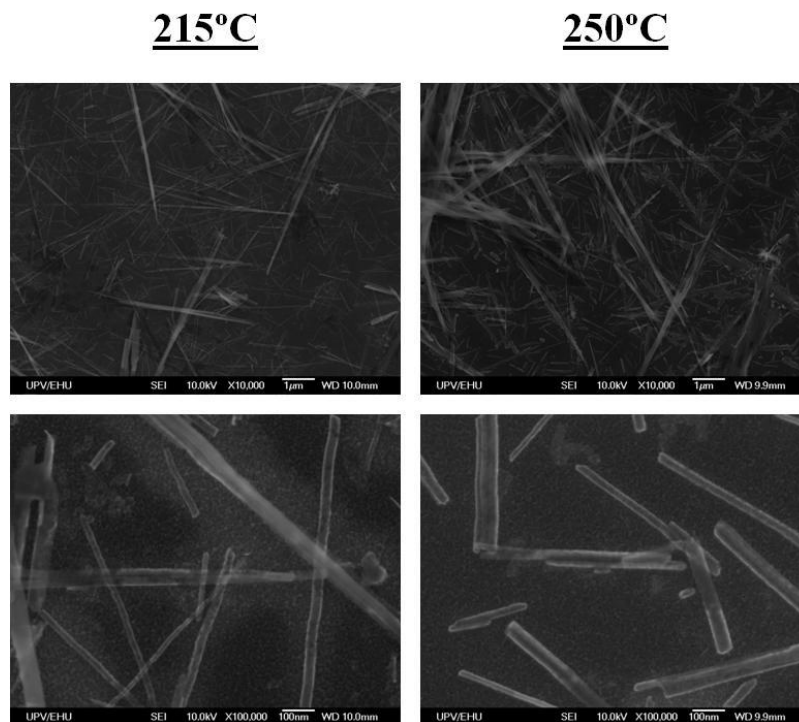
Figure III.1-3: SEM analysis of the xonotlite samples synthesized for 17 hours at 215ºC and 250ºC at two amplification levels.

As a conclusion, it could be said that the subcritical hydrothermal method is appropriate for the synthesis of crystalline nanometric xonotlite. Several precursors were studied; but, in order to avoid the production of secondary products, it was concluded that the most appropriate are nanosilica (Levasil 100) and waterglass for Si, and calcium oxide for the calcium source. The study concerning the reaction time and the temperature concluded that for low temperatures (215ºC), long reaction times are

required (17 hours) to obtain a crystalline product. For high temperatures (250ºC) this time is reduced to only two hours and the product obtained has the same morphology and characteristics.

III.1.2   Subcritical hydrothermal synthesis of tobermorite

The research group in Tecnalia had previous experience in synthesizing tobermorite under subcritical conditions[188]. Therefore, taking this knowledge, as a starting point, we decided to study the effect of Al substitution for Si on tobermorite's structure. The precursors employed were CaO, nano-SiO_2 and nano-Al_2O_3. The details of these compounds are summarized in Table III.1-3.

Table III.1-3 Precursors for subcritical hydrothermal synthesis of tobermorite.

	CaO	**Amorphous Nano-SiO_2**	**Nano-Al_2O_3**
Comercial distributor	Sigma Aldrich	Akzonobel Levasil 100	Nyacol Al2OSD
Description	White powder	Colloidal dispersion in water (45%)	White powder
Purity	96-100.5%	100%	94%
Particle size	//	5–100 nm	50 nm
Pretreatment	Thermal treatment at 800ºC for 4 hours	//	//

The experiments were carried out at different Al% from 0 to 20 atomic Al% of Silicon substitution (Al/(Si+Al)·100). This election was based on the bibliography that points out at the 15% Al as the most suitable dosage for the stability of the tobermorite[77][93][95]. All the experiments were carried out using the same precursors and with the same reaction conditions. The reactions were carried out in the hydrothermal batch reactor at 215ºC and autogenous pressure for 4 hours.   Each reaction specifications are sumarized in Table III.1-4. All the products were filtered and dried in a oven at 60ºC for 12 hours. The product, in every case, is a white powder that was analyzed with different characterization methods: XRD, SEM and NMR.

Table III.1-4 Formulation of the syntheses carried out with different Al contents.

Al%	Ca/(Si+Al)	CaO (g)	SiO_2 (g)	Al_2O_3(g)	H_2O (L)
0%	0.83	3.36	9.65	0.000	1.5
6%	0.80	3.36	9.35	0.023	1.5
10%	0.83	3.36	8.69	0.368	1.5
15%	0.83	3.36	8.19	0.550	1.5
20%	0.83	3.36	7.72	0.737	1.5

The XRD analyses of the different syntheses showed how the inclusion of the aluminum to the synthesis promotes the formation of crystalline tobermorite. Figure III.1-4 shows this effect clearly; all the syntheses were carried out under the same reaction conditions, so the differences between each synthesis are only related to the aluminum effect. In the XRD patterns it is possible to see that as the Al dosage increases, the tobermorite peaks are more defined and more intense. For low Al concentrations the sample is composed partially by a C-S-H gel and partially by tobermorite, as the Al dosage increases, there is less amount of the amorphous C-S-H gel and higher proportion of tobermorite. The pattern is compared with the PDF 00-045-1480 which is a natural specimen from Fuka (Japan).
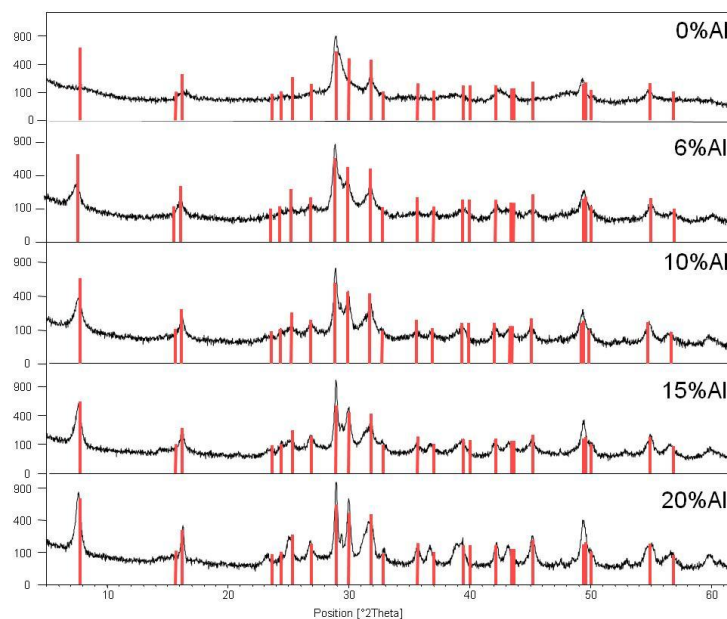
Figure III.1-4: XRD patterns of the subcritical tobermorite syntheses with different Al contents. In red is the tobermorite PDF 00-045-1480 pattern.

In Figure III.1-5 is represented only the first peak (0,0,2) where the increase of the peaks' intensity is more clear. Some authors attributed this effect to an acceleration of the crystallization rate along the c-axis because of the presence of Al [189]. These results are in accordance with the ones indicated by T. Mistsuda et al.[95] where they highlighted the effect of aluminum in the crystallization of tobermorite. In their work, they present the evolution of the crystallization as a function of the time. And, according to their results, the aluminum stabilizes somehow that the higher is the dosage of aluminum, the earlier is formed the crystalline phase of tobermorite. According to this basis, if longer reaction times are employed for those samples with lower Al%, crystalline tobermorite can be obtained. In the work of Mitsuda et al. it is not reflected the XRD signal to visualize the crystallization degree and the effect of the aluminum, but it is expected to follow a similar behavior to the results that we present in this work.
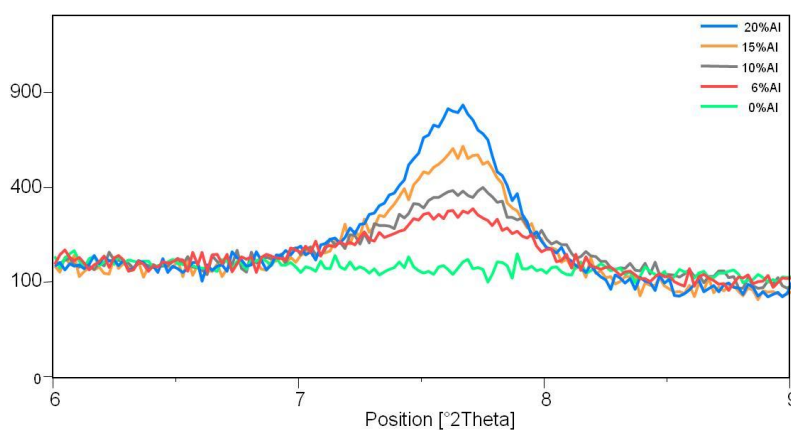
Figure III.1-5: Focus on the basal peak as a function of Al at%.

Two quantitative XRD-Rietveld analysis were carried out for two extreme aluminum dosage to quantify the crystallization degree of the sample; the 6% and the 20% (the one of 0% was not carried out because it was quite clear from the XRD that the crystallinity is very low). The results are sumarized in Table III.1-5.

Table III.1-5 Rietveld analysis composition of the 6%Al and 20%Al tobermorite.

	6%Al	20%Al
Amorphous phase	41.9±0.9	26.5±0.7
11Å Tobermorite	52.3±0.4	71.4±0.2
Calcite	5.5±0.4	2.0±0.2

The XRD-Rietveld analyses confirm the previous results and prove that the increase of crystalline tobermorite phase as function of the Al dosage. It was proved that with an increase of Al from 6% to 20% the crystalline tobermorite phase increased almost a 50%. It was not considered to analyze each of the samples with a dosage between 6% and 20%, but it is expected to follow the tendency of crystallization of tobermorite.

As it was mentioned in the introduction, the tobermorite can be found in two different structures, platelets and fibers. To know if the degree of crystallinity affected somehow the morphology, some SEM analyses were carried out.
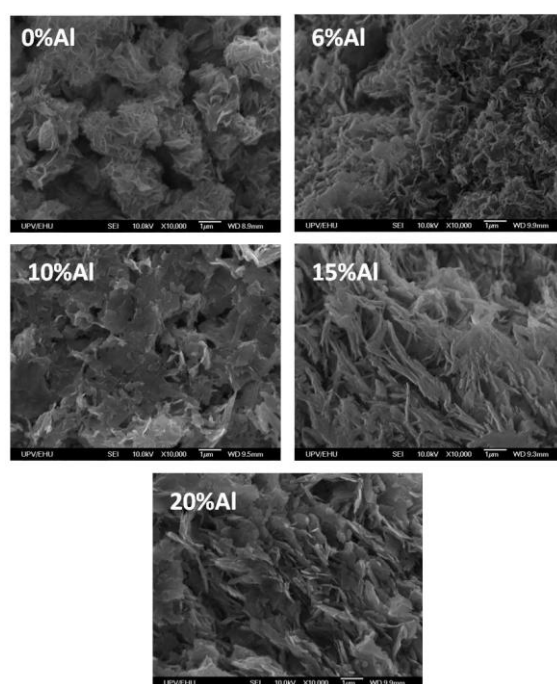
Figure III.1-6: SEM images of the tobermorite samples with different %Al content.

In the SEM images (Figure III.1-6) it is not easy to see a clear change in the morphology. It is not either clear the shape of the particles, or if there is a tendency to form one specific morphology as the proportion of crystalline tobermorite increases. It can be observed that for 0%Al the crystals are very small and agglomerated to each other and, as the Al dosage increases, the crystals are bigger and more homogeneous. This effect could alter the basal peak intensity if the particles tend to grow in the direction of (0,0,l) and they dispose in that direction preferentially during the XRD powder analysis.

A TEM analysis was also carried out to have more information about the morphology, and some slight differences were observed. With this technique, it was

possible to see that some parts were more similar to a "cloud" with an amorphous structure and only some tiny crystalline domains, while other parts were like thin paper sheets with a crystalline structure. The "clouds" are less predominant as the Al content is increased. A third structure is visible in the samples, it has fiber shape (which is characteristic of tobermorite); however, it might also be the edge of a sheet. This structure is not predominant but it is more common as the samples have more Al.
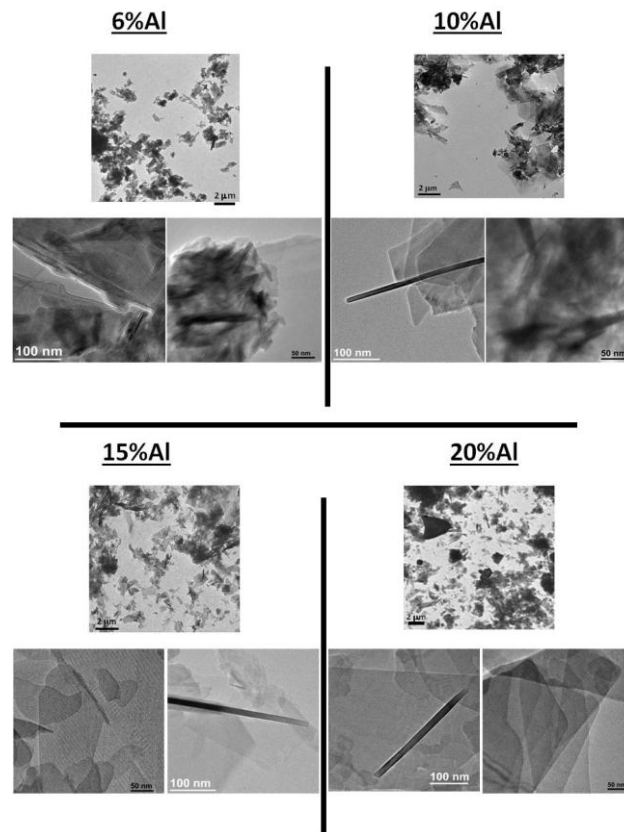
Figure III.1-7 TEM analyses of the subcritical hydrothermal tobermorite with different Al contents. Different morphologies (clouds, platelets, and fibers) are distinguished.

As it was mentioned in the introduction, there are two polytypes of 11Å tobermorite, the normal and the anomalous. It is possible to know what type of tobermorite is concerned, submitting the samples to a heating treatment at 300°C for 24 hours. For each Al dosage, several identical reactions were carried out as a large amount of product was required for the cement test. Each synthesis was analyzed to check its crystallinity degree, and some of them were also treated thermally to know if they were normal or anomalous.

(a)   For the 6% Al:

Sixteen samples were synthesized with this formulation; their XRD were all very similar to the one shown in Figure III.1-4. Among them the thermal treatment was applied to six samples obtaining three different behaviors which are shown in Figure III.1-8. In every case, the samples became more amorphous. The sample a) shows a clear normal behavior because after the treatment the distance between the two calcium layers was diminished to 9Å. However, this behavior was only found in two of the six samples treated at 300ºC. The sample b) shows another behavior, with a calcium distance of 10.4Å. It can correspond to a metastable phase in transformation from the 11Å phase to the 9Å one. This phase could be the one described by Biagioni et al. [190]. In this publication, they describe the formation of a 10Å tobermorite. However, the temperature required to obtain this phase is slightly higher (~420ºC) than the one employed in our experiment. This same peculiarity is observed in 3 of the samples. The sample c) shows a double behavior, on one side we can observe that metastable phase observed in the previous sample but also a small pick remaining of 11Å which would correspond to an anomalous behavior. This behavior was found in only one sample.

There are also two other peaks that are characteristic of the 11Å and 9Å tobermorite, respectively and where we can also observe the phase change. The first one is the one at 16.25º 2θ which is characteristic of the 11Å, and it is only observable in the b) and c) samples. However, the peak at 18.40º 2θ (characteristic of the 9Å tobermorite) is more pronounced in the sample a) than in the other two samples where it is still visible but more diffused.

The last two peaks that can differentiate the 11Å and the 9Å tobermorite are the ones at 28.97º and 29.61º respectively, which are the most intense ones. In the sample a) the intense peak is at 29.51 2θ, closer to the characteristic position in the 9Å tobermorite. However for samples b) and c) there are two peaks very close, at 29.02º and 29.41º which are in half way between the ones of 11Å and 9Å tobermorite.

Figure III.1-8: XRD pattern of the 6%Al tobermorite syntheses before and after the 300ºC thermal treatment. Three behaviors are observed: a) normal tobermorite, b) metastable transition phase and c) metastable transition phase + anomalous tobermorite

All the samples had the same treatment at 300ºC for 24h, so the different behaviors are linked to structural differences. So, in order to correlate it somehow with the structure, their original XRD were compared to check the differences among them. The only significant difference can be observed in the first peak (Figure III.1-9), the one which corresponds to the (0,0,2) direction. It can be observed that the sample a) (which presents a normal behavior) has that peak more intense than the other samples, and this behavior is repeated in the two samples classified as "normal tobermorite."

Figure III.1-9: Focus on the basal XRD band for the 6%Al tobermorite samples before thermal treatment. a) normal tobermorite, b) metastable transition phase and c) metastable transition phase + anomalous tobermorite

As the change of intensity of one specific peak in XRD measurements may be related to the morphology, and more specifically the preferential grow of the crystal, we checked if there was no morphological difference with SEM analysis.
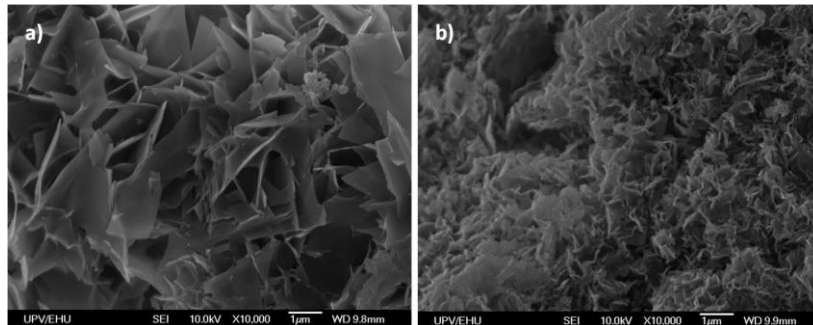
Figure III.1-10: SEM images of the samples with normal a) and metastable b) behavior.

The SEM images show a clear difference between the two samples (Figure III.1-10). The crystals in sample a) are bigger and more defined than in sample b) where the crystals are smaller and less organized. However, it is not clear that the sample a) grows in a preferential direction.

HR-TEM analysis was carried out to visualize the distance change between the Calcium layers. As some parts of the sample are crystalline, it was possible to see the distance between the calcium layers and measure it. Figure III.1-11a represents the sample with 6%Al which had a normal behavior, and its interlayer distance is 11.35Å; exactly the same as the one measured with XRD. Figure III.1-11b shows the same

sample after the dehydration thermal process. This sample is less crystalline, but it is still possible to visualize some crystalline phases with the new disposal. The interlayer distance was proved to be 9.64Å as it has been highlighted in XRD pattern.
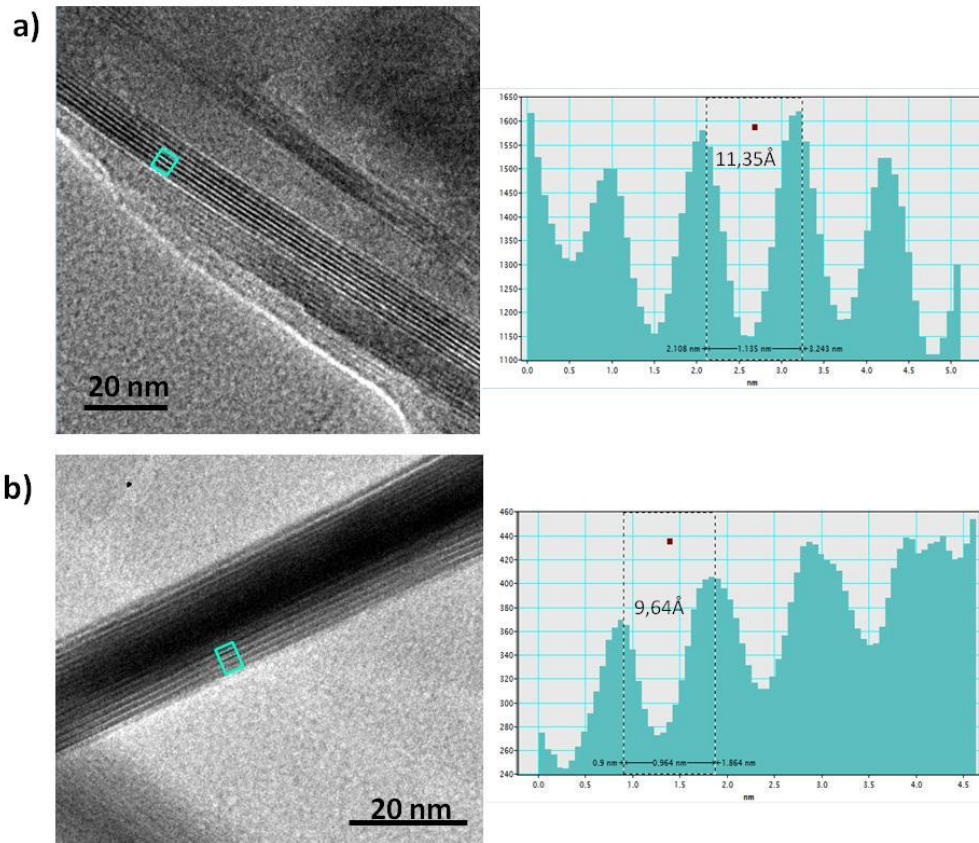
Figure III.1-11: TEM images of 6%Al normal tobermorite a) before heating treatment and b) after heating treatment. Representation of the profile of the sample in the selected area.

(b) For the 10%Al:

Nine samples were synthesized with this formulation; their XRD patterns were all very similar to the one shown in Figure III.1-4. Among them, the thermal treatment was applied to five samples, and the results are shown in Figure III.1-12. As in the 6%Al case, two polytypes were found, the normal tobermorite and the intermediary one at 10Å. The sample a) has a normal behavior because the distance between two consecutive calcium layers is reduced to 9Å (reflected in the first peak). This behavior was found in two of the five samples. The rest of the samples analyzed, three in total, had a different behavior as it is reflected in the Figure III.1-12b). In this case, it is also found a behavior similar to the one seen in the 6%Al b) sample where a metastable phase is formed with some characteristic peaks from both 11Å and 9Å configurations.

This sample has a double "first peak" with one maximum at 11.05Å corresponding to the anomalous behavior and the second one at 10.20Å.
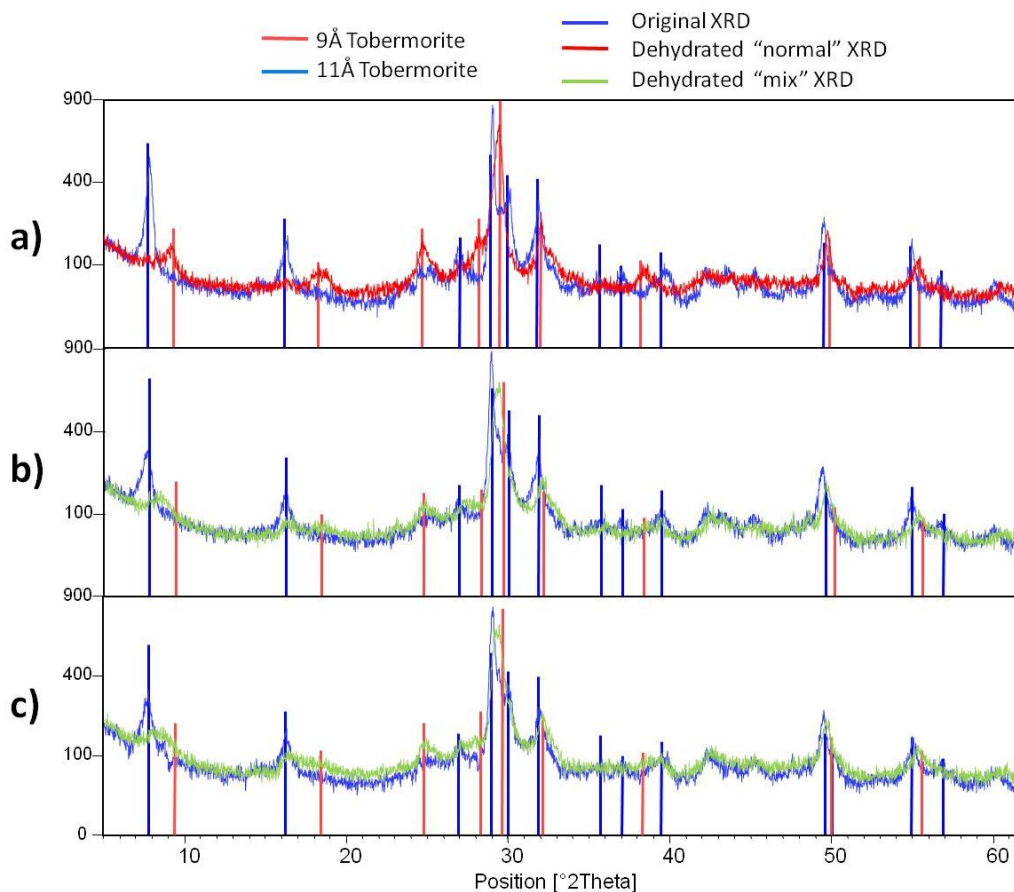

Figure III.1-12: XRD analysis of the 10%Al tobermorite syntheses before and after the 300ºC thermal treatment. Three behaviors are observed: a) normal tobermorite and b) metastable transition phase + anomalous tobermorite.

The other characteristic peaks that were mentioned for the 6%Al are also remarkable in these samples. In the case of the peaks at 16.25° and 28.97º, characteristic of 11Å tobermorite, they can be observed in sample b) and not in a). The peaks at 18.40º and 29.61° distinctive of the 9Å tobermorite are clearly visible in sample a) and less defined in sample b) but still distinguishable.

Following the same procedure as for the 6%Al samples, it was studied the original XRD analysis to seek differences among the samples synthesized which have different behaviors.
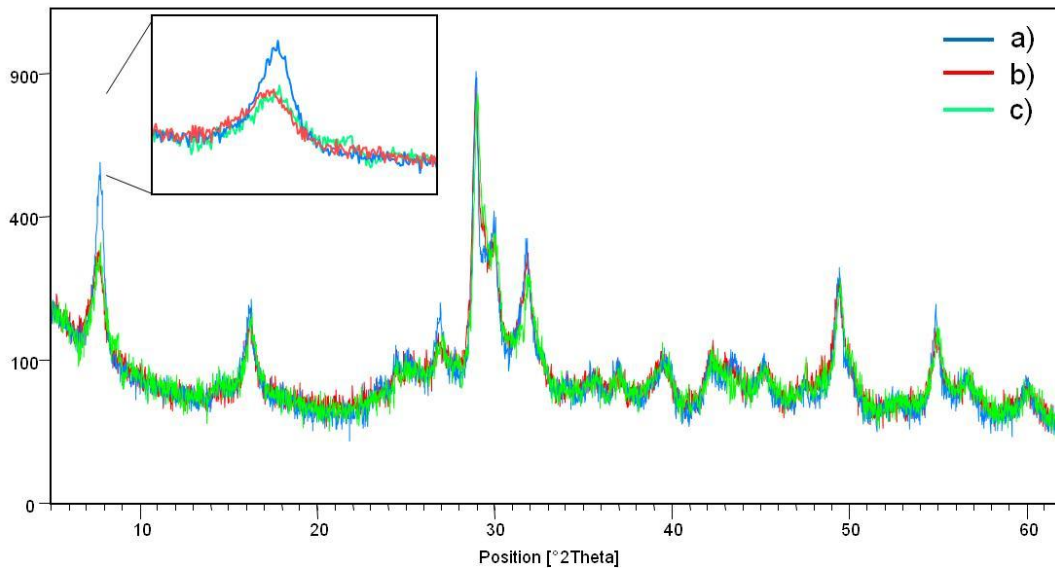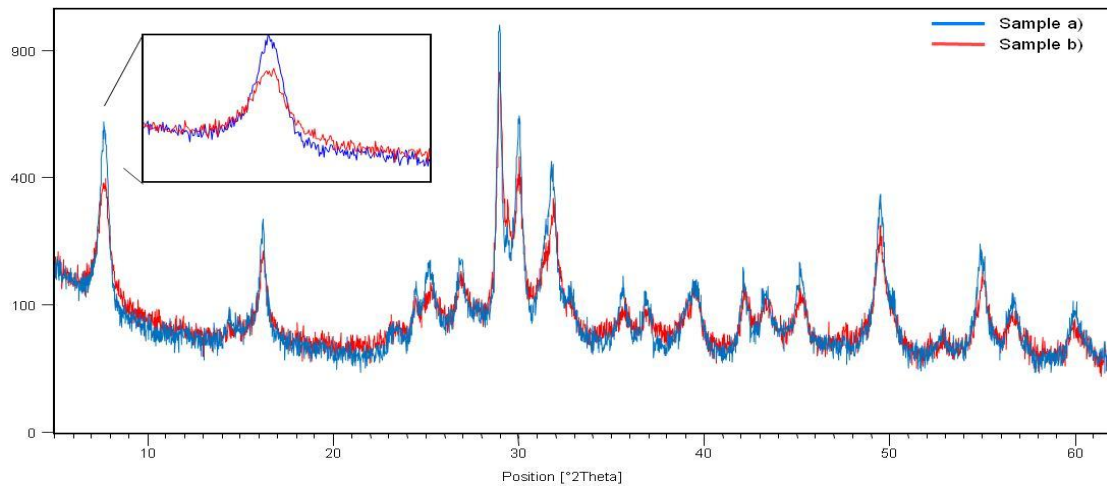
Figure III.1-13: Focus on the basal XRD band for the 10%Al tobermorite samples before thermal treatment. a) normal tobermorite and b) metastable transition phase + anomalous tobermorite.

In the Figure III.1-13 is represented the XRD analysis of the samples a) and b) before the thermal treatment. It can be observed that the sample a) (the one with normal behavior) is more crystalline than the sample b). This tendency was already observed in the 6% Al samples.

The morphology of the samples was also analyzed using SEM (Figure III.1-14); however, no significant difference was detected. Both samples have an irregular morphology with no preferential growing in any direction.
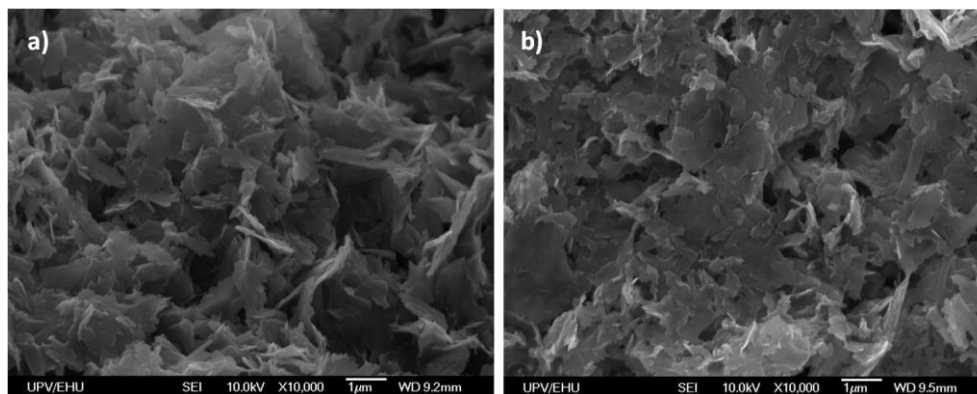
Figure III.1-14: SEM images of the samples with normal a) and metastable b) behavior.

(c)   For the 15%Al:

Sixteen samples were synthesized with the 15%Al formulation. A priori, the XRD analysis did not reflect anomalies among them, and they were all similar to the one shown in Figure III.1-4. It was selected four samples to apply the thermal treatment, and three different behaviors were found (Figure III.1-15): the normal, the anomalous

and the intermediary phase. The sample a) presents an anomalous behavior showing all the characteristic peaks of that phase. The sample b) can be considered as a mixture of both anomalous and normal tobermorite (not the metastable phase that we had seen before) as it can be observed peaks characteristics of both polytypes. The signals corresponding to the distance between Ca layers are at 11Å and 9Å, so it highlights the presence of both species and not the intermediary one. Also, the peaks at 16.25º and 30.04º shows the presence of 11Å tobermorite. Among the four samples analyzed, two were of this type. The sample c) is completely anomalous.
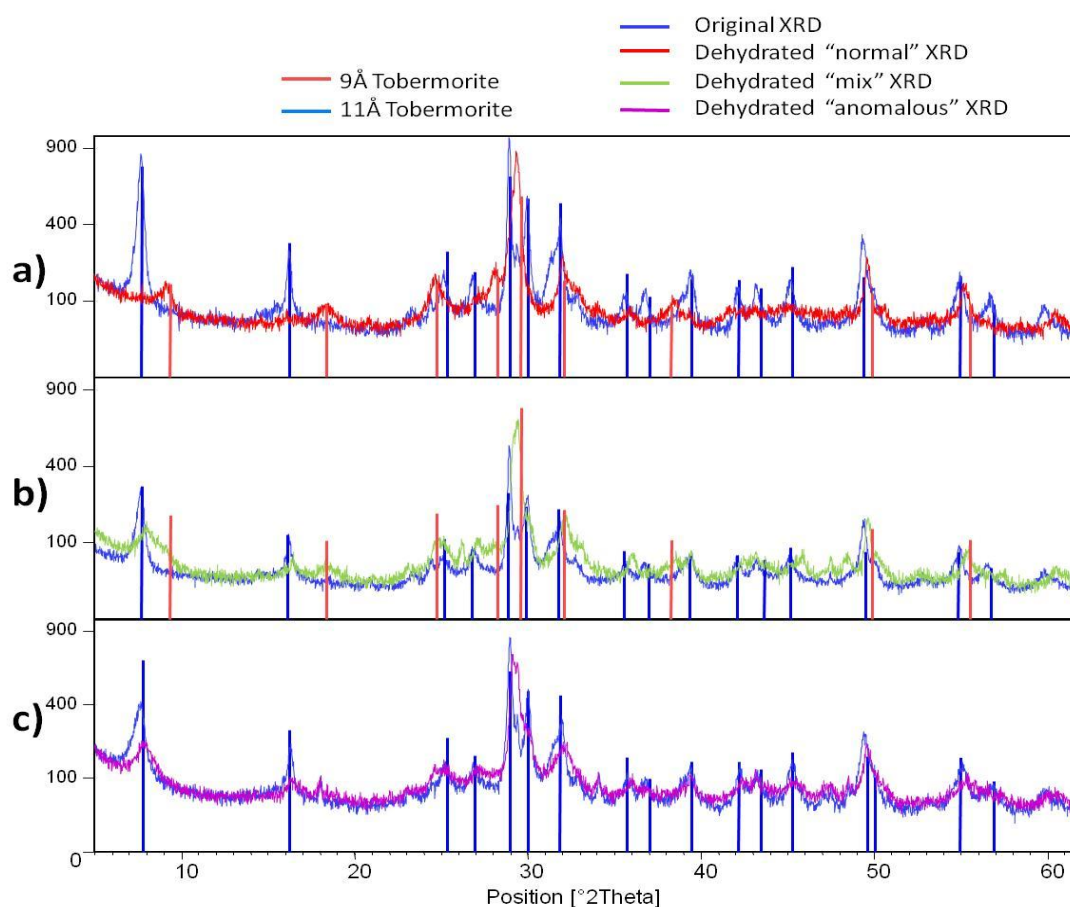
Figure III.1-15: XRD analysis of the 15%Al tobermorite syntheses before and after the 300ºC thermal treatment. Three behaviors are observed: a) normal tobermorite, b) a mixture of normal + anomalous tobermorite and c) anomalous tobermorite.

As it was done with the previous samples, the original X-ray diffracted patterns were analyzed to check if the tendency that had been observed previously was repeated in this case. As it can be observed in Figure III.1-16 the sample a), which is "normal" type, is in general more crystalline than the rest of the samples, and this effect is accentuated in the first peak. The least crystalline peak is the sample c) which is "anomalous." The sample b) has an intermediary behavior.
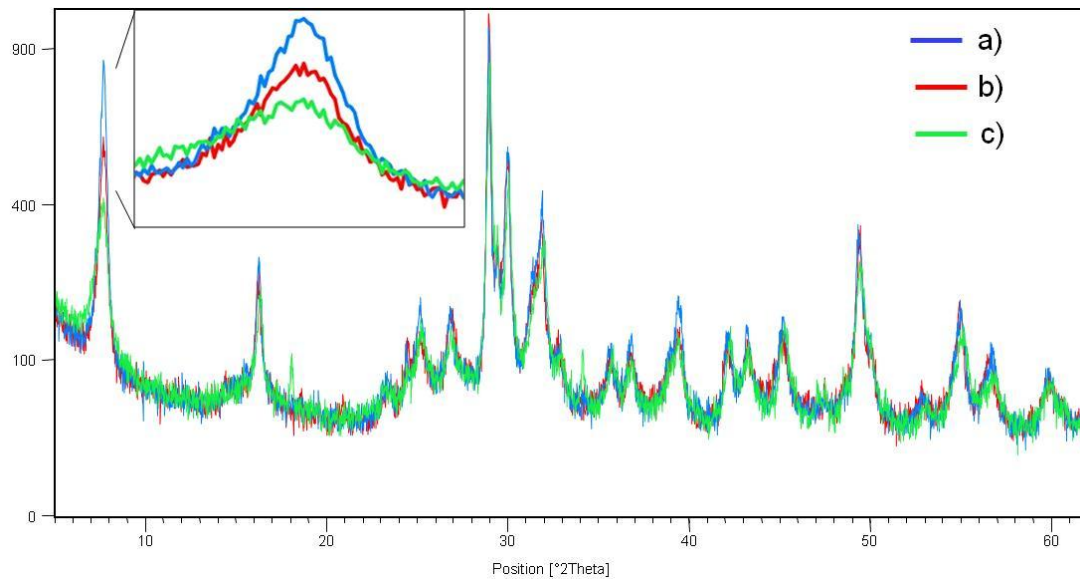
Figure III.1-16: Focus on the basal XRD peak for the 15%Al tobermorite samples before thermal treatment. a) normal tobermorite, b) a mixture of normal + anomalous tobermorite and c) anomalous tobermorite.

The samples a) and c) were analyzed by SEM (Figure III.1-17) but no significant difference was observed among then, both had a similar morphology.
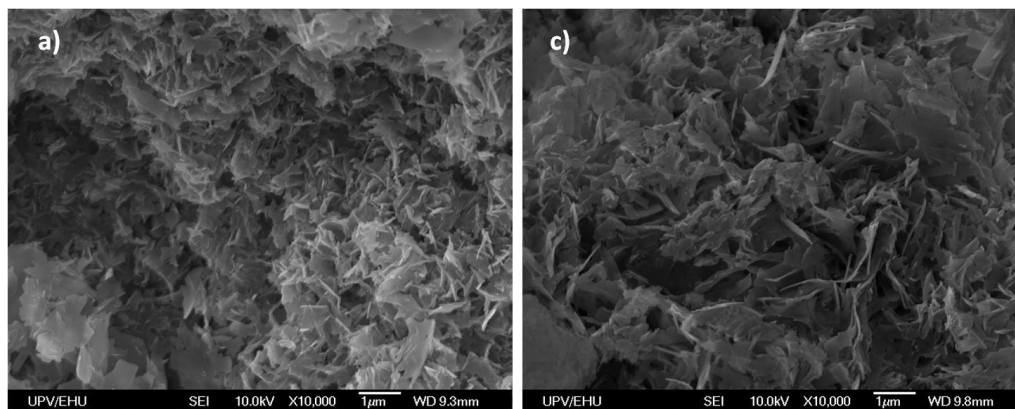
Figure III.1-17: SEM images of the samples with normal a) and anomalous c) behavior.

(d)   For the 20%Al:

For this dosage, seven samples were synthesized. There are no significant differences among them according to the XRD. Four samples were treated thermally to identify their polytopes. In this case, the samples were all equal with a mixed "normal" and "anomalous" behavior (Figure III.1-18).

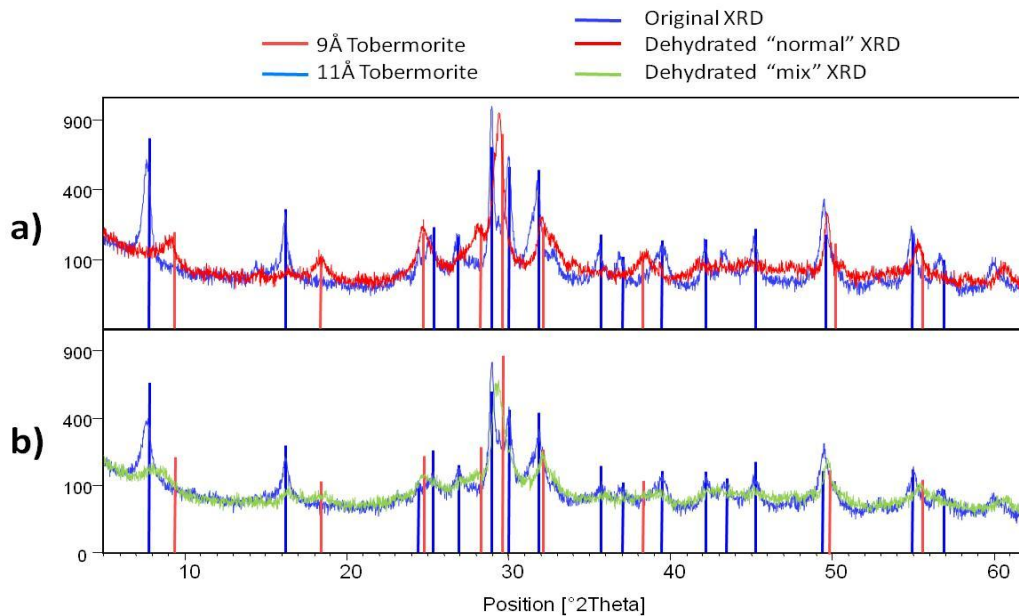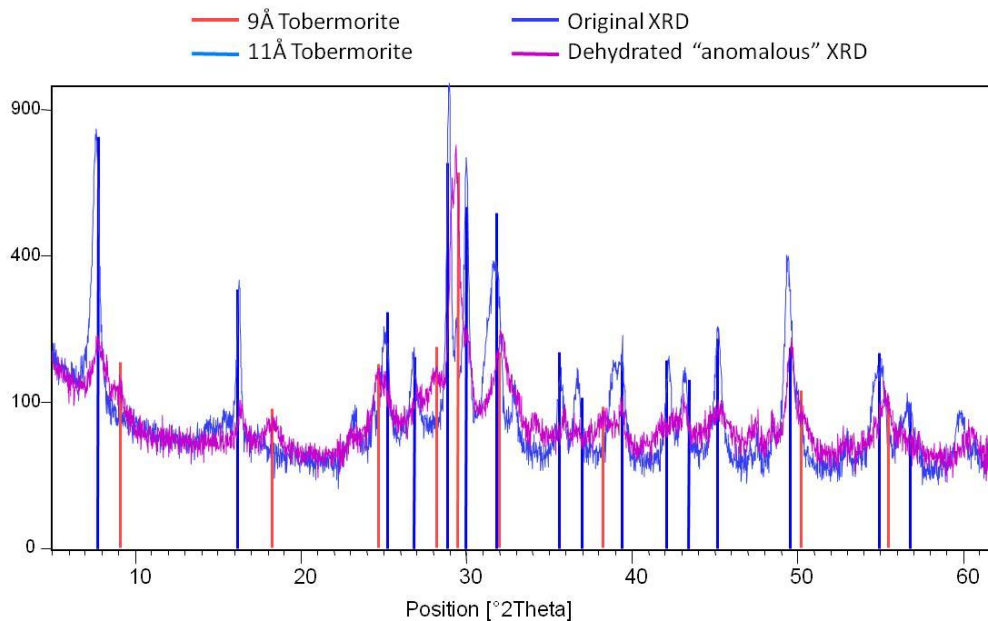**Figure III.1-18: XRD analysis of the 15%Al tobermorite syntheses before and after the 300ºC thermal treatment. The behavior observed was a mixture between "normal" and "anomalous" tobermorite.**

After this study, where some differences were observed in the structures, it was decided to make a more specific analysis on some of the samples to know how the aluminum affected to the structure of the silicate chains. As it was mentioned in the introduction, there are several theories about how the Al substitutes the Si in the sample. The most accepted model states that the Al enters preferentially in bridging and branching position [99][191] the possible signals would be: $Q_3 1Al$, the Q_3 the $Q_2 1Al$, the Q_2 and the Q_1. The different positions that the aluminum can take are represented in Figure III.1-19 and also the names that receive each Si position in the structure, that can give place to a different ^{29}Si-MAS NMR signal[191][98].
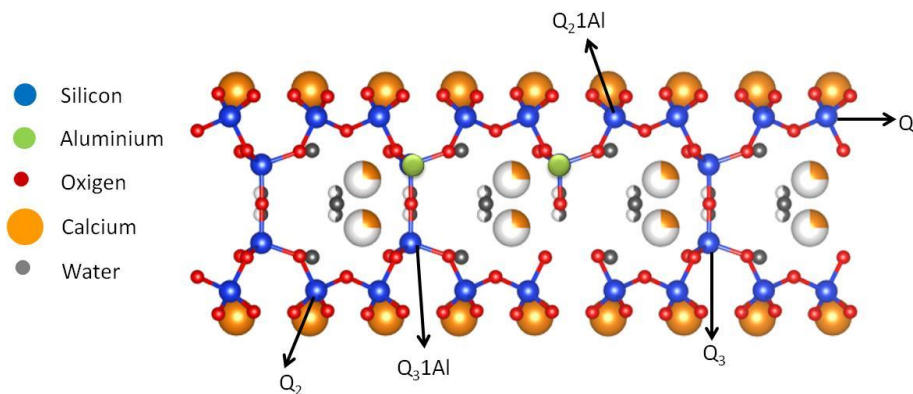
Figure III.1-19: Structure of 11Å tobermorite and the possible positions that the Al could have.

For this study it was selected a set of "normal" samples with 6%, 10% and 15% of aluminum and one sample of 20%Al which is a mixture of normal and anomalous phases, preferentially anomalous (Figure III.1-20).
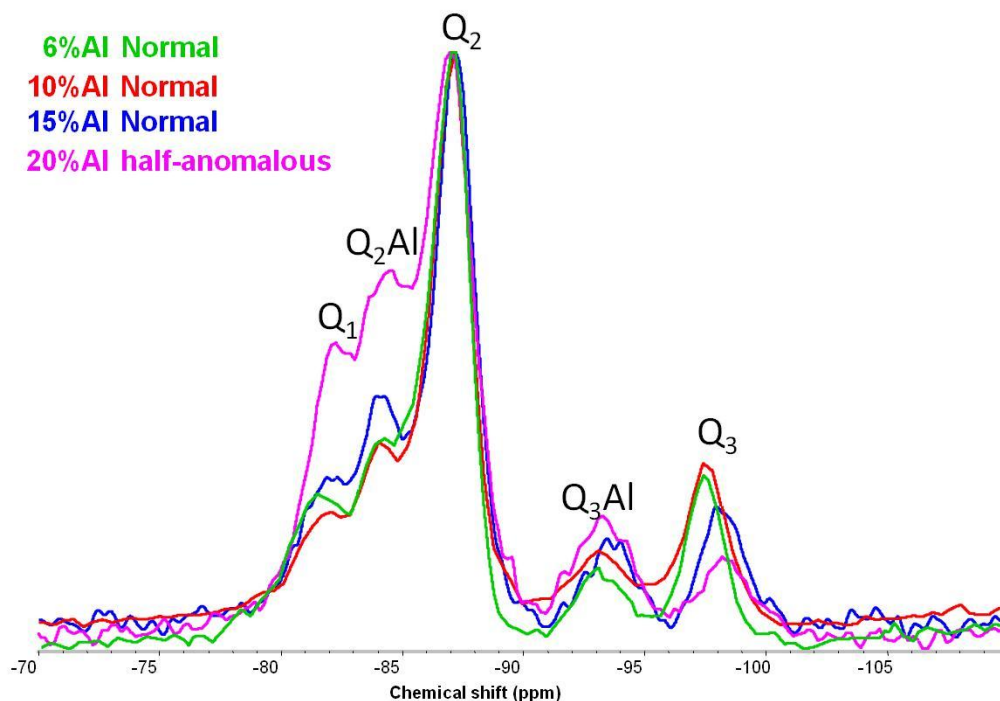
Figure III.1-20: ^{29}Si-MAS NMR analysis of tobermorite samples with different Al dosage: 6%,10%,15% and 20%.

The deconvolution of the spectrum was performed using OMNIC 7.2, assuming Voight line shapes and no loss of information to spinning side bands. It was carried out the deconvolution taking into count 5 main signals: Q_3 (~ -98 ppm), Q_3Al (~ -93.5 ppm), Q_2(~ -87 ppm), Q_2Al (~ -84 ppm) and Q_1 or Q_2(2Al) (~ -81.5 ppm). The spectra with the deconvolutions can be seen in Figure III.1-21.

Figure III.1-21: Deconvolution of the ^{29}Si-MAS NMR spectra. a) 6%Al normal tobermorite, b) 10%Al normal tobermorite, c) 15%Al normal tobermorite and d) 20%Al half-anomalous tobermorite.

The areas of each deconvoluted peak are described in Table III.1-6 and also the ratios Q_3/Q_3Al and Q_2/Q_2Al. Analyzing this information, it can be observed that the ratios diminish as the Al dosage is higher which demonstrates that the aluminum is entering in the structure of the tobermorite. The 6%,10% and 15% samples have normal behavior while the one of 20% has anomalous behavior. In the ^{29}Si-MAS NMR analysis we observe that for the normal samples the Q_3/Q_3Al ratio is 1 while for the anomalous one the ratio is 0.6. This shows that for anomalous structures the Al enters preferentially in branching positions giving stability to the structure and making it harder to break the Si-Al bond during the thermal dehydration and for that reason the structure does not compress to 9Å. It can be observed that for the sample with 20%Al the Q_1 signal is very intense, what would suggest that the chain length is shorter. However, there is another possible interpretation. This is that due to the large Al content, part of the contribution to such peak comes from $Q_2(2Al)$, which is in the same position[192]. Nevertheless this would imply that some Al atoms would occupy pairing positions that is not widely accepted in literature [193][99][194][191].

Table III.1-6: Percentage area of the deconvoluted peaks for each ^{29}Si-MAS NMR spectra.

	Q_3	Q_3Al	Q_2	Q_2Al	Q_1	Q_2/Q_2Al	Q_3/Q_3Al
6%Al	13%	7%	43%	24%	13%	1.787	1.935
10%Al	13%	8%	46%	26%	7%	1.736	1.644
15%Al	10%	7%	43%	27%	14%	1.612	1.466
20%Al	6%	9%	37%	29%	19%	1.303	0.621

In order to complete the information given by the ^{29}Si-MAS NMR analysis, a ^{27}Al-MAS-NMR analysis was carried out. Al can appear in three different forms: tetracoordinated, pentacoordinated and octacoordinated. The first group is reflected in the ^{29}Si-MAS NMR at ~50-70 ppm, the second group at ~30-40 ppm and the last group at ~0 ppm [194]. In the Figure III.1-22 it can be observed the ^{27}Al-MAS-NMR analysis carried out for the tobermorite samples with four different Al substitutions, 6%, 10%, 15% and 20%. It can be observed two clusters, one around 40-70 ppm and another one around 0 ppm, these are attributed to tetracoordinated and octacoordinated Al respectively. The tetracoordinated Al enters in the structure substituting the Si preferentially in bridging and branching positions[99][194][191]. There is no evidence in literature that the Al can enter in pairing position. The signal at ~63.5 ppm is assigned to the Al that enters in bridging and the one at ~56 ppm is assigned to the Al that enters in branching position [194] in good agreement with the ^{29}Si MAS-NMR results. This would mean that the silicate chains are not all linked to each other and there might be some defects in the structure. For the sample with 20%Al there is also some octacoordinated Al that might be related to an excess of Al. In an ideal tobermorite structure where the Al enters only in Q_3 positions and not in Q_2, the maximum of Al that could enter into the structure is 16.5%, so for this sample it might be normal to observe this excess. This Al could appear in two different forms. In the first one it would be in its original form Al_2O_3 where the aluminum is octacoordinated [191], so that means that the Al excess does not reaction or enter into the structure. However in the XRD pattern of the 20%Al sample (Figure III.1-4) it was not detected alumina, but this would be normal because we use amorphous nanoalumina as precursor. The second explanation is that the Al can enter in the position of a Ca in the tobermorite structure as X. Guio et Al. describe in their work [194].
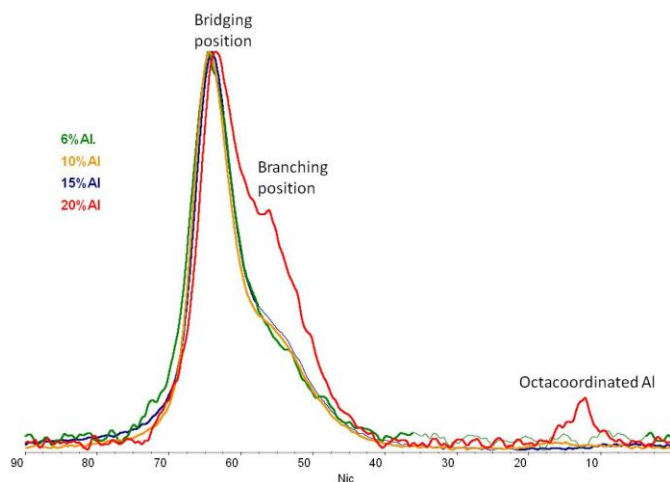
Figure III.1-22: ^{27}Al-MAS-NMR of tobermorite samples with 6%, 10%, 15% and 20% of Al in their structures

It was carried out a deconvolution of the two main bands in the ^{27}Al-MAS-NMR order to know the ratio between the Aluminum that enters in branching position and the one that it does in bridging position, these are reflected in Figure III.1-23.

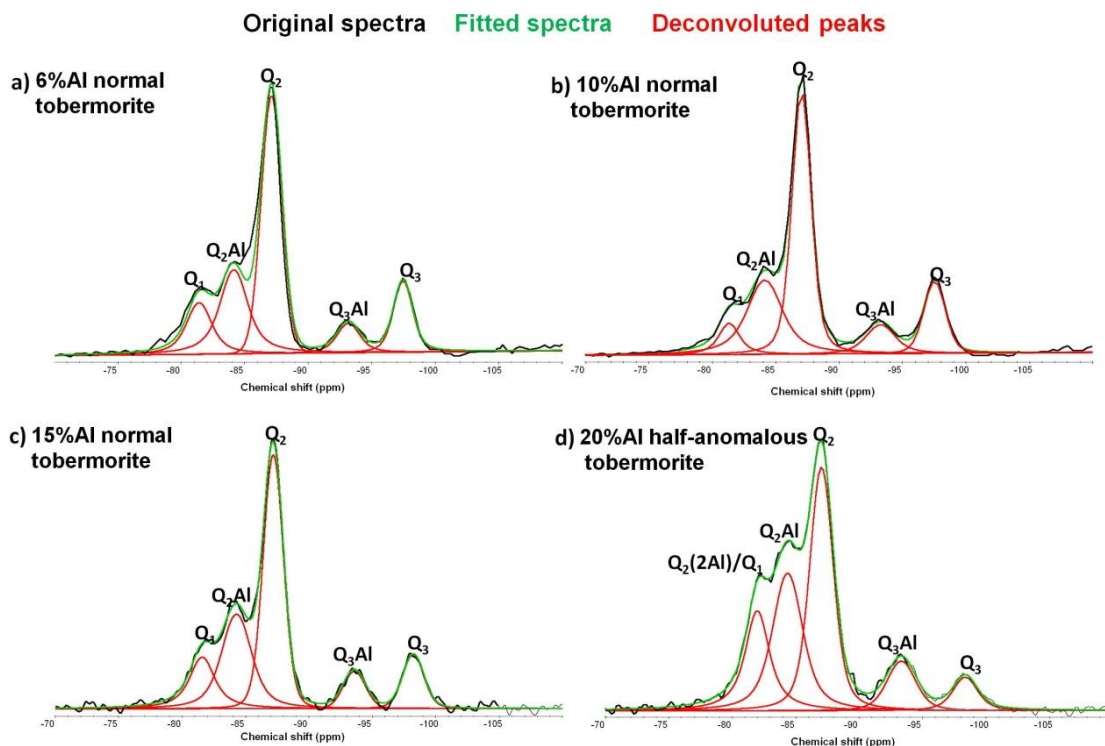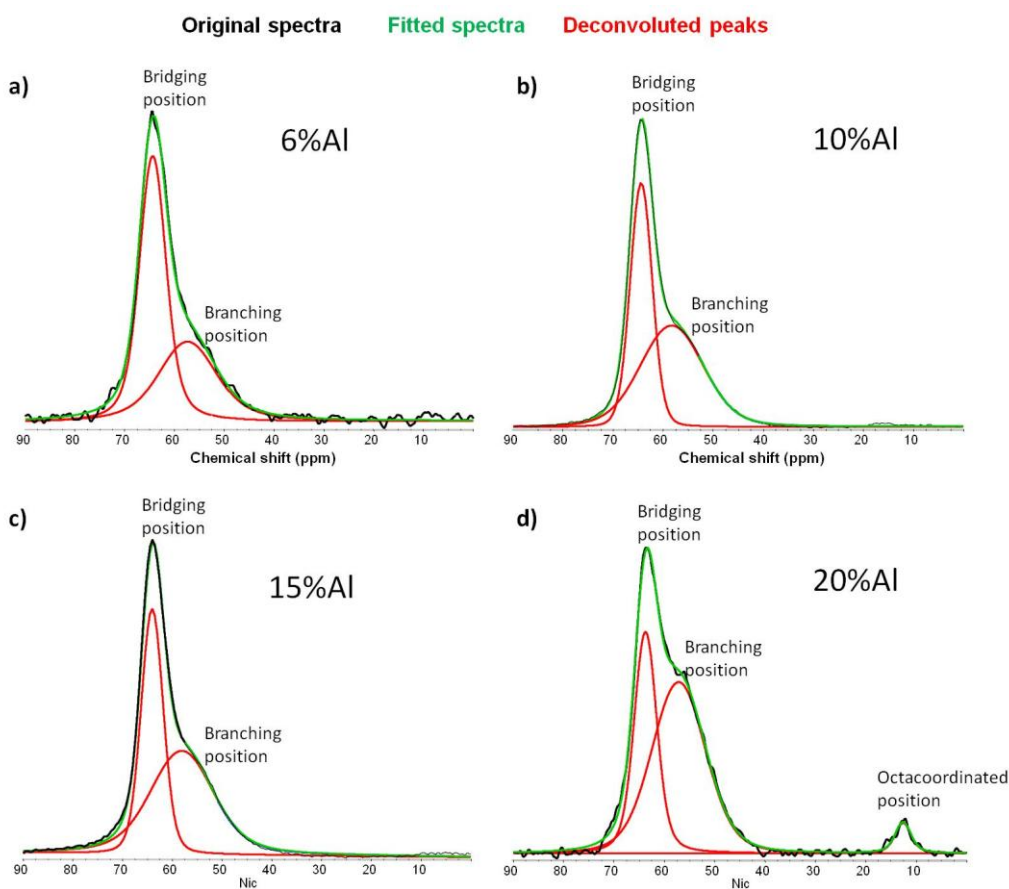**Figure III.1-23: Deconvolution of the ^{27}Al-MAS-NMR spectra. a) 6%Al normal tobermorite, b) 10%Al normal tobermorite, c) 15%Al normal tobermorite and d) 20%Al half-anomalous tobermorite.**

The percentage areas of the deconvolution are summarized in Table III.1-7. According to the results, it can be said that as the Al content is increased, the bridging positions diminish and the branching positions increase. This effect can be related with the one observed in the XRD analyses where the basal peak intensity increased with the increase of the Al content. Matsui et al. [189] relates this effect with an acceleration of the crystallization rate along the c-axis because of the presence of Al. The increase of order in the c-axis can be related with the formation of branching links observed in the ^{27}Al-MAS NMR analysis which occur in that direction. With XRD it was shown that for low Al dosages, there is a large proportion of amorphous C-S-H gel, and a small proportion of crystalline tobermorite. As the Al dosage is increase the proportion of tobermorite increases and the C-S-H gel decreases. This can be correlated with the conclusion extracted from the Q_3/Q_3Al comparison where it was observed that for high Al content, the sample had more Al in branching position. The fact that the Al enters in branching or in bridging does not affect to the total Q_2Al positions, for this reason the Q_2/Q_2Al ratio changes but not so drastically as it does for the Q_3/Q_3Al ratio. So the meaning of this change is only related with the increase of Al dosage.

Table III.1-7 Percentage area of the deconvoluted peaks for each ^{27}Al-MAS NMR spectra.

	Branching	Bridging	Octacoordinated
6%Al	39.6%	60.4%	//
10%Al	54.6%	45.4%	//
15%Al	55.7%	44.3%	//
20%Al	61.5%	34.7%	3.8%

In general, it can be concluded that it is possible to synthesize tobermorite under hydrothermal subcritical conditions. The synthesis was carried out with different atomic Al substitutions for Si in order to know the effect of Al in the formation of tobermorite. With the XRD analyses it was possible to observe that under the same reaction conditions, the higher it is the Al content, the more crystalline is the produced phase. These samples were thermally treated to a thermal treatment to know their behavior to the dehydration process and three different results were obtained. Some samples had

normal behavior, others had anomalous behavior and the third group had an intermediary behavior. However, no apparent reason was found to be form one kind of sample or another. With the SEM analysis it was observed that every sample obtained had platelet morphology preferentially. The Si and Al solid state NMR analyses verified that the Al does enter into the structure taking preferentially bridging positions for low Al dosages and branching positions for high Al dosages. For this reason it is more common to obtain anomalous samples for high Al dosages, because it is more complicated to break a Si-Al bond and therefore the structure does not constrain.

III.2   Supercritical hydrothermal synthesis

In this work we developed a new synthesis for xonotlite and tobermorite based in supercritical water technology. For the supercritical continuous synthesis, it was necessary to design the reactor first. As the xonotlite is more stable than tobermorite and as there was not previous knowledge in the supercritical synthesis of these species, it was decided to start the experiments with xonotlite, so the optimization of the reactor was carried out for this compound.

III.2.1   Supercritical hydrothermal synthesis of xonotlite

The first step before the synthesis was to design the reactor. As it was mentioned before, the supercritical continuous reactors are not commercial, so it was home-made and varied during the experiments to adjust it to our necessities.

In a continuous system, where the precursors are pumped, it is necessary to use soluble products. So, the first step was to choose soluble Si and Ca precursors. Traditionally it has been employed SiO_2 (amorphous and crystalline) and CaO as precursors [144][148][82], but these are not soluble enough, so other possibilities had to be found. After some bibliographic research, we found that some authors used $Na_2SiO_3 \cdot 9H_2O$ and $Ca(NO_3)_2 \cdot 4H_2O$ [151][152] which are highly soluble in water, we decided to use these precursors.

Some parameters must be taken into account for the design of the reactor; the most important one is the residence time of the reagents inside the reactor which will condition the reaction time. This parameter is controlled by different variables like the volume of the reactor, the flow of the precursors (and consequently the capacity of the pump) and the density of the solvent inside (at the temperature and pressure set) and outside the reactor. This is related by the following formula:

$$R_t = \frac{V}{Q} \cdot \frac{\varphi_{(P,T)}}{\varphi_{(P_0,T_0)}}$$

(Equation 7)

With:

$R_t \equiv$ Residence time (s),

$V \equiv$ Volume of the reactor (m^3),

$Q \equiv$ Flow (m^3/s),

$\varphi_{(P, T)} \equiv$ Solvent density inside the reactor ,

$\varphi_{(P0, T0)} \equiv$ Solvent density under atmospheric conditions.

As it is difficult to know the reaction time when it was done for the first time in supercritical conditions it is advisable to design a reactor which, taking into account the flow limits of the pump, can comprise a wide range of reaction times.

Another important factor to control in a continuous reactor is the mixing point. The co-flow mixing is composed of two concentric tubes (one inside of another). At the mixing point, the product pumped through the outer tube mixes with the product pumped through the inner tube. Depending on both flows, the particle is form in one part or another of the flow stream. The particle formation can be focused in the center of the flow stream controlling with the pump the outer and the inner flow (Figure III.2-1). The flow at the mixing point depends on the section of the tube in the mixing point and the flow rate. For an equal flowing velocity, if the outer section is different from the inner section, the flow would be different in the mixing point.
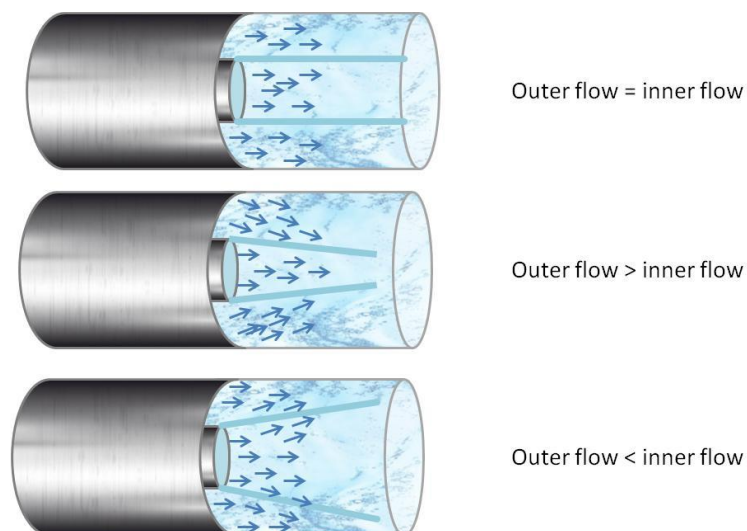
Figure III.2-1: Mixing point representation in function of the outer and inner flux.

As it is explained in Figure III.2-2, in a parallel flow, the velocity in the outer stream is equal to the one in the inner stream and the velocity is the flow divided by the

section of the tube. So, the inner and outer flow ratio is equal to the inner and outer section of the tubes. If the both the outer and the inner sections were equal, we could use the same flow in both pumps to have a parallel flow. However, commonly this does not happen, so the ratio between the inner and outer areas of the section is a constant that we call X. So, to obtain a confluent flow, the ratio between the inner flow and the outer flow should be lower than X. If different flows are employed to obtain a confluent flow, it has to be taken into account the stoichiometry of the reaction in that mixing point and not in the pumping point, so the concentration of the precursors should be re-adjusted in function of the flow applied.
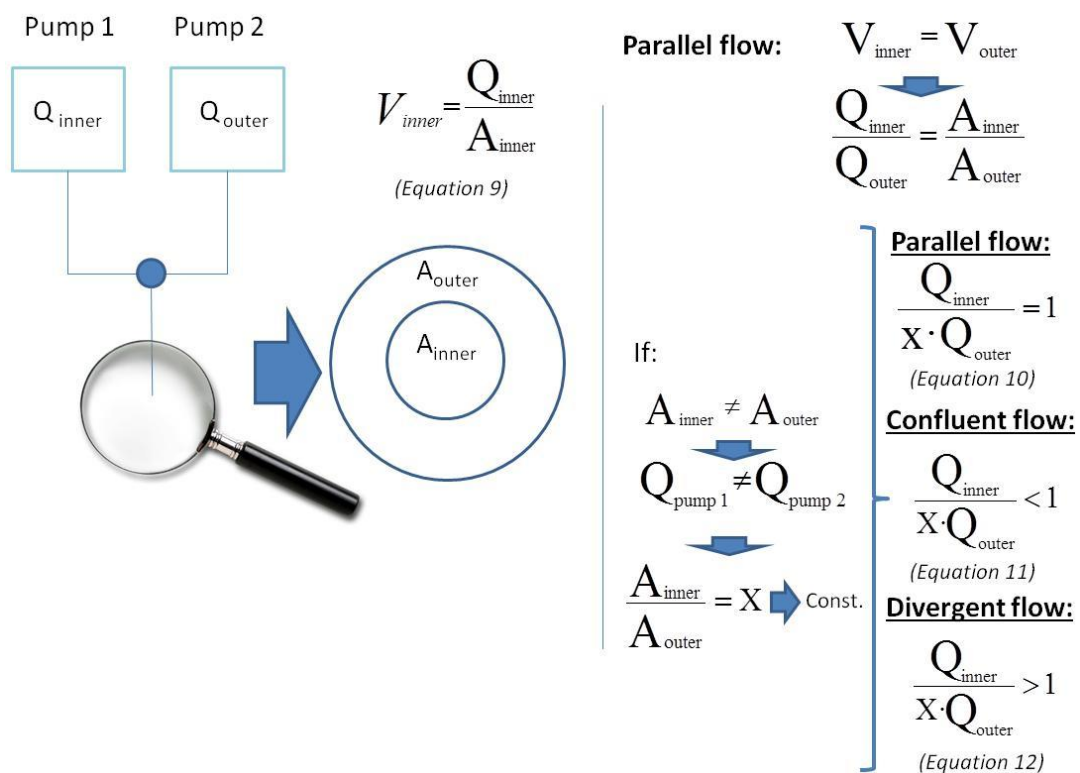
Figure III.2-2: Explanation of the co-flow mixing calculations. Q= flow (m³/s), A= area (m²), V= velocity (m/s)

Depending on the reactor design, it has also to be chosen the best way to heat the system to reach the temperature fast and homogeneously in the entire reactor. For this reason, in some designs, it might be necessary to control the temperature with different thermocouples. Also, the cooling area is important to quench the reaction. Working with supercritical water, when the experiment in supercritical water finishes, it is important to decrease first the temperature under 100ºC, while keeping the pressure and the flow, and then decrease the pressure. This way the system will never pass to gas phase, and

will be keep liquid (Figure III.2-3). Taking all this into account, various set-ups were built and tested until a satisfactory result was obtained.
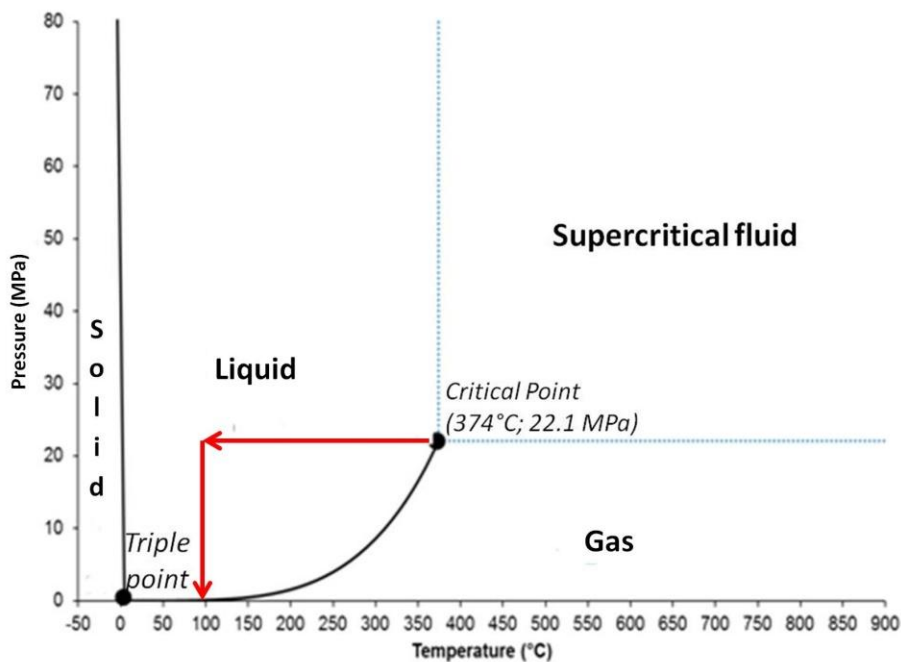
Figure III.2-3: Cooling process to avoid the gas phase

Taking into account these considerations, for the design of our reactor we took as a starting point the general scheme of a supercritical continuous reactor. As it can be observed in Figure III.2-4, it was composed of two pumps, a coflow type mixing point, a reactor made with 2 meters of a 1/16" diameter tube, a cartouche heating system, a quenching bath and a back pressure regulator. From this starting point we adapted the system to the necessities of our specific case up to obtaining of the optimal set up. In the following lines will be described the optimization process.
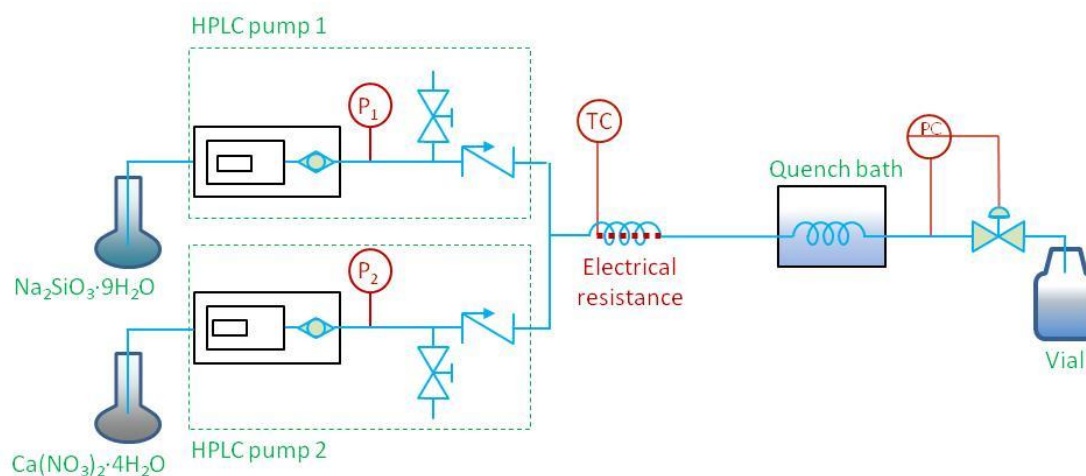
Figure III.2-4: First design done of the continuous hydrothermal supercritical reactor.

In this first design we had many problems of clogging due to the small size of the tubing that we had put. So in the first change we substituted the 1/16" tube of the reactor for 2 meters of a 1/8" size tube. Consequently we needed to change the heating system and put one adapted to the new size of the tube, so we put a ceramic band. With this reactor it was possible to carry out the first experiments and from now on we will refere to this set-up as 1a. Despite the increase in the tube size, there were still cloggings in the BPR, some product got stuck in the valve and just after few minutes of reaction, the system clogged. As a solution, it was proposed a filter to collect the product previous to the valve. A stainless steel fritted filter + reservoir was added after the reactor to collect the particles inside and to cool down the stream inside the filter (Figure III.2-5). We will refer to this set-up as set-up 1b).
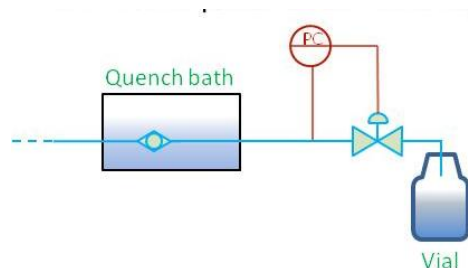
Figure III.2-5: In set-up 1b) was modified the quench line, with the introduction of a 50 μm filter.

Due to the clogging problems, it was also studied the co-flow mixing point. The main advantage of the co-flow is that the mixing point can be closer to the entrance of the reactor and the nucleation can be more controlled. In our case, an amorphous C-S-H gel precipitates as soon as the two precursors are in contact, so it was preferable to use a co-flow system. However, the calcium silicate particles have a big interaction with the reaction walls and can clog the pipes. For this reason it was decided to study our mixing point to control the nucleation point. In Figure III.2-6 is described the mixing point of this set-up and the flow conditions to each mixing type. Every case was tried experimentally but, despite all these efforts to avoid clogging using a confluent mixing type, there were still clogging problems.
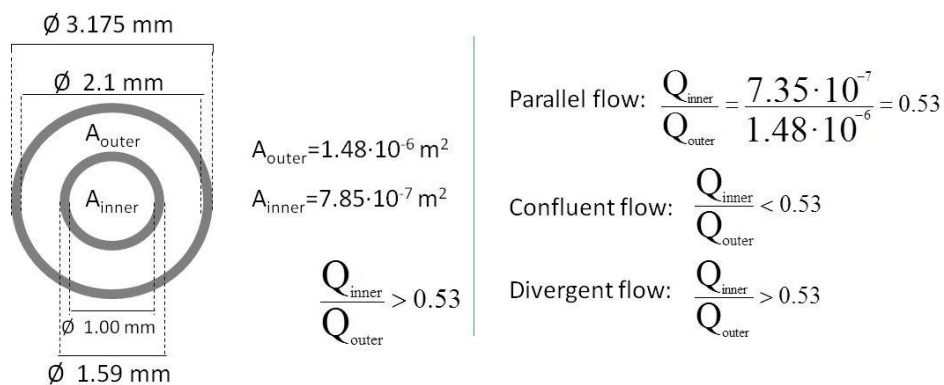
Figure III.2-6: Mixing point calculations for set-up 1.

At this point, for the first time it was possible to obtain Xonotlite. The reaction conditions are summarized in Table III.2-1.

Table III.2-1: Synthesis conditions employed in the set-up 1.

Si source	Ca source	Ca/Si	Temperature	Pressure	Residence time
$Na_2SiO_3 \cdot 9H_2O$ [0.005M]	$Ca(NO_3)_2 \cdot 4H_2O$ [0.005M]	1.00	400ºC	23.5 MPa	20s

However two problems were found, the production was very low, and the tube clogged easily within few minutes after the beginning of the reaction, and the formation of calcium carbonate as a by-product (Figure III.2-8 a). For that reason it was necessary to put a nitrogen source to decarbonate the precursor's solution. (Figure III.2-7). We will refer to this set-up as set-up 1c
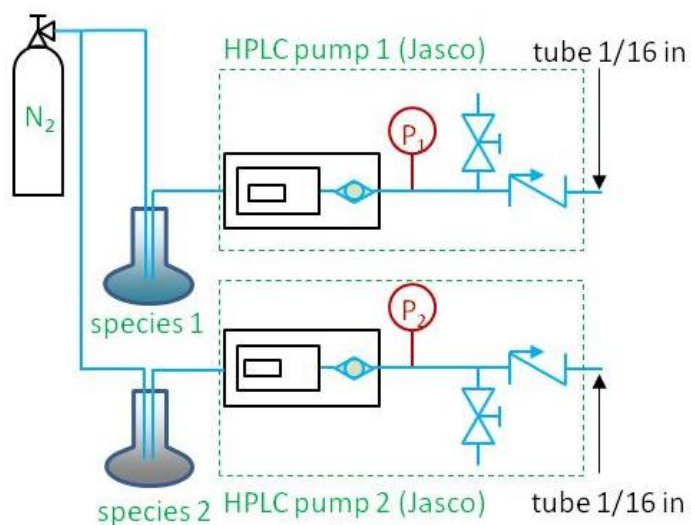
Figure III.2-7: Set-up 1c) with the modification in the inlet adding a nitrogen flow.

In the Figure III.2-8 are represented the XRD patterns of the syntheses carried out in the set-up 1a (Figure III.2-8 a) and 1c (Figure III.2-8 c). In the case of the sample a) it can be observed a very high degree of carbonation (calcite); the bad quality of the pattern is due to the very tiny amount of product that could be extracted from the reactor as a consequence of the clogging. In Figure III.2-8b) is observed the product that was obtained under the same reaction conditions but after the set-up modifications introduced, the XRD pattern is better, and there is no calcite.
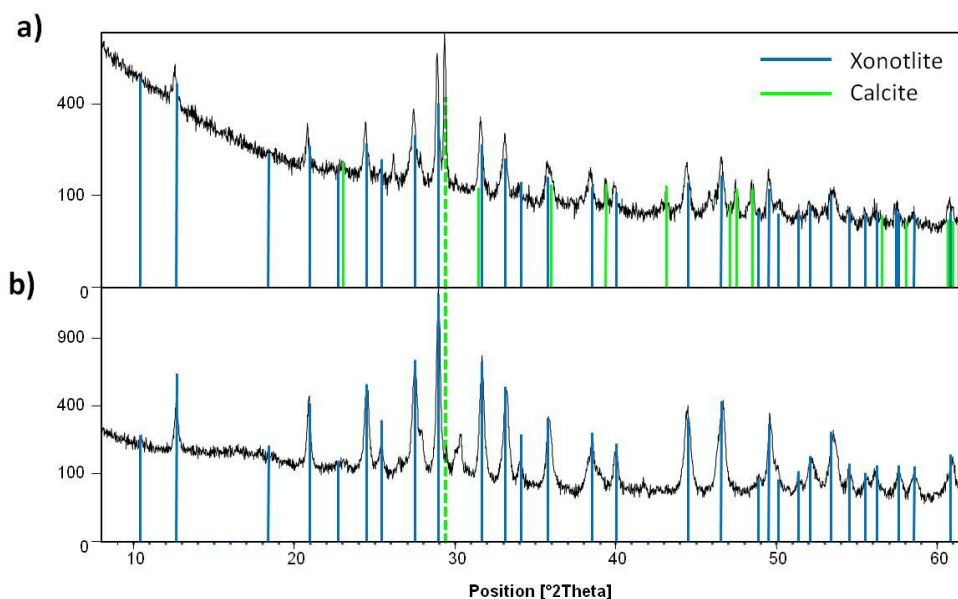
Figure III.2-8: XRD patterns of the product obtained from the supercritical continuous synthesis in the set-up 1a (a) and set-up 1c (b). It is highlighted with a dashed line the main peak of the calcite.

Despite having obtained the desired product in this reactor, the working conditions were not good, and the cloggings were constant, so we decided to modify the reactor one last time in order to obtain more quantity of product and do all the analyses necessaries to characterize the product. Therefore we modified the reactor tube and we replaced it for a system with tubes a 1/4" diameter size. The reactor is composed by 1.6m of 1/4" tube with 3mm internal diameter. In order to adapt he set-up to this size, a new heating system was used, a rolled wire. After each reaction, the set-up was cleaned with an open/close valve to expel all the retained particles and also cleaned with an acid to avoid cross-pollution between syntheses. This is the optimized reactor (Figure III.2-9) and from now on we will refer to it was set-up 2.
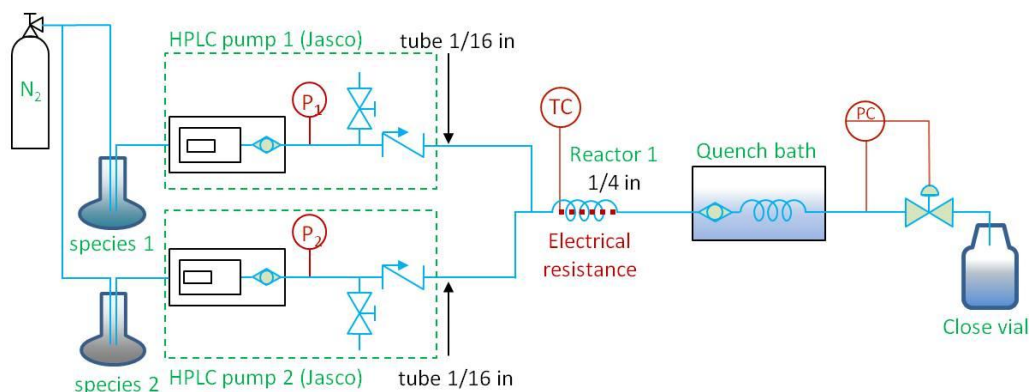
Figure III.2-9: Set-up 2 diagram.

In this reactor, it was possible to carry out the reaction, and several reactions were done under the conditions specified in Table III.2-2. The amount of product at this scale was not high enough to use it in the mechanical test; however, it was enough to study the chemistry.

Table III.2-2: Synthesis conditions employed in the set-up 2.

Si source	Ca source	Ca/Si	Temperature	Pressure	Residence time
$Na_2SiO_3 \cdot 9H_2O$ [0.005M]	$Ca(NO_3)_2 \cdot 4H_2O$ [0.005M]	1.00	400ºC	235 bar	20 s

In Figure III.2-10, we can observe the XRD analysis of the product which is pure crystalline xonotlite. The sample is compared with the pdf file (00-023-0125) which is a synthetic pattern from Osaka (Japan) prepared from equimolar amounts of lime and quartz at 200°C for 24h. L.Black et al. [82] reported that under hydrothermal conditions the extent of preferential orientation of the crystals along the directions (0,0,l) and (h,0,l) increases with increasing synthesis temperature. However, by comparison of the intensity distribution with the one of the powder diffraction file (PDF 00-023-0125), no preferential orientation was observed in this work, in spite of performing the synthesis at much higher temperatures than them. This might be due to the difference in the synthesis method and to the much shorter reaction time. It is also interesting to note that there is an almost perfect agreement between the positions of the peaks in our sample and the PDF 00-023-0125. The only exception corresponds to reflection at 25.4º (002) which is related to basal spacing. The d spacing obtained

(3.49Å) is slightly smaller than that of the powder diffraction file (3.50Å), suggesting a slight deviation from the perfect structure. Nevertheless, such deviation is too small like to be attributed to the systematic incorporation of foreign ions or defects into the structure.
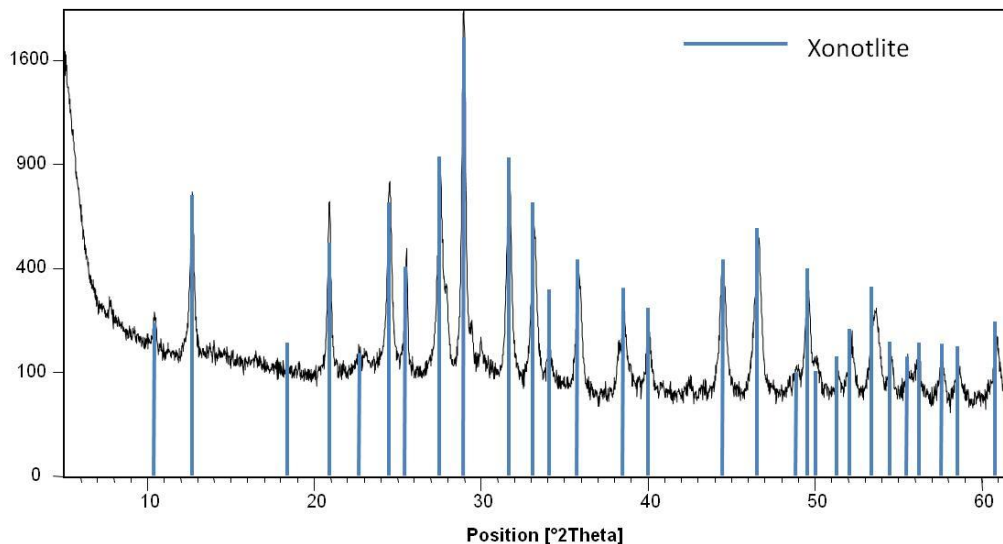
Figure III.2-10: XRD pattern of the product obtained in the set-up 2.

In the FTIR spectrum of the xonotlite sample, see Figure III.2-11, we can identify the main characteristic bands of the compound [148][195]: The ones at 611cm^{-1} and 671cm^{-1} correspond to the Si-O-Si bending vibrations. The band at 973cm^{-1} is attributed to the Si-O symmetric stretching modes. The one at 1082 cm^{-1} corresponds to the Si-O-Si symmetric stretching modes. The band at 1200 cm^{-1} is assigned to the Si-O stretching vibrations in Q^3 sites (the ones of the silica tetrahedral linked to 3 other tetrahedra), and the band at 455cm^{-1} are due to the bending rocking of Si-O-Si. Xonotlite shows a very sharp spike at 3614cm^{-1} which is due to Ca-OH stretching vibration and its bending mode at 632cm^{-1}. Xonotlite's structure has two hydroxyls in the Ca-O sheets which are the ones that are identified in this spectrum. The bands at 1638cm^{-1} and the one at 3452cm^{-1} are assigned to the water scissoring bending mode and its antisymmetric stretching vibration, respectively. In the case of the presence of Si-OH bonds, they would also be part of the wide band centered at 3413cm^{-1} what would make them difficult to distinguish [110]. The peak situated at 1000cm^{-1} might suggest the presence of Na-SiO bonds, although the absence of its asymmetric vibration at 897cm^{-1} generates doubts about such assignation [196]. Generally, xonotlite shows better resolved O-Si-O and Si-O-Si bands than other calcium silicates like tobermorite

because silicate chains are more ordered and occupy more symmetrical sites in the crystal structure.
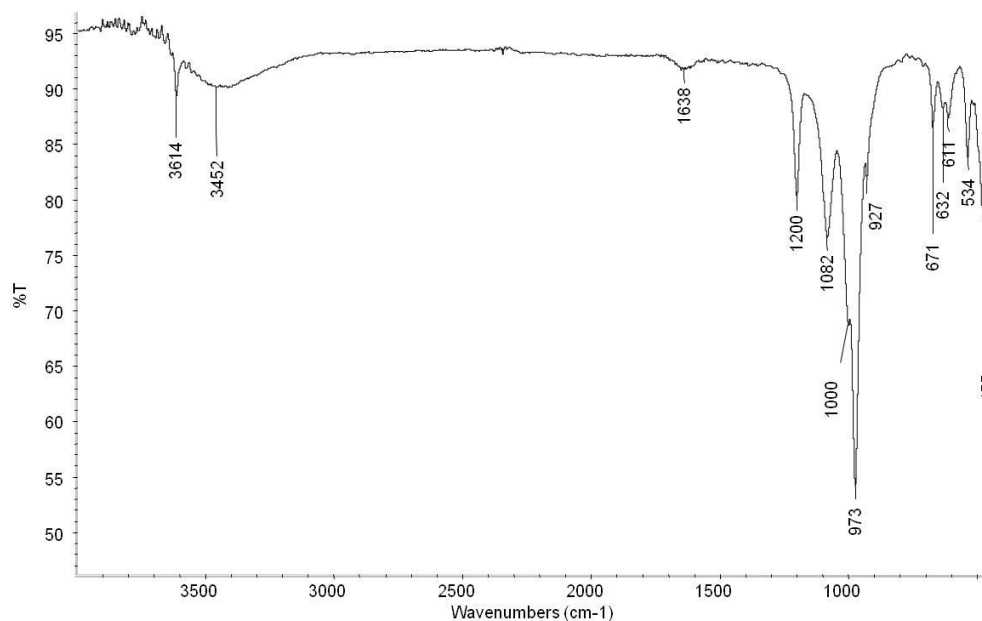
Figure III.2-11: FTIR spectrum of the xonotlite obtained in the continuous supercritical hydrothermal reaction in set-up 2.

^{29}Si MAS-NMR analysis was also carried out in order to study the local environment of Si atoms in the sample. Obtained spectrum, see Figure III.2-12, consists of two main peaks centered at -89ppm and -99ppm with an intensity ratio 2:1 similar to xonotlite synthesized by other methods[197][147][146][54]. Using common notation Qn, where "n" represents the number of bridging oxygen sites per silicon tetrahedron "Q", the peaks can be identified as Q^2 and Q^3, respectively. The deconvolution of the spectrum was performed using OMNIC 7.2, assuming Voigt line shapes and no loss of information to spinning side bands. The ratio of the areas of the deconvoluted peaks Q^2: Q^3 was approximately 2:0.7. However, the crystal structure of ideal xonotlite is composed of parallel SiO_4 chains with "dreierketten" arrangement which are bonded to each other every three SiO_4 tetrahedra. As a consequence, the ratio of Q^2: Q^3 should be 2:1. Such discrepancy indicates that some Q^3 Si sites are missing. Previous research works on both natural and synthetic xonotlite have also shown deviations from the ideal structure. For example, ^{1}H MAS NMR spectra proved the presence of Si–OH linkage [111], while perfect crystals should only contain one type of OH groups attached to Ca atoms like in portlandite [110]. Churacov et al. [110], after studying by computational simulation the substitution of OH groups for Q^2 and Q^3 types of Si atoms in the structure of xonotlite, concluded that substitution should take place preferentially in Q^3

positions, affecting simultaneously to the paired Q^3 Si atoms. However, this solution is not valid in our case because it would not vary Q^2:Q^3 ratio and, also, it would imply the apparition of Q^1 type of chain ends in a significant proportion which was not observed in this work. Comparison of cross-polarized ^{29}Si MAS-NMR data with the results of direct pulse proton decoupled experiments, see Figure III.2-12, indicated that the ratio of the areas Q^2:Q^3 is larger in the first case. This not only confirms the proximity of H atoms to Si atoms but it indicates that, on average, the interaction is stronger in the case of Q^2 atoms. Furthermore, the Q^2 peak of the direct pulse experiment contains two maxima. Although they are too close like to deconvolute them as two separate peaks, they are a clear evidence of two different Si environments. A possible explanation would be that some of the Si-O-Si bonds linking adjacent chains are missing and protons or other ions enter into the structure for charge balancing. Nevertheless, it would be normal to expect that this would induce a distortion of the crystal structure much more important than the slight variation in the basal spacing observed by X-ray diffraction; unless such change took place on the surface of the crystal.
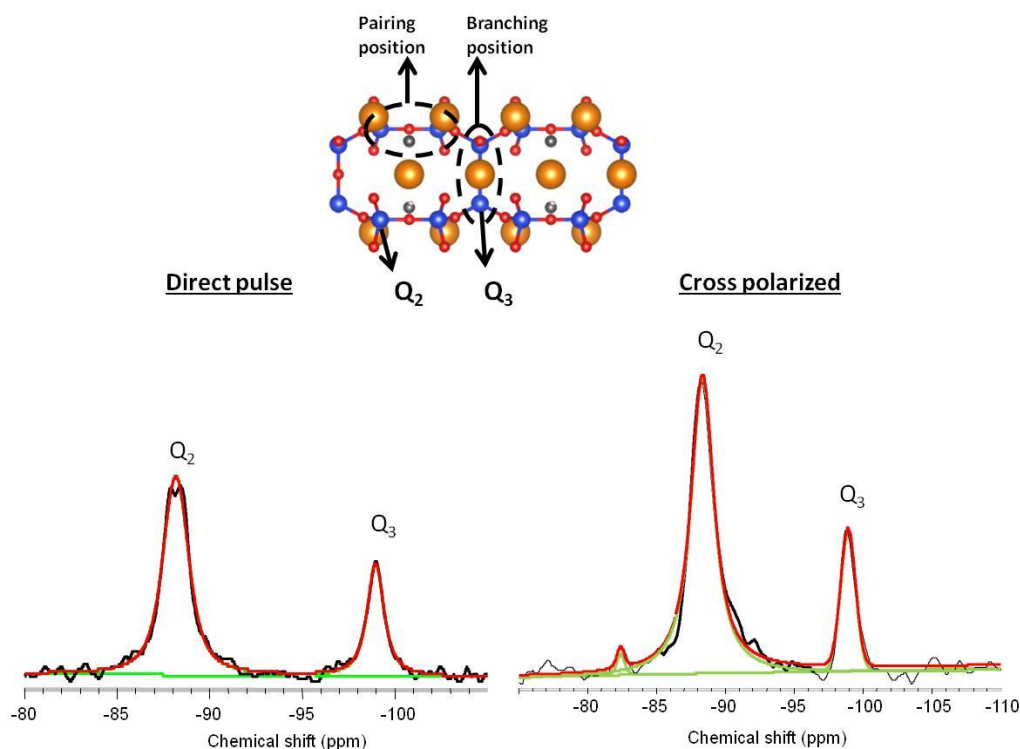
Figure III.2-12: ^{29}**Si MAS-NMR spectrum of the "supercritical" xonotlite. Orange spheres represent Ca, blue spheres, Si and red spheres are oxygen and small grey spheres represent water.**

As a first approximation, we assumed that the surfaces of the crystal in the direction (h,0,0) consists of single silicate chains, see Figure III.2-13, so it is possible to correlate the Q^2:Q^3 ratio with the length of the crystal along (h 0 0). Let's be a, b, c and A, B, C the dimensions of the unit cell and the crystal, respectively along the three crystallographic planes. Then, the number of dual silicate chains (NDC) in the crystal is given by:

$$NDC = 2 \times \frac{A - {a}/{2}}{a} \times \frac{C}{c} \qquad \textit{(Equation 13)}$$

And the number of Q^2 and Q^3 type Si atoms is:

$$Q^2 = 4 \times NDC \times \frac{B}{b} + 6 \times \frac{B}{b} \times \frac{C}{c} \qquad \textit{(Equation 14)}$$

$$Q^3 = 2 \times NDC \times \frac{B}{b} \qquad \textit{(Equation 15)}$$

Where the second term in the expression for Q^2, corresponds to the single chains in the two (h 0 0) surfaces of the crystal. From there the Q^2:Q^3 ratio would be given by:

$$Q^2 : Q^3 = \frac{4A + a}{2A - a} \qquad \textit{(Equation 16)}$$

It is interesting that with this approach Q^2:Q^3 ratio depends only on the dimensions of the crystal along the direction (h 0 0). Substitution of the Q^2:Q^3 ratio resulting from the deconvolution gives a value about 4nm for A.
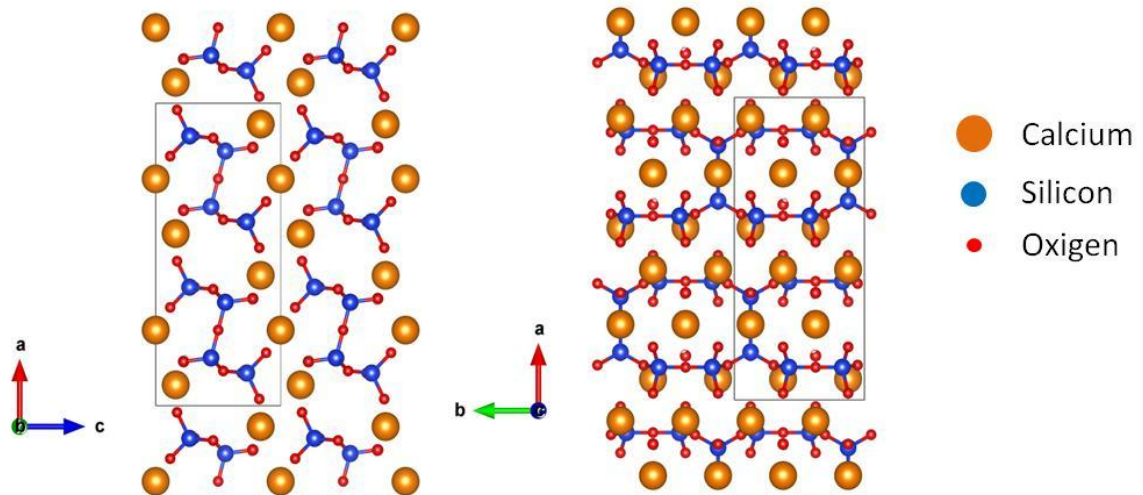
Figure III.2-13: Schematic representation of the crystal with top and bottom surfaces consisting of single silicate chains. The gray rectangle represents the limits of the unit cell. The axis of the nanofibers would be coincident with the axis b.

In order to know if this theory had a real meaning, and the assumption that we took that the crystal grows in the (h,0,0) plane on the surfaces was real, it was studied by SEM and TEM. As can be observed in Figure III.2-14, xonotlite crystallized in the form of flat fibers of 1-10µm long and 50-200nm wide. Lin et al., using the same reactants, obtained similar fibrous results but only after 24h of hydrothermal treatment at 200ºC [151].
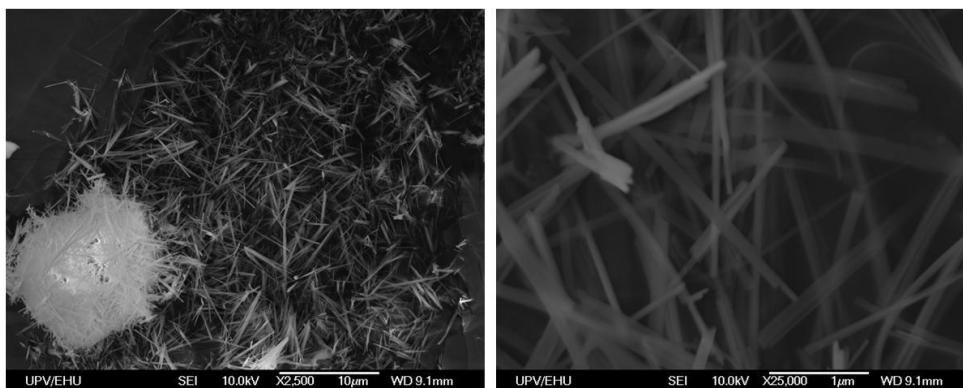
Figure III.2-14: SEM image of the xonotlite fibers obtained from the continuous supercritical hydrothermal synthesis.

In order to know the preferential growing direction of the crystal, a TEM analysis was carried out. As it can be observed in Figure III.2-15, the xonotlite is very crystalline, and it is possible to see some of the diffraction planes of the structure: such as the (2,0,0) and the (3,2,0). With this information, it is possible to know that the fiber grows along the direction of the silicate chains in b direction and the plane of the surface is the (0,0,l), so this evidence dismantles the theory proposed previously. The less favorable growing direction is the one corresponding to c-axis. So the defects in the structure are linked to the lack of Q_3 positions, but it cannot be related to a specific and continuous defect along the surface of the crystal but some random defects.
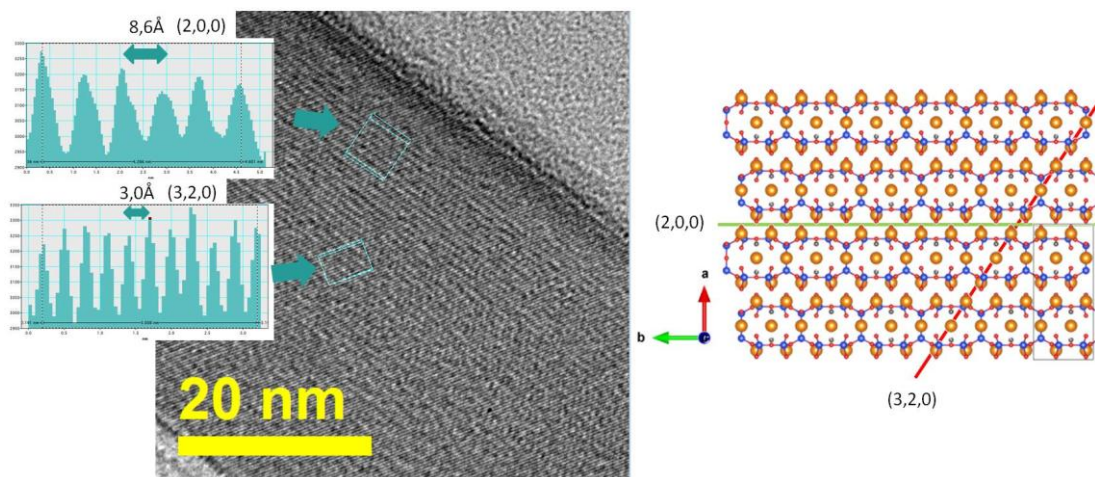
Figure III.2-15: TEM analysis of the xonotlite fibers and identification of two characteristic planes of the xonotlite structure. Orange spheres represent Ca, blue spheres, Si and red spheres are oxygen and small grey spheres represent water. The gray rectangle represents the limits of the unit cell.

This study proved the feasibility of producing inorganic nanofibers, in record breaking times, by means of continuous reactors working under supercritical water conditions. In particular, the synthesis time of xonotlite, which is normally larger than 5h, was reduced to only 17s by carrying the reaction at 400ºC and 23.5 MPa. Obtained product consisted of flat nanofibers of 1-10µm long with a length to diameter ratio of the order of 100. Structurally, synthesized xonotlite nanofibers were highly crystalline. However, some structural defects were observed in the structure.

III.2.2   Supercritical hydrothermal synthesis of tobermorite

For the synthesis of tobermorite, it was also employed as precursors $Na_2SiO_3 \cdot 9H_2O$ and $Ca(NO_3)_2 \cdot 4H_2O$. As it was mentioned in the introduction, for the synthesis of tobermorite, it is common to introduce aluminum as silicon substitute to stabilize earlier the tobermorite[95]; as a soluble Al precursor, $Al(NO_3)_3 \cdot 4H_2O$ was used. The decision of the Al dosage was based on the literature[95][92][77][191], so it was decided to use 15% of Al. It was possible to obtain tobermorite in two of the set-up designed.

In the set-up 1.c) were done more than sixty unsuccessful syntheses varying the composition the residence time, the %Al, the Ca/Si ratio… However, the constant problem of the clogging didn't allow us to work in good conditions and the product obtained from the reactions were not very reliable as we couldn't assure that the residence time was the one programmed. Due to the clogging, the product had been

stuck in the reactor for an unknown time, and the obtained product was not valid. The reaction conditions are summarized in Table III.2-3.

Table III.2-3: Reaction conditions employed in the continuous supercritical synthesis of tobermorite.

Si source	Ca source	Al source	$\dfrac{Ca}{(Si+Al)}$	$\dfrac{Al}{(Si+Al)}$	Temperature	Pressure	Residence time
$Na_2SiO_3 \cdot 9H_2O$	$Ca(NO_3)_2 \cdot 4H_2O$	$Al(NO_3)_3 \cdot 9H_2O$	0.83	0.15	400ºC	23.5 MPa	10 s

In the Figure III.2-16 we can observe the XRD carried out to the reaction product. As it can be observed, it was possible to obtain tobermorite but not pure. As it was mentioned in the introduction at high temperatures the tobermorite is a metastable phase that can transform into xonotlite which is the other phase that was found in this sample. However, with this set-up it was not easy to control the residence time of the reaction because of the clogging. This fact made it very hard to control the kinetic and get only the pure phase. There could also be problems of cross-contamination between reactions because the reactor was not properly clean.
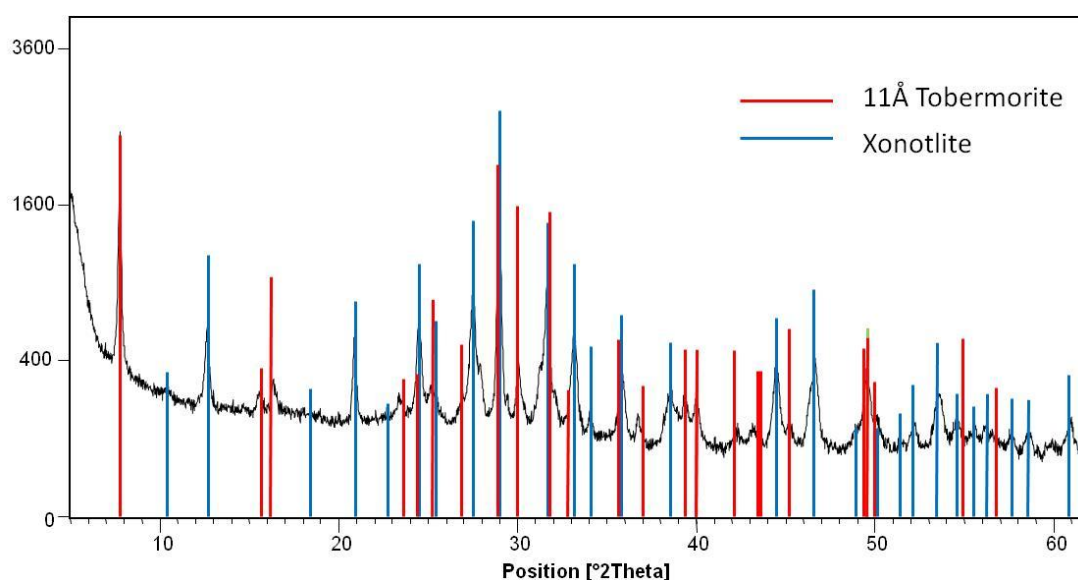
Figure III.2-16: XRD of the product obtained from the synthesis of tobermorite in the set-up 1c).

In the reactor 2 it was possible to do the synthesis at two reaction times (15 and 7 seconds). The XRD analyses of the products are shown in Figure III.2-17. The

positions of the main peaks of the obtained X-ray diffraction pattern match with those of tobermorite (pdf 01-083-1520) and xonotlite (pdf 00-023-0125). The intensity of xonotlite's peaks clearly decreases with decreasing synthesis residence time passing from being the main phase in the 15s to a minority in the 7s' one.

These results contradict what is commonly described about the tobermorite stability which has been widely described in the introduction. According to most of the authors, the tobermorite is methastable at high temperatures [137][144][77][140]. Depending on the author, it is described one temperature or another depending on the synthesis conditions employed for each case. These experiments expose the evidence that it is possible to obtain tobermorite above that temperature using supercritical water. The synthesis happens under metastable conditions for the tobermorite; however, the possibility to control the reaction time makes possible to control the system and obtain almost pure tobermorite. This accuracy in the reaction time, in terms of seconds, is only possible to obtain with the continuous reactor and the quenching at the exit of the reactor. The effect of the time in the crystallization of tobermorite and its transformation into xonotlite was studied by T.Mitsuda[95], El-Hemali[92] and S.Shaw[77]; however, none of them did the study in supercritical conditions.
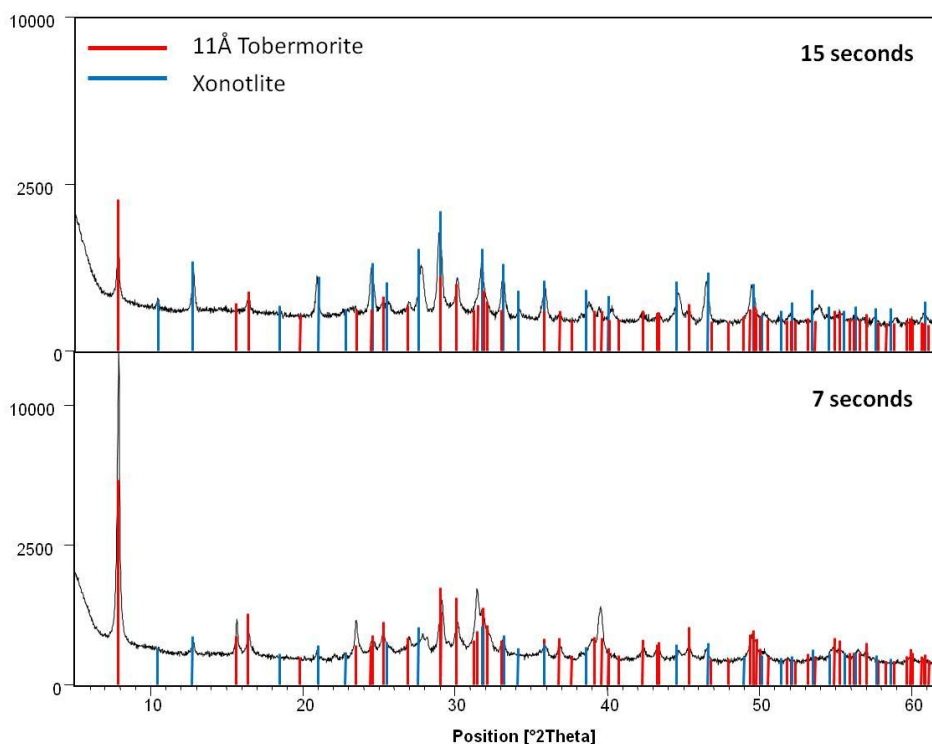
Figure III.2-17: XRD of the product obtained from the syntheses of tobermorite in the set-up 2 with 15 and 7 seconds of residence time respectively.

In the FTIR spectra (Figure III.2-18), it is easy to identify the characteristic bands common to many calcium silicate hydrates. The Si-O stretching (O-SiCa, O-Si2) at 970 cm^{-1}, the Si-O stretching (O-links bet. bridging tetr.) at 1166 cm^{-1}, the Si-O stretching (OH-SiCa in bridging tetr.) shoulder at 916 cm^{-1}, the O-Si-O bending at 668 cm^{-1}, the deformations of Si tetrahedral at 452 cm^{-1}, the OH stretching of absorbed molecular water (Si-OH····H2O) at 3427 cm^{-1} and the water bending at 1634 cm^{-1}. The small band at 3614 cm^{-1} corresponds to the Ca-OH vibration, and it is, therefore, characteristic of xonotlite. As can be observed, its intensity increases with increasing synthesis time, in good agreement with X-ray patterns. On the contrary, the band at 1166 cm^{-1} is, according to some authors [81][198], characteristic of anomalous tobermorite and can only be clearly identified in the shortest synthesis time (7s). Finally, it is worth to highlight that there is no evidence of the presence of secondary products like calcite (main band at 1434 cm^{-1}) or calcium hydroxide (main band at 3640 cm^{-1}).
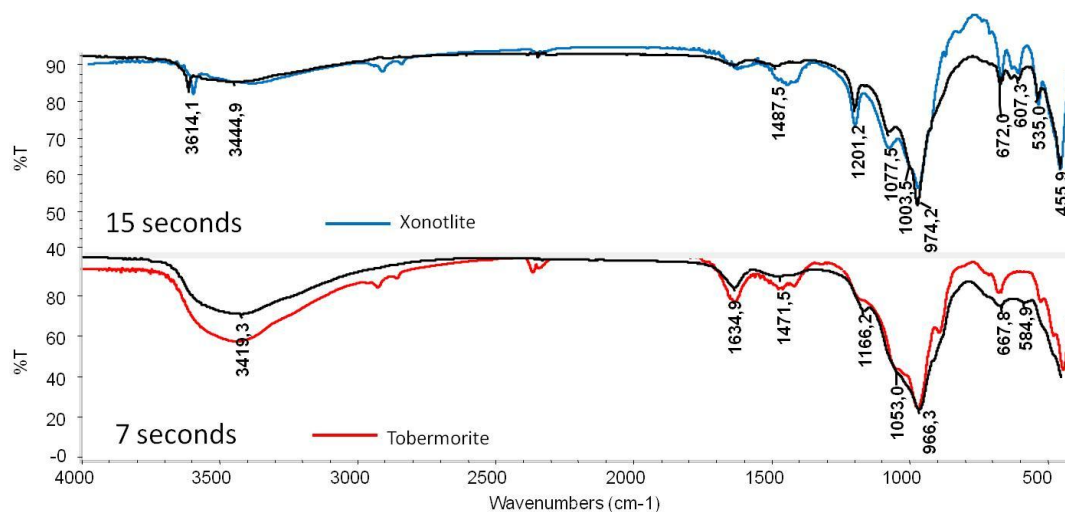
Figure III.2-18: FTIR of the products obtained after 7 and 15 seconds of reaction in supercritical conditions. The tobermorite and xonotlite pattern spectra (black) are extracted from RRUFF database [199]**.**

In the X-ray diffraction pattern of the sample synthesized in 7 seconds can be highlighted one fact, the anomalous increase of the peaks in one specific direction. The predominance of the (0,0,l) lattice component, Figure III.2-19, is particularly evident in the extremely large intensity of the basal reflection (0,0,2) observed at 7.8° 2θ. Some authors attributed this effect to an acceleration of the crystallization rate along the c-axis because of the presence of Al [189]. Nevertheless, comparison with tobermorite with similar Al content synthesized at 215ºC during 4h in a batch reactor questions such affirmation. The supercritical tobermorite was compared with the reference pdf 01-083-

1520 which is the measurement of a natural sample from Germany classified as "tolerable despite the unusual density" of the main peaks and studied by Hamid et Al.[200]. The subcritical sample instead was compared with the pdf 00-045-1480 which is a natural tobermorite from Fuka which is classified as "indexed"[201].
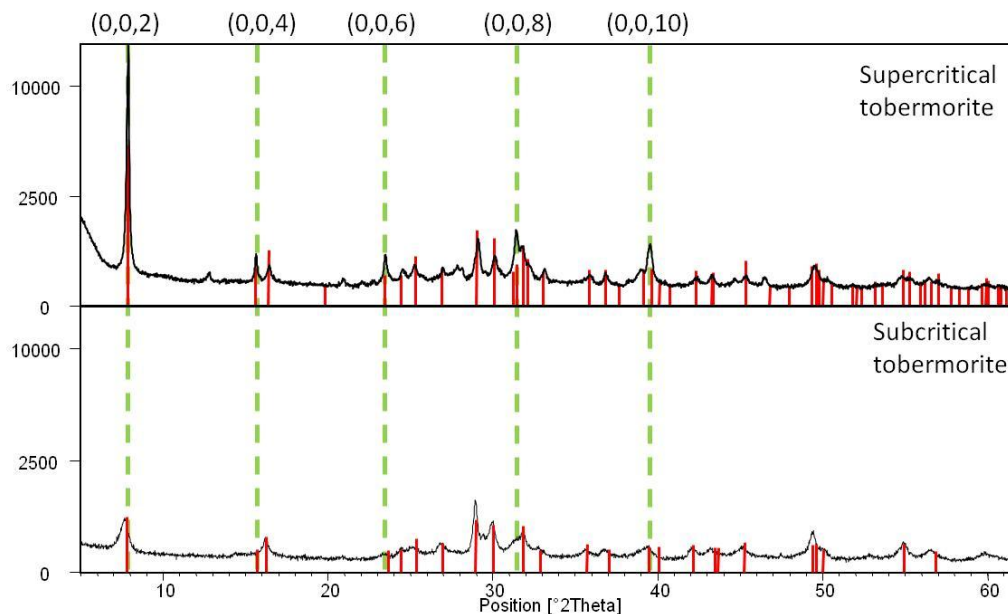
Figure III.2-19: Comparison between the patterns of the products obtained under supercritical and subcritical conditions. The dotted lines are the position of the signals in the (0,0,l) direction.

This preferential plane (0,0,l) is represented in Figure III.2-20. The high intensity of those peaks means that, in the powder, the crystals are preferentially oriented in that direction, and it could be due to morphological differences with the subcritical tobermorite.
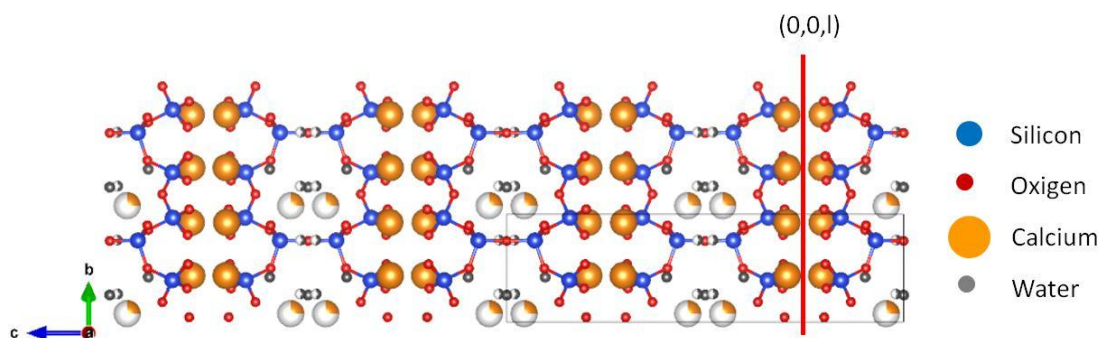
Figure III.2-20: 11Å tobermorite structure and the plane (0,0,l). The gray rectangle represents the limits of the unit cell.

Some image analyses were carried out to study the morphological differences. The SEM images of the supercritical product (Figure III.2-21a, b, and c) shows a very

well structured morphology with fibrous shape. The fact that aggregates of small fibers coexist with large individual fibers suggests that crystal growth takes place through a homogeneous nucleation process [80]. I.e. aggregates composed of small fibrous particles form first (Figure III.2-21c), then they grow forming bigger fibers (Figure III.2-21b) and finally, they disaggregate in large single units (Figure III.2-21a). In general, fiber length varies in the range of tenths of micrometers while their width is in the order of nanometers. However, some larger fibers are also present. It is interesting that such large fibers show splitting into smaller ones at their ends, suggesting that when they grow too much, thinner structures are more stable (Figure III.2-21b). L. Black et al. [82] called this phenomenon "feathering" when they observed it on xonotlite. They explained it by the dissolution of interlayer calcium at high temperature that led to fiber splitting; what might also be the case in tobermorite formation.
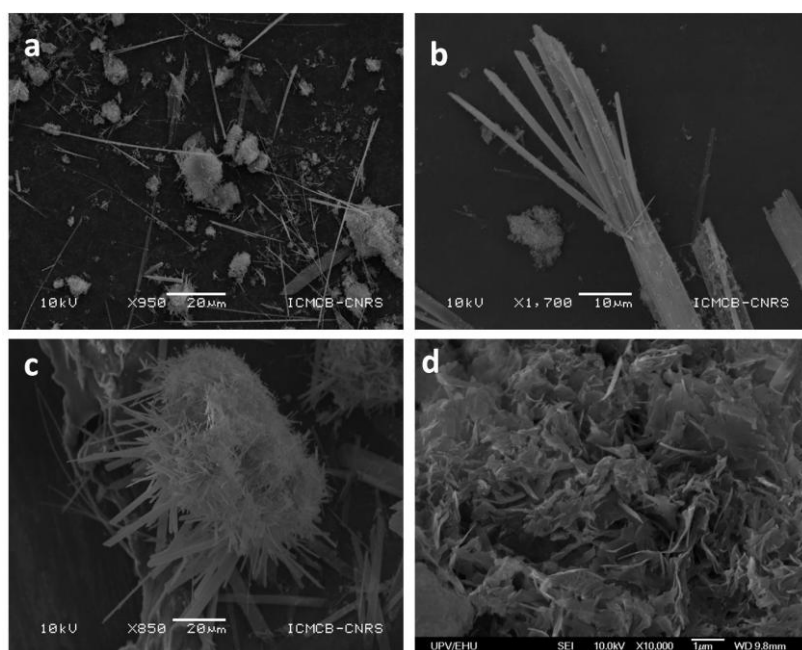
Figure III.2-21: SEM images of the tobermorite, a),b),c) under supercritical conditions and d) under subcritical conditions.

It is also worth stressing, that, compared to most artificial tobermorite samples, the product synthesized in this work is more similar to the natural one, suggesting that the new synthesis method captures more truthfully the formation process that takes place in nature. Generally, natural tobermorite crystallizes in the form of fibers, or plates [78][47][14][43]. On the contrary, synthetic tobermorite is normally obtained as foil like[16][5][28][43] unless templates are used to induce fiber formation[15][22]. At first thought, this difference might be related to a kinetic effect: natural tobermorite has

many years to crystallize while synthetic varieties have to form in much shorter time. However, this would imply that mineral tobermorite crystallizes at very low temperature because it is unstable at high temperatures. On the contrary, in the laboratory, the temperature must be increased as much as possible to speed up the process and only an accurate control of the reaction/crystallization time can prevent the formation of other phases. The problem is that such control is difficult to attain by traditional batch methods. Furthermore, at the mild temperatures normally used (<250ºC), the crystallization of tobermorite is still relatively slow and more stable phases begin to form before the process finishes. In consequence, the synthesis has to be prematurely stopped giving as a result foil-like structures instead of fiber. Using continuous flow reactors and supercritical water conditions, such problems are avoided, and fibrous tobermorite is obtained. This not only suggests that mineral tobermorite might form under similar conditions, but it also proves that this method is better than the traditional one.

The supercritical tobermorite was also analyzed with HR-TEM to visualize the structure order and see the preferential direction to grow. TEM image (Figure III.2-22) shows the basal distance between the calcium layers of approximately 11Å. The orientation of these calcium layers indicates that the c axis is perpendicular to the fibers. This suggests that the large intensity of the (0,0,l) peaks of the X-ray diffraction pattern might not only be due to the long range order along the c axis but also to the preferential orientation of the fibers during the measurement.
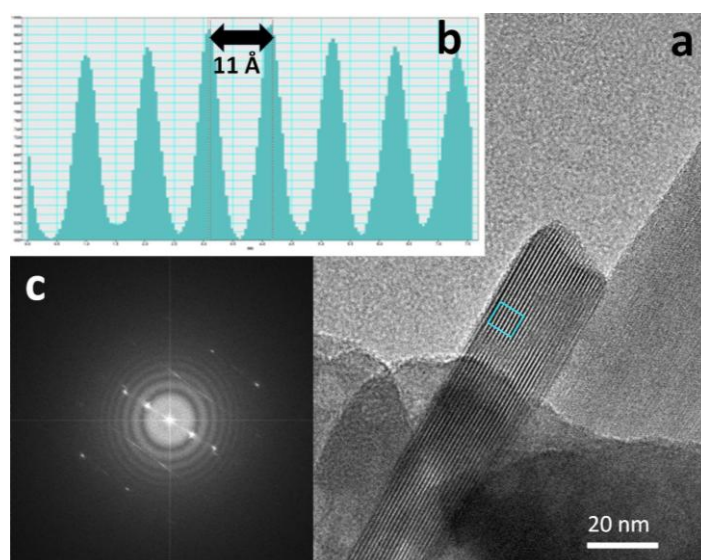
Figure III.2-22: TEM analysis of the 11Å tobermorite obtained under supercritical conditions. a) TEM image of a fiber, b) profile image representing the planes corresponding to the basal

peak with a distance of 11Å between planes and c) FFT image of the fiber also representing the basal planes.

To be sure if all the aluminum that had been introduced in the synthesis had reacted (and it didn't remain in solution), an XRF analysis was done. The results show a Al(Si+Al) ratio of 0.16, so it is in agreement with the amount introduced (0.15). This technique measures the total elemental Al, so it does not mean that all the Al has entered in the structure. In order to know that, a ^{27}Al-MAS-NMR should have been done.

In order to know how does that the aluminum enters into the structure, a solid state ^{29}Si-MAS NMR analysis was carried out. . The deconvolution of the spectrum was performed using OMNIC 7.2, assuming Voigt line shapes and no loss of information to spinning side bands. ^{29}Si MAS-NMR spectrum (Figure III.2-23) shows three distinctive peaks at -85, -88 and -98ppm, a clear shoulder at -92ppm and a tail downfield. The two most shielded peaks (-88 and -98ppm) are attributed to Si atoms bond solely to other Si atoms by O bridges (Q_2 and Q_3, respectively). On the contrary, the remaining peak and the shoulder ($Q_2 1Al$ and $Q_3 1Al$, respectively) confirm the substitution of Al for Si in the silicate chains

Finally, the tail downfield is more difficult to explain, since in perfect anomalous tobermorite Q_1 and bridging Q_2 should be small. Although it is generally accepted that Al substitution takes place preferentially at Q_3 positions, some works proved that it could also take place in bridging positions [191][194][99], what might explain not only the presence of that tail but why $Q_3 1Al$ is not so well defined.
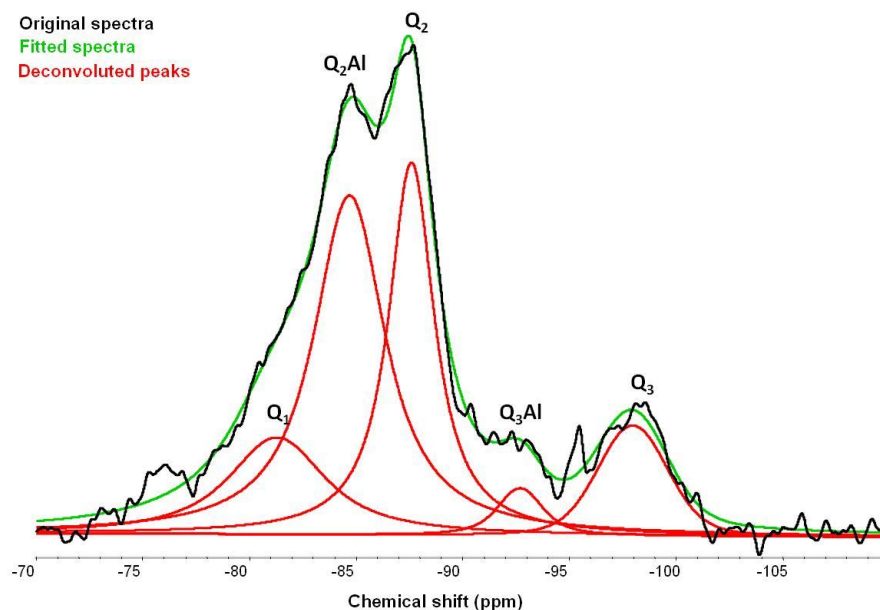
Figure III.2-23: ^{29}Si MAS-NMR spectrum of the supercritical tobermorite.

In Table III.2-4 are the areas of the ^{29}Si-MAS NMR deconvoluted signals. In order to know how the Al is introduced in the sample, a comparative study was carried out between the signal of the Si in Q_2 and Q_3 positions in comparison with the signals of Si also in Q_2 and Q_3 position but with the influence of Al in adjacent positions. It was observed that in this case enters preferentially in Q_2 positions rather than Q_3 positions. These results don't fit with what is generally described in literature that they say that the Al enters preferentially in branching position [191]. It might have been necessary to carry out a ^{27}Al-MAS NMR analysis to distinguish between bridging and branching positions but we had no more product remaining to do it.

Table III.2-4 Area of the deconvoluted ^{29}Si-MAS NMR peaks and the ratio between the signals of the Si and those with Al influence.

	Q_3	Q_3Al	Q_2	Q_2Al	Q_1	Q_2/Q_2Al	Q_3/Q_3Al
15%Al	10.3%	3.3%	30%	41%	15%	0.725	3.088

To fulfill the analysis of the sample it was done a thermal treatment at 300ºC for 24 hours to confirm its "anomalous" nature as it was shown in the infrared spectra. The resulting product was analyzed by XRD, and it resulted being "anomalous" (Figure III.2-24) because the basal peak remains fixed in the position at 11Å. It is remarkable that the first peak keeps being extraordinary big comparing with the amorphization observed in the subcritical samples (Figure III.1-5).
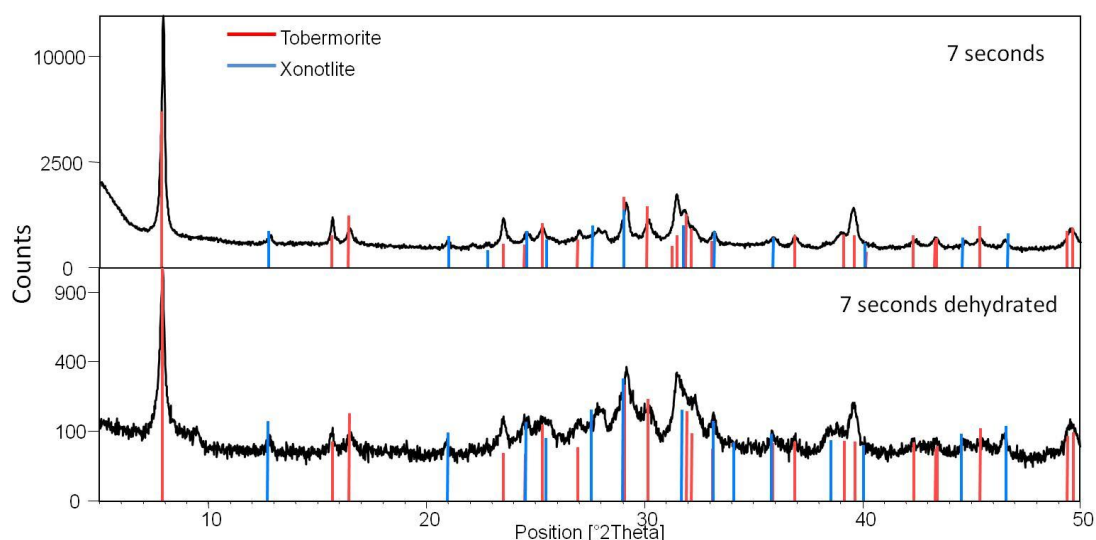
Figure III.2-24: XRD analysis of the supercritical tobermorite sample before and after the thermal treatment at 300ºC.

In conclusion, this work illustrates how the use of continuous reactors allows a better control of reaction time and synthesis conditions since it favors the crystallization of unstable phases like tobermorite far above its stability limit. In addition, under supercritical conditions reaction kinetics increase leading to a reduction of synthesis time from hours to seconds. Also with this continuous synthesis under supercritical hydrothermal conditions it was demonstrated the formation of fibrous tobermorite as single morphology.

In order to check if the formation of fibers was related to the continuous methodology or if it was due to the supercritical state, it was decided to carry out in Tecnalia another supercrítical synthesis in a batch reactor. This was just a preliminar study wich is not optimized due to the lack of time.

For the batch supercritical synthesis, the conditions employed were the following ones:

Table III.2-5: Formulation of the tobermorite syntheses carried out in the supercritical batch reactor.

Precursors	Weight (g)	Ca/(Si+Al)	Al/(Al+Si)
$Ca(NO_3)_2 \cdot 4H_2O$	2.41		
$Na_2SiO_3 \cdot 5H_2O$	2.14	0.83	0.15
$Al_2(NO_3)_3 \cdot 9H_2O$	0.69		

The precursors were all mixed in 0.5L of water, and a gel is precipitated. The mixture is introduced into the batch reactor and closed. The temperature was increased little by little to control the reaction properly. This increase is shown in Figure III.2-25a. This diagram describes the behavior of the mixture inside the reactor with the theoretical behavior of water. It can be observed that around 350ºC, the pressure is suddenly increased arriving at the supercritical pressure before arriving at the supercritical temperature, the pressure is stabilized at 25.0 MPa thanks to the back pressure regulator valve which was set at that pressure. This problem is related to the volume of the mixture, as it was explained in the introduction; when the reactor is filled more than an 80% of its volume, the systems achieve first the critical pressure than critical temperature and the entire product passes to the liquid phase. It only arrives at supercritical conditions when the temperature reaches the critical point.
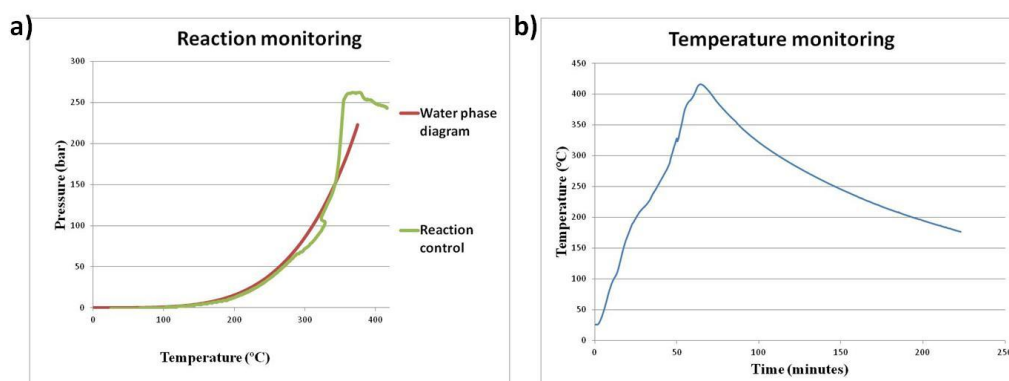
Figure III.2-25: Diagrams of the monitoring of the reaction, a) pressure/temperature and b) temperature/time

As soon as the reactor arrived at the supercritical state, the heating system was switched off, and the reaction was kept in the reactor until it arrived at 100ºC. As it can be seen in Figure III.2-25b, it took 55 minutes to reach the supercritical state, it remained 25 minutes in supercritical state, and it took around two hours to cool down. When the product was extracted from the reactor, it was filtered and dried overnight at 60ºC.

The product was analyzed by XRD. As it can be seen in Figure III.2-26, 11Å tobermorite was obtained but the product is not pure, and some many secondary products were obtained. The main secondary product is calcite due to the carbonation of the product during the synthesis; it would be convenient to add a nitrogen flow to the

vessel to avoid carbonation. In this reactor is not possible to quench the reaction so xonotlite was obtained as by-product. Due to the impossibility to control the reaction time and the kinetics, it might be hard to get pure tobermorite in this reactor. Also, it was obtained as a secondary product a calcium-aluminum silicate. Some other small peaks could not be identified, and they could be related to the degradation products.
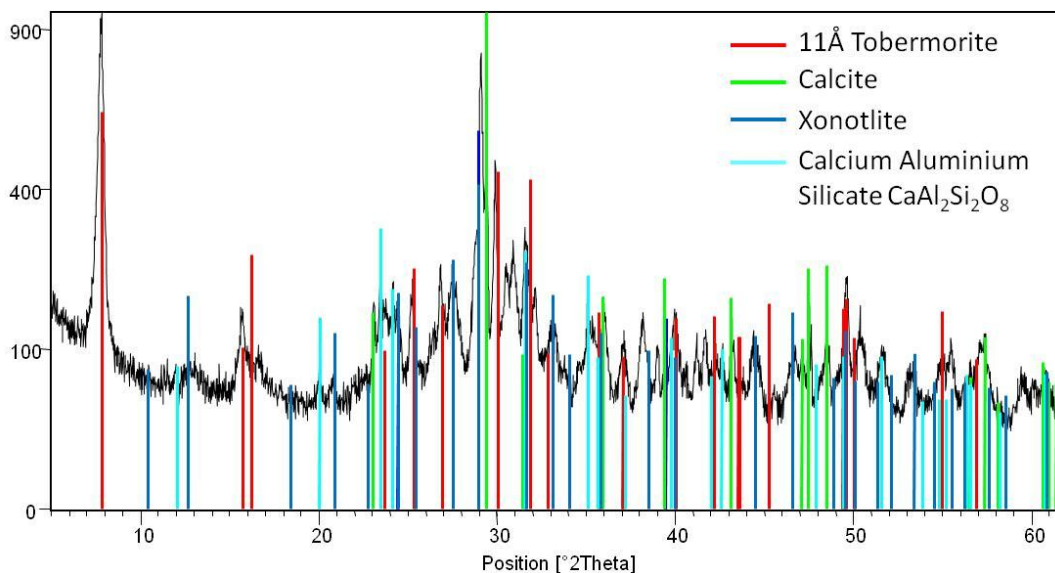
Figure III.2-26: XRD analysis of the product obtained from the supercritical batch synthesis of tobermorite.

The sample was submitted to the dehydration treatment during 24 hours at 300ºC. As it can be observed in Figure III.2-27, the sample is considered anomalous tobermorite as the sample keeps is structure after the thermal treatment (Figure III.2-27 Supercritical tobermorite before and after the heating treatment at 300ºC for 24h.).
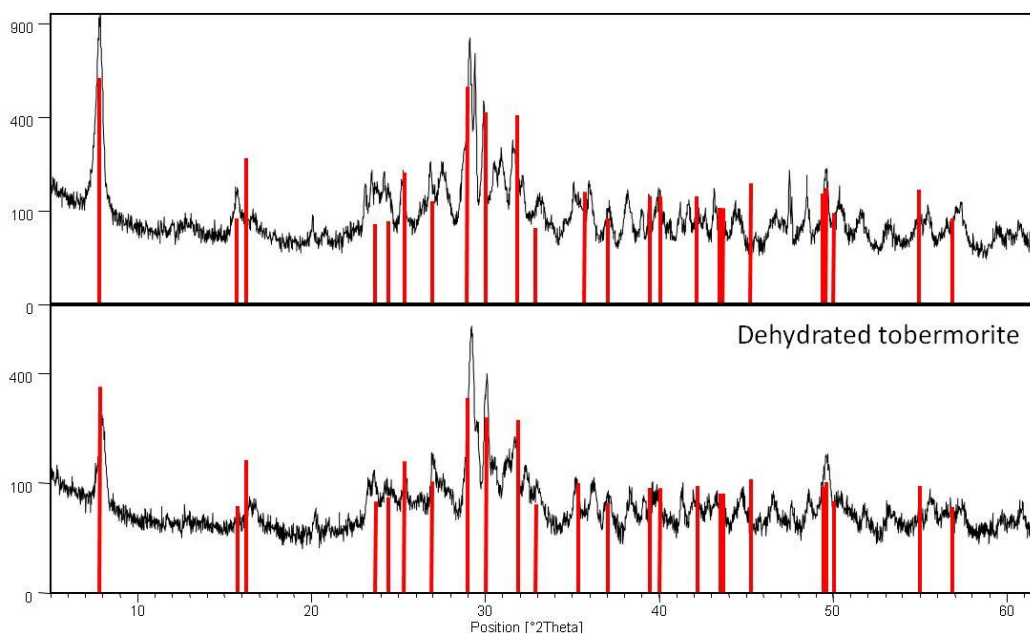
Figure III.2-27 Supercritical tobermorite before and after the heating treatment at 300°C for 24h.

In order to know the morphology of the sample, a SEM analysis was carried out. In the Figure III.2-28 it is possible to see that the product has fibrous morphology and that the agglomerations are composed of small size fibers. Unfortunately, it was not possible to carry out these measurements in a higher resolution microscope to identify better the morphology.
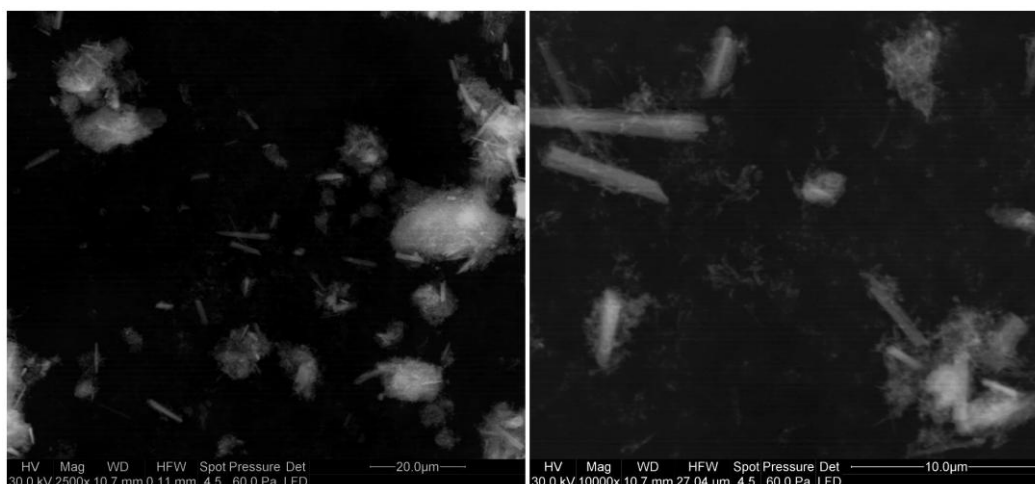
Figure III.2-28: SEM images of the tobermorite sample synthesized under supercritical conditions in the batch reactor.

This synthesis is still not optimized; this was a first attempt to obtain the tobermorite in the new supercritical batch reactor acquired by the group. However, observing the results obtained in this preliminary study, it will presumably be possible

to improve the results and obtain tobermorite fibers with this methodology. This synthesis allowed us to prove that the morphological shape is given by the supercritical estate and not is related to the continuous flowing system.

III.3 Conclusions

In this chapter has been included all the syntheses carried out for both tobermorite and xonotlite using different processes and technologies.

For the xonotlite in first place it was studied the different precursors to observe their influence in the synthesis. With the use of calcium nitrate as precursor, it was obtained nitratine (sodium nitrate) as a secondary product, so it was preferred to use nanosilica and waterglass for the Si source and calcium oxide for de Ca precursor. These gave place also to calcite as secondary product but the presence of this by-product was not as high as the nitratine. In second place two variables were studied simultaneously, the reaction time and the temperature. It was observed that at high temperatures (250ºC) very crystalline xonotlite is form independently of the reaction time. However, for low temperatures (215ºC) it was observed that to obtain highly crystalline xonotlite it was required long reaction times (17 hours). The samples have fibrous morphology for the xonotlite in every case.

Tobermorite was synthesized under hydrothermal subcritical conditions at 215ºC for 4 hours. In this case the variable studied was the substitution of Al for Si in the silicate chains for Al at variable dosages. In literature it was mentioned the stabilizing effect of this substitution but there was not enough structural information about it. It was proved that under the same synthesis conditions, the higher is the Al dosage, the higher is the crystallinity of the product. The structural study confirmed that the Al enters in bridging and branching positions. The crystallization increase with the Al dosage is reflected in a change in the structure. For low Al dosages, the Al enters preferentially on bridging positions (so the structure has more defects) while for high degrees of substitution Al enters preferentially in branching position increasing the crystallinity of the sample. For the highest Al dosage, it was observed an excess of Al that doesn't enter in the structure so this would confirm that there is a maximum of Al that can substitute the Si in the structure, this limit is between 15% and 20% Al.

The morphological study of the samples showed disordered platelet structures of small size. The high resolution image analysis revealed the coexistence of three different morphologies, a first amorphous one with cloudy shape, the second crystalline

one with plate morphology and a third one also crystalline with fibrous shape that can be a fibrous particle or the edge of a sheet. As the Al content increases, the cloudy morphology is less abundant, being predominant the platelet morphology. The "fiber shape" is not predominant but there are more "fibers" as the Al is increased.

Regarding the classification of the 11Å tobermorite, some products showed a normal behavior (meaning that the basal peak distance between CaO layers was reduced to 9Å) while others had an anomalous behavior. Also, a third type was identified when they dehydrated only up to 10Å of distance. The higher is the Al content; the lower is the probability to obtain normal tobermorite. Therefore Al seems to stabilize the structure preventing the shrinkage of basal distance. The reason might be that the Al-Si bond is more stable and difficult to break so the compression of the structure during the thermal dehydration process is less probable.

As a second synthesis method, it has been presented the supercritical synthesis as an innovative way of obtaining both tobermorite and xonotlite. In the first approach, a continuous reactor was developed. The main advantage of this type of reactor is that it allows an accurate control of synthesis conditions and it can be optimized to the requirements of the process.

In this reactor, xonotlite was synthesized in just 15 seconds. Instead of the hours/weeks reported in the literature. The morphology is fibrous, the normal one for this species. As it was mentioned in the first chapter, xonotlite has some potential industrial applications such as additive for friction materials, the synthesis of aerogels, and its use for some biological and orthopedic applications [123][202–204]. This new and fast synthesis route could be scaled-up and implemented in the mentioned applications for a more effective production.

In the case of the tobermorite, these results are revolutionary in the area of the synthesis of this product because traditionally it has been mentioned in the literature that tobermorite is a metastable phase that cannot be obtained at temperatures over 130ºC. However, in this work it has been demonstrated that it is possible to produce tobermorite under unstable conditions (400ºC) if the kinetic of the reaction is controlled. In the supercritical continuous reactor, it was possible to obtain tobermorite in only 7 seconds. This reaction time makes a big difference with the hours/days commonly described in the bibliography. The reason is that supercritical water is very energetic and can produce the crystalline phase faster than under subcritical conditions. Fast

production is very important from a technological point of view, increasing the possibilities of a future industrial application as cement addition, stabilization agent for the capture of contaminants [75,76,205–207], etc. The crystallinity of the sample is very high, and it can be highlighted the preferential growth in (0,0,l) direction. It is worth emphasizing that differently to what happens with subcritical synthesized tobermorite samples that have platelet morphology; the ones achieved by a supercritical treatment are fibrous, exhibiting a close structural and morphological similarity to the mineral phase. This finding suggests that the supercritical synthesis can reproduce, in an accelerated fashion, the geological formation of tobermorite and provide new clues to the mechanisms employed by nature to stabilize it. The answer could lay in the high solvation power of supercritical water [180] and its concomitant easier incorporation of foreign ions into the structure. In this sense, this work might serve as a starting point to the understanding of the geological processes that lead to the formation of tobermorite and other phases under geothermal conditions.

As a second step in the supercritical synthesis, it was tested the production of tobermorite in a batch reactor. This was just a preliminary attempt, so the process should be optimized. It was possible to synthesize tobermorite; however, the product obtained was not pure and many secondary products such as xonotlite and calcite were form. This is due to the impossibility to quench the reaction to control the kinetic. The tobermorite obtained has fibrous morphology. So, as a conclusion, it could be said that the supercritical conditions promote the fibrous morphology while under subcritical conditions only platelets are obtained. As a result of this observation it could be hypothesized that the fibrous morphology is energetically more favorable than the platelet one. However, to confirm this, it should be necessary to carry out some modeling of each case, which will be done in future works. The supercritical water might also encourage the formation of the fibers because of the high diffusivity in the media, and the collision between the particles.

CHAPTER IV: SEEDING EFFECT

IV.1   XONOTLITE SEEDING EFFECT

IV.2   TOBEMORITE SEEDING EFFECT

IV.3   COMPARISON BETWEEN XONOTLITE AND TOBERMORITE SEEDING EFFECT

IV.4   CONCLUSIONS

IV.1   Xonotlite seeding effect

One of the objectives of this work is to test the effect of tobermorite and xonotlite seeds into cement paste. To value this effect, two tests were carried out: calorimetric measurements to check if the reaction is accelerated and also mechanical test to compare the strength of the cement pastes with seeds with the ones without seeds. In the case of xonotlite only one variable was studied: the dosage of the seeds into the cement paste.

For both the calorimetric and mechanical tests, some cement pastes were prepared. The cement/water ratio used in the mix was 0.4 with a 40% of superplasticiser Auracast 280 (taking as reference the xonotlite dosage). The dosages studied were: 0.5%, 1%, 2% and 5%.

The preparation process of the cement paste samples is described in Figure IV.1-1. The mixing process is composed of 7 steps:

1. Mixing of the clinker + the seeds,
2. 1 minutes mixing at 300 rpm,
3. Add the water + superplasticiser,
4. Wait 10 seconds,
5. 1.5 minutes mixing at 750 rpm,
6. 1 minute of wait,
7. 1.5 minutes mixing at 750 rpm.
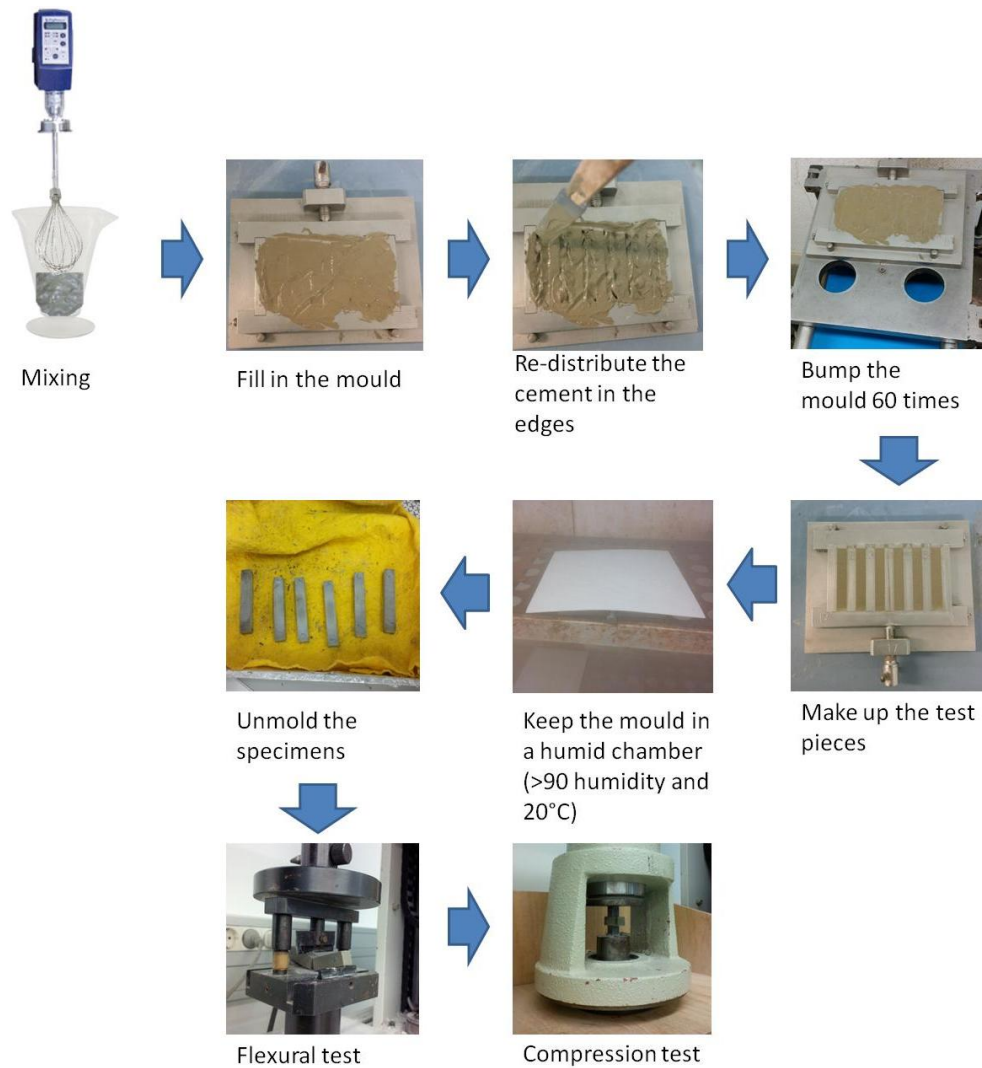
Figure IV.1-1: Preparation process of the samples employed in the mechanical test.

IV.1.1 Calorimetric test

For the calorimetric tests, six grams of the cement paste were introduced into the calorimetric vials, and the measurement was carried out.

In Figure IV.1-2 is represented the calorimetric curve of each dosage. As it can be observed, there is an accelerating effect as a consequence of the addition of xonotlite nanoseeds. The accelerating tendency is similar to the one observed in tobermorite, the higher is the seed dosage, and bigger is the accelerating effect.
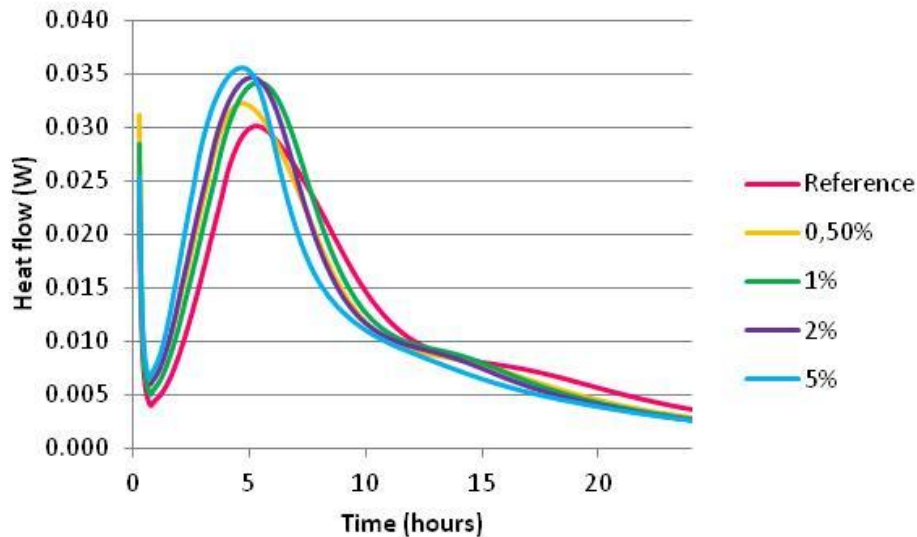
Figure IV.1-2: Calorimetric curves for xonotlite additions in dosages: 0.5%, 1%, 2% and 5%

With this calorimetric measurement it was demonstrated the accelerating effect of xonotlite in comparison with the reference sample.

IV.1.2   Mechanical test

The mechanical tests were carried out for three dosage levels: 0.5%, 1% and 2% at different points of the setting process: 6 hours, one day, one week and 28 days. These times were chosen because they are the most common ones employed in cement paste strength test. For the flexural test (Figure IV.1-3), however, it was not possible to carry out the test on the 6 hours samples because they were too brittle and they broke very easily. In these tests we can observe that the introduction of xonotlite slightly improves the resistance at the beginning of the setting and then remains equal to the reference. However, it would have been desirable to see also the results at shorter times to really see the seeding effect. The flexural strength results have a big variability, so the results are not very accurate, and these results are just to observe the tendency but not to take into account the strength value.
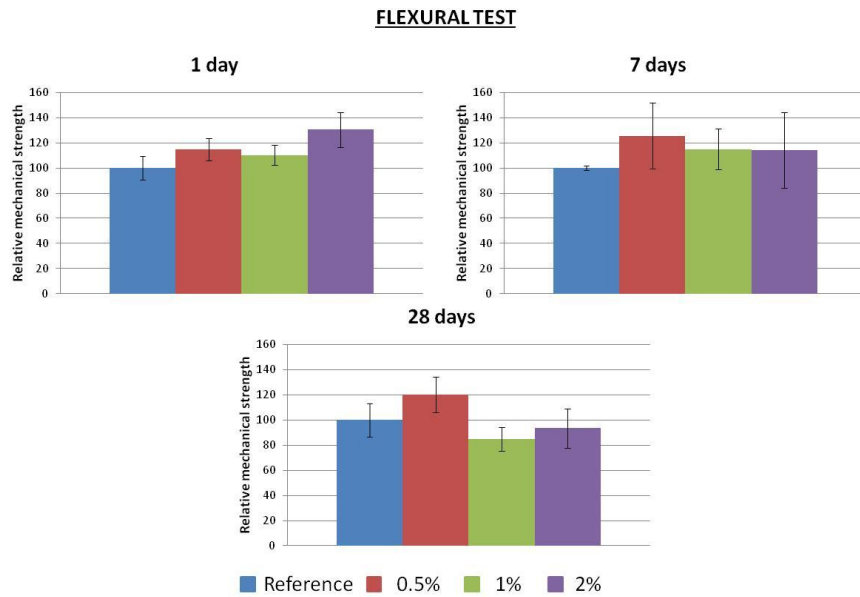
FLEXURAL TEST

Figure IV.1-3: Flexural test for samples with xonotlite additions at different times and dosages. Comparison as function of the dosage.

The compression test (Figure IV.1-4) could be carried out at shorter setting times (6 hours), and it is possible to see that, in comparison with the rest of the results, the highest accelerating effect is observed at this point. The introduction of high xonotlite dosage doesn't improve the resistance at long times in comparison with lower dosages. However at shorter setting times, it is observed that the higher is the dosage, the better is the resistance of the sample.
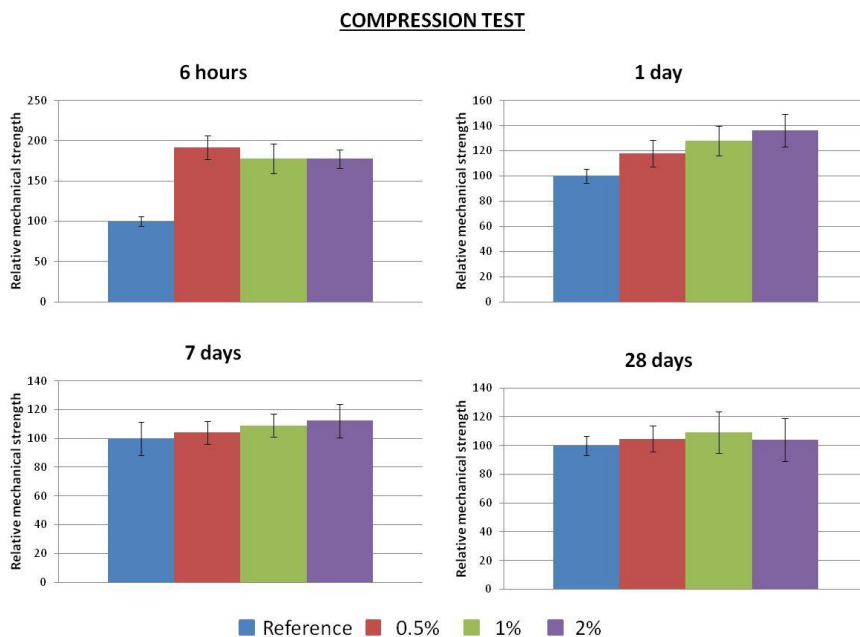
COMPRESSION TEST

Figure IV.1-4: Compression test for samples with xonotlite additions at different times and dosages. Comparison in function of the dosage.

In view of these results it can be said that the xonotlite has an accelerating effect at short times, obtaining better results for the flexural test at 1 day when high dosages of xonotlite are added. In the case of the compression test, where it was also possible to carry out a test at 6 hours, it can be observed that at such early times the strength with the xonotlite seeds is doubled.

IV.2 Tobermorite seeding effect

For this study, a different methodology was designed to test the effect of several variables described in Table IV.2-1. It was decided to change the methodology in comparison with the one carried out for xonotlite because more variables were introduced and the mechanical tests were also carried out at earlier times. Every combination of the variables was studied.

Table IV.2-1: Variables studied to test the seeding effect of tobermorite

Variable studied	
%Al substituting Si in Tobermorite	0%Al
	6%Al
	10%Al
	15%Al
	20%Al
Dosage of the seeds	0% (reference)
	0.5%
	1%
	2%
	3%
	4%
	5%

Dispersion of the seeds	Dried seeds and redispersed
	Not dried seeds (with and without superplasticizer)
Synthesis method of the seeds	Subcritical synthesis
	Supercritical synthesis

The aim of studying the %Al substitution of Si in tobermorite is to know if the aluminum content, or the crystallinity variations, could affect to the seeding effect. Another variable studied was the dosage of the seeds into the cement paste. This is a very common variable for the admixtures in cement paste. This variable measures the optimal dosage to obtain the desired effect and avoid problems derived to a too high dosage (points where the particles are especially concentrated and which can be a weak point for degradation or strength) or too low dosage where the seeding effect is not detected. The common dosage is usually between 1% and 20% [70][69]. For this work, we decided to use six degrees of dosage from 0.5% to 5% because when using nanoseeds usually the dosages are lower because of the workability of the paste[208][209].

Another variable that we were interested in was the way of applying the nanoparticles into the cement paste. When the hydrothermal synthesis is finished, we obtain a dispersion of the particles. The first option that we studied was to filter and dry the nanoparticles to obtain a powder that we could afterward re-disperse in water with an ultrasonic tip (2 minutes at 30% power) and added into the cement paste. The second option was to use the particles directly as they came out of the reactor, and preconcentrate them up to the exact point to have a dispersion containing the exact dosage of nanoparticles desired and also the exact amount of water needed for the cement paste preparation. For this process, it was taken a 20g aliquot of the reaction product dispersion and evaporated at 100°C up to constant weight to know the concentration of the particles in the reactor outcome. As function of the dosage, it was possible to evaporate the particles up to the desired concentration. The reason to study this variable is that it was observed that when the tobermorite is dried, it gets strongly

agglomerated and the re-dispersion might not be as effective as the use of the outcome product. It was also observed that the water in tobermorite is very embedded in between the particles. It was possible to arrive at this conclusion as there was a big difference between the 5% dosage that had been re-dispersed and the one that had been concentrated (Figure IV.2-1). In the first case, the sample was a limp paste (texture like cream) and the second case was a very dry paste. Taking into account that both samples had the same amount of water and tobermorite; it could be extracted as a conclusion that, during the drying process, the particles aggregate somehow that, after the redispersion, it is not possible to turn back to the original state. It was pointed out this fact as important, and for that reason, we decided to study the effect of this as nanoseed. It was thought that it could affect in the seeding effect as the dispersion is better with the concentrated product.

Figure IV.2-1: Comparison between the texture of the seeds mixtures and the cement pastes when the seeds are added dried or not dried.

The last variable studied was the method employed for the synthesis of each tobermorite, the subcritical and the supercritical. This variable was not widely studied as we didn't have enough supercritical tobermorite to develop this aspect exhaustively.

The seeding effect was studied both by calorimetric analysis and mechanical test at a short setting time. For the calorimetry every case was studied because it didn't imply the use of large amounts of product. The mechanical test, however, were only carried out for two of the samples (6%Al and 15%Al). The reason for this decision is that to carry out the mechanical test for each variable (at six different timings), implied

the use of large amounts of product which was impossible to synthesize. So, it was decided to do it with only two levels of Al content. Also, for the not-dried samples, it was only used for the 6% Al sample and three dosage levels 0.5%, 2% and 5% due to the same reason and also because of the hard work that it takes to evaporate the sample up to the desired amount of water.

IV.2.1   Calorimetric test

The preparation of the sample was different as function of the dispersion mode of the tobermorite, as described in Figure IV.2-2. In this case, differently to what it was made for the xonotlite, the samples were not taken from cement mixes but prepared manually because we wanted to measure a big amount of variables and it was not possible to carry out a big cement mixture of each sample due to the lack of product.
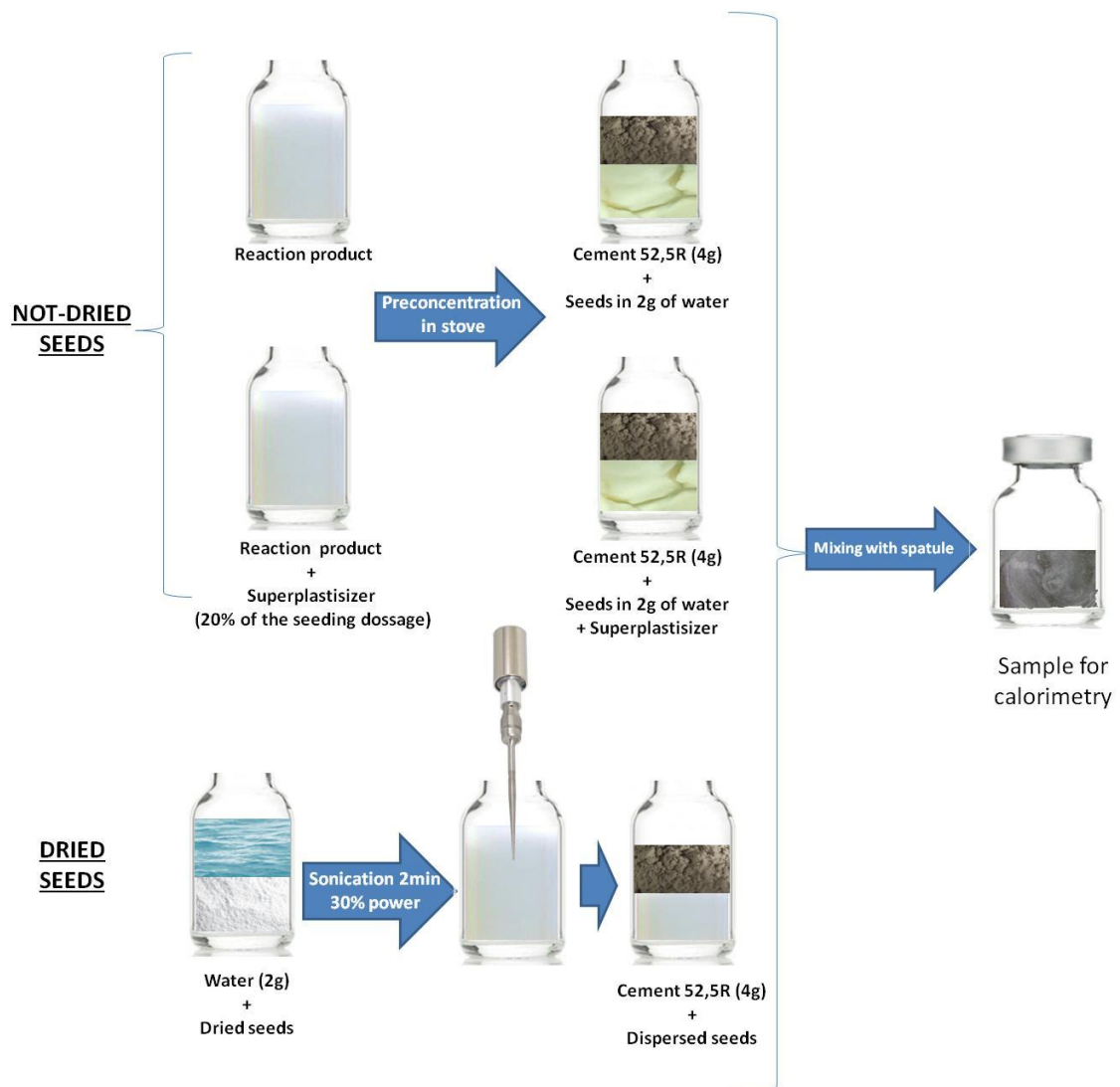
Figure IV.2-2: Sample preparation for calorimetric measurements.

(a)   Study of the Tobermorite %Al:

For every dosage it was observed an accelerating effect, using dried seeds, compared to the reference (Figure IV.2-3). The calorimetric measurements employing not-dried seeds are very similar; they are included in the appendix III. This effect is more intense as the dosage is higher.
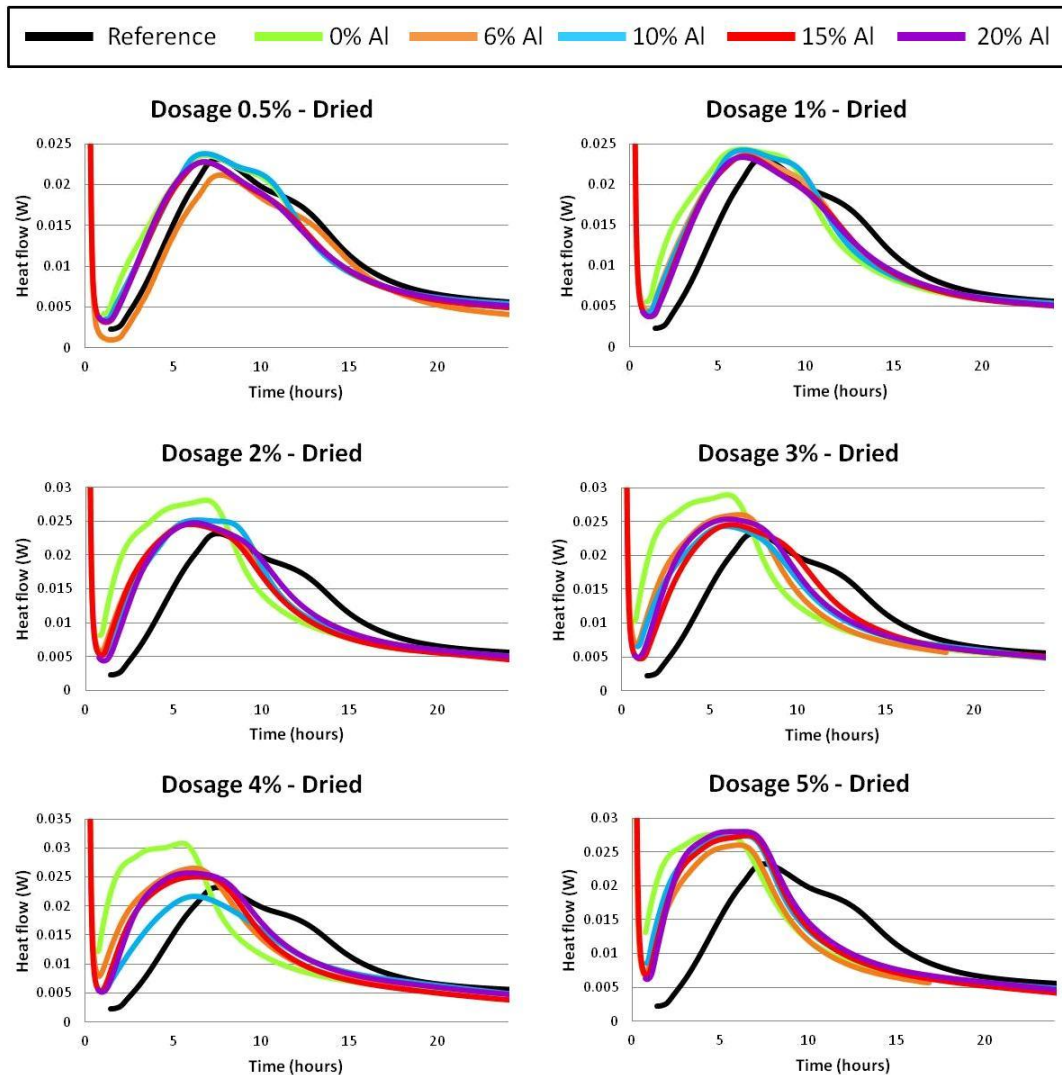
Figure IV.2-3: Calorimetric measurements of the cement paste with dried seed addition in dosage ranging from 0.5% to 5% and with different Al content in the tobermorite.

In Figure IV.2-4 we show in more detail the results obtained for the 5% dosage, which has the biggest accelerating effect. In Figure IV.2-4a) are represented the calorimetries of the cement paste with dry seeds. As it can be observed, all the samples have an accelerating effect comparing with the reference. However, no tendency can be observed in the samples with different %Al. In Figure IV.2-4b) are represented the calorimetries of the cement paste with not-dried seeds. In this case, also can be observed

an accelerating effect but the behavior is not that homogeneous as in the previous case, and it doesn't follow a clear tendency. This could be due to the workability difference between the cement paste with the dried seeds and the paste with not-dried seeds. As it was mentioned before, the not-dried tobermorite absorbs much more water and its consistency is like a paste, not a dispersion. As a consequence, the cement paste is also less workable. In order to improve the workability of the samples, it was decided to add a superplasticizer (Fosroc Auracast 280) at a concentration of 20% in reference to the tobermorite dosage. The paste was more workable, similar to the paste with dried seeds. The results of these measurements can be observed in Figure IV.2-4: Calorimetric measurements of different %Al contents in the tobermorite seed for: a) dried nanoseeds with 5% addition, b) not-dried nanoseed with 5% addition and c) not-dried nanoseeds with 5% addition with superplastisizer. As a result, the acceleration effect was increased, but no distinction could be made among the samples with different Al%.
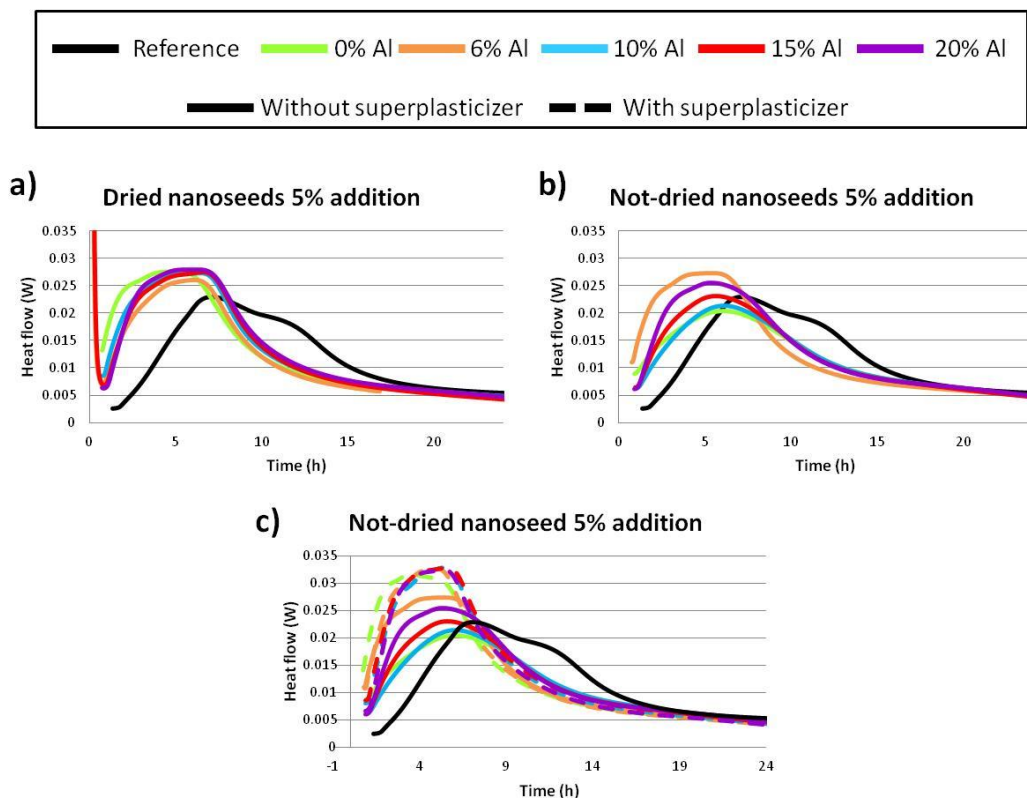
Figure IV.2-4: Calorimetric measurements of different %Al contents in the tobermorite seed for: a) dried nanoseeds with 5% addition, b) not-dried nanoseed with 5% addition and c) not-dried nanoseeds with 5% addition with superplastisizer.

(b)   Seed dosage study

As a second variable, it was studied the dosage of the seeds in the cement paste. All the done experiments can be seen in the appendix IV. As no difference was observed among the tobermorite with different %Al, the one of 15%Al has been selected to show the case. In Figure IV.2-5a) are represented the samples prepared with dried tobermorite 15%Al. It can be seen a clear tendency; the higher is the dosage, the higher is the accelerating effect.   In Figure IV.2-5b) are represented the not-dried samples; in this case it can be observed an increasing accelerating effect for the 0.5%, 1%, 2% and 3%. However, for the 4 and 5%, the effect is lower. In these cases also the loose of effectiveness is related with the low workability. Therefore, a 0.6% of superplasticizer was added. In Figure IV.2-5c) is represented the effect of the superplasticizer in the not-dried samples and the comparison with the dried ones. In the reference case can be observed that the superplasticizer has a retarding effect in the cement paste. For the 3% dosage it was observed that the seeds accelerate a little bit the reaction in comparition with the reference. The workability of this paste is good, so the small improvement that the superplastisicer could have in the dispersion of the seeds, is countered by the retarding effect. So in the end no change is observed in comparison with the samples without supercplastisizer. For the 5% dosage it is clear that the superplasticizer improves the accelerating effect of the not-dried samples. The accelerating effect of the not-dried seeds is so strong that not only counters the retarding effect of the superplasticizer but also overcomes the accelerating rate of the sample with dried seeds (with no superplasticizer). So it could be said that the not-dried nano-seeds have a higher accelerating impact than the dried ones.
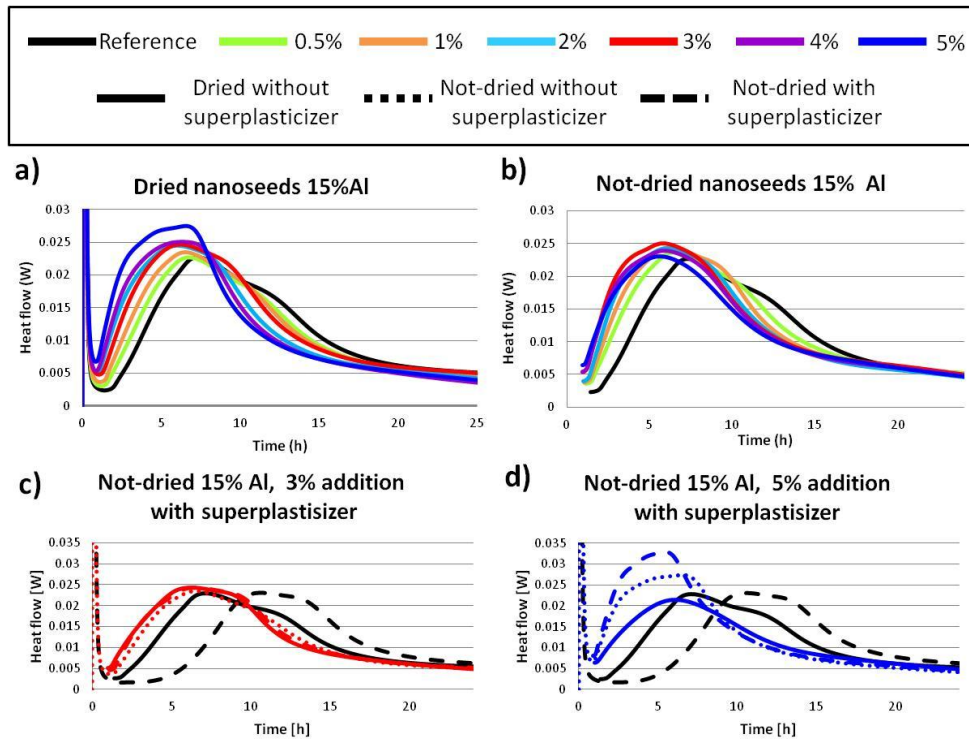
Figure IV.2-5: Calorimetric measurements of different tobermorite seed dosages for: a) dried nanoseeds 15%Al, b) not-dried nanoseeds 15%Al and c) and d) addition of superplasticiser.

(c)   Study of the seed synthesis method:

The last variable measured was the tobermorite synthesis method, using both the supercritical and the subcritical method. In Figure IV.2-6 is represented the result, as it can be observed the particles synthesized supercritically presents and a slight improvement in the acceleration. However the lack of sample did now allow as to carry out more test with the supercritical tobermorite, so this case should be further studied to give solid conclusions.
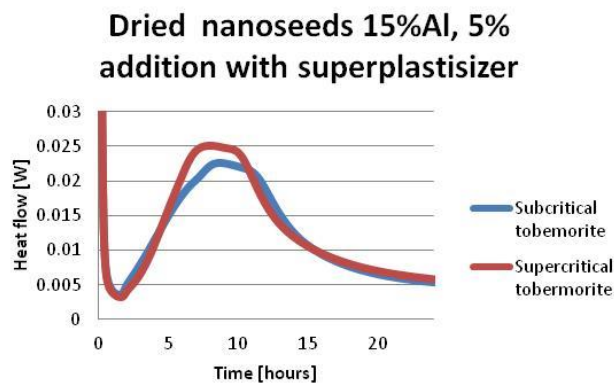
Figure IV.2-6: Calorimetric measurements of seeds synthesized under different conditions.

As a result of the calorimetric experiments, some conclusions were obtained. The first conclusion is that the Al% in the tobermorite doesn't affect to the calorimetries. As a second conclusion, it was proved that the tobermorite acts like an accelerator and the seed dosage influenced in the effect. As last conclusion, it was proved the necessity of using superplasticizer to improve the workability of the cement paste when not-dried seeds were used, especially for high dosages.

IV.2.2 Mechanical test

To complete the seeding effect study we decided to do some mechanical test. It was decided to carry out the mechanical test at short setting times as the accelerating seeding effect is expected to be more intense at early times. For the preparation of the cement paste, the water/clinker ratio employed was 0.4 and the proportion of superplasticiser 20% taking the tobermorite dosage as a reference (both of dried and not dried seeds). The tobermorite seeds used for the first set of experiments were the dried ones with 6%Al and 15%Al, with dosages of 0.5%, 2%, and 5%. The workability of these samples was very good for every dosage. The mechanical tests were performed after 6, 8, 16, 24, 40 and 72 hours of setting of the cement paste. For the second set of experiments, it was used not-dried seeds with 6%Al and dosages of 0.5%, 2%, and 5%. The workability in this case instead, was not homogeneous, as it can be seen in Figure IV.2-7. For the sample of 0.5% the workability was good. For the sample 2%, it was more plastic, but nevertheless, it was possible to mold it. However, for the 5% the sample was so dry that it was almost impossible to mold it and the test pieces were too weak. In this case, the mechanical tests were only performed after 6, 16 and 24 hours of setting.
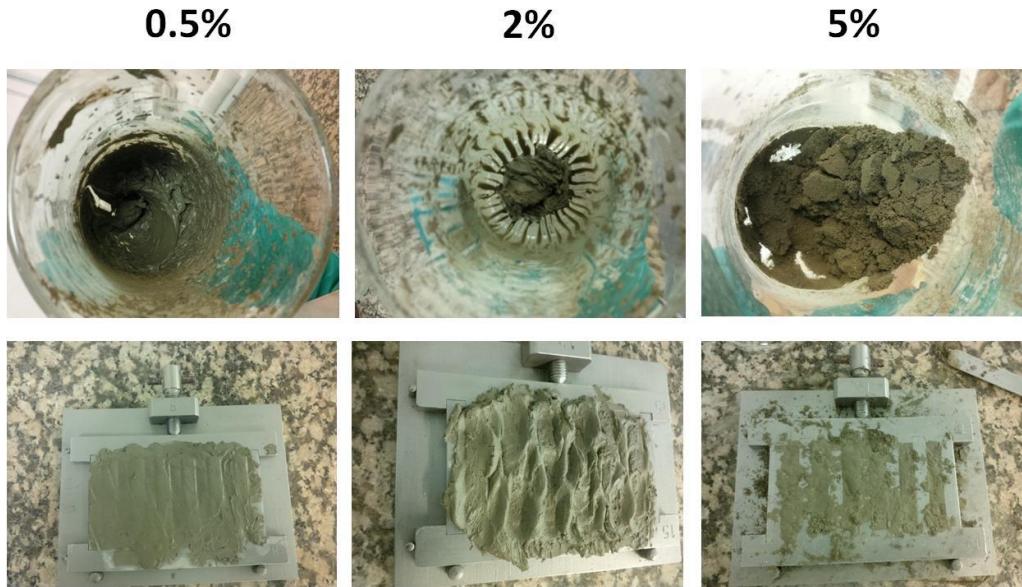
Figure IV.2-7: Differences in the cement paste texture as function of the dosage when not-dried nanoseeds are added.

As it was mentioned before also, in this case, the same variables as for the calorimetric test were taken into count: the Al% of the tobermorite, the dosage and also the way that the seeds were introduced into the cement paste.

(a)   Study of the Tobermorite %Al:

The first one studied was the Al content in the flexural test (Figure IV.2-8). The results are not very clear because the variability among the different samples is very big. Both 6%Al and 15%Al samples present a performance improvement after 6 and 8 hours comparing with the reference, but no clear difference is observed among the two cases studied. In the same way in the compression test (Figure IV.2-9). It's possible to appreciate an acceleration effect of the samples with seeds in comparison with the reference. However for the comparison between the samples with different Al dosages the effect is not clear. Only at short setting times (6 and 8 hours) and medium-high dosage (2% and 5%), there is a slight difference with better results for the tobermorite with 6% of Aluminum. However, the difference is so small that it can be considered irreverent.
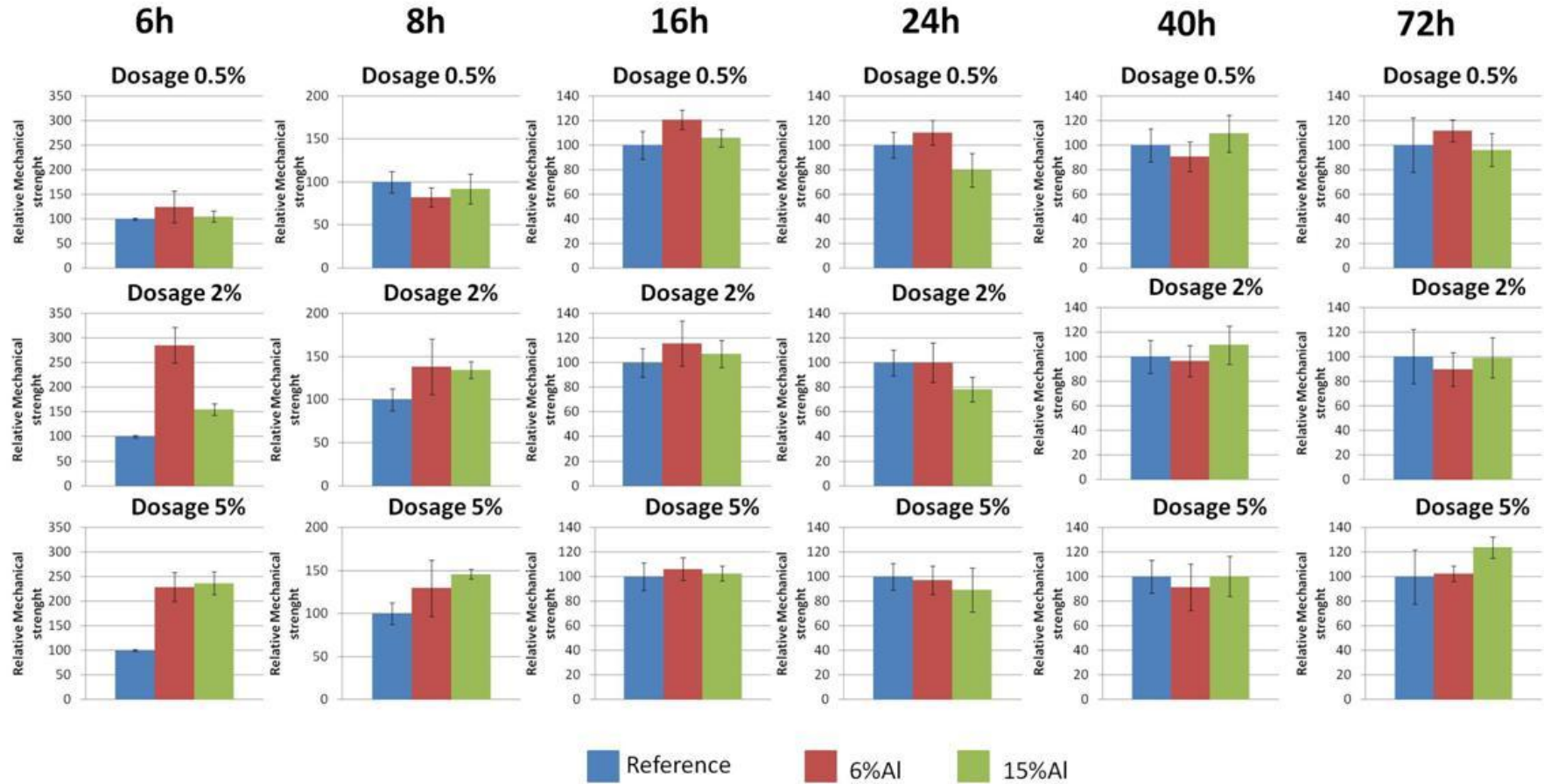
FLEXURAL TEST

Figure IV.2-8: Flexural test for dried samples of different times, dosages, and %Al. Comparison as function of the Al content.

COMPRESSION TEST
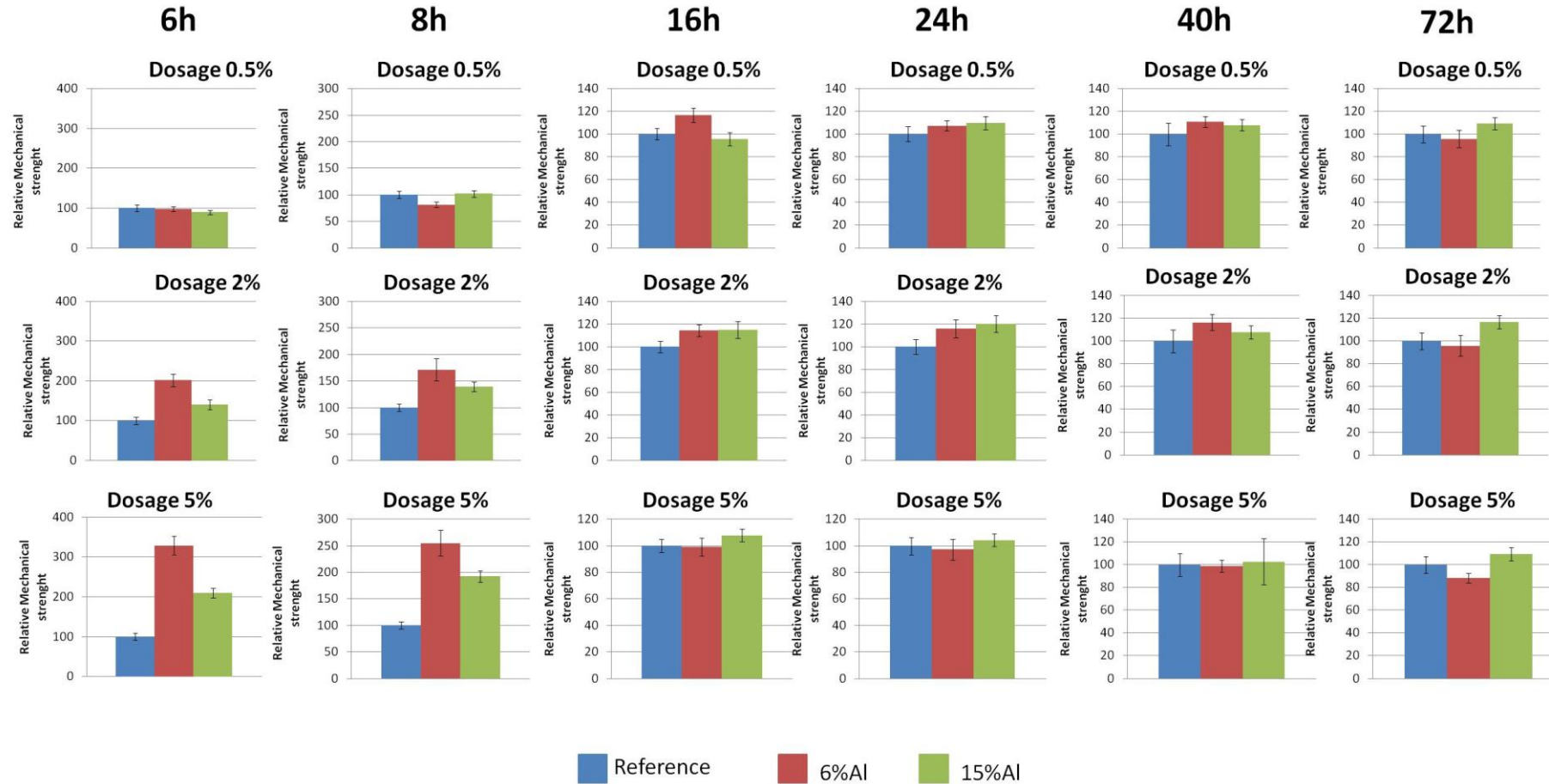
Figure IV.2-9: Compression test for dried samples of different times, dosages, and %Al. Comparison as function of the Al content.

(b)   Seed dosage study

A second variable taken into account was the seed dosage. For the flexural test (Figure IV.2-10) it can be observed a tendency for the shortest setting times, 6 and 8 hours. The resistance of the 2% and 5% dosage is higher than the reference and the 0.5% dosage. At longer setting times the values are matched. However, as it was mentioned before, the variability between measurements is very big, and the error bars very big.
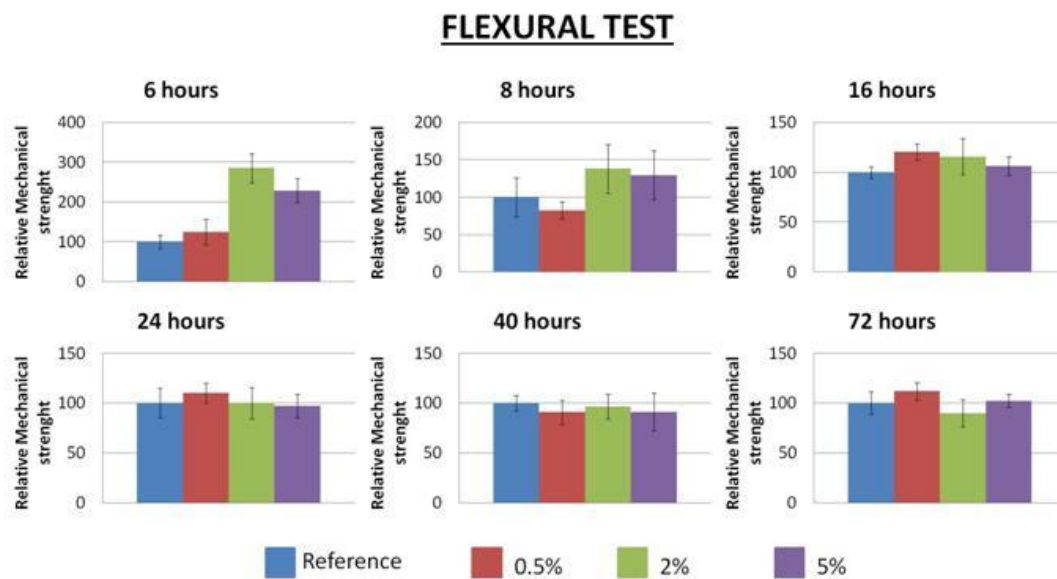
Figure IV.2-10: Flexural test for 6%Al dried tobermorite samples of different times and dosages. Comparison as function of the dosage.

For the compression test (Figure IV.2-11) there is a clear accelerating tendency. The dosage 0.5% has a very similar behavior to the reference, such small amount of seeds is not enough to see an effect in the cement paste. For the 2% dosage, it is found a clear increase of the strength at short setting times (6 and 8 hours) highlighting the acceleration effect of the tobermorite seeds. For the 5% dosage the accelerating effect is accentuated, and it is even higher than for the 2% dosage. Once more, this effect is visible for the earliest times (6 and 8 hours). Afterwards the effect is matched to the reference as it was expected. These results are consistent with the ones observed in the calorimetries. As it was mentioned, the Al content in the seeds doesn't affect to the acceleration effect. However, the dosage does have influence, the higher is the dosage, the more is the acceleration rate.
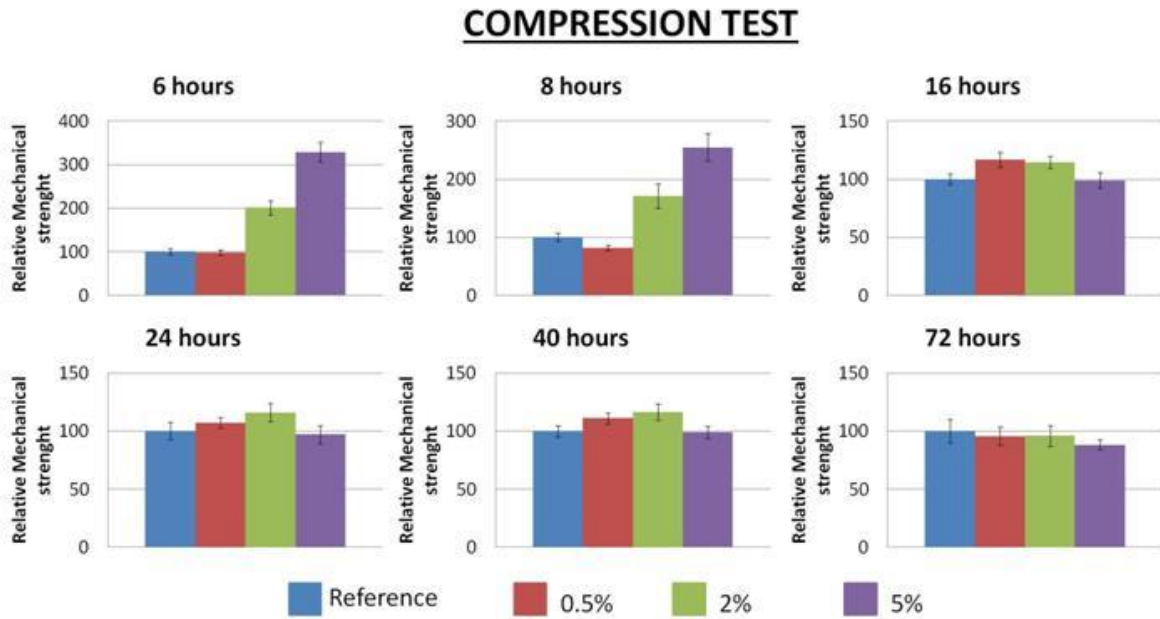
COMPRESSION TEST

Figure IV.2-11: Compression test for 6%Al dried tobermorite samples of different times and dosages. Comparison as function of the dosage.

(c)   Study of the seeds pretreatment:

The third variable taken into account is the way that the seeds are introduced into the sample: dried or no-dried (pre-concentrated). In Figure IV.2-12 are represented the flexural tests carried out in the two types of samples for two dosage levels: 0.5% and 2%. It can be observed that for the earlier setting time, 6 hours, the strength of the samples with not-dried seeds is better than the samples with dried seeds. For the dosage of 0.5% this improve is note very high in comparison with the sample with dried seeds but it is almost the double in comparison with the reference. For the 2% dosage the strength is almost two times higher when using not-dried seeds in comparison with the dried ones and almost five times higher in comparison with the reference. At long hours the effect is equilibrated obtaining similar strength results for every dosage and in comparison with the reference. However, as happened in the previous analysis, the variability between flexural measurements is very high, and these results could slightly change.
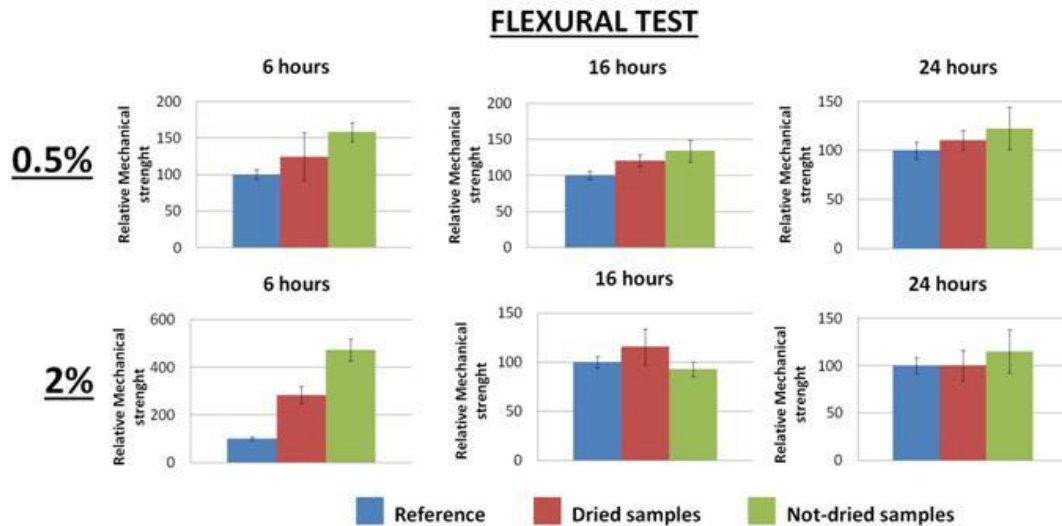
Figure IV.2-12: Flexural test for 6%Al tobermorite samples of different times and dosages. Comparison as function of the dried-or not-dried nature of the seeds.

The results of the compression tests (Figure IV.2-13) are similar to the ones of the flexural test. In this case, the difference between the two seeds types is emphasized. For both dosages, after 6 hours of setting the strength of the cement paste with not-dried seeds higher than the strength of the dried seeds. For the 0.5% dosage is two times higher and for the 2% dosage is three times higher (and 6 times higher in comparison with the reference). For longer reaction times this effect is blunted and despite there is still some differences between the samples, they don't differ much.
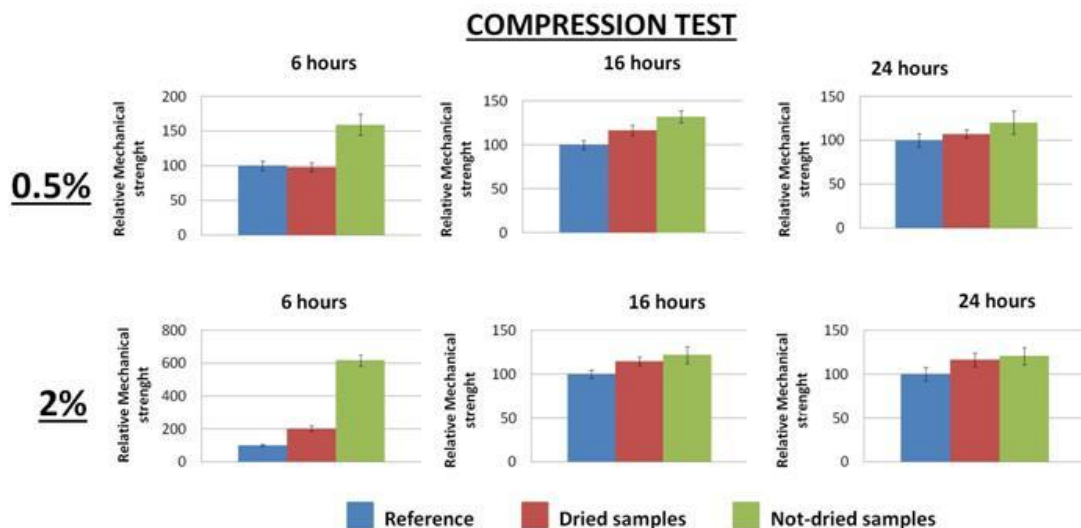
Figure IV.2-13: Compression test for 6%Al tobermorite samples of different times and dosages. Comparison as function of the dried-or not-dried nature of the seeds.

IV.3   Comparison between xonotlite and tobermorite seeding effects

It was carried out a comparison between the calorimetric measurements done to the cement pastes with either xonotlite or tobermorite. The cement pastes were prepared the same way for the samples with xonotlite and tobermorite, the only difference between both is that for xonotlite it was used superplasticizer in a dosage of 40% (taking as reference the xonotlite dosage) while for tobermorite the superplasticizer dosage used was 20% (taking as reference the tobermorite dosage).

As it can be observed in Figure IV.3-1, for every dosage there is an accelerating effect. For the 0.5% dosage, the lower effect is observed for the dried tobermorite. In the case of not dried tobermorite seeds, the maximum heat flow is lower than for xonotlite; however, the peak is wider so the total of product reacted is higher. For the 2% dosage, the lower effect is observed for the dried xonotlite. For dried tobermorite the total heat flow is higher than in the previous case but the maximum of the peak is a little bit retarded. For the not-dried tobermorite seeds a big change was observed, the accelerating effect is multiplied and the maximum heat release is observed two hours before it does for dried tobermorite. This certifies what it was observed in the previous sections. For the 5% dosage the accelerating effect is higher for dried xonotlite than for dried tobermorite. It was not possible to measure the accelerating effect of not-dried tobermorite for this dosage because the low workability of the cement paste.
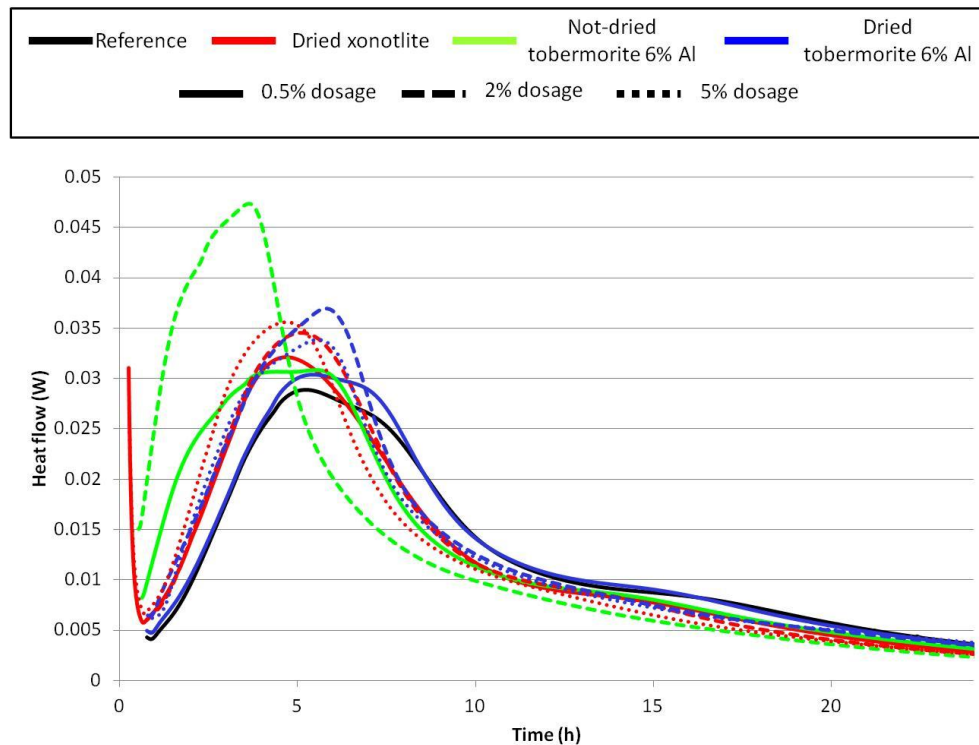
Figure IV.3-1: Comparison between the calorimetries done to the cement pastes prepared in the previous sections with xonotlite and tobermorite as seeding agents.

In Figure IV.3-2 is represented the mechanical test comparison between the acceleration effect on cement paste of xonotlite and tobermorite (dried and not) seeds. As it can observed, for short setting times and low dosages (0.5%), the effect of xonotlite and not-dried tobermorite seeds is very similar. However, for higher dosages (2%) the effect of the not-dried tobermorite samples is 3.5 times higher than the effect of xonotlite. At this short setting time it is not possible to compare the flexural test because it was impossible to carry it out for the samples with xonotlite. For longer setting time (24 hours), the mechanical strength of every sample is equilibrated, being slightly higher the resistances of the samples with xonotlite rather than the ones with tobermorite.
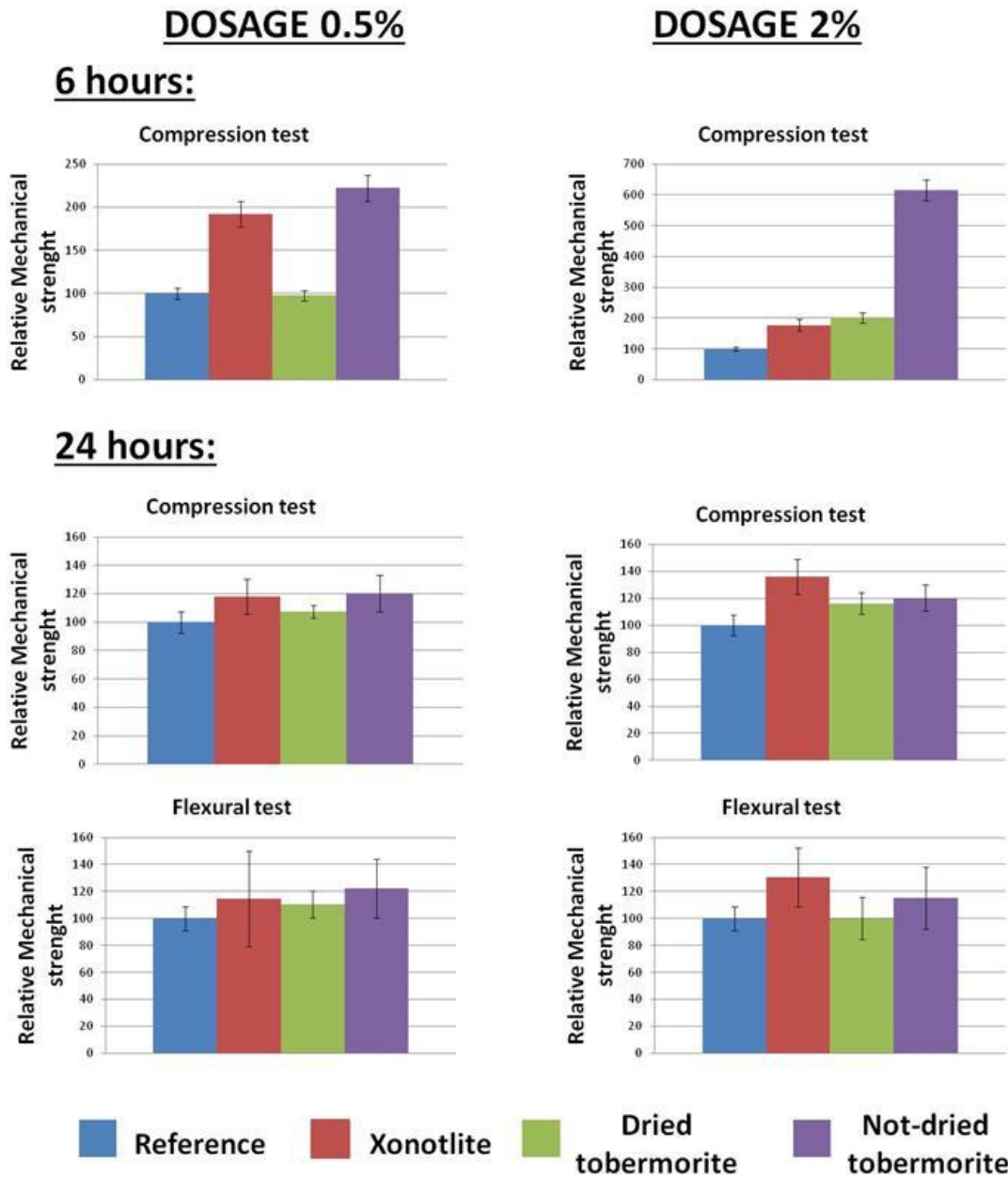
Figure IV.3-2: Comparison between the mechanical resistances of cement pastes with xonotlite seeds, dried tobermorite seeds and not-dried tobermorite seeds at different times and dosages.

In future works it would be interesting to analyze also the not-dried xonotlite and the supercritical tobermorite. Due to the fibrous morphology and the lower aggregation of the supercritical tobermorite, it would be interesting to see if it's translated into a difference in the accelerating effect due to a different dispersion in the cementitious matrix.

IV.4 Conclusions

In this chapter has been described the seeding effect of both tobermorite and xonotlite in cement. Two methodologies were employed for it: the calorimetric measurements and the mechanical test.

For the calorimetric analysis of xonotlite only one variable was studied, the dosage of the seeds. It was observed that the higher was the dosage, the more was the accelerating effect of the seeds. So the optimal dosage would be 5%.

In the calorimetric analysis of tobermorite as seed, many variables were studied in order to know how each variable does influence the accelerating effect. It was demonstrated that in every case the tobermorite acted as an accelerator, but some variables have more influence than others. For example, it was proved that the aluminum content in tobermorite has no influence on the accelerating effect. The second conclusion extracted was that the higher is the dosage, the higher is the accelerating effect. In the comparison between dried seeds or not-dried ones, it was highlighted the necessity of using a superplasticizer when using not-dried seeds. Despite the retarding effect of the superplasticizer (observed in the reference), the seeding effect of not-dried seeds was so high that it counterbalanced the retarding effect of the superplasticizer and the overall effect was even higher than for the dried seeds. So from these results, it could be deduced that the not-dried seeds have a higher impact on the acceleration effect in cement pastes. This can be related to the dispersion of the samples. As it was mentioned, the dried samples during the drying process tend to aggregate and increase the size; therefore the dispersion of the seeds is not so optimal. The better behavior of the not-dried samples might reside in the better dispersion of these in the cement paste.

The last variable measured in the calorimetric test was the synthesis method (subcritical or supercritical), which would be linked to the morphology of the particles, platelets, and fibers, respectively. In the results, it cannot be appreciated differences among them. However, further experiments should be carried out as this time it was not possible due to the low amount of product produced in the supercritical continuous synthesis.

In the comparison between the calorimetric analysis of xonotlite and tobermorite, it could be observed a higher accelerating effect of xonotlite over tobermorite. This can be related to the morphology, the size or the aggregation of the particles. It would be interesting to carry out this comparison in the future with the supercritical tobermorite seeds which also have fibrous shape.

For the mechanical study carried out for xonotlite seeds, it could be appreciated that at short times (one day) the seeding effect is visible for every dosage in comparison with the reference for both flexural and compression strength tests. However, the flexural test is not very accurate because of the high variability among each sample of the test.

For the tobermorite, several variables were also studied, the same ones as for the calorimetries. In this case, also it was proved that the Al content in tobermorite does not affect to the mechanical strength. On the contrary, the higher is the dosage, the higher is the compression strength. For the analysis of dried or not-dried seeds, it was only possible to carry out the test on samples with 0.5% and 2% seed dosage because the workability of the one with 5% was very low. The results, in this case, showed a big improvement at short times in the resistance of the samples with not-dried seeds in both flexural and compression tests. In this case, the difference between both tests could be related to the dispersion. In the case of the dried seed, they were first mixed with the cement and then the water was added to the mixture while in the not-dried ones the water was embedded. So this could make a difference in the seeds size and also the dispersion in the cement paste. The better is the dispersion and the lower is the size of the seed, the higher is the accelerating effect. This happens because there are more nucleation points and the reactive surface of the small seeds is higher, so it can react faster.

As a general conclusion it could be said that both xonotlite and tobermorite have an accelerating effect on cement pastes. The calorimetric and mechanical results highlight that for short setting times, the effect of the use of not-dried tobermorite seeds is higher; however, for long setting times (24h hours) the effect of the samples with xonotlite is slightly better. Nevertheless, it should be carried out further experiments under similar conditions to compare the results.

CHAPTER V: GENERAL CONCLUSIONS AND FUTURE WORK

The work carried out in this thesis is divided into two main parts. The first one is the synthesis of tobermorite and xonotlite with different hydrothermal methodologies and characterization of the samples. And the second one is the test of the seeding effect of tobermorite and xonotlite into cement paste.

From the first part, some general conclusions can be obtained. Related to the subcritical batch reaction we can conclude that it is possible to obtain xonotlite and tobermorite at relatively low timing comparing to the one described in the literature. For xonotlite it was proved that if high temperatures are used in the reaction (250ºC) the formation of highly crystalline xonotlite is independent of the reaction time (with a minimum of 2 hours), but for low reaction temperatures (215ºC), long reaction times (17 h) are required to obtain highly crystalline xonotlite.

It was also proved the important role of aluminum in the formation of the tobermorite. In literature, it is described that aluminum gives stability to the tobermorite, but in this work, we have carried a deep study about how the aluminum does affect the structure of the tobermorite. It was proved that, under same reaction condition, the higher is the aluminum content, the more crystalline is the tobermorite. However it was observed that for high dosages (20%) there is some Al that doesn't enter into the silicate chain. This suggest that the maximum amount of Al substitution for Si is below 20% in good agreement with the 17% inferred from most widely accepted structural models. For low Al content an irregular "cloudy" morphology was predominant. As the Al content increased, the "cloudy" morphology disappeared and the predominant was a "paper like" sheets. The structural analysis of the samples proved that the Al enters in the tobermorite structure occupying both bridging and branching positions. For low Al dosages, there are more bridging positions than for high Al dosage where the branching positions are predominants. When higher amounts of Al are added, the structure is more ordered, have more branching positions than bridging and the structure is more similar to the one of the crystalline tobermorite instead of a C-S-H gel. The structural analysis has also through some light about the two types of 11Å tobermorite, the normal and the

anomalous. In the anomalous sample there is a big difference in the number of Al in branching position in comparison with the normal samples. So, due to the high stability of the Al-Si bond, the thermal treatment does not allow it to break and constrain the structure and it remains anomalous. However further analyses should be carried out to study deeper this theory. These samples were also analyzed by broadband dielectric spectroscopy (BDS) as part of the collaboration with Silvina Cerveny and Guido Goracci in the "Materials Physics Center" of San Sebastian. With this technique is possible to analyze the dynamics of polar molecules in different environments in a broad frequency and temperature range. In particular in the case of tobermorite here analyzed, it is possible to access the molecular movements of the water molecules confined in the zeolitic cavities. Since these measurements are sensitive to the environment surrounding the water molecules, it is possible to detect differences among the tobermorites synthesized with different Al content.

Analyzing the variation of the water dynamics in tobermorite with different Al content, it has been possible to conclude that the samples with less Al content (0 and 3 wt %) resemble the response observed for C-S-H gel, i.e. the dynamics of water is similar to that observed in the amorphous C-S-H gel. However, increasing the Al content (6 and 10 wt%) the water dynamics look like as that in the natural and crystalline tobermorite. However, these results are still being processed and will be included in a future publication.

In this first part of the thesis, it was also experimented a new hydrothermal synthetic route using a supercritical continuous reactor. The first step was to design a reactor, and in this work, we have presented an optimized reactor suitable for the synthesis of crystalline and pure xonotlite and tobermorite. As a result, we confirm the viability to produce both pure tobermorite and xonotlite at supercritical conditions (400ºC and 23.5 MPa). This result is especially interesting in the case of tobermorite because in the literature it was described that this compound is unstable over 130ºC and it transforms into xonotlite. However, with this synthetic route, we have demonstrated that if we control the kinetic of the reaction, not only it is possible to obtain pure tobermorite, but also it is obtained in only 7 seconds, while under subcritical conditions the reactions take hours or even days. Another interesting result obtained is that the morphology of the product is fibrous, which is more similar to the natural

tobermorite. So it could be said that this synthesis route might reproduce more accurately what it could be happening in nature when tobermorite is formed. In the case of the xonotlite synthesis, it was possible to obtain the product within only 11 seconds, while under subcritical conditions several hours are required. Concerning the reactor, the model that we have used is for a laboratory scale. So, in order to produce higher quantities, it would be advisable in the future to scale-up the system and obtain a more suitable reactor for big productions. This could be interesting for the industrial uses of the tobermorite.

Following this line of the supercritical synthesis, one more synthesis was carried out in a batch reactor. This was just a preliminary study were crystalline fibrous tobermorite was obtained; however, the products were not pure. Nevertheless it was demonstrated that the fibrous morphology is given by the energetic supercritical phase, not for the continuous flow. Also it was highlighted the necessity of controlling the kinetic in order to obtain pure tobermorite.

In the second part of the thesis was studied the effect of the xonotlite and the tobermorite as a seed in cement paste. Through the use of two methods, calorimetric and mechanical test it was demonstrated the accelerating effect of both compounds.

In the calorimetric test for the xonotlite, it was possible to see that the setting process is accelerated in comparison to the reference. Different dosages were used: 0.5%, 1%, 2% and 5% and at no dosage was perceptible the accelerating effect, being more intense at the highest dosage. The mechanical test for xonotlite showed an improvement of the compression strength at early times (8 hours) comparing with the reference. At long times both strengths are equal. So it accelerates the process but doesn't have a negative effect at long times. For this test, only one variable was taken into account, the dosage. It was proved that the dosage has little effect on the compression test at short times, it is observed a slight improvement for the highest dosage 5%, but this is not so big.

For the tobermorite calorimetric test, different variables were employed. The conclusions obtained were in the first place that the Al content in the sample, and therefore the crystallinity of the product, does not affect to the acceleration. Also, that the higher is the dosage, the more intense is the effect and at least that when the seeds are added as dispersion, without previous drying process, the effect is higher, but it is necessary the use of a superplasticizer. In the mechanical test, the same variables were

employed and, also in this type of test, no improvement in the strength was observed when it was used a tobermorite with different % of Al. For the dosage, it was proved that the highest dose 5% gives an improvement of the double at early times (6 hours) and the strength remains stable at longer times. Another important result is that when the mix is prepared with not-dried seeds at a 2% dosage, the compression resistance is six times higher at short times (6 hours) than the reference and three times more strength than the sample with dried seeds. However, the cement paste done employing not-dried seeds was not very fluid, and this made not possible to introduce dosages above 2% because the workability was very low.

To summarize, this thesis follows the complete path from the hypothesis that xonotlite and tobermorite could work as acceleration additions in cement paste, up to the test of their effect in cement paste, passing through the development of a new synthesis route to produce them.

BIBLIOGRAPHY

[1]   B. Herring, *Constructor* **2002**, 13–15.

[2]   P. R. S. Moorey, *Ancient Mesopotamian Materials and Industries*, Eisenbrauns, Indiana, **1999**.

[3]   S. Pavía, S. Caro, *Constr. Build. Mater.* **2008**, *22*, 1807–1811.

[4]   M. Vitruvius, *De Architectura*, **25AD**.

[5]   R. Zawawi, Artificial Hydraulic Lime Mortar Obtained by Calcining Limestone and Siliceous Waste Materials, **2010**.

[6]   L. Coppola, *BETONROSSI BASIC CONCRETE Prescrivere, Confezionare E Mettere in Opera Calcestruzzi Durevoli*, **2002**.

[7]   J. P. Mercier, G. Zambelli, W. Kurz, *Introduction À La Science Des Matériaux*, Presses Polytechniques Et Universitaires Romandes, **1999**.

[8]   A. R. Martínez, Estudio Del Sector Cementero a Nivel Mundial Y Nacional, Con Particularización de Una Empresa Cementera Situada En La Comunidad Valenciana, Universidad Politécnica de Valencia, **2014**.

[9]   Cembureau, *Activity Report 2015*, **2007**.

[10]   Portland Cement Association, *Portl. Cem. Assoc.* **2013**.

[11]   P. Wray, *Am. Ceram. Soc. Bull.* **2012**, 47–50.

[12]   N. Mahasenan, S. Smith, K. Humphreys, in *Greenh. Gas Control Technol. - 6th Int. Conf.*, **2003**, pp. 995–1000.

[13]   M. S. Imbabi, C. Carrigan, S. McKenna, *Int. J. Sustain. Built Environ.* **2012**, *1*, 194–216.

[14]   Federación interamericana del cemento, **2013**, 41.

[15]   World Business Council for Sustainable Developmemt, International Energy Agency, **2009**, 36.

[16]   U.S. Environmental Protection Agency, *Portland Cement Manufacturing*, **1995**.

[17]   C. J. Engelsen, *Quality Improvers in Cement Making – State of the Art*, **2008**.

[18]   F. M. Lea, *Encycl. Br.* **n.d.**

[19]   H. Manzano, Atomistic Simulation Studies of the Cement Paste Components, Universidad del País Vasco, **2009**.

[20]   M. N. De Noirfontaine, S. Tusseau-Nenez, C. Girod-Labianca, V. Pontikis, *J. Mater. Sci.* **2012**, *47*, 1471–1479.

[21]   H. F. W. Taylor, *Cement Chemistry*, Thomas Telford, **1997**.

[22]   I. Sharpley, The Effect of Hydration on the Microstructural Properties of Individual Phases of Ordinary Portland Cement, University College London,

2015.

[23] F. M. Lea, P. C. Hewlett, *Lea's Chemistry of Cement and Concrete*, Arnold, **1998**.

[24] J. Thomas, H. M. Jennings, "The science of concrete," can be found under http://iti.northwestern.edu/cement/index.html, **n.d.**

[25] H. Zhang, J. Zhuang, S. Huang, X. Cheng, Q. Hu, Q. Guo, J. Guo, *RSC Adv.* **2015**, *5*, 55428–55437.

[26] A. Ioannidou, Precipitation , Gelation and Mechanical Properties of Calcium-Silicate-Hydrate Gels, **2014**.

[27] B. J. Dalgleish, A. Ghose, H. M. Jennings, P. L. Pratt, in *Proc. RILEM Colloq.* (Ed.: E.A. ANPC), Paris, **1982**, p. 137.

[28] B. J. Dalgleish, P. L. Pratt, E. Toulson, *J. Mater. Sci.* **1982**, *17*, 2199–2207.

[29] D. D. Double, A. Hellawell, S. J. Perry, *Proc R Soc London Ser A* **1978**, *359*, 435–451.

[30] G. W. Groves, *J. Mater. Sci.* **1981**, *16*, 1063–1070.

[31] P. L. Pratt, A. Ghose, J. Skalny, P. C. Hewlett, *Phil. Trans. R. Soc. Lond.* **1983**, *310*, 93–103.

[32] J. P. Skalny, K. . Scrivener, in (Ed.: J.P. Skalny), Columbus, OH (USA); American Ceramic Society Inc., **1989**, p. 127.

[33] K. L. Scrivener, P. L. Pratt, in *Proc. Br. Ceram. Soc.*, **1984**, p. 207.

[34] H. Manzano, A. N. Enyashin, J. S. Dolado, A. Ayuela, J. Frenzel, G. Seifert, *Adv. Mater.* **2012**, *24*, 3239–3245.

[35] H. F. W. TAYLOR, *J. Am. Ceram. Soc.* **1986**, *69*, 464–467.

[36] I. G. Richardson, G. W. Groves, *Cem. Concr. Res.* **1992**, *22*, 1001–1010.

[37] I. . Richardson, *Cem. Concr. Compos.* **2000**, *22*, 97–113.

[38] I. . Richardson, *Cem. Concr. Res.* **1999**, *29*, 1131–1147.

[39] H. Manzano, Atomistic Simulation Studies of the Cement Paste Components, **2009**.

[40] H. L. Chatelier, J. L. Mack, *Experimental Researches on the Constitution of Hydraulic Mortars*, McGraw Publishing Company, **1905**.

[41] S. B. Newberry, M. M. Smith, *J. Soc. Chem. Ind.* **1903**, *22*, 94–95.

[42] R. H. Bogue, *The Chemistry of Portland Cement*, Reinhold Pub. Corp., **1955**.

[43] J. S. Dolado, M. Griebel, J. Hamaekers, *J. Am. Ceram. Soc.* **2007**, *90*, 3938–3942.

[44] V. S. Ramachandran, J. J. Beaudoin, *Handbook of Analytical Techniques in Concrete Science and Technology*, Noyes Publications, **2001**.

[45] H. M. Jennings, J. J. Thomas, J. S. Gevrenov, G. Constantinides, F. J. Ulm, *Cem. Concr. Res.* **2007**, *37*, 329–336.

[46] J. W. Jeffery, J. D. Bernal, H. F. W. Taylor, *Mag. Concr. Res.* **1952**, *4*, 49–54.

[47] H. F. W. Taylor, *J. Chem. Soc.* **1950**, 3682–3690.

[48] H. F. W. Taylor, *J. Am. Ceram. Soc.* **1986**, *69*, 464–467.

[49] I. G. Richardson, *Cem. Concr. Res.* **2004**, *34*, 1733–1777.

[50] H. W. F. Taylor, in *Proc. Fifth Int. Symp. Chem. Cem. Tokyo, 1968 Chem. Cem. Clinker* (Ed.: K. Semento), Cement Association Of Japan, **1969**, pp. 1–26.

[51] M. D. Andersen, H. J. Jakobsen, J. Skibsted, *Cem. Concr. Res.* **2004**, *34*, 857–868.

[52] J. A. Gard, H. F. W. Taylor, *Cem. Concr. Res.* **1976**, *6*, 667–677.

[53] H. F. W. Taylor, J. W. Howison, *Clay Miner. Bull.* **1956**, *3*, 98–111.

[54] X. Cong, R. J. Kirkpatrick, *Adv. Cem. Based Mater.* **1996**, *3*, 144–156.

[55] X. Cong, R. J. Kirkpatrick, *J Am Ceram Soc* **1996**, *79*, DOI 10.1111/j.1151-2916.1996.tb08768.x.

[56] P. Yu, R. J. Kirkpatrick, B. Poe, P. F. McMillan, X. Cong, *J. Am. Ceram. Soc.* **1999**, *82*, 742–748.

[57] D. Viehland, L. J. Yuan, Z. Xu, X.-D. Cong, R. J. Kirkpatrick, *J. Am. Ceram. Soc.* **1997**, *80*, 3021–3028.

[58] J. J. Thomas, J. J. Chen, H. M. Jennings, D. A. Neumann, *Chem. Mater.* **2003**, *15*, 3813–3817.

[59] H. Manzano, A. Ayuela, J. S. Dolado, *J. Comput. Mater. Des.* **2007**, *14*, 45–51.

[60] M. D. Jackson, S. R. Chae, S. R. Mulcahy, C. Meral, R. Taylor, P. Li, A.-H. Emwas, J. Moon, S. Yoon, G. Vola, et al., *Am. Mineral.* **2013**, *98*, 1669 LP-1687.

[61] M. D. Jackson, J. Moon, E. Gotti, R. Taylor, S. R. Chae, M. Kunz, a. H. Emwas, C. Meral, P. Guttmann, P. Levitz, et al., *J. Am. Ceram. Soc.* **2013**, *96*, 2598–2606.

[62] B. K. Violetta, Kari L. Yuers, J. M. Aldred, N. S. Berke, C. J. Bognacki, M. L. Brown, L. J. Cook, T. Durning, R. Eller, H. Farzam, et al., *REPORT ON CHEMICAL ADMIXTURES FOR CONCRETE Report on Chemical Admixtures for Concrete*, **2016**.

[63] C. Aggregates, *Quality* **2001**, *4*, 1–9.

[64] R. L. Angstadt, F. R. Hurley, *Spodumene Accelerated Portland Cement*, **1967**, US3331695 A.

[65] H. N. Stein, J. M. Stevels, *J. Appl. Chem.* **1964**, *14*, 338–346.

[66] J. A. Nelson, J. F. Young, *Cem. Concr. Res.* **1977**, *7*, 277–282.

[67] Z.-Q. Wu, J. F. Young, *J. Mater. Sci.* **1984**, *19*, 3477–3486.

[68] W. Kurdowski, W. Nocuń-Wczelik, *Cem. Concr. Res.* **1983**, *13*, 341–348.

[69] R. Alizadeh, L. Raki, J. M. Makar, J. Beaudoin, I. Moudrakovski, **2009**, 7937–7946.

[70] P. Bost, M. Regnier, M. Horgnies, *Comparison of the Accelerating Effect of Various Additions on the Early Hydration of Portland Cement*, **2016**.

[71] G. Land, D. Stephan, *Nanotechnol. Constr.* **2015**, 377–382.

[72] J. J. Thomas, H. M. Jennings, J. J. Chen, *J Phys Chem c* **2009**, *113*, 4327–4334.

[73] S. Ditter, S. Hauck, R. Konig, *bft Int.* **2013**, *january*, 44–51.

[74] G. Land, D. Stephan, *Cem. Concr. Compos.* **2015**, *57*, 64–67.

[75] U. Berg, D. Donnert, P. G. Weidler, E. Kaschka, G. Knoll, R. Nüesch, *Water Sci. Technol.* **2006**, *53*, 131–138.

[76] O. P. Shrivastava, R. Shrivastava, *Bull. Mater. Sci.* **2000**, *23*, 515–520.

[77] S. Shaw, S. M. Clark, C. M. B. Henderson, *Chem. Geol.* **2000**, *167*, 129–140.

[78] S. Merlino, E. Bonaccorsi, T. Armbruster, *Eur. J. Mineral.* **2001**, *13*, 577–590.

[79] R. J. Myers, E. L'Hôpital, J. L. Provis, B. Lothenbach, *Cem. Concr. Res.* **2015**, *68*, 83–93.

[80] N. S. Bell, S. Venigalla, P. M. Gill, J. H. Adair, *J. Am. Ceram. Soc.* **1996**, *79*, 2175–2178.

[81] A. Vidmer, G. Sclauzero, A. Pasquarello, *Cem. Concr. Res.* **2014**, *60*, 11–23.

[82] L. Black, K. Garbev, a. Stumm, *Adv. Appl. Ceram.* **2009**, *108*, 137–144.

[83] E. Bonaccorsi, S. Merlino, A. R. Kampf, *J. Am. Ceram. Soc.* **2005**, *88*, 505–512.

[84] H. F. W. Taylor, in *6th Natl. Conf. Clays Clay Miner.*, **1959**, pp. 101–109.

[85] T. Mitsuda, H. W. F. Taylor, *Mineral. Mag.* **1978**, *42*, 229–235.

[86] J. D. C. McConnell, *Mineral. Mag.* **1954**, *30*, 293–305.

[87] H. D. Megaw, C. H. Kelsey, *Nature* **1956**, *177*, 390–391.

[88] S. A. Hamid, *Z. Krist.* **1981**, *1981*, 189–198.

[89] S. Merlino, E. Bonaccorsi, T. Armbruster, *Am. Mineral.* **1999**, *84*, 1613–1621.

[90] S. Merlino, E. Bonaccorsi, T. Armbruster, *Eur. J. Mineral.* **2000**, *12*, 411–429.

[91] S. P. Jakobsson, I. Museum, **1986**, 648–659.

[92] S. A. S. El-Hemaly, T. Mitsuda, H. F. W. Taylor, *Cem. Concr. Res.* **1977**, *7*, 429–438.

[93] M. Sakiyama, T. Mitsuda, *Cem. Concr. Res.* **1977**, *7*, 681–685.

[94] R. Gabrovšek, B. Kurbus, D. Mueller, W. Wieker, *Cem Concr Res* **1993**, *23*, 321–328.

[95] T. Mitsuda, H. F. W. Taylor, *Cem Concr Res* **1975**, *5*, 203–210.

[96] G. L. Kalousek, *J. Am. Ceram. Soc.* **1957**, *40*, 74–80.

[97] S. Diamond, *J. Am. Ceram. Soc.* **1964**, *47*, 593–594.

[98] X. Pardal, F. Brunet, T. Charpentier, I. Pochard, A. Nonat, *Inorg. Chem.* **2012**, *51*, 1827–1836.

[99] Z. Wang, S. Ma, S. Zheng, X. Wang, *J. Am. Ceram. Soc.* **2016**, 792–799.

[100] M. W. Barnes, B. E. Scheetz, in *Mat. Res. Soc. Symp. Proc*, **1991**, pp. 243–272.

[101] S. Diamond, J. . White, W. . Dolch, *Effects of Isomorphous Subtitution in Hydrothermally Synthesised Tobermorite*, **1964**.

[102] S. Komarneni, *Clays Clay Miner.* **1987**, *35*, 385–390.

[103] N. J. Coleman, *Int. J. Environ. Waste Manag.* **2011**, *8*, 366–382.

[104] W. Ma, P. W. Brown, S. Komarneni, *J. Am. Ceram. Soc.* **1996**, *79*, 1707–1710.

[105] N. J. Coleman, Q. Li, A. Raza, *Physicochem. Probl. Miner. Process.* **2014**, *50*, 5–16.

[106] S. Komarneni, E. Breval, D. M. Roy, R. Roy, *Cem. Concr. Res.* **1988**, *18*, 204–220.

[107] C. Rammelsberg, *Zeitschrift der Dtsch. Geol. Gesellschaft* **1866**, *18*, 33–34.

[108] C. Hejny, T. Armbruster, *Z. Krist.* **2001**, *216*, 396–408.

[109] E. Burzo, in *Gr. III Condens. Matter Vol. 27 Magn. Prop. Non-Metallic Inorg. Compd. Based Transit. Elem. Subvolume I4* (Ed.: H.P.. Wijn), Springer Berlin Heidelberg, New York, **2011**, pp. 371–378.

[110] S. V. Churakov, P. Mandaliev, *Cem. Concr. Res.* **2008**, *38*, 300–311.

[111] G. L. Kalousek, T. Mitsuda, H. F. W. Taylor, *Cem. Concr. Res.* **1977**, *7*, 305–312.

[112] S. Komarneni, R. Roy, D. M. Roy, *Cem. Concr. Res.* **1986**, *16*, 47–58.

[113] O. P. Shrivastava, S. Komarneni, E. Breval, *Cem. Concr. Res.* **1991**, *21*, 83–90.

[114] O. Anton, A. Eckert, A. Eckert, **1991**.

[115] N. M. P. Low, J. J. Beaudoin, *Cem. Concr. Res.* **1993**, *23*, 1016–1028.

[116] K. Luke, *J. Sustain. Cem. Mater.* **2015**.

[117] X. Li, J. Chang, *Chem. Lett.* **2004**, *33*, 1458–1459.

[118] P. Siriphannon, Y. Kameshima, A. Yasumori, K. Okada, S. Hayashi, **2000**.

[119] X. Liu, C. Ding, *Mater. Lett.* **2002**, *57*, 652–655.

[120] X. Liu, C. Ding, P. K. Chu, *Biomaterials* **2004**, *25*, 1755–1761.

[121] K. Lin, W. Zhai, S. Ni, J. Chang, Y. Zeng, W. Qian, *Ceram. Int.* **2005**, *31*, 323–326.

[122] P. . De Aza, Z. . Luklinska, M. . Anseau, F. Guitian, S. De Aza, *J. Dent.* **1999**, *27*, 107–113.

[123] X. Li, J. Chang, *J. Mater. Sci.* **2006**, *41*, 4944–4947.

[124] K. Byrappa, M. Yoshimura, *Handbook of Hydrothermal Technology*, **2001**.

[125] G. W. Morey, *J. Am. Ceram. Soc.* **1953**, *36*, 279–285.

[126] P. W. Bridgman, *The Physics of High Pressure.*, **1933**.

[127] K. F. E. Schafhault, *Gelehtre Anzeigen Bayer. Akad.* **1845**, *20*.

[128] R. Nacken, *Artificial Quartz Crystals*, **1946**.

[129] R. M. Barrer, *J. Chem. Soc.* **1948**, 2158–2163.

[130] R. A. Laudise, A. A. Ballman, *Kirk-Othmer Encycl. Chem. Technol.* **1969**, 105.

[131] R. A. Laudise, A. A. Ballman, *J. Am. Chem. Soc* **1958**, *80*, 2655–2657.

[132] A. R. West, *Solid State Chemistry and Its Applications*, **2013**.

[133] S. D. Hamann, *Phys. Chem. Earth* **1981**, *13*, 89–111.

[134] G. Brunner, *Hydrothermal and Supercritical Water Processes*, Elsevier Science, **2014**.

[135] U. Schubert, N. Hüsing, *Synthesis of Inorganic Materials*, Wiley, **2012**.

[136] H. W. F. Taylor, in *Chem. Cem. Vol I*, **1964**, pp. 167–232.

[137] I. Harker, *J. Am. Ceram. Soc.* **1964**, *47*.

[138] E. Bonaccorsi, S. Merlino, *Rev. Mineral. Geochemistry* **2005**, *57*, 241–290.

[139] S. A. Hamid, *J. Cryst. Growth* **1979**, *46*, 421–426.

[140] S. Y. Hong, F. P. Glasser, *Cem. Concr. Res.* **2004**, *34*, 1529–1534.

[141] D. A. Buckner, D. M. Roy, R. Roy, *Am. J. Sci.* **1960**, *258*, 132–147.

[142] L. Black, K. Garbev, P. Stemmermann, K. R. Hallam, G. C. Allen, *Cem. Concr. Res.* **2003**, *33*, 899–911.

[143] L. Heller, H. F. W. Taylor, *J. Chem. Soc.* **1951**, 2397–2401.

[144] K. Speakman, **1968**, *30*.

[145] P. E. Flint, H. F. McMurdie, L. S. Wells, *J. Res. Natl. Bur. Standars* **1938**, *21*.

[146] X. Cong, R. J. Kirkpatrick, *Adv. Cem. Based Mater.* **1996**, *3*, 133–143.

[147] M. R. Hansen, H. J. Jakobsen, J. Skibsted, *Inorg. Chem.* **2003**, *42*, 2368–2377.

[148] N. Y. Mostafa, a. a. Shaltout, H. Omar, S. a. Abo-El-Enein, *J. Alloys Compd.* **2009**, *467*, 332–337.

[149] A. Yazdani, H. R. Rezaie, H. Ghassai, *J. Ceram. Process. Res.* **2010**, *11*, 348–353.

[150] A. Hartmann, D. Schulenberg, J. Buhl, **2015**, 39–55.

[151] K. Lin, J. Chang, G. Chen, M. Ruan, C. Ning, *J. Cryst. Growth* **2007**, *300*, 267–271.

[152] W. Tan, G. Zhu, Y. Liu, Z. Zhang, L. Liu, *Cem. Concr. Res.* **2015**, *72*, 69–75.

[153] J. Cao, F. Liu, Q. Lin, Y. Zhang, *Prog. Nat. Sci.* **2008**, *18*, 1147–1153.

[154] X. Huang, D. Jiang, S. Tan, *J. Eur. Ceram. Soc.* **2003**, *23*, 123–126.

[155] S. Tränkle, D. Jahn, T. Neumann, L. Nicoleau, N. Hüsing, D. Volkmer, *J. Mater. Chem. A* **2013**, *1*, 10318.

[156] A. Hartmann, J. Buhl, *Mater. Res. Bull.* **2010**, *45*, 396–402.

[157] A. Hartmann, M. Khakhutov, J. Buhl, *Mater. Res. Bull.* **2014**, *51*, 389–396.

[158] K. Lin, J. Chang, J. Lu, *Mater. Lett.* **2006**, *60*, 3007–3010.

[159] J. Reinik, I. Heinmaa, U. Kirso, T. Kallaste, J. Ritamäki, D. Boström, E. Pongrácz, M. Huuhtanen, W. Larsson, R. Keiski, et al., *J. Hazard. Mater.* **2011**, *196*, 180–186.

[160] N. J. Coleman, C. J. Trice, J. W. Nicholson, *Int. J. Miner. Process.* **2009**, *93*, 73–78.

[161] N. J. Coleman, *Mater. Res. Bull.* **2005**, *40*, 2000–2013.

[162] D. Palubinskaite, a Kantautas, *Mater. Sci.* **2006**, *24*, 395–403.

[163] X. Huang, D. Jiang, S. Tan, *Mater. Res. Bull.* **2002**, *37*, 1885–1892.

[164] S. Tränkle, D. Jahn, T. Neumann, L. Nicoleau, N. Hüsing, D. Volkmer, *J. Mater. Chem. A* **2013**, *1*, 10318.

[165] P. G. Jessop, W. Leitner, *Chemical Synthesis Using Supercritical Fluids*, Wiley, **2008**.

[166] B. Berche, M. Henkel, R. Kenna, *Rev. Bras. Ensino Física* **2009**, *31*, 2602.1-2602.4.

[167] C. Cagniard de la Tour, in *Ann. Chim. Phys.* (Eds.: F. Arago, J.L. Gay-Lussac), Crochard, **1822**.

[168] C. Cagniard de la Tour, in *Ann. Chim. Phys.* (Eds.: F. Arago, J.L. Gay-Lussac), Crochard, **1823**.

[169] M. Faraday, *Philos. Trans. R. Soc. London* **1845**, *135*, 155–i.

[170] D. Mendelejeff, *Justus Liebigs Ann. Chem.* **1861**, *119*, 1–11.

[171] T. Andrews, *Philos. Trans. R. Soc. London* **1869**, *159*, 575–590.

[172] R. Askin, S. Otles, *Acta Sci.Pol. Technol. Aliment.* **2005**, *4*, 3–16.

[173] J. B. Hannay, J. Hogarth, *Proceeding R. Soc. London* **1879**, *29*, 324–326.

[174] K. Zosel, **1981**.

[175] T. Adschiri, K. Kanazawa, K. Arai, *J. Am. Ceram. Soc.* **1992**, *75*, 1019–1022.

[176] C. Aymonier, A. Loppinet-serani, H. Rever, Y. Garrabos, *J. Supercrit. Fluids* **2006**, *38*, 242–251.

[177] F. Cansell, C. Aymonnier, *J. Supercrit. Fluids* **2009**, *3*, 508–516.

[178] A. Chakrabarty, S. Marre, R. F. Landis, V. M. Rotello, U. Maitra, A. Del Guerzo, C. Aymonier, *J. Mater. Chem. C* **2015**, *3*, 7561–7566.

[179] K. Byrappa, T. Adschiri, *Prog. Cryst. Growth Charact. Mater.* **2007**, *53*, 117–166.

[180] P. S. Shah, T. Hanrath, K. P. Johnston, B. a. Korgel, *J. Phys. Chem. B* **2004**, *35*, 9574–9587.

[181] A. Chaudhry, S. Haque, S. Kellici, P. Boldrin, I. Rehman, F. a Khalid, J. a Darr, *Chem. Commun. (Camb).* **2006**, 2286–2288.

[182] R. I. Gruar, C. J. Tighe, P. Southern, Q. a. Pankhurst, J. a. Darr, *Ind. Eng. Chem. Res.* **2015**, *54*, 7436–7451.

[183] G. Philippot, E. D. Boejesen, C. Elissalde, M. Maglione, C. Aymonier, B. B. Iversen, *Chem. Mater.* **2016**, *28*, 3391–3400.

[184] G. Philippot, K. M. Ø. Jensen, M. Christensen, C. Elissalde, M. Maglione, B. B. Iversen, C. Aymonier, *J. Supercrit. Fluids* **2014**, *87*, 111–117.

[185] D. Bröll, C. Kaul, A. Krämer, P. Krammer, T. Richter, M. Jung, H. Vogel, P. Zehner, *Angew. Chemie - Int. Ed.* **1999**, *38*, 2998–3014.

[186] Y. Marcus, *Fluid Phase Equilib.* **1999**, *164*, 131–142.

[187] D. E. Winterbone, *Advanced Thermodynamics for Engineers*, **1997**.

[188] M. Monasterio, J. J. Gaitero, H. Manzano, J. S. Dolado, S. Cerveny, *Langmuir* **2015**, *31*, 4964–4972.

[189] K. Matsui, A. Ogawa, J. Kikuma, M. Tsunashima, T. Ishikawa, S. Matsuno, in *Denver X-Ray Conf. Appl. X-Ray Anal.*, **2009**, pp. 1–7.

[190] C. Biagioni, E. Bonaccorsi, S. Merlino, D. Bersani, C. Forte, *Eur. J. Mineral.* **2012**, *24*, 991–1004.

[191] J. R. Houston, R. S. Maxwell, S. A. Carroll, *Geochem. Trans.* **2009**, *10*, 1–14.

[192] W. M. Kriven, J. Wang, T. Fischer, D. Zhu, S. Kirihara, *Developments in Strategic Ceramic Materials: Ceramic Engineering and Science Proceedings, Volume 36*, Wiley, **2016**.

[193] H. Manzano, J. S. Dolado, M. Griebel, J. Hamaekers, *Phys. Status Solidi Appl. Mater. Sci.* **2008**, *205*, 1324–1329.

[194] X. Guo, F. Meng, H. Shi, *Constr. Build. Mater.* **2017**, *133*, 253–260.

[195] M. Mehrali, E. Moghaddam, S. F. S. Shirazi, S. Baradaran, M. Mehrali, S. T. Latibari, H. S. C. Metselaar, N. A. Kadri, K. Zandi, N. A. A. Osman, *ACS Appl. Mater. Interfaces* **2014**, *6*, 3947–62.

[196] I. Halasz, R. Li, M. Agarwal, N. Miller, *From Zeolites to Porous MOF Materials - The 40th Anniversary of International Zeolite Conference, Proceedings of the 15th International Zeolite Conference*, Elsevier, **2007**.

[197] H. Noma, Y. Adachi, Y. Matsuda, T. Yokoyama, *Chem. Lett.* **1998**, *27*.

[198] M. Monasterio, J. J. Gaitero, H. Manzano, J. S. Dolado, S. Cerveny, *Langmuir* **2015**, *31*, 4964–4972.

[199] B. Lafuente, R. T. Downs, H. Yang, N. Stone, *Highlights Mineral. Crystallogr.* **2015**, 1–30.

[200] S. A. Hamid, *Zeitschrift für Krist. - Cryst. Mater.* **1981**, *154*, 189–198.

[201] T. Maeshima, H. Noma, M. Sakiyama, T. Mitsuda, *Cem. Concr. Res.* **2003**, *33*, 1515–1523.

[202] G. Wei, Y. Liu, X. Zhang, F. Yu, X. Du, *Int. J. Heat Mass Transf.* **2011**, *54*, 2355.

[203] Smeets, L., van de Worp, B., and Dewald, K., *SAE Tech. Pap.* **2011**.

[204] E. Kloimsteln, R. Eatermann, *United States Patent [191 Patent Number :*, **1990**.

[205] S. Komarneni, D. M. Roy, *Science (80-.).* **1983**, *221*, 647–648.

[206] S. Komarneni, E. Breval, D. M. Roy, R. Roy, *Cem. Concr. Res.* **1988**, *18*, 204–220.

[207] M. Tsuji, S. Komarneni, P. Malla, *J. Am. Ceram. Soc.* **1991**, *74*, 274–279.

[208] K. Sobolev, M. F. Gutiérrez, *Am. Ceram. Soc. Bull.* **2005**, *84*, 14–18.

[209] L. Raki, J. Beaudoin, R. Alizadeh, J. Makar, T. Sato, *Materials (Basel).* **2010**, *3*, 918–942.

APPENDIX

Appendix I: Xonotlite hydrothermal synthesis

<table>
<tr>
<th colspan="4">Reference</th>
<th colspan="6">Reaction conditions</th>
</tr>
<tr>
<th>Ref. number</th>
<th>Year</th>
<th>Authors</th>
<th>Title</th>
<th>Reactives</th>
<th>Ca/(Si+Al)</th>
<th>Water/Solid</th>
<th>Temperature (ºC)</th>
<th>Reaction time</th>
<th>Product</th>
</tr>
<tr>
<td rowspan="15">[1]</td>
<td rowspan="15">1938</td>
<td rowspan="15">Einar P. Flint
H.F. McMurdie
Lansing S. Wells</td>
<td rowspan="15">Formation of hydrated calcium silicates at elevated temperatures and pressures</td>
<td rowspan="15">CaO
+
SiO</td>
<td rowspan="2">0.8</td>
<td rowspan="2">//</td>
<td>300</td>
<td>14 days</td>
<td>Xonotlite</td>
</tr>
<tr>
<td>350</td>
<td>10 days</td>
<td>Xonotlite</td>
</tr>
<tr>
<td rowspan="7">1.0</td>
<td rowspan="7">//</td>
<td>175</td>
<td>79 days</td>
<td>Xonotlite</td>
</tr>
<tr>
<td>200</td>
<td>73 days</td>
<td>Xonotlite</td>
</tr>
<tr>
<td>250</td>
<td>10 days</td>
<td>Xonotlite</td>
</tr>
<tr>
<td>320</td>
<td>7 days</td>
<td>Xonotlite</td>
</tr>
<tr>
<td>370</td>
<td>4 days</td>
<td>Xonotlite</td>
</tr>
<tr>
<td>380</td>
<td>4 days</td>
<td>Xonotlite</td>
</tr>
<tr>
<td>390</td>
<td>4 days</td>
<td>Xonotlite</td>
</tr>
<tr>
<td rowspan="4">1.5</td>
<td rowspan="4">//</td>
<td>250</td>
<td>14 days</td>
<td>Xonotlite + ?</td>
</tr>
<tr>
<td>300</td>
<td>14 days</td>
<td>Xonotlite + ?</td>
</tr>
<tr>
<td>350</td>
<td>14 days</td>
<td>Xonotlite + ?</td>
</tr>
<tr>
<td>400</td>
<td>5 days</td>
<td>Xonotlite + ?</td>
</tr>
<tr>
<td rowspan="9">[2]</td>
<td rowspan="9">1968</td>
<td rowspan="9">K. Speakman</td>
<td rowspan="9">The stability of tobermorite in the system CaO-SiO$_2$-H$_2$O at elevated temperatures and pressures</td>
<td rowspan="5">Ca(OH)$_2$
+
Quartz</td>
<td>0.83</td>
<td>//</td>
<td>225</td>
<td>38 days</td>
<td>Xonotlite + quartz + tobermorite (traces)</td>
</tr>
<tr>
<td>0.67</td>
<td>//</td>
<td>264</td>
<td>26 days</td>
<td>Xonotlite + quartz</td>
</tr>
<tr>
<td rowspan="3">1.33</td>
<td rowspan="3">//</td>
<td>193</td>
<td>34 days</td>
<td>Xonotlite + hillebrandite</td>
</tr>
<tr>
<td>205</td>
<td>14 days</td>
<td>Xonotlite + hillebrandite</td>
</tr>
<tr>
<td>246</td>
<td>14 days</td>
<td>Xonotlite + hillebrandite</td>
</tr>
<tr>
<td rowspan="4">Ca(OH)$_2$
+
Silica gel</td>
<td rowspan="4">1.00</td>
<td rowspan="4">//</td>
<td>160</td>
<td>149 days</td>
<td>Xonotlite</td>
</tr>
<tr>
<td>208</td>
<td>28 days</td>
<td>Xonotlite</td>
</tr>
<tr>
<td>256</td>
<td>8 days</td>
<td>Xonotlite</td>
</tr>
<tr>
<td>273</td>
<td>13 days</td>
<td>Xonotlite</td>
</tr>
</table>

Reference				Reaction conditions					
Ref. number	Year	Authors	Title	Reactives	Ca/(Si+Al)	Water/Solid	Temperature (ºC)	Reaction time	Product
[2]	1968	K. Speakman	The stability of tobermorite in the system CaO-SiO₂-H₂O at elevated temperatures and pressures	Gel of Ca(OH)₂ + Colloidal silica	0.83	//	316	13 days	Xonotlite + truscottite
							150	133 days	Xonotlite
							170	133 days	Xonotlite
							202	7 days	Xonotlite
							246	7 days	Xonotlite
							291	10 days	Xonotlite
					0.917	//	228	7 days	Xonotlite + tobermorite
							271	7 days	Xonotlite + tobermorite
							285 (low pressure)	7 days	Xonotlite + truscottite
							285 (high pressure)	7 days	Xonotlite + tobermorite (trace)
							304	7 days	Xonotlite + truscottite (trace)
				Gel prepared by hydrolysis of Si(OC₂H₅)₄ in the presence of Ca(NO₃)₂	0.83	//	272	17 days	Xonotlite + gyrolite + tobermorite
							287	16 days	Xonotlite + truscottite
							302	17 days	Xonotlite + truscottite
							302	16 days	Xonotlite + truscottite + scawtite
					1.00	//	150	133 days	Xonotlite + scawtite
							248	7 days	Xonotlite
							252	7 days	Xonotlite
				Glass	1.00	//	226	7 days	Xonotlite
							260	7 days	Xonotlite
							275	7 days	Xonotlite
							295	8 days	Xonotlite
							300	7 days	Xonotlite
							305	11 days	Xonotlite

Reference				Reaction conditions					
Ref. number	Year	Authors	Title	Reactives	Ca/(Si+Al)	Water/Solid	Temperature (°C)	Reaction time	Product
[3]	1979	S.A. Hamid	Electron microscopic characterization of the hydrothermal growth of synthetic 11Å tobermorite crystals	CaO + SiO$_2$	1.0	1	175	70h	Xonotlite
					0.1	1	200	72 h	Xonotlite + quartz
[4]	1993	N.M.P. Low J.J. Beaudoin	Mechanical properties and microstructure of cement binders reinforced with synthesized xonotlite micro-fibres	Ca(OH)$_2$ + SiO$_2$	1.0	20	218	24 h	Xonotlite
[5]	1996	X. Cong R. Kirkpatrick	^{29}Si and ^{17}O NMR investigation of the structure of some crystalline calcium silicate hydrates	CaO + Quartz	1.0	7.5	230	5 days	Xonotlite

Reference				Reaction conditions					
Ref. number	Year	Authors	Title	Reactives	Ca/(Si+Al)	Water/Solid	Temperature (ºC)	Reaction time	Product
[6]	2000	S. Shaw S.M Clark C.M.B. Henderson	Hydrothermal formation of the calcium silicate hydrates tobermorite, and xonotlite: an in situ synchrotron study	Calcsilicate alkoxide gel	0.83	5	270	5 h	Xonotlite
[7]	2003	L. Black, K. Garbev, P.Stemmermann, K.R.Hallam G.C Allen	Characterisation of crystalline C-S-H phases by X-ray photoelectron spectroscopy	CaO + SiO_2 1º Milling (12h) 2º Hydrothermal	1.00	4	220	14 days	Xonotlite
[8]	2003	M.R. Hansen H.J. Jakobsen J. Skibsted	[29]Si Chemical Shift Anisotropies in Calcium Silicates from High-Field ^{29}Si MAS NMR Spectroscopy	CaO + SiO_2	1.00	//	250	6 days	Xonotlite
[9]	2004	S.-Y. Hong F.P. Glasser	Phase relations in the CaO–SiO2–H2O system to 200°C at saturated steam pressure	C-S-H gel formed (during 6-24 months) from Aerosil 300 (SiO_2) + $Ca(OH)_2$	1.00	//	200	90 days	Xonotlite

XONOTLITE HYDROTHERMAL SYNTHESIS

Reference				Reaction conditions					
Ref. number	Year	Authors	Title	Reactives	Ca/(Si+Al)	Water/Solid	Temperature (ºC)	Reaction time	Product
[10]	2006	X. Li J. Chang	A novel hydrothermal route to the synthesis of xonotlite nanofibers and investigation on their bioactivity	TEOS + CTAB + Ca(NO$_3$)$_2$ + NaOH (pH=11.8)	//	//	180	30 h	Xonotlite
[11]	2007	K.Lin J.Chang G.Chen M.Ruan C.Ning	A simple method to synthesize single-crystalline wollastonite nanowires	Na$_2$SiO$_3$·9H$_2$O + Ca(NO$_3$)$_2$·4H$_2$O	1.00	//	200	24 h	Xonotlite
[12]	2009	N.Y Mostafa, A.A Shaltout, H. Omar, S.A. Abo-El-Enein,	Hydrothermal synthesis and characterization of aluminium and sulfate substituted 1.1 nm tobermorites	SiO$_2$ + CaO	1.00	10	220	24 h	Xonotlite
[13]	2009	L. Black K.Garev A.Stumm	Structure, bonding and morphology of hydrothermally synthesised xonotlite	SiO$_2$ + CaO	1.0	//	200	7 days	Low crystalline xonotlite + calcite (traces)
							220	7 days	Crystalline xonotlite + calcite (traces)
								14 days	Crystalline xonotlite + calcite
							250	7 days	High crystalline xonotlite + calcite (traces)

Reference				Reaction conditions					
Ref. number	Year	Authors	Title	Reactives	Ca/(Si+Al)	Water/Solid	Temperature (ºC)	Reaction time	Product
[14]	2008	J.Cao F.Liu Q.Lin Y.Zhang	Hydrothermal synthesis of xonotlite from carbide slag	SiO$_2$ + Carbide slag	1.00	30	205	8h	Tobermorite + xonotlite
							215	8h	Xonotlite
							220	6h	Tobermorite + xonotlite
								8h	Xonotlite
								10h	Xonotlite
							225	8h	Xonotlite
[15]	2010	A.Yazdani H.R.Rezaie H.Ghassai	Investigation of hydrothermal synthesis of wollastonite using silica and nano silica at different pressures	SiO$_2$ + CaO	0.54	2	200 °C (P=3atm)	2 h	Dicalcium silicate hidrate +quartz +calcium hydroxide
							200 °C (P=5atm)	2 h	Dicalcium silicate hidrate +quartz +calcium hydroxide
							200 °C (P=7atm)	2 h	Dicalcium silicate hidrate +quartz +calcium hydroxide
					0.8	2	200 °C (P=3atm)	2 h	Dicalcium silicate hidrate +quartz +calcium hydroxide
							200 °C (P=5atm)	2 h	Dicalcium silicate hidrate +quartz +calcium hydroxide
							200 °C (P=7atm)	2 h	Dicalcium silicate hidrate +quartz +calcium hydroxide
					1.0	2	200 °C (P=3atm)	2 h	Xonotlite + dicalcium silicate hidrate +quartz +calcium hydroxide
							200 °C (P=5atm)	2 h	Xonotlite + dicalcium silicate hidrate +quartz +calcium hydroxide
							200 °C (P=7atm)	2 h	Xonotlite + dicalcium silicate hidrate +quartz +calcium hydroxide

Reference				Reaction conditions					
Ref. number	Year	Authors	Title	Reactives	Ca/(Si+Al)	Water/Solid	Temperature (°C)	Reaction time	Product
[15]	2010	A.Yazdani H.R.Rezaie H.Ghassai	Investigation of hydrothermal synthesis of wollastonite using silica and nano silica at different pressures	Nano - SiO₂ + CaO	0.54	2	200 °C (P=3atm)	2 h	Calcium hydroxide
							200 °C (P=5atm)	2 h	Xonotlite + calcium hydroxide
							200 °C (P=7atm)	2 h	Xonotlite + calcium hydroxide
					0.8	2	200 °C (P=3atm)	2 h	Xonotlite + quartz +calcium hydroxide
							200 °C (P=5atm)	2 h	Xonotlite + dicalcium silicate hidrate +quartz +calcium hydroxide
							200 °C (P=7atm)	2 h	Xonotlite + dicalcium silicate hidrate +quartz +calcium hydroxide
					1.0	2	200 °C (P=3atm)	2 h	Xonotlite + dicalcium silicate hidrate +quartz +calcium hydroxide
							200 °C (P=5atm)	2 h	Xonotlite + dicalcium silicate hidrate +quartz +calcium hydroxide
							200 °C (P=7atm)	2 h	Xonotlite + dicalcium silicate hidrate +quartz +calcium hydroxide

Reference				Reaction conditions					
Ref. number	Year	Authors	Title	Reactives	Ca/(Si+Al)	Water/Solid	Temperature (ºC)	Reaction time	Product
[16]	2015	W.Tan G.Zhu Y.Liu Z.Zhang L.Liu	Effects and mechanism research of the crystalline state for the semi-crystalline calcium silicate	$Na_2SiO_3 \cdot 9H_2O$ + $Ca(OH)_2$ + $NaOH$ (pH=11-13)	1.0	//	200	2h	Poor crystalline xonotlite
								8h	High crystalline xonotlite
				$Na_2SiO_3 \cdot 9H_2O$ + $Ca(OH)_2$ + $NaOH$ (pH=11-13) + Na_3AlO_3 (Al/Si=0.1)	1.0	//	200	1h	High crystalline xonotlite
[29]	2015	A. Hartmann D. Schulenberg J.C. Buhl	Synthesis and Structural Characterization of CSH-Phases in the Range of C / S = 0 . 41 - 1 . 66 at Temperatures of the Tobermorite Xonotlite Crossover	SiO_2 + CaO	0.55	7.5	230	40.5	Xonotlite + quartz+ tobermorite (trace)
					0.83	7.5	230	40.5	Xonotlite + quartz+ tobermorite (trace)
					1.24	7.5	230	40.5	Xonotlite + quartz+ tobermorite (trace)

Appendix II: Tobermorite hydrothermal synthesis

Reference				Reaction conditions						
Ref. number	Year	Authors	Title	Reactives	Ca/(Si+Al)	Al/(Si+Al)	Water/Solid	Temperature (°C)	Reaction time	Product
[1]	1938	E. P. Flint H.F. McMurdie L. S. Wells	Formation of hydrated calcium silicates at elevated temperatures and pressures	CaO + SiO	0.8	0.00	//	150	42 days	Tobermorite
								225	14 days	Tobermorite
								250	7 days	Tobermorite
					0.76	0.00	//	275	21 days	Tobermorite
[2]	1957	G. Kalousek	Crystal Chemistry of Hydrous Calcium Silicates: I, Substitution of Aluminum in Lattice of Tobermorite	*Kaolin (Al_2O_3) *Micricrystalline quartz (SiO_2) *Quicklime ($Ca(OH)_2$)	0.80	0.0041	//	175	24 h	100% Tobermorite
					0.80	0.1244	//	175	24 h	95% Tobermorite + C_3ASH_4
					0.80	0.2060	//	175	24 h	85% Tobermorite + C_3ASH_4
					0.80	0.2900	//	175	24 h	75% Tobermorite + C_3ASH_4
					1.00	0.0045	//	175	15 h	100% Tobermorite
					1.00	0.1350	//	170	72 h	Tobermorite + hydrogarnet
					1.00	0.2280	//	170	72 h	Tobermorite + hydrogarnet
					1.00	0.3200	//	170	72 h	Tobermorite + hydrogarnet
					1.00	0.5000	//	170	72 h	Tobermorite + hydrogarnet
[3]	1968	K. Speakman	The stability of tobermorite in the system CaO-SiO$_2$-H$_2$O at elevated temperatures and pressures	$Ca(OH)_2$ + Silica gel	0.80	0.00	//	110	180 days	Tobermorite
				$Ca(OH)_2$ + Quartz	0.80	0.00	//	140	196 days	Tobermorite + xonotlite (traces)
					0.83	0.00	//	140	196 days	Tobermorite + gyrolite + quartz +xonotlite (traces)
						0.00	//	160	196 days	Tobermorite + xonotlite + quartz (traces)
					0.5	0.00	//	210	21 days	Tobermorite + quartz + xonotlite
					0.67	0.00	//	200	19 days	Tobermorite + quartz + xonotlite (traces)

Reference				Reaction conditions						
Ref. number	Year	Authors	Title	Reactives	Ca/(Si+Al)	Al/(Si+Al)	Water/Solid	Temperature (ºC)	Reaction time	Product
[3]	1968	K. Speakman	The stability of tobermorite in the system CaO-SiO$_2$-H$_2$O at elevated temperatures and pressures	Ca(OH)$_2$ + Quartz	0.67	0.00	//	213	22 days	Tobermorite + xonotlite + quartz
				Gel of Ca(OH)$_2$ + Colloidal silica		0.00	//	254	7 days	Tobermorite + gyrolite + xonotlite
						0.00	//	276	7 days	Tobermorite + gyrolite + xonotlite
					1.00	0.00	//	149	7 days	Tobermorite + xonotlite
					0.917	0.00	//	278	10 days	Tobermorite + xonotlite
				Gel prepared by hydrolysis of Si(OC$_2$H$_5$)$_4$ in the presence of Ca(NO$_3$)$_2$	1.00	0.00	//	152	7 days	Tobermorite + xonotlite (traces)
				Glass	0.80	0.00	//	204	32 days	Tobermorite
[4]	1975	T. Mitsuda H.F.W. Taylor	Influence of aluminium on the conversión od calcium silicate hydrate gels into 11Å tobermorite at 90ºC and 120ºC	Colloidal SiO$_2$ CaO γ−Al$_2$O$_3$	0.8	0.00	//	90	4 weeks	Very poor tobermorite
						0.00	//	120	4 weeks	Very poor tobermorite
						0.05	//	90	1 week	//
						0.05	//	120	1 week	High crystalline tobermorite
						0.10	//	90	1 week	Poor crystallized tobermorite
						0.10	//	120	1 week	High crystalline tobermorite
						0.15	//	90	1 week	Poor crystallized tobermorite
						0.15	//	120	16 h	High crystalline tobermorite
					1.0	0.00	//	90	4 weeks	Very poor tobermorite
						0.00	//	120	4 weeks	Poor crystallized tobermorite
						0.05	//	90	1 week	Very poor tobermorite
						0.05	//	120	1 week	Very poor tobermorite
						0.10	//	90	1 week	Very poor tobermorite

Reference				Reaction conditions						
Ref. number	Year	Authors	Title	Reactives	Ca/(Si+Al)	Al/(Si+Al)	Water/Solid	Temperature (ºC)	Reaction time	Product
[4]	1975	T. Mitsuda H.F.W. Taylor	Influence of aluminium on the conversión od calcium silicate hydrate gels into 11Å tobermorite at 90ºC and 120ºC	Colloidal SiO$_2$ CaO $\gamma-Al_2O_3$	1.0	0.10	//	120	1 week	Poor crystallized tobermorite
						0.15	//	90	1 week	Poor crystallized tobermorite
								120	1 week	High crystalline tobermorite
				Aluminosilicic gel CaO	0.8	0.05	//	90	4 weeks	High crystalline tobermorite
								120	4 weeks	High crystalline tobermorite
						0.10	//	90	1 week	High crystalline tobermorite
								120	1 day	High crystalline tobermorite
						0.15	//	90	4 week	High crystalline tobermorite
								120	16h	High crystalline tobermorite
					1.0	0.05	//	90	1 week	Very poor tobermorite
								120	1 week	Poor crystallized tobermorite
						0.10	//	90	1 week	High crystalline tobermorite
								120	1 week	High crystalline tobermorite
						0.15	//	90	1 week	High crystalline tobermorite
								120	1 week	High crystalline tobermorite
				Clinoptilolite CaO	0.8	0.16	//	90	1 week	High crystalline tobermorite
								120	1 week	High crystalline tobermorite
					1.0	0.16	//	90	4 weeks	High crystalline tobermorite
								120	1 week	High crystalline tobermorite
[5]	1977	S.A.S El-Hemaly T. Mitsuda H.F.W. Taylor	Synthesis of normal and anomalous tobermorites	CaO Quartz (10-20 µm)	0.8	0.00	20	180	10h	Anomalous tobermorite
				CaO Colloidal silica	0.8	0.00	20	180	96h	Normal tobermorite
				CaO Colloidal silica $\gamma-Al_2O_3$	0.8	0.10	20	180	2 h	Normal tobermorite

Reference				Reaction conditions						
Ref. number	Year	Authors	Title	Reactives	Ca/(Si+Al)	Al/(Si+Al)	Water/Solid	Temperature (ºC)	Reaction time	Product
[5]	1977	S.A.S El-Hemaly T. Mitsuda H.F.W. Taylor	Synthesis of normal and anomalous tobermorites	CaO By-product SiO$_2$	0.8	0.00	20	180	10h	Anomalous tobermorite
				CaO Cristobalite	0.8	0.00	20	180	5h	Mix tobermorite
				CaO Quartz (<10μm) γ−Al$_2$O$_3$	0.8	0.05	20	180	72h	High crystalline tobermorite
						0.10	20	180	15h	High crystalline anomalous tobermorite
								120	14 days	Normal tobermorite
						0.15	20	180	15h	High crystalline tobermorite
					1.0	0.10	20	180	15h	Anomalous tobermorite + Quartz
				CaO Quartz (<10μm)	0.8	0.00	20	180	72h	High crystalline tobermorite
					1.0	0.00	20	120	14 days	Normal tobermorite
								180	15h	Mix tobermorite
				CaO Quartz (<10μm) γ−Al$_2$O$_3$ Alkali (Sodium silicate)	0.8	0.15	20	120	14 days	Anomalous tobermorite
					1.0	0.15	20	120	14 days	Anomalous tobermorite

Reference				Reaction conditions						
Ref. number	Year	Authors	Title	Reactives	Ca/(Si+Al)	Al/(Si+Al)	Water/Solid	Temperature (°C)	Reaction time	Product
[6]	1977	M. Sakiyama T. Mitsuda	Hydrothermal reaction between C-S-H and Kaolinite for the formation of tobermorite at 180°C	C-S-H prepared from CaO and SiO$_2$ (Ca/Si= 1.14) at 130°C for 2 hours + Kaolinite	0.8	0.00	//	180	1 h?	High crystalline tobermorite
				C-S-H prepared from CaO and SiO$_2$ (Ca/Si= 1.14) at 180°C for 2 hours + Kaolinite	0.8	0.00	//	180	4h	High crystalline tobermorite
[7]	1978	C.F. Chan T.Mitsuda	Formation of 11Å tobermorite from mixtures of lime and colloidal silica with quartz	CaO + Colloidal silica + Quartz $\left(\frac{quartz}{tot\ SiO_2} = 0.6\right)$	0.8	0.00	//	180	3h	High crystalline tobermorite

Reference				Reaction conditions						
Ref. number	Year	Authors	Title	Reactives	Ca/(Si+Al)	Al/(Si+Al)	Water/Solid	Temperature (°C)	Reaction time	Product
[7]	1978	C.F. Chan T.Mitsuda	Formation of 11Å tobermorite from mixtures of lime and colloidal silica with quartz	CaO + Colloidal silica + Quartz $\left(\frac{quartz}{tot\ SiO_2} = 0.47\right)$	0.8	0.00	//	180	3h	High crystalline tobermorite
				CaO + Colloidal silica Quartz $\left(\frac{quartz}{tot\ SiO_2} = 0.47\right)$	0.8	0.00	//	180	3h	High crystalline tobermorite
[8]	1978	N. Hara C.F. Chan T. Mitsuda	Formation of 14Å tobermorite	CaO + Quartz	1.0	0.00	20	140 + 60	20h + 10 months	14Å tobermorite + quartz
					0.9	0.10	20	140 + 60	20h + 10 months	14Å tobermorite + quartz
					0.8	0.00	20	140 + 60	20h + 10 months	14Å tobermorite + quartz

Reference				Reaction conditions						
Ref. number	Year	Authors	Title	Reactives	Ca/(Si+Al)	Al/(Si+Al)	Water/Solid	Temperature (°C)	Reaction time	Product
[8]	1978	N. Hara C.F. Chan T. Mitsuda	Formation of 14Å tobermorite	CaO + Quartz + $\gamma-Al_2O_3$	0.8	0.00	20	140 + 60	20h + 10 months	14Å tobermorite + quartz
				CaO + Cristobalite	1.0	0.00	20	140 + 60	20h + 10 months	14Å tobermorite
					0.9	0.10	20	140 + 60	20h + 10 months	14Å tobermorite
					0.8	0.00	20	140 + 60	20h + 10 months	14Å tobermorite
				CaO + Cristobalite + $\gamma-Al_2O_3$	0.8	0.00	20	140 + 60	20h + 10 months	14Å tobermorite
				CaO + By-product silica	1.0	0.00	20	140 + 60	20h + 10 months	14Å tobermorite

Reference				Reaction conditions						
Ref. number	Year	Authors	Title	Reactives	Ca/(Si+Al)	Al/(Si+Al)	Water/Solid	Temperature (ºC)	Reaction time	Product
[8]	1978	N. Hara C.F. Chan T. Mitsuda	Formation of 14Å tobermorite	CaO + By-product silica	0.9	0.00	20	140 + 60	20h + 10 months	14Å tobermorite
[9]	1979	S.A. Hamid	Electron microscopic characterization of the hydrothermal growth of synthetic 11Å tobermorite crystals	CaO + SiO_2	1.2	0.00	1	140	80h	Tobermorite
					1.0	0.00	1	140	80h	Tobermorite
					1.0	0.00	1	175	40h	Tobermorite + xonotlite
					0.83	0.00	1	140	60h	Tobermorite
[10]	1985	S. Komarneni R. Roy D.M. Roy C.A. Fyfe G.J. Kennedy A.A. Bothner J. Dadok A.S. Chesnick	^{27}Al and ^{29}Si magic angle spinning nuclear magnetic resonance spectroscopy of Al-substituted tobermorites	Quartz + CaO	0.83	Si/Al=0	//	175	18h	Anomalous tobermorite
				Na_2SiO_3 + $FeCl_3$ + CaO	0.83	Si/Al=0	//	175	14 day	Anomalous tobermorite + calcite + goethite

TOBERMORITE HYDROTHERMAL SYNTHESIS

Reference				Reaction conditions						
Ref. number	Year	Authors	Title	Reactives	Ca/(Si+Al)	Al/(Si+Al)	Water/Solid	Temperature (°C)	Reaction time	Product
[10]	1985	S. Komarneni R. Roy D.M. Roy C.A. Fyfe G.J. Kennedy A.A. Bothner J. Dadok A.S. Chesnick	^{27}Al and ^{29}Si magic angle spinning nuclear magnetic resonance spectroscopy of Al-substituted tobermorites	Amorphous SiO_2 + Kaolinite + KOH	0.83	Si/Al=20	//	175	7day	Anomalous tobermorite + calcite
				Na_2SiO_3 + $AlCl_3$ + CaO	0.83	Si/Al=9	//	180	7day	Anomalous tobermorite + calcite
					0.83	Si/Al=9	//	85	4day	Normal tobermorite + calcite
					0.83	Si/Al=9	//	180	1day	Anomalous tobermorite + calcite
				Amorphous SiO_2 + Kaolinite + CaO + NaOH	0.83	Si/Al=20	//	175	7day	Anomalous tobermorite + calcite
				Amorphous SiO_2 + Zeolite Linde 3A + CaO + NaOH	0.83	Si/Al=5.7	//	80	22 days	Normal tobermorite + calcite

Reference				Reaction conditions						
Ref. number	Year	Authors	Title	Reactives	Ca/(Si+Al)	Al/(Si+Al)	Water/Solid	Temperature (°C)	Reaction time	Product
[10]	1985	S. Komarneni R. Roy D.M. Roy C.A. Fyfe G.J. Kennedy A.A. Bothner J. Dadok A.S. Chesnick	^{27}Al and ^{29}Si magic angle spinning nuclear magnetic resonance spectroscopy of Al-substituted tobermorites	Amorphous SiO_2 + Kaolinite + CaO + KCl	0.83	Si/Al=20	//	175	7day	Anomalous tobermorite + xonotlite (trace)
				Clinoptilolite + CaO	0.83	Si/Al=3.7	//	175	7day	Anomalous tobermorite + calcite
				Phillipsite + CaO	0.83	Si/Al=3	//	225	5day	Normal tobermorite
				Amorphous SiO_2 + Zeolite	0.83	Si/Al=7.7	//	85	120 day	Anomalous tobermorite + calcite
				Fumed silica + $\gamma-Al_2O_3$ + CaO	0.83	Si/Al=5	//	80	120 day	Normal tobermorite
[11]	1992	H. Sato M. Grutzeck	Effect of Starting Materials on the Synthesis of Tobermorite	CaO + Quartz	0.8	0.00	5	180	4h	High crystalline tobermorite

TOBERMORITE HYDROTHERMAL SYNTHESIS

Reference				Reaction conditions						
Ref. number	Year	Authors	Title	Reactives	Ca/(Si+Al)	Al/(Si+Al)	Water/Solid	Temperature (ºC)	Reaction time	Product
[11]	1992	H. Sato M. Grutzeck	Effect of Starting Materials on the Synthesis of Tobermorite	CaO + Silicic Acid	0.8	0.00	5	180	8h	Low crystalline tobermorite
				CaO + Colloidal Silica Fume	0.8	0.00	5	180	24 h	Low crystalline tobermorite
[12]	1992	R. Gabrovšek B. Kurbus D. Mueller W. Wieker	Tobermorite formation in the system CaO, C_3S-SiO_2-Al_2O_3-NaOH-H_2O under hydrothermal conditions	CaO + Quartz flour	0.83	0.00	20	180	12h	Tobermorite + SiO_2
				CaO + Quartz flour + Al_2O_3	0.83	0.10	20	180	12h	Tobermorite
				C_3S + Quartz flour	0.83	0.00	20	180	12h	Tobermorite + SiO_2
				C_3S + Quartz flour + Al_2O_3	0.83	0.10	20	180	12h	Tobermorite
[13]	1996	X. Cong R. Kirkpatrick	^{29}Si and ^{17}O NMR investigation of the structure of some crystalline calcium silicate hydrates	CaO + Quartz	0.8	0.00	5	175	2 days	11Å Tobermorite
					0.9	0.00	5	80	133 days	14Å Tobermorite

Reference				Reaction conditions						
Ref. number	Year	Authors	Title	Reactives	Ca/(Si+Al)	Al/(Si+Al)	Water/Solid	Temperature (°C)	Reaction time	Product
[14]	1996	N.S. Bell S. Venigalla P.M. Gill J.H. Adair	Morphological forms of tobermorite in hydrothermally treated calcium silicate hydrate gels	SiO_2 + CaO + NaOH (pH 12.6)	0.83	0.00	//	150	14 days	11Å Tobermorite
[15]	2000	S. Shaw S.M Clark C.M.B. Henderson	Hydrothermal formation of the calcium silicate hydrates tobermorite, and xonotlite: an in situ synchrotron study	Calcsilicate alkoxide gel	0.83	0.15	5	240	5h	11Å Tobermorite
[16]	2002	X. Huang, D. Jiang, S. Tan,	Novel hydrothermal synthesis method for tobermorite fibers and investigation on their thermal stability	$Ca(OH)_2$ Amorphous SiO_2 EDTA (EDTA/Ca=1.0) KOH	2.00	0.00	//	200	3h	Low crystalline 11Å Tobermorite
									10h	Fibrous high crystalline 11Å Tobermorite

Reference				Reaction conditions						
Ref. number	Year	Authors	Title	Reactives	Ca/(Si+Al)	Al/(Si+Al)	Water/Solid	Temperature (°C)	Reaction time	Product
[17]	2003	X. Huang, D. Jiang, S. Tan,	Novel hydrothermal synthesis of tobermorite fibers using Ca(II)-EDTA complex precursor	$Ca(OH)_2$ Amorphous SiO_2 EDTA (EDTA/Ca=1.0) KOH pH= 13.0	1.00	0.00	//	200	3h	Fibrous high crystalline 11Å Tobermorite
					1.25	0.00	//	200	5h	Fibrous high crystalline 11Å Tobermorite
					1.50	0.00	//	200	10h	Fibrous high crystalline 11Å Tobermorite
				$Ca(OH)_2$ Amorphous SiO_2 EDTA (EDTA/Ca=1.0) KOH pH= 12.0	2.00	0.00	//	200	10h	Platy high crystalline 11Å Tobermorite
[18]	2003	L. Black, K. Garbeva, P. Stemmermann, K.R. Hallamb, G.C. Allen	Characterisation of crystalline C-S-H phases by X-ray photoelectron spectroscopy	Aerosil 300 (SiO_2) + CaO 1° milling 12 h 2° hydrothermal	0.83	0.00	4	170	5 days	Crystalline 11Å Tobermorite
[19]	2004	S.-Y. Hong F.P. Glasser	Phase relations in the CaO–SiO2–H2O system to 200°C at saturated steam pressure	C-S-H gel formed (during 6-24 months) from Aerosil 300 (SiO_2) + $Ca(OH)_2$	0.83	0.00	10	140	90 days	High 11Å Tobermorite

Reference				Reaction conditions						
Ref. number	Year	Authors	Title	Reactives	Ca/(Si+Al)	Al/(Si+Al)	Water/Solid	Temperature (ºC)	Reaction time	Product
[20]	2005	N.J. Coleman	Synthesis, structure and ion exchange properties of 11Å tobermorites from newsprint recycling residue	Newsprint de-inking sludge mineral part (25%) (CaO + CaO 41% + SiO_2 31% + Al_2O_3 18%) + NaOH (4M)	0.855	0.4	17	100	48h	Low crystalline tobermorite + katoite + gehlenite
				Newsprint de-inking sludge mineral part (25%) (CaO + CaO 41% + SiO_2 31% + Al_2O_3 18%) + $Na_2SiO_3 \cdot 5H_2O$ + CaO	0.75	0.15	17	100	168h	High crystalline tobermorite + gehlenite (traces)

TOBERMORITE HYDROTHERMAL SYNTHESIS

Reference				Reaction conditions						
Ref. number	Year	Authors	Title	Reactives	Ca/(Si+Al)	Al/(Si+Al)	Water/Solid	Temperature (ºC)	Reaction time	Product
[20]	2005	N.J. Coleman	Synthesis, structure and ion exchange properties of 11Å tobermorites from newsprint recycling residue	Newsprint de-inking sludge mineral part (25%) (CaO + CaO 41% + SiO_2 31% + Al_2O_3 18%) + $Na_2SiO_3 \cdot 5H_2O$ + CaO + NaOH (4M)	0.75	0.15	17	100	168h	Low crystalline tobermorite + katoite
[21]	2006	K. Lin, J. Chang, J. Lu	Synthesis of wollastonite nanowires via hydrothermal microemulsion methods	CTAB + n-pentanol + $Ca(NO_3)_2$ + Na_2SiO_3 + NH_4^+ (pH=10.8) 1° Microemulsion 2° Hydrothermal	1.00	0.00	//	200	18h	Fibrous 11Å Tobermorite

Reference				Reaction conditions						
Ref. number	Year	Authors	Title	Reactives	Ca/(Si+Al)	Al/(Si+Al)	Water/Solid	Temperature (ºC)	Reaction time	Product
[22]	2006	D. Palubinskaite A. Kantautas,	Influence of tribomechanical milling and activation of primary mixtures on the synthesis of calcium silicate hydrates	CaO + SiO_2 + Al_2O_3 + NaOH 1° Milling 2° Hydrothermal	0.83	0.025	10	175	24h	Tobermorite
[23]	2009	J.R. Houston, R.S Maxwell, S.A.Carroll	Transformation of meta-stable calcium silicate hydrates to tobermorite: reaction kinetics and molecular structure from XRD and NMR spectroscopy	CaO + Amorphous SiO_2 + Al_2O_3 + NaOH (pH=13.3)	0.83	0.15	10	150	8 days	11Å Tobermorite

Reference				Reaction conditions						
Ref. number	Year	Authors	Title	Reactives	Ca/(Si+Al)	Al/(Si+Al)	Water/Solid	Temperature (°C)	Reaction time	Product
[24]	2009	N.Y Mostafa, A.A Shaltout, H. Omar, S.A. Abo-El-Enein,	Hydrothermal synthesis and characterization of aluminium and sulfate substituted 1.1 nm tobermorites	CaO + SiO_2 + $CaSO_4$ + $Al_2(SO_4)_3$ (2%)	0.83	0.02	10	175	4h	Low crystalline 11Å Tobermorite
									24h	High crystalline 11Å Tobermorite
[25]	2009	N.J. Coleman C.J. Trice J.W. Nicholson	11Å tobermorite from cement bypass dust and waste container glass: a feasibility study	Cement bypass dust (58% CaO + 14% SiO_2+ 5% Al_2O_3 +2% Fe_2O_3 + 1% Na_2O) + Soda-lime-silica glass (11% SiO_2 + 73% SiO_2 +13% Na_2O + 1% Al_2O_3 +	0.85	0.08	10.5	100	14 days	11Å Tobermorite + quartz + calcite

Reference				Reaction conditions						
Ref. number	Year	Authors	Title	Reactives	Ca/(Si+Al)	Al/(Si+Al)	Water/Solid	Temperature (ºC)	Reaction time	Product
[26]	2010	A. Hartmann, J. Buhl	The influence of sucrose on the crystallization behaviour in the system $CaO - SiO_2 - C_{12}H_{22}O_{11} - H_2O$ under hydrothermal conditions	CaO + SiO_2 + Sucrose	0.5	0.00	//	200	40 h	High crystalline 11Å Tobermorite
					0.8	0.00	//	200	40h	Fibrous 11Å Tobermorite
[27]	2011	K. Matsui, A.Ogawa, J. Kikuma, M.Tsunashima T. Ishikawa, S. Matsuno	In situ time-resolved X-Ray diffraction of tobermorite formation process under hydrothermal condition: influence of reactive Al compound	Quartz (SiO_2) + CaO + Portland cement + Gypsum	//	0.00	0.75	190	12h	Low crystalline 11Å Tobermorite
				Quartz (SiO_2) + CaO + Portland cement + Gypsum + $\gamma-Al_2O_3$	//	0.05	0.75	190	5h	High crystalline 11Å Tobermorite

Reference				Reaction conditions						
Ref. number	Year	Authors	Title	Reactives	Ca/(Si+Al)	Al/(Si+Al)	Water/Solid	Temperature (°C)	Reaction time	Product
[28]	2011	J. Reinik I.Heinmaa U.Kirso T.Kallaste J.Ritamäki D.Boström E.Pongácz M.Huuhtanen W.Larsson R.Keiski K.Kordás J.P. Mikkola	Alkaline modified oil shale fly ash: optimal synthesis conditions and preliminary test on CO_2 adsorption	Oil shale fly ash (50%CaO + 22% SiO_2 + 5% Al_2O_3) + NaOH 1M	1.94	0.21	0.003	130	24h	Tobermorite 11Å + quartz + calcite + katoite
					1.94	0.21	0.003	160	24h	Tobermorite 11Å + calcite + katoite
				Oil shale fly ash (50%CaO + 22% SiO_2 + 5% Al_2O_3) + NaOH 8M		0.21	0.003	130	24h	Tobermorite 11Å + calcite + katoite + quartz (traces)
						0.21	0.003	160	24h	Tobermorite 11Å + calcite + katoite

Reference				Reaction conditions						
Ref. number	Year	Authors	Title	Reactives	Ca/(Si+Al)	Al/(Si+Al)	Water/Solid	Temperature (ºC)	Reaction time	Product
[29]	2013	S. Tränkle, D. Jahn, T. Neumann, L. Nicoleau, N. Hüsing, D.Volkmer	Conventional and microwave assisted hydrothermal syntheses of 11 Å tobermorite	H Y D O T H E R M A L	$Ca(OH)_2$ + Silicic Acid + Borosilicate + EDTA + KOH (pH=13)	0.36	0.00	//	200	7 days	11Å Tobermorite + Gyrolite
					$Ca(OH)_2$ + Silicic Acid + Borosilicate + KOH (pH=13)	0.36	0.00	//	200	7 days	11Å Tobermorite + Gyrolite
					$Ca(OH)_2$ + Borosilicate + KOH (pH=13)	0.36	0.00	//	200	7 days	11Å Tobermorite + Gayrolite
						0.44	0.00	//	200	7 days	11Å Tobermorite
						0.60	0.00	//	200	7 days	11Å Tobermorite
						0.89	0.00	//	200	7 days	11Å Tobermorite + Xonotlite
					$Ca(OH)_2$ + Quartz (SiO_2) + KOH (pH=13)	0.44	0.00	//	200	7 days	Low crystalline 11Å Tobermorite
					$Ca(OH)_2$ + Silicic Acid + KOH (pH=13)	0.36	0.00	//	200	7 days	Low crystalline 11Å Tobermorite

TOBERMORITE HYDROTHERMAL SYNTHESIS

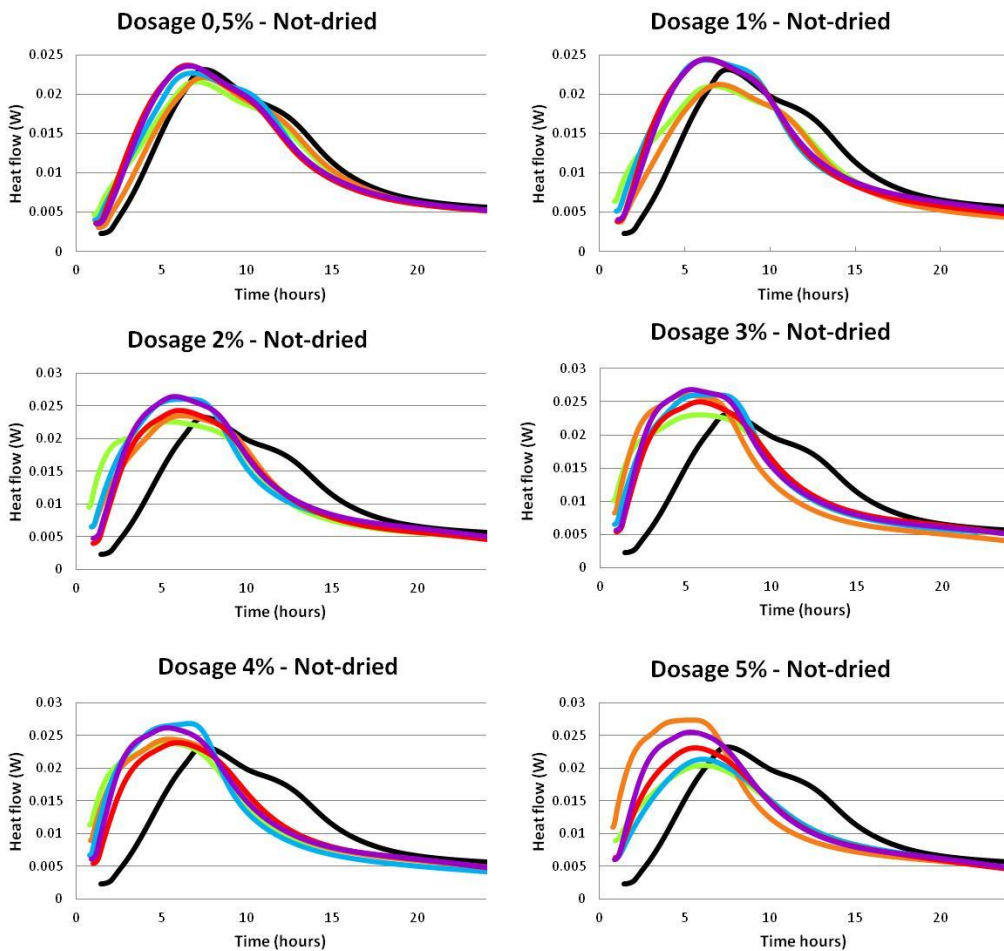| Reference				Reaction conditions						
Ref. number	Year	Authors	Title	Reactives	Ca/(Si+Al)	Al/(Si+Al)	Water/Solid	Temperature (°C)	Reaction time	Product
[29]	2013	S. Tränkle, D. Jahn, T. Neumann, L. Nicoleau, N. Hüsing, D.Volkmer	Conventional and microwave assisted hydrothermal syntheses of 11 Å tobermorite	MICROWAVE $Ca(OH)_2$ + Silicic Acid + Quartz (SiO_2) + KOH (pH=13)	0.36	0.00	//	200	8 hours	Low crystalline 11Å Tobermorite + quartz
					0.45	0.00	//	200	8 hours	11Å Tobermorite + quartz
					0.60	0.00	//	200	8 hours	11Å Tobermorite + quartz
					0.70	0.00	//	200	8 hours	Low crystalline 11Å Tobermorite + quartz
					0.83	0.00	//	200	8 hours	Low crystalline 11Å Tobermorite + quartz
[30]	2014	X. Yang, C.Cui, X.Cui, G. Tang, H. Ma,	High-temperature phase transition and the activity of tobermorite	CaO + SiO_2	0.83	0.00	10	180	10 h	11Å Tobermorite
[31]	2014	A. Hartmann, M. Khakhutov, J. Buhl	Hydrothermal synthesis of CSH-phases (tobermorite) under influence of Ca-formate	SiO_2 + CaO + Ca-formate	0.67	0.00	//	200	40.5 h	Quartz + Low crystalline 11Å Tobermorite

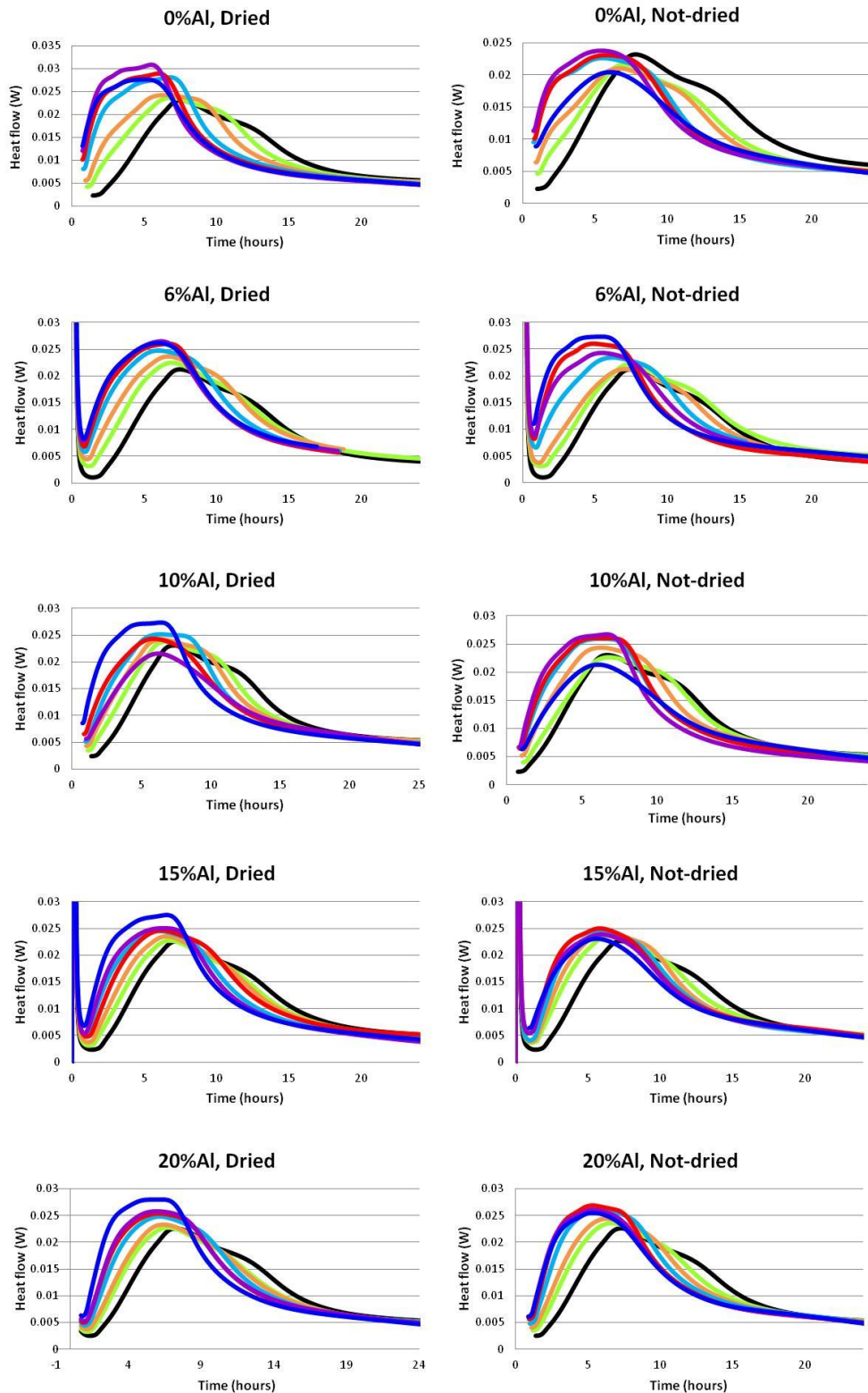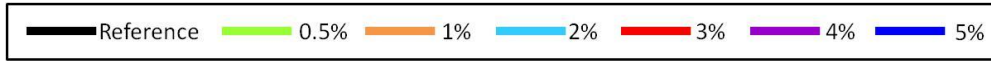| Reference				Reaction conditions						
Ref. number	Year	Authors	Title	Reactives	Ca/(Si+Al)	Al/(Si+Al)	Water/Solid	Temperature (ºC)	Reaction time	Product
[32]	2014	N.J. Coleman Q. Li A.Raza	Synthesis, structure and performance of calcium silica ion exchangers from recycled container glass	Soda-Lime-Silica glass (72% SiO_2 + 13% Na_2O + 11% CaO + 1% Al_2O_3) + CaO + NaOH (1M)	0.78	0.02	12	100	168h	Poor crystalline 11Å tobermorite
				Soda-Lime-Silica glass (72% SiO_2 + 13% Na_2O + 11% CaO + 1% Al_2O_3) + CaO + NaOH (2M)	0.72	0.02	12	100	168h	Poor crystalline 11Å tobermorite

TOBERMORITE HYDROTHERMAL SYNTHESIS

Reference				Reaction conditions						
Ref. number	Year	Authors	Title	Reactives	Ca/(Si+Al)	Al/(Si+Al)	Water/Solid	Temperature (ºC)	Reaction time	Product
[32]	2014	N.J. Coleman Q. Li A.Raza	Synthesis, structure and performance of calcium silica ion exchangers from recycled container glass	Soda-Lime-Silica glass (72% SiO_2 + 13% Na_2O + 11% CaO + 1% Al_2O_3) + CaO + NaOH (4M)	0.72	0.02	12	100	168h	Poor crystalline 11Å tobermorite
[33]	2015	A. Hartmann D. Schulenberg J.C. Buhl	Synthesis and Structural Characterization of CSH-Phases in the Range of C / S = 0 . 41 - 1 . 66 at Temperatures of the Tobermorite Xonotlite Crossover	SiO_2 + CaO	0.41	0.00	7.5	180	40.5 h	11Å Tobermorite + Quartz
								230	40.5 h	Low crystalline 11Å Tobermorite + quartz
					0.55	0.00	7.5	180	40.5 h	11Å Tobermorite + Quartz
								230	40.5 h	Low crystalline 11Å Tobermorite + quartz + xonotlite
					0.83	0.00	7.5	180	40.5 h	11Å Tobermorite + Quartz + Xonotlite
								230	40.5 h	Low crystalline 11Å Tobermorite + quartz + xonotlite

Reference				Reaction conditions						
Ref. number	Year	Authors	Title	Reactives	Ca/(Si+Al)	Al/(Si+Al)	Water/Solid	Temperature (ºC)	Reaction time	Product
[34]	2015	M.Monasterio J.J Gaitero H.Manzano J.S Dolado S. Cerveny	Effect of Chemical Environment on the Dynamics of Water Confined in Calcium Silicate Minerals: Natural and Synthetic Tobermorite	Nano-SiO$_2$ (Levasil 45%) + CaO + Al$_2$O$_3$ (Nyacol)	0.85	0.06	115	200	4h	11Å Tobermorite

Appendix III: Tobermorite not-dried seeds at different dosages and Al content calorimetries.